annual report 1978

nuclear physics laboratory
university of washington

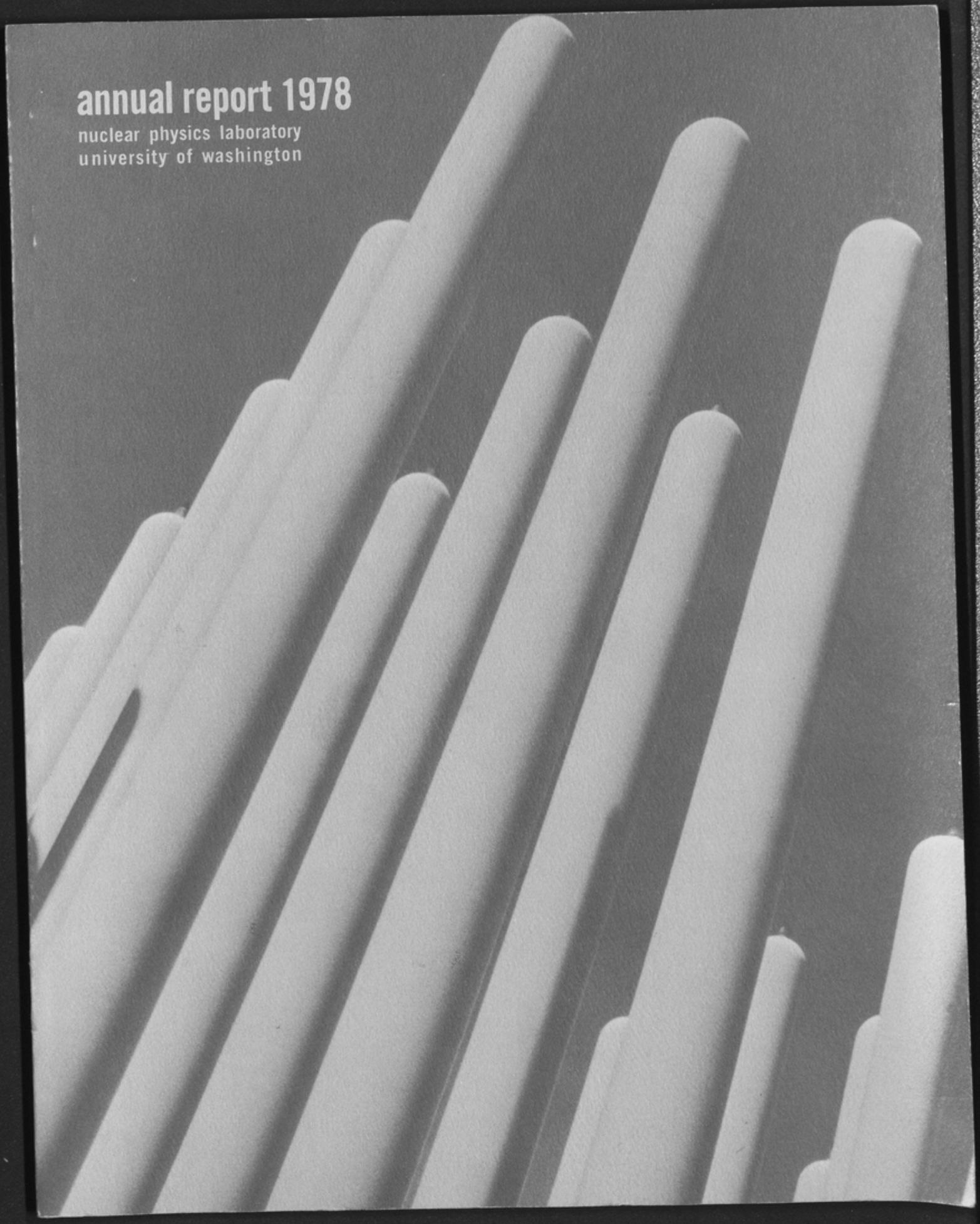

ANNUAL REPORT

Nuclear Physics Laboratory
University of Washington
July, 1978

Supported in part by the United States Department of Energy under contract EY-78-C-06-1388 Program A.

THE COVER DESIGN

For our cover picture we continue the tradition of the past several years and show the photograph of the high pressure gas cylinders which store the nitrogen and carbon dioxide mixture used for insulating the high potential terminals of the two Van de Graaff machines. They form a group of towers which front on the Van de Graaff building and have aroused considerable local interest and curiosity.

INTRODUCTION

This Annual Report is the twenty-third of its kind describing research done at the University of Washington Nuclear Physics Laboratory. The first of the series, the 1956 Annual Report, covered the period ending June 15, 1956 (and it has been customary since that time to publish the Annual Report for a given year before that year is over).

The 1956 Annual Report, the first such report to be printed and circulated in quantity by the Laboratory, was 43 pages long. It reported work done with the new external beam of the UW 60" Cyclotron, and reported that "a number of experiments have been performed with a beam of a few millimicroamperes of alpha particles delivered to a scattering chamber". It contained research reports covering 16 topics (principally in the areas of beta spectroscopy, alpha scattering, fission, and reaction mechanism studies), and listed 2 publications in Physical Review, 4 abstracts in BAPS, and one PhD Thesis for that year. It listed 6 faculty members, 3 research faculty, and 12 graduate students as members of the laboratory research staff, and a technical support staff of 17. (I note that a large number of the then graduate students are active and prominent nuclear physicists today.)

The 1978 Annual Report, 143 pages long, continues this tradition. The beams come primarily from the 3-stage FN Tandem accelerator and are often more intense than a "millimicroampere", but scattering and reaction mechanism studies still play a prominent role in the activities of the laboratory. This year's report contains research reports on 68 topics, and lists 22 journal publications, 7 invited papers, 11 papers published in conference proceedings, 11 contributed abstracts, and 2 PhD theses. We now list 9 teaching faculty, 3 research faculty, 6 research associates, and 12 graduate students. The research support staff now consists of 18 permanent employees plus a variable number of undergraduate hourly workers averaging about 15. (One might be tempted to conclude that since the other numbers have remained about the same, the large increase in research activity indicated by the publications is attributable to the addition to the laboratory of research associates and hourly workers.)

We find in the 1978 Annual Report evidence of vigorous continuing programs in a number of areas, as well as some efforts in new directions. The program in nuclear astrophysics continues with systematic studies of cross sections for gamma-ray astronomy and also turns some attention to the more esoteric problems of neutrino detection and antimatter astronomy. The program in fundamental symmetries reports parity experiments on the nuclei ^{18}F, ^{19}F, and ^{21}Ne and describes the beginning phases of a major experiment to measure in the hydrogen atom parity mixing resulting from neutral weak currents.

Other highlights include a report of a nuclear "time-delay" experiment which detects the interference between the into-the-atom amplitude and the energy-shifted out-of-the-atom amplitude for exciting a narrow resonance in $^{58}Ni + p$; continuing polarized proton studies of giant resonances, analog states, and continuum analyzing power; heavy ion studies including investigations of the transition in qualitative scattering characteristics between "light" ions (^{4}He and ^{6}Li) and "heavy" ions (^{12}C and ^{16}O), and quantitative angular correlation studies of the angular momentum transfer in deeply inelastic scattering;

and medium energy studies using the scattering of pions to investigate giant resonances and other nuclear properties.

Technical reports include a description of the installation of the first half of the laboratory's new dual PDP 11/60 computer system, a number of innovative instrumentation projects, and improvements of the tandem aimed at making it a super-sensitive mass spectrometer for radioisotope identification and dating. There are also a number of reports from the varied and active outside user groups who employ the accelerator facilities of the laboratory for a range of applied projects from materials studies to cancer therapy.

We close this introduction with the standard reminder that the articles in this report describe work in progress and are not to be regarded as publications nor quoted without permission of the investigators. The names of the investigators on each article have been listed alphabetically but where appropriate the name of the person primarily responsible for the report has been underlined.

As always, we welcome applications from outsiders for the use of our facilities. As a handy reference for potential users we list in the table on the following page the vital statistics of our accelerators. For further information please write or telephone Dr. W. G. Weitkamp, Technical Director, Nuclear Physics Laboratory, University of Washington, Seattle, WA 98195; (206) 543-4080.

John G. Cramer
Editor, 1978 Annual Report

August 8, 1978

THREE STAGE TANDEM VAN DE GRAAFF ACCELERATOR

(A High Voltage Engineering Corp. Model FN)

Completed: 1967
Funding: Purchased with NSF funds; maintained by ERDA funds and some funds from the State of Washington.

Beams currently available: (See also W.G. Weitkamp and F.H. Schmidt "The University of Washington Three Stage Van de Graaff Accelerator" Nucl. Instrum. Methods *122*, 65 (1974).

Ion	Typ.Current 2 stage(μA)	Max.Practical Energy 2 Stage (MeV)	Typ.Current 3 stage(μA)	Max.Practical Energy 3 Stage (MeV)
p,d	15	18	10	25
polarized p,d	0.1	18	--	--
^{3,4}He	3	27	--	--
^{6,7}Li	0.5	36	--	--
C	2	63	1	70
N	2	72	1	79
O	10	81	3	88
Si	0.2	90	--	--
Cl	0.2	117	0.2	124
Ni	0.5	117		
Br	0.1	125		
Ag	0.01	125		

CYCLOTRON

(A 60-inch fixed energy machine)

Completed: 1952
Funding: Constructed primarily with State funds and subsequently supported by AEC funds. Now sustained by funds from outside users.

Beams currently available:

Ion	Typical Current (μA)	Maximum Practical Energy (MeV)
p	100	11
d	150	22
^{4}He	30	42

THREE STAGE TANDEM VAN DE GRAAFF ACCELERATOR

(A High Voltage Engineering Corp. Model TM)

Completed: 1967

Funding: Purchased with NSF funds; maintained by ERDA funds and some funds from the State of Washington.

Beams currently available: (See also W.G. Weitkamp and F.M. Schmidt, "The University of Washington Three Stage Van de Graaff Accelerator" Nucl. Instrum. Methods 128, 65 (1974).

Ion	Typ.Current (μA)	Max.Practical Energy 2 Stage (MeV)	Typ.Current (μA)	Max.Practical Energy 3 Stage (MeV)
p	10	18	0.1	25
d	10	18	0.1	37
^{3}He	5	27	--	--
^{6},^{7}Li	0.5	38	--	--
C	2	63	1	70
N	2	72	2	72
O	10	81	6	86
Si	0.2	90	--	--
Cl	0.2	117	0.2	124
Ni	0.5	117		
Br	0.1	125		
Ag	0.01	125		

CYCLOTRON

(A 60-inch fixed energy machine)

Completed: 1952

Funding: Constructed primarily with State funds and subsequently supported by AEC funds. Now sustained by funds from outside sources.

Beams currently available:

Ion	Typical Current (μA)	Maximum Practical Energy (MeV)
p	100	11
d	150	22
^{3}He	30	42

TABLE OF CONTENTS

Page

1. ASTROPHYSICS AND COSMOLOGY

1.1 Cross Sections Relevant to Gamma-Ray Astronomy

D. Bodansky, P. Dyer†, and D. R. Maxson††

Measurements have been completed on gamma ray yields for reaction involving nuclei of relatively high cosmic abundance, namely for protons and alpha particles on ^{12}C, ^{14}N, ^{16}O, ^{20}Ne, ^{24}Mg, ^{28}Si, and ^{56}Fe. The measurements were made, for the most part, at incident proton energies from threshold to 24 MeV and at incident alpha-particle energies from threshold to 27 MeV. As discussed in previous Reports,[1] laboratory investigations of gamma ray spectra can provide data necessary to the interpretation of astronomical gamma-ray line spectra in terms of the abundances, energy spectra, and, possibly, directions of the interacting nuclei.

For all targets studied other than ^{16}O, the most prominent lines involved gamma rays with multipolarities of two or less. In such cases, the total cross section can be found from differential cross sections measured at the zeros of $P_4(\cos\theta)$. Therefore, measurements were made with a pair of Ge(Li) detectors at 109.9° and 30.5°. For ^{16}O, measurements were made at four angles.

Table 1.1-1. Prominent Gamma-Ray Lines in Proton Bombardments

Target Nucleus	Residual Nucleus	Transition (Levels)	Energy (MeV)	Comment
^{12}C	^{12}C	1→0	4.439	
^{14}N	^{14}N	2→1	1.635	
	^{14}N	1→0	2.313	
	^{13}C	2→0	3.683	strong for E_p > 20 MeV
^{16}O	^{12}C	2→0	4.439	
	^{16}O	2→0	6.130	use escape peaks
	^{16}O	4→0	7.117	
^{20}Ne	^{20}Ne	1→0	1.634	
	^{16}O	2→0	6.130	
^{24}Mg	^{24}Mg	1→0	1.369	
	^{20}Ne	1→0	1.634	
^{28}Si	^{24}Mg	1→0	1.369	
	^{28}Si	1→0	1.779	
^{56}Fe	^{56}Co	4→1	0.816	
	^{56}Fe	1→0	0.847	
	^{56}Fe	2→1	1.238	
	^{56}Fe	3→1	1.811	

We are currently in the process of extracing cross sections from the observed gamma ray spectra. Particularly prominent lines for the proton

bombardments are listed in Table 1.1-1. Typical results are presented in Table 1.1-2, where total cross sections are listed for 1.78-MeV gamma rays from protons incident upon ^{28}Si. The measured cross sections for individual points have

Table 1.1-2. Average total cross sections in 1-MeV bins: $p + {}^{28}Si$, 1.78-MeV gamma ray production. (Systematic uncertainties are approximately 10%; statistical uncertainties are much smaller.)

Central Energy (MeV)	σ Tot (mb)	Central Energy (MeV)	σ Tot (mb)
2	0	13	410
3	21	14	384
4	73	15	391
5	140	16	352
6	217	17	312
7	292	18	284
8	307	19	245
9	352	20	207
10	379	21	180
11	408	22	164
12	421	23	151

been summed to obtain the average cross section over bins of 1-MeV width. At the lower energies, where the cross section varies most rapidly, successive data points were taken at energies separated by amounts less than the energy loss in the target (typically, ∿100 keV).

When gamma-ray line spectra from astronomical sources become available, it can be expected that the information which will be most immediately extractible will be the relative abundances of the most abundant (heavy) nuclei, such as ^{12}C, ^{16}O, ^{20}Ne, etc. To relate the observed gamma-ray line fluxes to these abundances, only the cross sections for the very strongest lines will be needed--along with some surmise as to the energy spectra of the interacting nuclei.

However, some of the individual spectra are rich in potential information if one looks at a larger number of lines. For example, in the alpha-particle bombardment of ^{56}Fe at 24 MeV, the following lines are prominent: 0.847 MeV (^{56}Fe, $1 \rightarrow 0$), 1.050 MeV (^{58}Co, $10 \rightarrow 0$), 1.19 MeV (^{59}Co, $2 \rightarrow 0$ and/or ^{59}Ni, $4 \rightarrow 0$), 1.238 MeV (^{56}Fe, $\alpha \rightarrow 1$), 1.428 MeV (^{59}Ni, $10 \rightarrow 1$), and 1.454 MeV (^{58}Ni, $1 \rightarrow 0$). The ^{58}Co and ^{58}Ni lines do not become conspicuous until about 24 MeV, while the ^{56}Fe and ^{59}Ni lines are already strong at an alpha-particle energy of 8 MeV. Thus, in principle, the relative strengths of these several lines should provide information on the shape of the alpha-particle energy

spectrum. The A=58 and A=59 lines are particularly interesting because the relatively low cosmic abundances of all nuclei for A > 56 means that lines from the A=58 and A=59 isotopes are especially good indicators of alpha-particle fluxes (as distinct from proton fluxes). However, further analysis, including consideration of the probable background from reactions with targets other than ^{56}Fe, is necessary before it will be possible to judge the extent to which this potential will in fact be exploitable.

One can anticipate complexity in the interpretation of astronomical fluxes of some of the gamma ray lines, because of the many sources of these lines. Thus, we have observed the ^{16}O 6.13-MeV line in proton bombardments of ^{16}O and ^{20}Ne and in alpha-particle bombardments of ^{14}N, ^{16}O, and ^{20}Ne. These bombardments have been made primarily using gas targets and the lines show the expected large Doppler broadening. We have not as yet explored the extent, if any, to which differences in Doppler widths could be used to indicate the relative importance of the different contributing interactions (including the reverse reactions, e.g., ^{16}O on ^{4}He). However, one anticipated result is dramatically seen: a sharp 6.13-MeV line is seen from stopped ^{16}O nuclei in bombardments of silicon oxide targets, illustrating the suggestion of Ramaty and Lingenfelter[2] that observation of this sharp line could be used as evidence for interactions in interstellar grains (as distinct from gas).

---

† Present address: Cyclotron Lab, Michigan State University, East Lansing, Michigan 48824.

†† Permanent address: Brown University, Providence, Rhode Island 02912.

1. Nuclear Physics Laboratory Annual Report, University of Washington (1976), p. 51; *ibid* (1977), p. 1.
2. E. Lingenfelter and R. Ramaty, Ap. J. Lett. 211, L19 (1977).

1.2 Investigation of Solar Neutrino Detection Experiments using Long-Lived Product Nuclei

J. G. Cramer, W. G. Lynch, and R. Loveman

With the recent advances in laser isotope identification[1] and in employment of accelerators as mass spectrometers,[2] it has become (at least in principle) possible to detect one atom of isotope A of element Z in the presence of Avogadro's number of atoms of isotope A±1 of the same element by direct detection, without the requirement that isotope A undergo radioactive decay. It therefore seems appropriate to restudy the problem of detecting solar neutrinos from a slightly different point of view than has been done by the Brookhaven group,[3] in that the requirement of a promptly decaying reaction product ($T_{\frac{1}{2}} \lesssim 5$ years) can be relaxed and reaction products with much longer half lives can be considered. This, in turn, raises the possibility that one can consider experiments integrating over geological time scales by employing naturally occurring "targets" in deeply buried high purity ores. (We note here that after beginning these investigations, we learned that the group at ANL headed by Mel Freedman has been pursuing the same line of investigation, centered about using ^{205}Tl as a "target," for several years.[4])

In order to study the possible neutrino-induced reactions in a systematic way, a computer program was prepared which calculates the neutrino absorption cross section for a given transition as a function of neutrino energy and integrates this cross section with the calculated neutrino fluxes of Bachall[5] to obtain a transition rate. This is then combined with the half-life of the product nucleus to compute the equilibrium ratio of product nucleus to target nucleus which will be present in a given sample which is in equilibrium with the solar flux. Table 1.2 lists 16 product nuclei which might be produced

Table 1.2. Comparison of Neutrino-Induced Reactions

Product	Z	A	Q-value(keV)	Log-ft	T(1/2) (sec)	Ratio
^{205}Pb	82	205	62.3	5.3(?)	4.8 E14	2.8 E-19
	82	205	60.0	10.2	4.8 E14	3.5 E-24
^{55}Mn	25	53	976	5.0(?)	6.0 E13	1.4 E-22
^{81}Kr	36	81	459	5.0(?)	6.3 E13	7.4 E-23
^{97}Tc	43	97	535	6.4(?)	7.8 E13	4.1 E-23
	43	97	644	6.4(?)	7.8 E13	3.3 E-23
^{137}La	57	137	610	5.3(?)	1.8 E12	1.8 E-23
^{93}Mo	42	93	1765	4.8(?)	1.0 E11	3.8 E-25
	42	93	1875	5.8(?)	1.0 E11	3.7 E-26
	42	93	1919	5.2(?)	1.0 E11	1.4 E-25
^{41}Ca	20	41	2430	6.0(?)	3.9 E12	3.9 E-25
^{157}Tb	65	157	383	5.3(?)	4.5 E9	1.7 E-25
^{145}Pm	61	145	141	6.6	5.3 E8	3.8 E-27
	61	145	221	7.4(?)	5.3 E8	2.9 E-28
^{179}Ta	73	179	115	6.0	4.9 E7	2.7 E-27
^{7}Be	4	7	862	3.3	4.5 E6	4.0 E-28
^{71}Ge	32	71	233	4.3	1.0 E6	2.0 E-28
^{37}Ar	18	37	5803	3.5	3.0 E6	1.5 E-29
	18	37	862	5.0	3.0 E6	8.4 E-30

in this way, ordered by decreasing product-to-target ratio as given in the right hand column. Double entries indicate cases where a transition to an excited state of the product nucleus has also been considered, and can be distinguished by the differing reaction Q-values.

As can be seen from Table 1.2, the reaction $^{205}Tl(\nu,e^-)^{205}Pb$ offers the most favorable equilibrium product-to-target ratio of the isotopes considered, and in terms of this criterion considered alone is some ten orders of magnitude better than the $^{37}Cl(\nu,e^-)^{37}Ar$ reaction employed by the Brookhaven group[3] in their work at the Homestake mine. However, this ratio does not reveal the complete story and other factors such as isotopic abundance of the target, background due to competing processes (e.g., muon and neutron induced transitions), and ease and efficiency of detection of the product isotope must be carefully considered in evaluating various alternative experiments. In the particular case of $^{205}Tl(\nu,e^-)^{205}Pb$ there is an additional complication in that the transition of interest goes to the first excited state of ^{205}Pb (the g.s. transition is highly inhibited, with a Log-ft value of 10.2). The transition rate for this transition is not known because the inverse decay cannot be observed as a k-

capture. Moreover, the transition matrix element must be known to about 20% if experimental measurements of the solar neutrino flux are to be of astrophysical interest. This presents a very challenging nuclear physics problem: how can the $^{205}Tl \rightarrow ^{205}Pb$ matrix element be measured or predicted to accuracy?

We have considered the following alternatives:

(1) Use the known weak-interaction decays in the neighborhood, (and possibly measure a few more), together with shell-model calculations, to predict the unknown fT value. This method does not appear to be able to predict the fT value to better than a factor of 1.5 to 2, because of uncertainties in the shell model.

(2) Use strong interaction charge exchange reactions, e.g., (^{3}He,t), (t,^{3}He), (p,n), and (n,p). These would be "calibrated" by measurements with known weak-interaction transition matrix elements and then used to predict the unknown matrix element from its strong-interaction transition rate in a charge exchange reaction (e.g., $^{205}Tl(^3He,t)^{205}Pb(\frac{1}{2}^-, 2.5\ keV)$ or $^{205}Tl(p,n)$ to the same state). We estimate that because of the differences between the radial regions sampled in strong- and weak-interaction charge exchange reactions this method would only be good to about a factor of 2 in estimating the unknown matrix element.

(3) The electromagnetic decay from the analog in ^{205}Pb of the ^{205}Tl ground state to the first excited state of $^{205}Pb(\frac{1}{2}^-, 2.3\ KeV)$ is the electromagnetic analog of the Fermi part of the weak interaction transition from $^{205}Tl_{gs}$ to $^{206}Pb_1$. Thus if the gamma-ray transition could be observed for this case the weak interaction matrix element could be estimated with accuracy at the 20% level. The problem here is experimental, for it would involve measurements on a radioactive target [$^{205}Pb(p,p'\gamma_1)$] and would require an energy resolution in the gamma ray detection which are beyond the present state of the art for large sodium iodide detectors for resolving γ_1 from γ_2 and γ_3. Thus, though tempting, this method does not appear to be experimentally feasible.

(4) One could produce ^{205}Pb in its metastable first excited state and attempt to observe k-capture decays from the weak interaction branch which competes with the dominant m- and n-electron conversion transitions. We estimate that this branching ratio is only about 1 in 10^{-12} and thus does not appear to be experimentally measurable.

In summary, then, there does not appear to be an experimentally feasible method presently available for determining the unknown weak-interaction matrix element to the desired accuracy. While method (3) above is perhaps the least unpromising, it requires a radioactive target and a high-resolution high-efficiency detector for 16 MeV gamma rays which does not presently exist.

We are presently studying some of the other neutrino induced reactions listed in Table 1.2 to see if one of these might offer a feasible "natural" experiment.

---

1. Sam Hurst, Oak Ridge National Laboratory, (private communication), (1978).

2. R.A. Muller, L.W. Alvarez, W.R. Holley, and E.J. Stephenson, Science 196, 521 (1977); *Physics Today*, December 1977, pp 17-19.
3. R. Davis, Jr., Phys. Rev. Lett. 12, 303 (1964); Invited paper at BNL Conference on the Status and Future of Solar Neutrino Research, January 5-7, 1978.
4. M.S. Freedman, C.M. Stevens, E.P. Horowitz, L.M. Fuchs, J.L. Lerner, L.S. Goodman, W.J. Childs, and J. Hesser, Science 193, 1117 (1976); M.S. Freedman, Contribution to BNL Conference on the Status and Future Of Solar Neutrino Research, January 5-7, 1978.
5. J.N. Bachall and R.L. Sears, Annual Reviews of Astronomy and Astrophysics 10, 25 (1972).

1.3 Status of the Neutrino Absorber-Theory Experiment

J. G. Cramer and A. G. Seamster

An experiment described in the previous year's Annual Report[1] has been initiated to provide an experimental test of the Wheeler-Feynman Absorber Theory[2] as it applies to the emission of neutrinos. This experiment has the advantage of being 180° symmetric in its sensitivity and thus overcomes certain criticisms of previous Absorber-Theory experiments[3] which have been suggested[4] or carried out.[5]

The execution of the present experiment was delayed by the unexpected demands of the ^{19}F parity experiment for the ND2400 analyzer and tape drive unit until December, 1977. At the beginning of this year we were able to take over the analyzer from the parity group and begin test runs. Gain stability requirements of the experiment indicated that a light pulser system be added to the experimental setup so that an external light flash could be delivered to both detector systems by light pipes from the same photodiode.

Special electronics for stabilization, routing, and operation of the light-pulser has been constructed and tested. Several items of NIM electronics have been purchased so that they can be tied up in the experiment without interfering with other experiments at the laboratory. We are now proceeding with stability checks and other tests of the system, and expect to begin data runs in about 1-2 months.

---

1. Nuclear Physics Laboratory Annual Report, University of Washington (1977), p. 3.
2. J.A. Wheeler and R.P. Feynman, Rev. Mod. Physics 17, 157 (1945); Rev. Mod. Physics 21, 425 (1949); also Phys. Rev. 59, 683 (1941).
3. P.C.W. Davis, Journal of Physics A: Math., Nucl. Gen. 8, 272 (1975).
4 P.L. Csonka, Phys. Rev. 180, 1266 (1969); M.L. Heron and D.T. Pegg, J. Phys. A: Math., Nucl. Gen. 7, 1 (1965).
5. R.B. Partridge, Nature 244, 263 (1973).

1.4 Search for Antimatter Supernovae using Photon Helicity Detection

J. G. Cramer, R. Loveman, and W. J. Braithwaite†

Work on this scheme for detecting antimatter at intergalactic distances, as described in last year's Annual Report,[1] has continued. A paper describing the method was published last Fall in Physical Review Letters.[2] Our further efforts have centered around (1) seeking ways of extending the distance over which the method could be applied and (2) conducting a more detailed investigation into the design of a space-mounted polarimeter capable of the required directionality and sensitivity to accomplish the measurements of interest.

For the first of these objectives, we have considered the effect of integrating the flux from a cluster of galaxies rather than concentrating on a single galaxy. In particular, the Virgo Cluster contains about 2×10^4 galaxies with an average distance from earth of about 15 Megaparsecs. If we take the rate of supernovae occurrence in an average galaxy of the cluster to be 1 supernova in 50 years, and the time over which a supernova emits the radiation of interest to be about 2 years, then at a given time some 800 galaxies contain active supernova remnants which are producing the polarized radiation of interest. Thus, a comparison of the radiation from the Virgo cluster with that from a supernova in a member of the Local Group at a distance of 1 megaparsec shows that the integrated flux from VC should be $800/(15)^2 = 3.6$ times more intense than that from the LG. Moreover, in this case the measurements can be made at any time and there is no necessity of waiting until a LG supernova occurs and no limit to the time over which counts may be collected. It should be noted that the above calculation assumes that all of the members of the Virgo Cluster are uniquely composed of the same stuff, either matter or antimatter. If half of the galazies were composed of one and half of the other, then there would be no net polarization to the observed radiation.

In pursuit of objective (2) above, we have begun detailed investigation of the suitability of the newly developed liquid argon and xenon ion chambers[3] for polarization sensitive gamma ray detectors, suitable for measurements of the polarization of secondary radiation from supernovae. In this connection, Dr. Charles R. Gruhn of LASL has been working with us, and we expect this collaboration to continue and to become more intensive in the coming year.

---

† Colleague at the University of Texas, Austin, Texas 78712.

1. Nuclear Physics Laboratory Annual Report, University of Washington, (1977), p. 6.
2. J.G. Cramer and W.J. Braithwaite, Physical Review Letters 39, 1104 (1977).
3. C.R. Gruhn and M.D. Edmiston, Physical Review Letters 40, 407 (1978); and C.R. Gruhn, Los Alamos Scientific Laboratory (private communication).

2. FUNDAMENTAL SYMMETRIES

2.1 Parity Mixing in the Ground State J=1/2 Doublet of ^{19}F

E. G. Adelberger, H. E. Swanson, T. A. Trainor, and R. Von Lintig

We have made considerable progress on our new experiment to measure the parity mixing in the ground ($1/2^+$) and 110 keV ($1/2^-$) levels of ^{19}F. Our first version of this experiment has been published[1] and some details of the new version are given in previous annual reports.[2] During the last year we have concentrated on: 1) improving the performance of the polarized ion source fast spin-flip system and the 4 counter on-line polarimeter, 2) measuring (or setting limits on) systematic errors in our appartus, and 3) acquiring data on the parity violating asymmetry δ of the 110 keV radiation.

The digital feedback system for the spin direction, based on the 4-counter polarimeter is now used routinely. A major advance was the discovery of a number of subtle problems in the 4-counter polarimeter which were traced to build up of a silicon contaminant on the thin C plus Au foil and to pile up of the scattered proton pulses. These were eliminated by removing Si O-ring grease from the system, doubling the thickness of the C plus Au foil, decreasing the solid angles of the 4 proton counters, and slightly modifying the method of analyzing the polarimeter data.

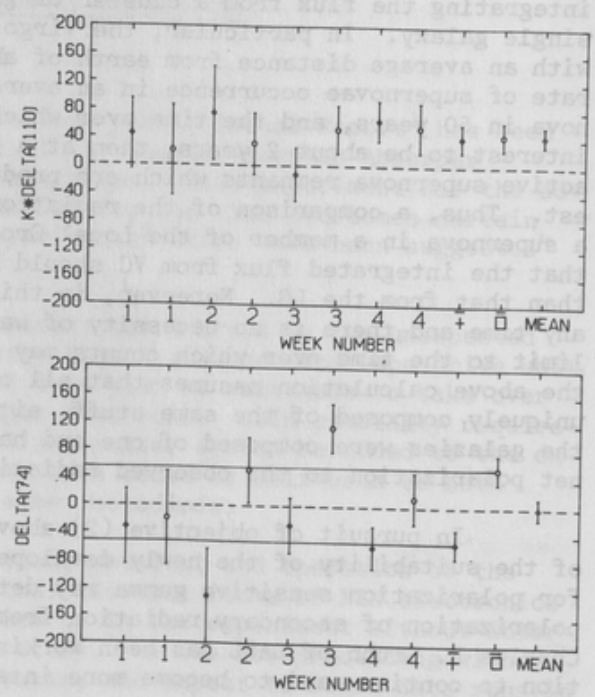

Fig. 2.1-1. The asymmetry, δ, in the 74 keV and 110 keV gamma rays in units of 10^{-6}. Data are shown with the Wien precession "normal" and "reversed." Also shown are the means of the individual Wien directions and the over-all mean.

The performance of the fast spin flip system has steadily been improved. Our most recent values are $P_0 = (P_+ + P_-)/2 = 81\%$, $P_1 = (P_+ - P_-)/2 = 5\%$, $i^+/i^- = 2\times10^{-4}$, when P_+ and P_- are the proton polarization on target in the two states + and - (T-coil on and off respectively) and i_+ and i_- are the corresponding beam currents.

During the last year we have had 4 data-taking runs on the ^{19}F experiment, each roughly 1 week long. During each run we acquired roughly equal statistics with the Wien spin precessor "normal" and "reversed" in order to compensate for any fake effect correlated with the T-coil state rather than the spin direction. Preliminary results from these runs are shown in Fig. 1, where we display

$$K\delta_{110} = \frac{1}{4P_p}\left[\frac{L^+R^-}{L^-R^+}\Big|_{110} - 1\right] \text{ and } \delta_{74} = \frac{1}{4P_p}\left[\frac{L^+R^-}{L^-R^+}\Big|_{74} - 1\right].$$

The notation has been defined in previous annual reports. We have improved our method of data analysis. The small residual current modulation ($i_+/i_- \approx 10^{-4}$) causes a small centroid shift between the (+) and (-) routes; peak areas are now extracted using a peak tracking routine. This does not however produce a significant change in our result. Any non-vanishing value for δ_{74} must be due to instrumental asymmetries since a 0^+ state can have no true anisotropy. Our preliminary experimental values are $\delta_{74} = (0\pm15)\times10^{-6}$ and $K\delta_{110} = (47\pm14)\times10^{-6}$. This implies $\delta_{110} = -(8.5\pm2.6)\times10^{-5}$. In each case we are quoting statistical standard errors. Although the observed asymmetry for the 74 keV γ ray is gratifyingly small, there is clearly a difference between the runs with the Wien precessor "normal" and "reversed," which is being cancelled in our final value because we acquire essentially equal amounts of data in the two precessor states. We are currently investigating the origin of this effect. It is very clear however that our experimental value for δ_{110} is definely smaller than predictions[3] based on the Weinberg-Salam model of the weak interactions $\delta_{110} = -31\times10^{-5}$.

We have tried to set limits on fake effects due to spin correlated modulation of the proton beam emittance and intensity by deliberately misadjusting the electric and magnetic fields used to flip the spin and measuring the spin correlated modulations in the beam using the beam correlation analyzer described in ref. 1. For example, we normally obtain data with both polarities of the T-coil field. Correlated beam motion was measured using only one T-coil polarity and found to correspond to a δ_{74} of about 20×10^{-6}. Since the measured effect changed sign when the T-coil polarity was reversed, our normal mode of data taking should cancel this to a high degree.

Tests for spurious asymmetries in the detection electronics were performed using the 59.5 keV line from a ^{241}Am source. The amplifier gains were adjusted to place the peak in the regions normally occupied by the 74 and 110 keV peaks respectively.

The apparent asymmetry in these measurements are $K\delta_{110} = (21\pm16)\times10^{-6}$ and $\delta_{74} = (0\pm12)\times10^{-6}$. The small size of these results rules out an electronic origin for the behavior of the 74 keV γ ray.

---

1. E.G. Adelberger, H.E. Swanson, M.D. Cooper, J.W. Tape, and R.A. Trainor, Phys. Rev. Lett. 34, 402 (1975).
2. E.G. Adelberger and H.E. Swanson, Nuclear Physics Laboratory Annual Report, University of Washington (1976), p. 36. E.G. Adelberger, Z. Iqbal, H.E. Swanson, T.A. Trainor, R. Von Lintig, Nuclear Physics Laboratory Annual Report, University of Washington (1977), p. 9.
3. M.A. Box, A.J. Gabric, and B.H.J. McKellar, Nucl. Phys. A271, 412 (1976).

2.2 Design and Construction of an Apparatus to Detect $2s_{1/2}$-$2p_{1/2}$ Mixing in Hydrogen Atoms

E.G. Adelberger, W.B. Ingalls, and T. A. Trainor

The hydrogen parity mixing experiment requires: 1) an intense, low-emittance source of H(2s) atoms, 2) a very uniform magnetic field to cross the 2s and 2p states, 3) a microwave cavity to drive the $2s \rightarrow 2p$ transitions and generate the stark mixing, 4) a very good vacuum to minimize the background of $\alpha \rightarrow \beta$ transition induced by collisions with residual gas.

The following measures have been taken during the past year.

1. A room has been found in the cyclotron lab where the experiment will be performed. The room has been fitted with 100 Amp 3 phase 208 VAC power. Water and compressed-air services were already in place.

2. An ion source very similar to that used on the polarized ion source has been constructed. Improvements to the extractor and decel electrodes and to the extractor power supply have been incorporated. The recirculatory Cs canal used to produce the H(2s) atoms is described in a separate section below.

3. A rigid frame capable of supporting the $\sim$1.5 ton apparatus while maintaining alignment to $\sim$5 mils is made. The ion pump and main solenoid are mounted on trolleys which ride on mechanical rails. The frame is 12 feet long.

4. A three-stage vacuum system is employed in our apparatus. The ion source box is maintained at 4×10^{-6} torr by a LN_2 trapped 6" diffusion pump. The atomic beam passes through a differential pumping impedance into a two-stage ultra-high vacuum system. The first stage is ion pumped by a unit having a pumping speed for hydrogen of 1500 l/sec. Components for this stage have arrived and are being assembled. We expect the vacuum in this stage to be better than 10^{-8} torr. Then the beam passes through a second pumping impedance into the main solenoid which is cryopumped. A 10 watt compressor which drives two 2-watt heads has been delivered and tested with prototype cryopanels. We hope to achieve a vacuum of $\sim10^{-10}$ torr in the solenoid.

5. The main solenoid has been designed. A 1/3 scale prototype of this has been built and tested and is described in a contribution below. The full scale solenoid will be $\sim$50" long, have an ID of 10.5" and will weigh $\sim$1 ton. All material for this solenoid has been delivered.

6. We have used two different L_α detectors - a "solar-blind" photomultiplier and a NO filled ion chamber. The PMT has been very useful for beam diagnostics because of its high signal to noise ratio. The ion chamber was supplied by a commercial firm[1] and gave us an absolute calibration of the L_α flux. However we have experienced problems with the reliability of these detectors. Some studies of detection geometries are discussed below.

---

1. Artech Corp., Falls Church, Virginia.

2.3 Study of a Recirculating Cesium Canal with a Surface Ionization Probe

R. Risler and T. A. Trainor

The metastable hydrogen beam for the hydrogen parity-violation experiment is produced by passing the proton beam from a duoplasmatron through a cesium vapor region. This cesium canal is a cylinder with a stainless steel mesh on the inside wall to allow recirculation of the cesium by capillary forces.[1] It was provided by R. A. Hardekopf, Los Alamos Scientific Laboratory.[2] The canal is 152 mm long with an inner diameter of 12.7 mm. The center part is heated to ∿100° C while the ends are water cooled to ∿25° C. The canal is filled with cesium from a separately heated reservoir which can be closed off.

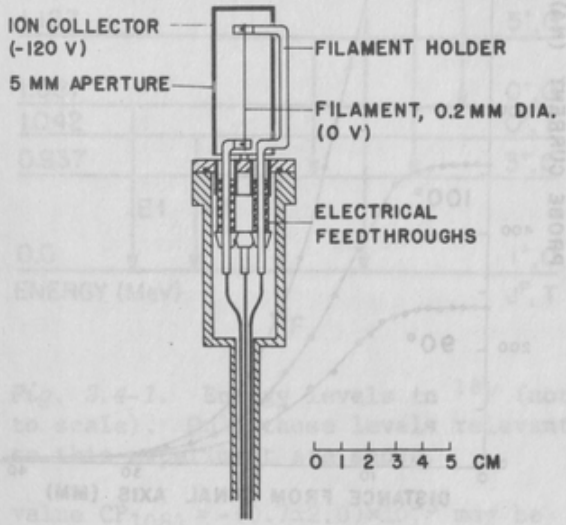

Fig. 2.3-1. **The surface ionization probe for measuring cesium flow from the canal.**

In order to study the behavior of the canal, a surface ionization probe was built, which measures the flow of cesium from the canal as well as its angular distribution. It is based on the long known effect that alkali atoms are ionized with practically 100% efficiency on a hot tungsten surface. The probe is essentially a selective partial pressure gauge for cesium.[3]

Figure 2.3-1 shows a schematic cut of the probe. Cesium atoms enter through a 5 mm diameter hole in the collector and hit the tungsten wire. The filament has a diameter of 0.2 mm and is 40 mm long. A DC current of two Amperes heats it to 1000° C. The cesium atoms are ionized on the hot surface and are accelerated by a negative voltage (-120 V) to the surrounding cylinder where they are collected, and the resulting current is measured. The probe is mounted on a hollow shaft containing the electrical connections, which runs through the chamber wall. The whole device can be moved across the canal axis, and a profile of the cesium coming out can be measured. To determine the background signal resulting from undirected cesium atoms in the residual gas the aperture can be rotated away from the canal.

The probe has become a reliable instrument to check the status of the canal while filling it from the reservoir or to determine the loss of cesium during longer running periods. The background reading gives valuable information on any spill of cesium in the vacuum box and helps to identify a malfunction of the canal very quickly.

The collector current reading is insensitive to large changes in collector voltage and filament current. The collector bias is provided by a battery, and no change of the current reading was observed between 90 V and 270 V.

Varying the filament current between 1.7 and 2.3 A changes the collector current by less than 1%. Below 1.7 A the temperature of the filament becomes too low, above 2.3 A the probe is heated up and outgassing leads to a higher background current and less precise reading.

Figure 2.3-2 shows three probe scans 65 mm from the canal end, taken with three different center temperatures and an end temperature of 25° C. The background current which is typically below 10 nA has been subtracted. By integrating the profile the cesium loss from the canal can be estimated. The 100° scan gives a total loss from both ends of 4 mg/hour. The amount of cesium coming from the canal decreases exponentially with time with a half life of $T_{\frac{1}{2}} \sim 13$ h (100°/ 25°, duoplasmatron off). The beam from the duoplasmatron heats the canal and thus increases the cesium flow by as much as 50%.

To reduce losses from the ends a new system with longer cooled end zones and small diameter apertures is in construction.

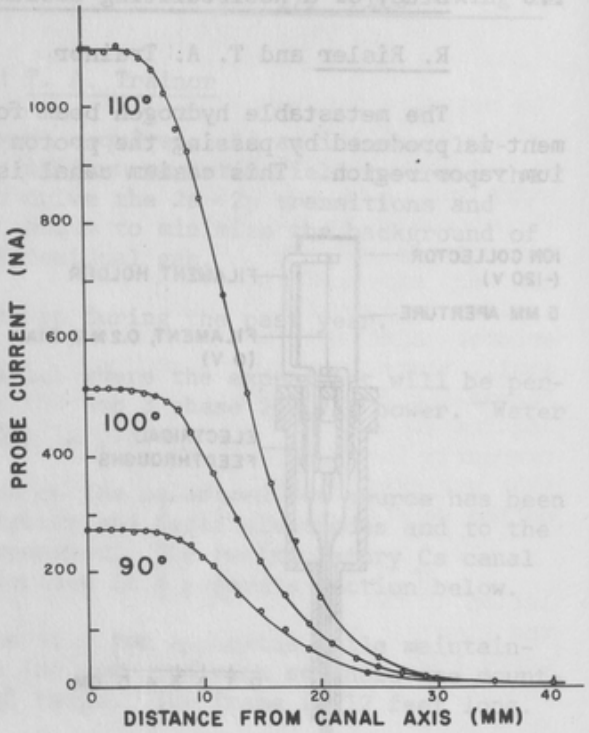

Fig. 2.3-2. Experimental scans of the cesium intensity 65 mm from the canal end at different center temperatures. No corrections have been applied for probe geometry.

1. M. Bacal, N. Olier, and W. Reichelt, Symposium on Ion Sources and Formation of Ion Beams, Brookhaven, 1971 (post deadline paper).
2. R.A. Hardekopf, Proceedings of the Fourth International Symposium on Polarization Phenomena in Nuclear Reactions, eds. W. Grüebler and V. König, Zürich 1975, p. 865.
3. J.B. Taylor and I. Langmuir, Phys. Rev. 51, 753 (1973).

2.4 Parity Mixing in the 1 MeV J=0 Doublet in ^{18}F*

E. G. Adelberger, C. A. Barnes†, J. Davidson†, M. L. Lowry†, R. E. Marrs, F. B. Moringo††, and H. E. Swanson

The $J^{\pi}=0^{+}$, T=1 and $J^{\pi}=0^{-}$ levels at $E_x \approx 1$ MeV in ^{18}F form an unusually "clear" and sensitive system for measuring the $\Delta T=1$ parity nonconserving N-N force. For a discussion of this point and details of our apparatus to measure the parity mixing in the J=0 doublet see previous annual reports.[2]

Our ^{18}F experiment was brought to a conclusion once our errors on the circular polarization of the 1081 keV γ-ray (see Fig. 2.4-1) were reduced to the designed level of ∿1/3 of a prediction[1] based on the Weinberg-Salam model of the neutral currents. This required ∿1500 hours of data taking on the CSULA accelerator. Our cumulative data is shown in Fig. 2.4-2. Our experimental

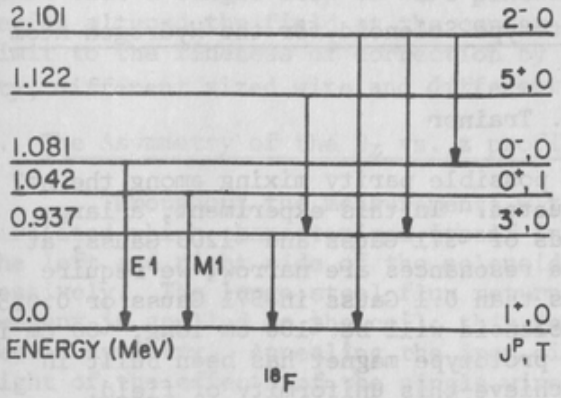

Fig. 2.4-1. Energy levels in ^{18}F (not to scale). Only those levels relevant to this experiment are shown.

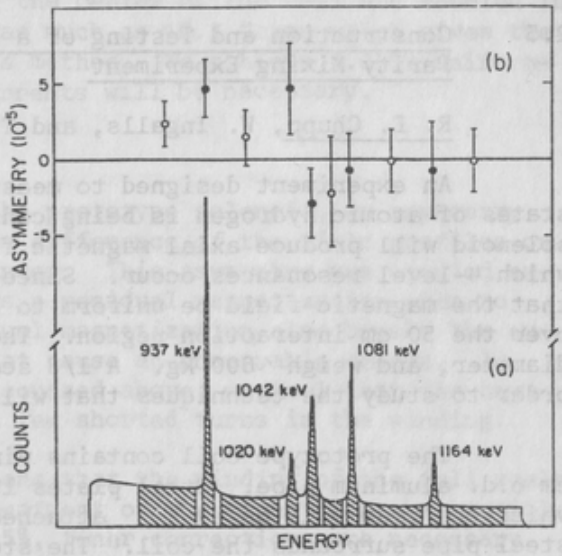

Fig. 2.4-2. a) Typical pulse height spectral regions for which asymmetries were determined are shaded. b) The measured asymmetries $A = \left(1-(R_-L_+/R_+L_-)\right)/4$ where $R_\pm$ and $L_\pm$ refer to the counting rates in the right (R) and left (L) detectors during the two polarimeter magnetization states (+ and -). The error bars denote statistical standard deviations. The open and closed circles are for the background and peak regions, respectively, shown in part (a).

value $CP_{1081} = -(0.7\pm2.0)\times10^{-3}$ may be compared to Cabibbo model predictions $|CP_{1081}| = 3.6\times10^{-3}$ [1] and $|CP_{1081}| = 3.4\times10^{-3}$ [3] and a prediction[1] of 5.7×10^{-3} based on the Weinberg-Salam model assuming that the nuclear structure aspects of the calculations are reliable, our result establishes an upper limit of 7.5 for any enhancement over the Cabibbo value of the ΔT=1 parity nonconserving N-N force. Previous theoretical estimates for this "enhancement factor" were 16 [4] and ∿10. [5] Our experiment is the only one which has achieved sufficient sensitivity to test whether pure ΔT=1 transitions are enhanced by such large factors. An account of this work has recently appeared in print.[6]

---

* Supported in part by the NSF (Caltech) and the State of California (CSULA).

† California Institute of Technology, Pasadena, CA. 91125.

†† California State University at Los Angeles, Los Angeles, CA. 90032.

1. M. Gari, J.B. McGrory, and J. Offerman, Phys. Lett. 55B, 277 (1975).
2. E.G. Adelberger *et al.*, Nuclear Physics Laboratory Annual Report, University of Washington (1976), p. 36; (1977) p. 8.
3. B.H.J. McKellar, private communication (1977).

4. M. Gari and J. Reid, Phys. Lett. 53B, 237 (1974).
5. B. Desplangues and J. Micheli, Phys. Lett. 68B, 339 (1977).
6. C.A. Barnes, M.M. Lowry, J.M. Davidson, R.E. Marrs, F.B. Morinigo, B. Chang, E.G. Adelberger, and H.E. Swanson, Phys. Rev. Lett. 40, 840 (1978).

2.5 Construction and Testing of a Prototype Solenoid for the Hydrogen Atom Parity Mixing Experiment

R. E. Chupp, W. Ingalls, and T. A. Trainor

An experiment designed to measure possible parity mixing among the n=2 states of atomic hydrogen is being constructed. In this experiment, a large solenoid will produce axial magnetic fields of ∿571 Gauss and ∿1200 Gauss, at which 4-level resonances occur. Since the resonances are narrow, we require that the magnetic field be uniform to less than 0.1 Gauss in 571 Gauss or 0.015% over the 50 cm interaction region. The solenoid will be ∿130 cm long, ∿60 cm in diameter, and weigh ∿600 kg. A 1/3 scale prototype magnet has been built in order to study the techniques that will achieve this uniformity of field.

The prototype coil contains windings of #15 copper magnet wire on a 10 cm o.d. aluminum pipe. Steel plates 19 cm ϕ with holes in the center (through which the beam will pass) attached at the ends, and a large 20 cm o.d. steel pipe surrounds the coil. The steel serves to return the flux and clamp the field. The over-all length of the prototype solenoid is 40 cm.

Measurements of the axial field profile were made using a Bell 620 Gaussmeter with a longitudinal probe and a chart recorder which produced plots of B_z vs. z. We studied: A) The effect of the size of the end plate holes on the field profile; B) The uniformity which we could achieve; C) The sources of an asymmetry in the B_z vs. z profile. Two coils were wound, the first with 1748 turns in 7 layers (which produces a net current in the z-direction) and the second with 2050 turns in 8 layers (no net I_z).

A. The Effect of the size of endplate holes on the field profile

The beam of atomic hydrogen produced by the duoplasmatron source should have a maximum cross-sectional diameter of ∿1.5 cm. Since maximum beam current is desired, reducing the cross-sectional area of the holes in the solenoid endplates is undersirable. We therefore examine the effects of 2.5 cm, 3.75 cm and 5 cm diameter holes on the field profile. As expected, the axial field strength diminishes more quickly away from the center of the solenoid for larger holes. However, the gradient of B_z is not in linear proportion to the size of the hole. The difference between 2.5 cm and 3.75 cm is much less than the difference between 3.75 cm and 5 cm. Though it will be desirable to make the endplate holes small in the final solenoid, there is clearly no need to obstruct the beam.

B. The Uniformity of the field

With the surrounding steel endplates and flux return, the magnetic field does not fall as rapidly from its maximum value at the center as it would without

the steel. Yet the field of such a coil is not uniform over any distance. A computer code was employed to find the approximate configuration of additional windings which would produce the desired uniformity. Correction coils were wound at the ends of the solenoid, each consisting of 36 turns in 9 layers of the same #15 wire. These were connected in series with the main coil. A field uniform to 0.1 Gauss in 90 Gauss or 0.11% over 20 cm was produced. We also found that a single loop of wire placed at the center of the coil and mounted in series altered the field at the center by as much as ∿0.1 Gauss which gives the limit to the fineness of correction by this method. To achieve 0.015% uniformity, different sized wire and different currents will be necessary.

C. The Asymmetry of the B_z vs. z profile

Throughout the measurements with the prototype solenoid, an asymmetry persisted which characterized itself in the difference of the field profiles on the left and right side of the solenoid center. This asymmetry was studied extensively. The large steel flux return has a residual magnetization when no current is applied to the coil; this residual magnetization also breaks the expected symmetry. Annealing the iron did not cause an observable change. In light of the effects of the single wire discussed above, we feel that the asymmetry may also arise in part from one or a few shorted turns in the winding.

It is clear from these investigations that the winding of the full scale solenoid and the quality and commercial treatment of the magnet ion are crucial. In order to achieve the uniformity of 0.015%, finer corrections are necessary than those achieved with the prototype thus far, or than can be achieved by the methods described. Further study with prototype will be carried out to develop the techniques which will produce a field uniform to 0.015%.

2.6 Calculations of Atomic Substate Populations for Metastable Hydrogen

E. G. Adelberger, M. Z. Iqbal, and T. A. Trainor

In order to determine the best experimental configuration, and in order to interpret the results of the hydrogen parity violation experiment we have performed rather detailed calculations of hydrogen metastable-state populations and explored the dependence of these populations on the various experimental parameters. This report describes a computer code developed to perform the required calculations and some typical results.

The calculations are done in a straight-forward way by solving exactly the time-dependent Schrödinger equation for appropriate two-, three- and four-level problems. The eight states involved in the calculation are,

$$|\alpha+\rangle = 2s\left|\tfrac{1}{2}\tfrac{1}{2}\right\rangle$$

$$|\alpha o\rangle = 2s\left(\cos\theta\left|\tfrac{1}{2}-\tfrac{1}{2}\right\rangle + \sin\theta\left|-\tfrac{1}{2}\tfrac{1}{2}\right\rangle\right)$$

$$|\beta o\rangle = 2s\left(-\sin\theta\left|\tfrac{1}{2}-\tfrac{1}{2}\right\rangle + \cos\theta\left|-\tfrac{1}{2}\tfrac{1}{2}\right\rangle\right)$$

$$|\beta-\rangle = 2s\left|-\tfrac{1}{2}-\tfrac{1}{2}\right\rangle$$

$$|e+\rangle = 2P|\tfrac{1}{2}\tfrac{1}{2}\rangle$$
$$|eo\rangle = 2P(\cos\theta|\tfrac{1}{2}-\tfrac{1}{2}\rangle + \sin\theta|-\tfrac{1}{2}\tfrac{1}{2}\rangle)$$
$$|fo\rangle = 2P(-\sin\theta|\tfrac{1}{2}-\tfrac{1}{2}\rangle + \cos\theta|-\tfrac{1}{2}\tfrac{1}{2}\rangle)$$
$$|f-\rangle = 2P|-\tfrac{1}{2}-\tfrac{1}{2}\rangle$$

where M_J and M_I for each state vector $|M_J,M_I\rangle$ are magnetic quantum numbers for the electronic angular momentum $\vec{J}$ and nuclear spin $\vec{I}$ respectively. The hyperfine mixing angle θ is given by $\tan 2\theta = \Delta/2\mu B$ where Δ is the hyperfine splitting, $\mu = \mu_J + \mu_N$ and B is the axial magnetic field.

The Schrödinger equation

$$i\hbar\frac{\partial}{\partial t}|\psi\rangle = \left(Ho + e\vec{E}(t)\cdot\vec{r} + V_{PV}\right)\psi\rangle$$

has to be solved for the four important processes:

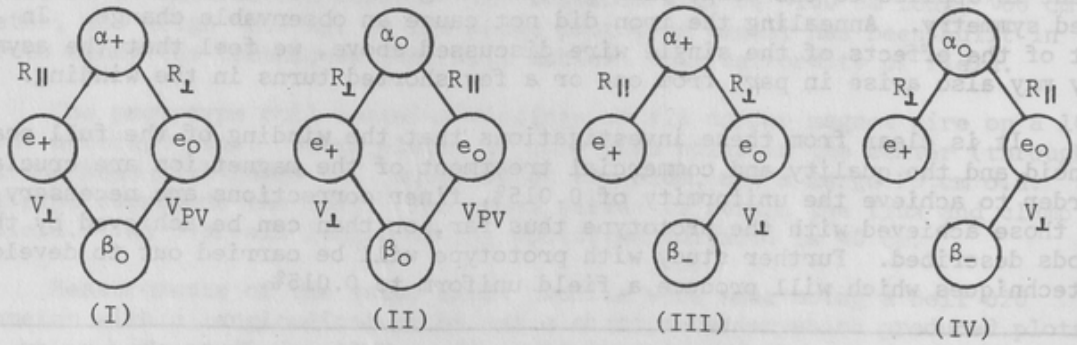

where $R_\parallel = E_\parallel \cos\omega t$ is an axial RF electric field.

$R_\perp = E_\perp \cos\omega t$ is a perpendicular RF electric field.

$V_\perp$ = Perpendicular static electric field.

Process II gives rise to a parity-violating resonance near 570 Gauss.

If the atomic state is written as

$$|\psi\rangle = a(t)e^{-iE_{\alpha+}t/\hbar}|\alpha+\rangle + b(t)e^{-iE_{\beta o}t/\hbar}|\beta o\rangle + c(t)e^{-iE_{e+}t/\hbar}|e+\rangle + d(t)e^{-iE_{eo}t/\hbar}|eo\rangle$$

and trial solutions are assumed of the type $a(t) = \sum_k A_k e^{-\mu_k t}$ for example, one gets a quartic equation in μ from the condition that the A_k be non zero. Solving this quartic equation and using initial values for the amplitudes (e.g., $a(o) = \sum_k A_k = a_o$, etc.) one can find a(t), b(t), c(t) and d(t) in terms of the initial values a_o, b_o, c_o, d_o, the electromagnetic field matrix elements, and the time spent in the fields.

The population derived from exact calculations for process I through IV are now combined as classical probabilities to obtain over-all α and β state populations as functions of axial magnetic field, etc. The justification for

this treatment involves arguments based on detailed calculations but, in general, depends on the distinguishability of the $\alpha - \beta$ processes I through IV, on the narrowness of the various three-level resonances under these conditions, and on the nature of the initial conditions.

In general,

$$|a|^2 = |a_I|^2 \times |a_{III}|^2 + |a_{II}|^2 \times |a_{IV}|^2$$

$$|b|^2 = |b_I|^2 + |b_{II}|^2 + |b_{III}|^2 + |b_{IV}|^2$$

where a_I indicates the α population calculated from process I, etc.

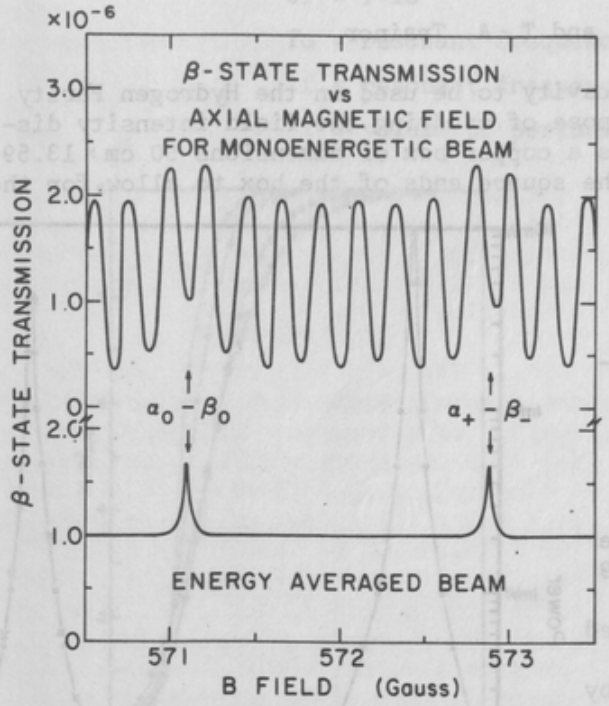

Fig. 2.6-1. The β state ($m_J = -1/2$) for monoenergetic beam (upper curve) and energy averaged beam (lower curve) vs. magnetic field evaluated at t=1.6 μs for r.f. = 1608 MH_z.

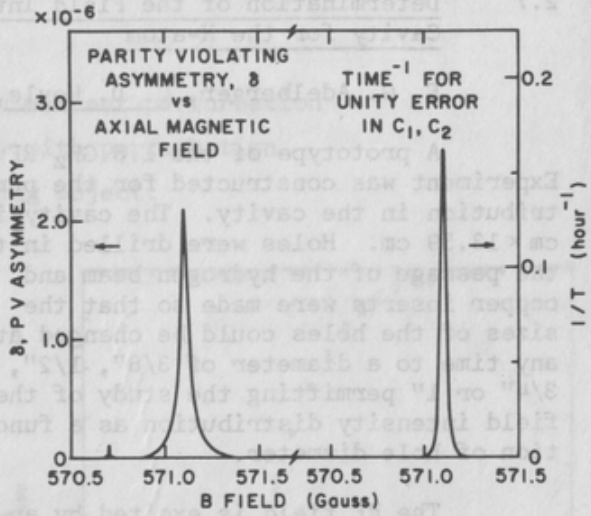

Fig. 2.6-2. The variation of parity violating asymmetry, δ (left curve) and inverse of integration time (right curve) vs. magnetic field evaluated at t=1.6 μs for r.f. = 1608 MH_z.

The calculated β population exhibits two very sharp resonances (FWHM ~0.1 Gauss), one showing a parity violating asymmetry (α_0-β_0, 571.1 Gauss), and one showing no asymmetry (α_+-β_-, 572.8 Gauss) when averaged over the energy spread of the hydrogen beam. For a monoenergetic beam, the resonances are superposed on high-frequency oscillations as shown in Fig. 2.6-1.

Since $|b_{II}|^2 \sim \frac{V_{PV} R_{II}}{R_\perp V_\perp}$,

the parity-violating asymmetry δ can be calculated for the (α_0-β_0) resonance as

$$\delta = \frac{|b^+|^2 - |b^-|^2}{|b^+|^2 + |b^-|^2}$$

where $|b^+|^2$ ($|b^-|^2$) is $|b|^2$ calculated for $V_\perp(-V_\perp)$. The Stark resonance $\alpha_+ - \beta_-$ gives a null result for δ. A rough estimate of the time required for the expected value of δ to be equal to one error bar can be found assuming 1. microamp equivalent of metastable hydrogen beam in each $2s_{1/2}$ state. The best values for the field strengths are found by maximizing δ and minimizing the integration time. Some typical results are shown in Fig. 2.6-2.

2.7 Determination of the Field Intensity Distribution of a Prototype RF Cavity for the H-atom

E. G. Adelberger, C. D. Hoyle, and T. A. Trainor

A prototype of the 1.6 GH_z RF cavity to be used in the Hydrogen Parity Experiment was constructed for the purpose of studying the field intensity distribution in the cavity. The cavity is a copper box of dimensions 50 cm × 13.59 cm × 13.59 cm. Holes were drilled in the square ends of the box to allow for the the passage of the hydrogen beam and copper inserts were made so that the sizes of the holes could be changed at any time to a diameter of 3/8", 1/2", 3/4" or 1" permitting the study of the field intensity distribution as a function of hole diameter.

The RF field is excited by applying an RF signal to a small copper loop (approximately 1 cm in diameter) inserted into the cavity through a hole in the center of one of the 50 cm × 13.9 cm sides. The plane of the loop is parallel to the beam so that the desired TM_{110} mode is excited. The resonant frequency of this mode was determined by the use of a smaller loop (approximately 1/2 cm in diameter). The power picked up by this smaller loop was measured along with the frequency of the input signal; maximum power was then observed at the resonant frequency. The frequencies corresponding to an observed power of one-half the maximum power were also measured to obtain the Q of the cavity. The observed power is plotted as a function of frequency in Fig. 2.7-1. The peak at 1567 MH_z corresponds to the desired mode whereas the peak at 1594 MH_z corresponds to the

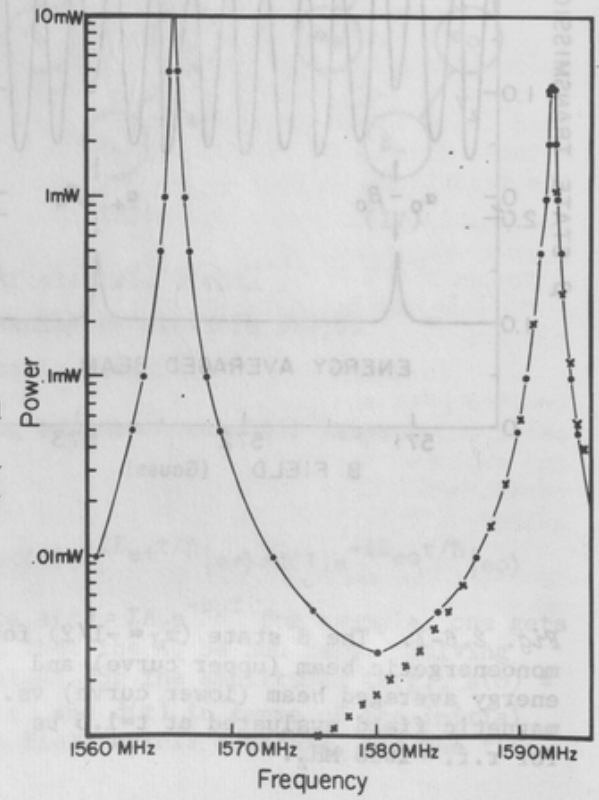

Fig. 2.7-1. Observed power vs. frequency.

degenerate TM_{111} and TE_{111} modes which are the modes nearest the desired mode. For the desired peak the Q = 3419 and for the 1594 MH_z peak the Q = 3317. The x's on the plot are theoretical points indicating that, when the cavity is driven at the desired frequency, the power picked up from exciting the next nearest modes is down by over four orders of magnitude.

The Slater perturbation method was used to measure the field intensity distribution. With this method the shift in resonant frequency is given by

$$\frac{\delta f}{fo} = \frac{-3\varepsilon o E^2 \tau}{4u}$$

where u = stored energy

E = electric field

δf = f-fo

fo = resonant frequency without perturbation

f = resonant frequency with perturbation

τ = volume of perturbing object.

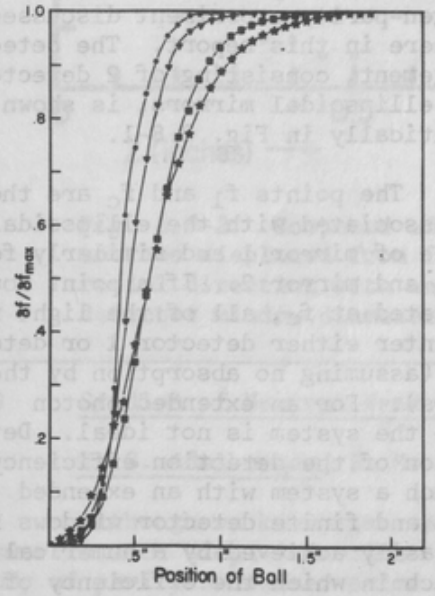

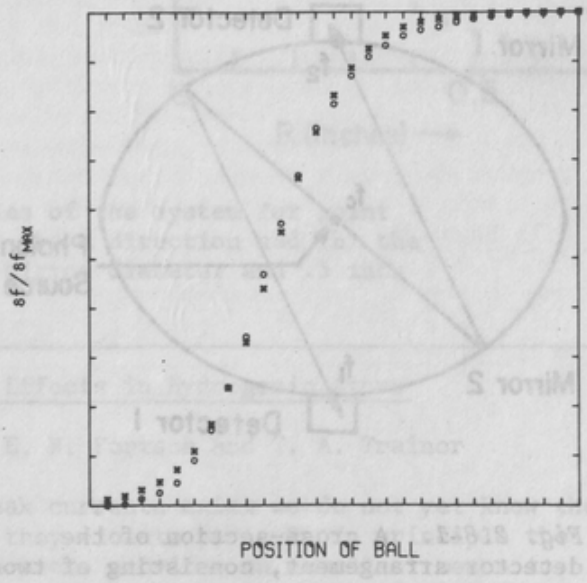

Fig. 2.7-2. Curve plotted with · is for a 3/8" hole, curve with ▼ is for a 1/2" hole, curve with ■ is for a 3/4' hole and curve with * is for a 1" hole.

Fig. 2.7-3. O represents data, X are computed values assuming $E^2 \propto \tanh(K(Z-Zo))$.

The perturbing object used was a 5/16" steel ball bearing. Figure 2.7-2 shows plots of $\delta f/_{\delta f\ max}$ for different hole diameters.

The effect of the finite size of the ball is unfolded from the data

by assuming a parameterized form for the field intensity distribution and numerically integrating the field intensity over the volume of the ball to obtain a frequency shift distribution. Figure 2.7-3 shows a fit to the 3/4" hole data using a parameterization of the form tanh $\left(K(Z-Zo)\right)$ where K and Zo are the adjustable parameter. Once determined, the reduced electric field intensities will permit the calculation of transition rates between states mixed by the electric field. Since the rates depend on the integral of the electric field, the shape of the electric field distribution is an important element in the calculation of the transition rates.

2.8 Computer Modeling of a Lyman-α Detector Geometry

K. J. Davis, E. N. Fortson, and T. A. Trainor

A familiar property of ellipsoidal mirrors is that light emitted from a point source located at one of the foci is reflected and brought to a point at at the other focus. A Lyman-α detector system exploiting this property is being studied for possible use in the hydrogen-parity experiment discussed elsewhere in this report. The detector arrangement, consisting of 2 detectors and 2 ellipsoidal mirrors, is shown schematically in Fig. 2.8-1.

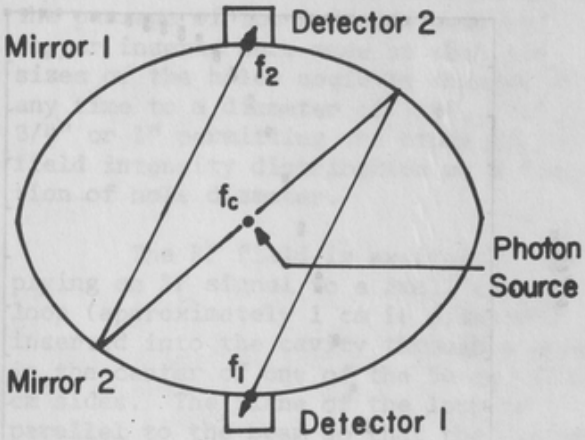

Fig. 2.8-1. **A cross-section of the detector arrangement, consisting of two ellipsoidal mirrors and two detectors with a Lyman-α source located at f_c.**

The points f_1 and f_c are the foci associated with the ellipsoidal surface of mirror 1 and similarly for f_2, f_c and mirror 2. If a point source is located at f_c, all of the light rays will enter either detector 1 or detector 2 (assuming no absorption by the mirrors). For an extended photon source the system is not ideal. Determination of the detection efficiency for such a system with an extended source and finite detector windows is most easily achieved by a numerical approach in which the efficiency of the system for point sources displaced from f_c is determined. Such an approach permits the generation of surfaces of equal efficiency about f_c. These are useful in the design of the metastable hydrogen quenching region to be located at f_c.

A code has been written which computes the geometrical efficiency of the system for points displaced from f_c. Some computed efficiencies for displacements (Z) along the axis of azimuthal symmetry (passing through f_1 and f_2) and for displacements (R) in the radial direction are shown in Fig. 2.8-2. The code will be extended to account for absorption by the mirrors and detector efficiency, which varies with angle of incidence.

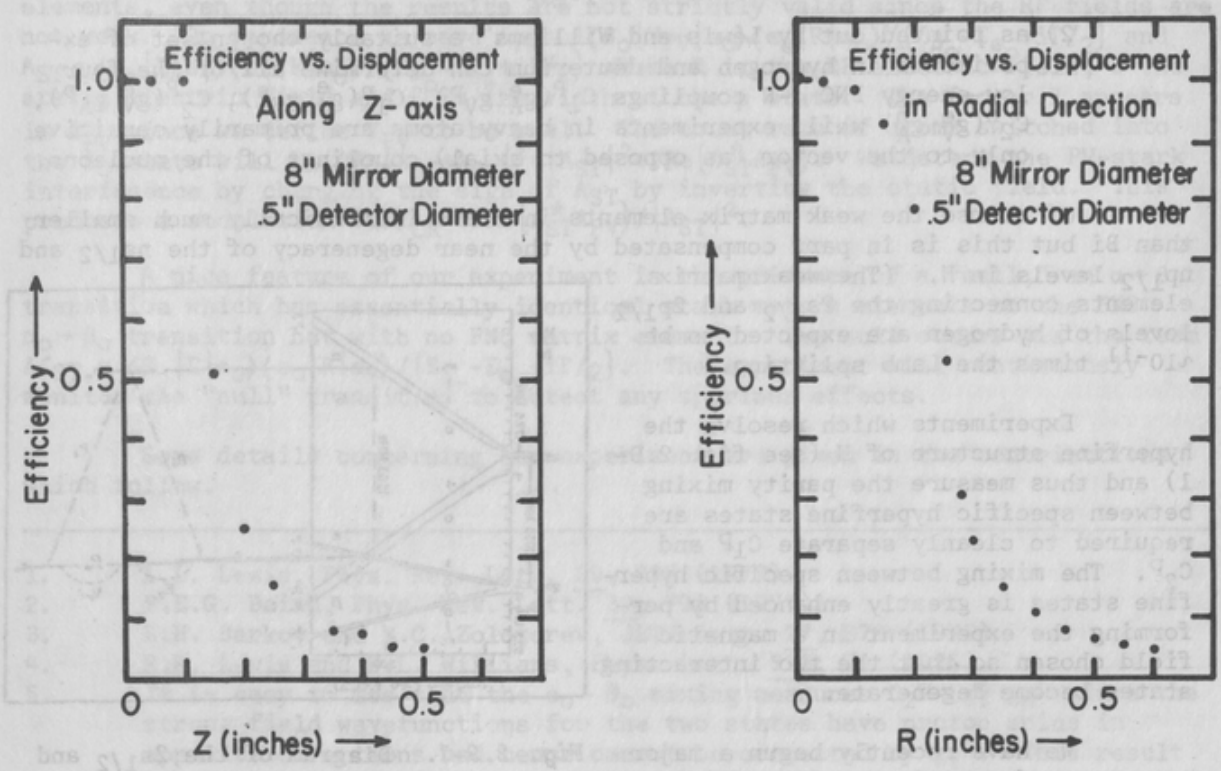

Fig. 2.8-2. Computed efficiencies of the system for point sources displaced from f_c in (a) the z direction and (b) the radial direction with an 8 inch mirror diameter and .5 inch detector window diameter.

2.9 Studies of Neutral Weak Current Effects in Hydrogenic Atoms

E. G. Adelberger, E. M. Henley, E. N. Fortson and T. A. Trainor

Although we know that neutral weak currents exist we do not yet know the answer to such simple questions as: do they violate parity? In principle the study of parity nonconservation (PNC) in atoms provides an excellent means to answer this question since atomic PNC is a semileptonic (and therefore caculable) process. Due to the high electron momentum and the coherence of the isoscalar, Lorentz-vector weak charge one expects the experimentally observable effects to be largest in heavy atoms. The first precise experiments have been done done in Bismuth. Two groups (at Seattle[1] and Oxford[2]) find no effect at a level considerably smaller than predictions based in the Weinberg-Salam model while a group at Novosibirsk[3] claims to have a result consistent with Weinberg-Salam. However the situation in Bismuth is resolved, it is important to study PNC in the simplest atom of all - the one-electron system. This follows from two considerations:

1) there are no uncertainties in the atomic structure which may obscure

the basic weak interaction physics

2) as pointed out by Lewis and Williams[4] a suitably chosen set of experiments in hydrogen and deuterium can determine all of the four low-energy PNC d-N couplings $C_1^P(g_A^e\, g_V^P)$, $C_1^n(g_A^e\, g_V^P)$, $C_2^P(g_V^e\, g_A^P)$, $C_2^n(g_V^e\, g_A^n)$ while experiments in heavy atoms are primarily sensitive only to the vector (as opposed to axial) couplings of the nucleons.

Of course the weak matrix elements in H are intrinsically much smaller than Bi but this is in part compensated by the near degeneracy of the $ns_{1/2}$ and $np_{1/2}$ levels in H. (The weak matrix elements connecting the $2s_{1/2}$ and $2p_{1/2}$ levels of hydrogen are expected to be $\sim 10^{-11}$ times the Lamb splitting.)

Experiments which resolve the hyperfine structure of H (see fig. 2.9-1) and thus measure the parity mixing between specific hyperfine states are required to cleanly separate C_1^P and C_2^P. The mixing between specific hyperfine states is greatly enhanced by performing the experiment in a magnetic field chosen so that the two interacting states become degenerate.

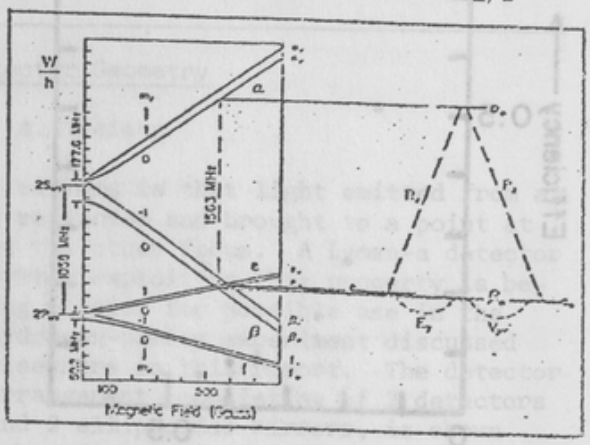

Fig. 2.9-1. **Diagram of the $2s_{1/2}$ and $2p_{1/2}$ states of hydrogen.**

We have recently begun a major program to detect $2s_{1/2} - 2p_{1/2}$ mixing in hydrogen and deuterium atoms. We will begin by trying to measure the $\beta_o - e_o$ mixing which is sensitive only to C_2^P.[5] This requires a magnetic field of $\sim$570 gauss. The apparatus is constructed so that we can attain a magnetic field of $\sim$1200 gauss which will be needed later to study the $\beta_o - f_o$ and $\beta_- - f_-$ mixings which are sensitive to both C_1^P and C_2^P.

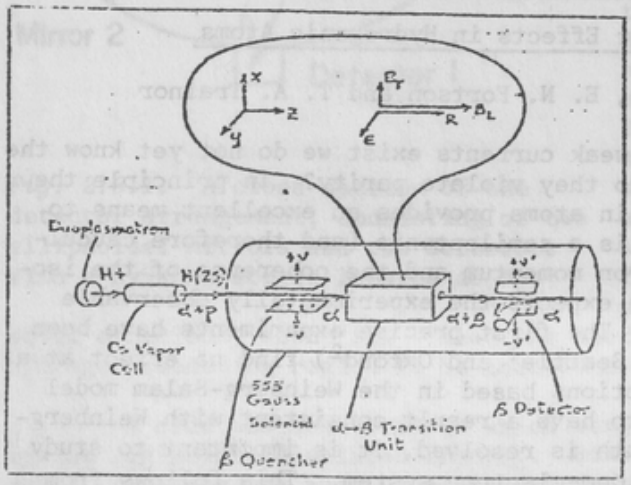

Fig. 2.9-2. **Schematic representation of the Seattle H atom experiment.**

The basic idea of our experiment can be understood using the schematic diagram in Fig. 2.9-2. We prepare a beam of H atoms in the states α_o and then make transitions from $\alpha_o \to \beta_o$. The transitions occur via two mechanisms and we detect the interference between the two paths. In the first (or PV) path an E1 microwave field in z direction connects the α_o state to the e_o parity impurity in β_o level. In the second (or Stark) path an E1 microwave field along $\hat{x}$ connects the α_o level to the piece of the e_+ level which is mixed into the β_o state by an external E field along $\hat{y}$. One can get some insight from perturbation theory expressions for the matrix

elements, even though the results are not strictly valid since the RF fields are not weak. On resonance we have $A_{PV} = i\langle\beta_o|V_{PV}|e_o\rangle\langle e_o|R|\alpha_o\rangle/(E_{\beta_o}-E_{e_o}+i\Gamma/2)$ and $A_{ST} = \langle\beta_o|E|e_+\rangle\langle e_+|R|\alpha_o\rangle/(E_{\beta_o}-E_{e_+}+i\Gamma/2)$ where R is the RF electric field, E the static electric field and Γ^o is the width of the p state. The factor i appears in A_{PV} since we define V_{PV} to be real. The count rate of atoms switched into the β_o state will be $CR \propto |A_{ST}+A_{PV}|^2 \approx |A_{ST}|^2 + 2Re(A^*_{ST}A_{PV})$. We detect the PV-stark interference by changing the sign of A_{ST} by inverting the static field. This produces a modulation $\delta CR/_{CR} = \pm 2Re(A^*_{ST}A_{PV})/|A_{ST}|^2$.

A nice feature of our experiment is the presence of a "null," an $\alpha \to \beta$ transition which has essentially identical stark matrix elements to the PNC $\alpha_o \to \beta_o$ transition but with no PNC matrix element. The null occurs via the term $A'_{ST} = \langle\beta_-|E|e_o\rangle\langle e_o|R|\alpha_+\rangle/(E_{\beta_-}-E_{e_o}+i\Gamma/2)$. The experiment will continuously monitor the "null" transition to detect any spurious effects.

Some details concerning our experiment are given in the contributions which follow.

---

1. L.L. Lewis, Phys. Rev. Lett. 39, 795 (1977).
2. P.E.G. Baird, Phys. Rev. Lett. 39, 798 (1977).
3. L.H. Barkov and M.C. Zolotorev, JETP Lett. 27, 379 (1978).
4. R.R. Lewis and W.L. Williams, Phys. Lett. 59B, 70 (1975).
5. It is easy to see that the $e_o - \beta_o$ mixing measures $C_2^P = g_V^e\, g_A^P$ since the strong field wavefunctions for the two states have proton spins in opposite directions and hence cannot be connected by g_V^P. This result is not restricted to strong field wavefunctions, but holds even when realistic wavefunctions are used.

2.10 Parity Mixing in ^{21}Ne I: Motivation, Importance of Mixing Ratios, and the $1/2^- \to 5/2^+$ Mixing Ratio Measurement

K. A. Snover, R. Von Lintig, P. Ikossi, and E. K. Warburton†

A. Motivation

A particularly interesting system for studying nuclear parity mixing occurs at $E_x = 2.8$ MeV in ^{21}Ne where a $J^\pi = 1/2^+$ and a $J^\pi = 1/2^-$ level are separated by only 6.7±0.7 keV (see ref. 1 and Fig. 2.10-1). A measurement in this system would be particularly interesting for two reasons which we discuss more fully below: First, a measurement of parity mixing in ^{21}Ne would be the first in an odd N, even Z nucleus where the parity nonconserving (PNC) matrix element connecting two levels of opposite parity can be inferred directly from a measurement of the pseudoscalar observable; and second, the ^{21}Ne system is unusually sensitive - a very small PNC matrix element produces relatively large experimental effects.

All positive measurements of PNC effects in odd A = N+Z nuclei have been in odd Z nuclei. In the single particle approximation the PNC effects in all these odd Z nuclei measure nearly the same linear combination of the basic PNC N-N amplitudes. By studying an odd N nucleus one probes a different linear

combination. For example, consider a schematic model where the J = 1/2 doublet in ^{19}F (odd Z) consists of a proton hole in the T=0 ^{20}Ne core while the similar levels in ^{21}Ne (odd N) consist mainly of a nucleon hole in the mass = 22 T=1 core. From simple isospin considerations the ratio of isovector to isoscalar PNC mixing in ^{21}Ne will be -1/3 that of ^{19}F. For ^{21}Ne parentage to $^{22}Na(T=0)\otimes$proton hole the corresponding factor is +1; inclusion of this parentage further reduces the relative importance of isovector PNC mixing in ^{21}Ne compared to ^{19}F (this ratio calculated by Millener[1] including all parentage is ≈ -1/1.7). Thus experimental and theoretical results in ^{21}Ne could be combined with ^{19}F[2] (and ^{18}F[3]) to yield the isoscalar and isovector components of the PNC nucleon-nucleon force. Then it will be possible to determine whether or not ΔT=1 PNC nuclear transitions are enhanced by neutral weak currents as has been predicted by calculations[4] based on the Weinberg-Salam model.

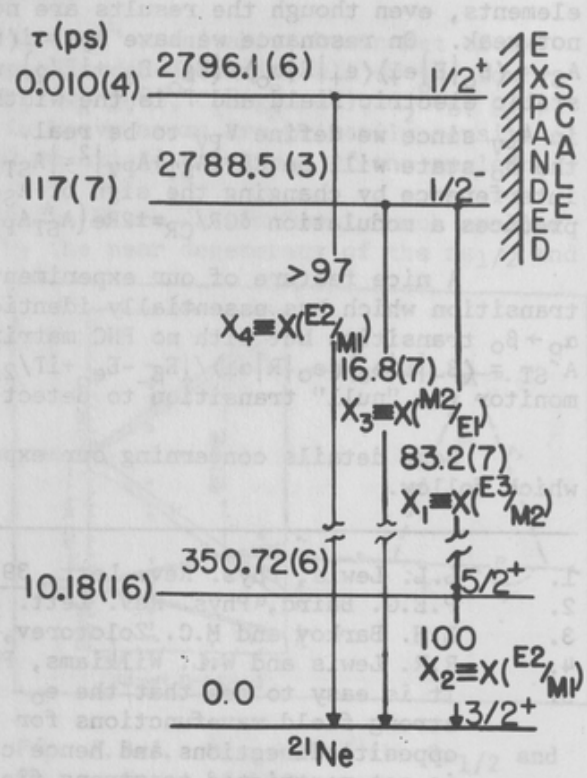

Fig. 2.10-1. **Energy levels, lifetimes and mixing ratios for the ^{21}Ne levels relevant to this discussion.**

It is easy to understand the great sensitivity of the ^{21}Ne system. The parity impurities in the 2.789 MeV $1/2^-$ and 2.796 MeV $1/2^+$ levels (see Fig. 2.10-1) are well approximated by simple two-level mixing:

$$|2.789\rangle = |-\rangle + \varepsilon|+\rangle$$
$$|2.796\rangle = |+\rangle - \varepsilon|-\rangle$$

where $\varepsilon = \langle +|H^{PNC}|-\rangle/\Delta E$

The parity mixing produces a circular polarization, P_γ of the gamma rays deexciting the two states which, to first order in the $M2/_{E1}$ and $E2/_{M1}$ mixing ratios of the $1/2^\pm \rightarrow$ g.s. decays is given by

$$P_\gamma(2.789) = 2\varepsilon\langle M1\rangle/\langle E1\rangle \quad \text{and} \quad P_\gamma(2.796) = -2\varepsilon\langle E1\rangle\langle M1\rangle.$$

The dipole matrix elements $\langle M1\rangle$ and $\langle E1\rangle$ can be deduced from the known lifetimes and branching ratios (we assume the 2.789 MeV gamma ray is predominantly E1). The decays $2.789 \rightarrow 0.0$ are highly retarded ($\tau_{\gamma_0} = \tau/B.R. = 696\pm51$ ps [see ref. 1]) while the M1 decays $2.797 \rightarrow 0.0$ are fast ($\tau_{\gamma_0} = 10\pm4$ fs).[5] This leads to a large expected value for $P_\gamma(2.789)$ and a negligible $P_\gamma(2.796)$. The result is $P_\gamma(2.789) = 9.5\pm10^{-2}eV^{-1}\langle +|H^{PNC}|-\rangle$ using the theoretical lifeline of 5.3 fs for the $1/2^+$ state. Thus if $\langle H^{PNC}\rangle$ is comparable to the value obtained in ref. 2 for ^{19}F (0.9 eV) one obtains $P_\gamma(2.789) = 8.6\%$ in ^{21}Ne compared to the asymmetry $A_\gamma = -(18\pm9)\times10^{-5}$ observed[2] in ^{19}F.

B. Importance of Mixing Ratios

Our first attempts to observe parity violation in ^{21}Ne involve circular polarization measurements (see Sec. 2.1). However, the sign of a measured P_γ (2.789) can be turned into a sign for the parity mixing amplitude (which is necessary for the isospin decomposition discussed above) only if the sign of $\langle M1\rangle/\langle E1\rangle$ is known. The sign of the strong $\langle M1\rangle$ matrix element may be confidently taken from theory; however the sign of the very weak $\langle E1\rangle$ matrix element may not be theoretically reliable. A measurement of the M2/E1 $1/2^- \rightarrow$ g.s. mixing ratio χ_3 would provide an opportunity to tie the sign of $\langle E1\rangle$ to the theoretical $\langle M2\rangle$ sign, which may be more reliable.

If the $1/2^\pm$ parity mixing is small, then the alternative technique of measuring parity mixing by detecting an asymmetry in the $1/2^- \rightarrow$ g.s. decay of a polarized initial state may be competitive, if a favorable reaction with a reasonable polarization transfer can be found. However, the γ-asymmetry is sensitive to the mixing ratios χ_3 and χ_4 since the latter enter linearly in this case. χ_4 is expected to be small, but χ_3 could even cause the γ-asymmetry for the $1/2^- \rightarrow$ g.s. decay to vanish independent of the parity mixing.

The best way to determine χ_3 would appear to be the difficult experiment of measuring the ratio of circular polarizations for the $1/2^- \rightarrow 3/2^+$ and $1/2^- \rightarrow 5/2^+$ transitions following formation with a polarized beam, provided the E3/M2 mixing ratio χ_1 of the latter transition is known. In addition, the circular polarization of the $1/2^- \rightarrow 5/2^+$ decay would be the best indicator of the degree of $1/2^-$ polarization (induced by a reaction with a polarized beam) if the mixing ratio χ_1 is known. Knowledge of the $1/2^-$ polarization would also be necessary for a quantitative interpretation of a γ-asymmetry measurement.

C. Measurement of the E3/M2 Mixing Ratio χ_1 of the $1/2^- \rightarrow 5/2^+$ Transition

Here we describe the results of angular correlation measurements for the $1/2^- \gamma_2 \rightarrow 5/2^+ \gamma_1 \rightarrow 3/2^+$ γ-γ cascade ($E_{\gamma_1} = 2.44$ MeV and $E_{\gamma_2} = 0.35$ MeV). The $1/2^-$ level was populated in the ^{18}O(α,n)^{21}Ne reaction at $E_\alpha = 5.10$ MeV. This α-energy corresponds to a maximum excitation energy of 3.47 MeV in ^{21}Ne, so that the only levels above the $1/2^-$ which were populated were the $1/2^+$(2.796) and $9/2^+$(2.866) levels. A 70 nA α^+ beam was produced by the University of Washington FN Tandem Van de Graaff and stopped in a tantalum target of thickness 0.012 μm, with an oxidized ^{18}O surface layer of thickness ∿220 μg/cm^2. A 4.45 cm ϕ by 5.08 cm cylindrical NaI crystal mounted on an RCA 8575 phototube was used to detect the 350 keV γ-rays, while an ORTEC coaxial Ge(Li) detector of 15% efficiency (relative to a 3"×3" NaI) was used to detect γ-rays between the energies of 0.75 and 3.0 MeV. The front face of the NaI was located at 8.3 cm from the target, and the front face of the Ge(Li) at 8.9 cm from the target. The NaI was fixed at an angle of -135° with respect to the beam axis, while the coplanar Ge(Li) detector was set at angles of 45°, 15°, -15° and -45° to the beam axis, corresponding to the relative γ-γ correlation angles $\theta = 180°$, 150°, 120° and 90°. This arrangement insured that the Ge(Li) detector would see the same beam-related background (and the same Doppler-shifted background γ-rays) for $\phi = 180°$ and 90°, the most important correlation angles.

Signals corresponding to fast coincidences between the two detectors

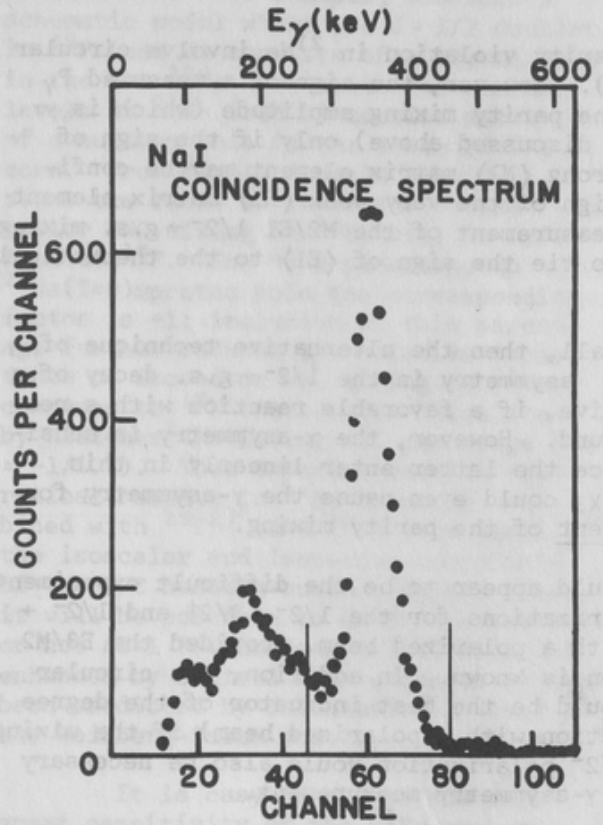

Fig. 2.10-2. NaI coincidence spectrum corresponding to a TAC real window and a window about the 2.44 MeV Ge(Li) peak. The peak window is indicated by vertical lines.

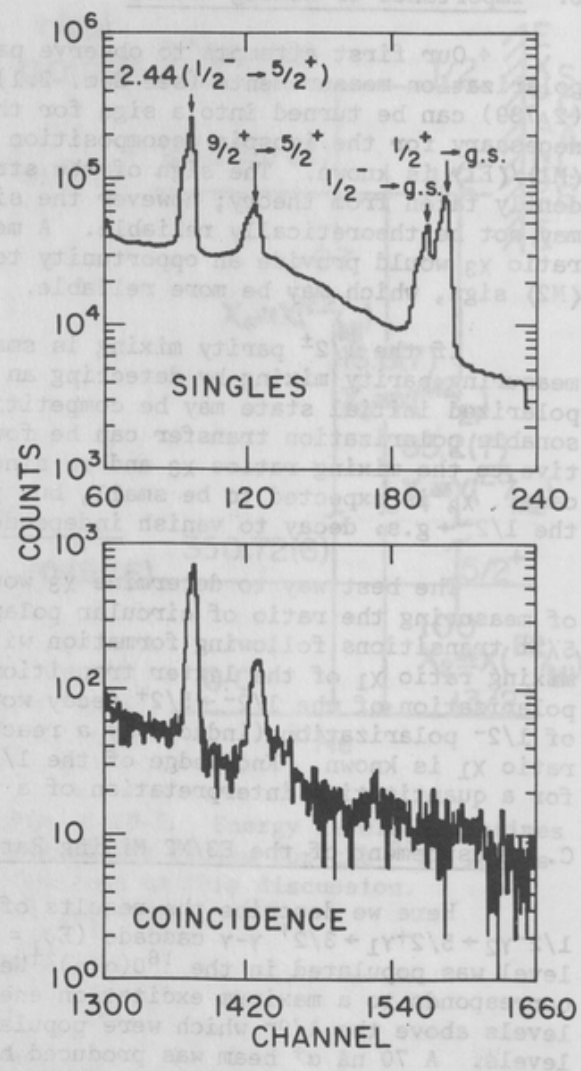

Fig. 2.10-3. Coincidence (a) and singles (b) Ge(Li) γ-ray spectra for 2.2 $<E_\gamma<3.0$ MeV at $\theta = 150°$ ($\theta_{beam}=15°$) from the $^{18}O(\alpha,n\gamma)^{21}Ne$ reaction at $E_\gamma =$ 5.1 MeV. Background windows are indicated by the vertical lines.

were produced in a time-to-amplitude converter (TAC) using leading edge timing for the short rise time NaI signals and extrapolated zero strobe timing for the Ge(Li). Three-parameter coincidence events (parameters E_γ[NaI], E_γ [Ge(Li)] and TAC amplitude) were recorded in a computer, along with Ge(Li) singles recorded in a separate analyzer. A gain stabilizer centered on the 350-keV γ-ray was used with the NaI detector.

Coincidence data analysis was performed in 2 stages. First, NaI spectra were generated corresponding to a window set on the 2.44 peak in the Ge(Li) spectrum and on the TAC peak; an example is shown in Fig. 2.10-2. These spectra are dominated by the 350 keV line, with no evidence for other significant contributions. Centroids calculated from these spectra were used to compute small residual gain correction factors (which differed from unity by only ±0.3%) which

were applied to the results discussed below. Second, Ge(Li) difference spectra were generated corresponding to a window centered on the 350 keV line in the NaI spectrum and (real + random) minus (random) TAC windows (the random correction was ∿3%) - an example is shown in Fig. 2.10-3(a). A substantial real continuum background is apparent in this spectrum, along with some apparent real contribution from the 2.8 → 0 γ-decays presumably arising from n-γ coincidences where the neutron was detected in the NaI. Coincidence yields for the cascade of interest were then extracted from these spectra by summing counts above a symmetric background determined from regions above and below the centroid of the 2.44 Ge(Li) peak.

Care was taken in the choice of background windows here and in the singles analysis to minimize the effect of a possible $1/2^+ \rightarrow 5/2^+$ branch. There is no evidence from the present data for such a branch. A proper accounting of the uncertainty in background shape in the region where such a peak is expected leads to an upper limit of 3% for this decay relative to the $1/2^+ \rightarrow$ g.s. decay, which is similar to that obtained previously.

The Ge(Li) singles spectra were analyzed with a similar background subtraction to determine the 2.44 and 2.80 (combined $1/2^+$ and $1/2^- \rightarrow$ g.s.) γ-yields [see Fig. 3(b)]. Since these peaks arise from decays of J=1/2 initial states, their intensities should be isotropic. However, small systematic variations as a function of angle and fluctuating variations independent of angle were present in these yields when normalized to total integrated beam current. These variations could arise from a small geometrical misalignment, and an inaccuracy in beam-current integration, respectively. Since such variations would affect equally the singles and coincidence yields, our best values for the normalized relative coincidence yield W(θ) are given by the ratio of measured coincidence counts to 2.44 MeV singles counts. This ratio, which includes small (≤1%) relative dead time corrections, is shown plotted against $P_2(\cos\theta)$ in Fig. 2.10-4.

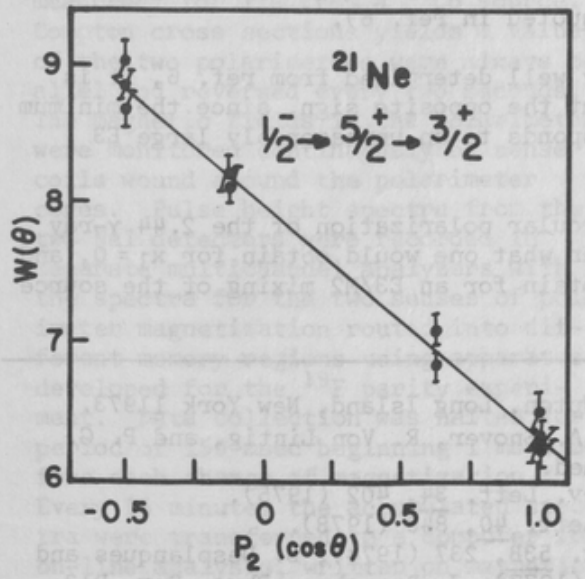

Fig. 2.10-4. Results for the ^{21}Ne $1/2^- \rightarrow 5/2^+ \rightarrow 3/2^+$ relative γ-γ correlation W(θ) versus $P_2(\cos\theta)$. The solid line is the best fit allowing only A_0 and a_2 to vary and is indistinguishable from a fit in which a_4 was also free to vary.

A fit to all the data points in Fig. 2.10-4 yield $a_2 = -0.2127 \pm 0.0088$ and $a_4 = +0.004 \pm 0.011$, with $\chi^2 = 1.3$. A fit with a_4 constrained to be zero produces the straight line shown in Fig. 2.10-4, with $a_2 = -0.2106 \pm 0.0065$ and $\chi^2 = 1.2$. A fit excluding the 120° and 150° data gives essentially the same a_2. A fit to the 90° and 180° coincidence yield normalized to the <u>average</u> 2.44 singles yield at each angle gives $a_2 = -0.2091 \pm 0.0070$.

Various other analyses were performed to investigate effects of systematic errors in the analysis. Different types of coincidence background subtraction were performed; normalizations were also calculated relative to the 2.80 singles yields, which were found to be less sensitive to background subtraction than the 2.44 singles yields. From fits to all of these results with a_4 constrained to be zero we arrive at a best value of $a_2 = -0.2130 \pm 0.0076$, where the above error contains a contribution of ± 0.004 folded with the statistical error to represent the variation observed from the different analyses. Fits in which a_4 was allowed to vary produced values which ranged over $\pm 1\sigma$ ($\sigma = 0.011$) for the different analyses; hence our best value is $a_4 = 0.00 \pm 0.015$. The χ^2 for all of these fits were $\lesssim 1.3$. Attenuation coefficients were calculated from the known geometry of the detectors; the result is $Q_2(\mathrm{NaI})Q_2(\mathrm{GeLi}) = 0.931$ and $Q_4(\mathrm{NaI})Q_4(\mathrm{GeLi}) = 0.79$. Hence from

$$a_2 = (-0.2717 \pm 0.0046) Q_2[\mathrm{NaI}] Q_2[\mathrm{Ge(Li)}] f_2(x_1)$$

and

$$f_2(x_1) = [1 + \sqrt{2} x_1 + 1.5 x_1^2]/(1 + x_1^2)$$

we find $f_2(x_1) = 0.842 \pm 0.033$ and x_1 -0.12 ± 0.03 (the other solution is $x_1 = -2.03 \pm 0.14$ which is ruled out since it would correspond to an E3 strength of ~ 870 W.U.). The expected a_4 based on the above x_1 is well within the experimental uncertainty of the measured value. This value of x_1 is also in agreement with an earlier, less accurate result[6] of $x_1 = 0.0 \pm 0.14$ (the corrected uncertainty quoted here is based on the measured a_2 quoted in ref. 6).

Although the sign of x_2 is fairly well determined from ref. 6, it is useful to note that the above a_2 rules out the opposite sign, since the minimum x_1 solution for $x_2 = -0.0739 \pm 0.0048$ corresponds to an unreasonably large E3 strength of 350 ± 100 W.U.

This value of x_1 enhances the circular polarization of the 2.44 γ-ray for a given $1/2^-$ polarization by $\sim 50\%$ over what one would obtain for $x_1 = 0$, and by a factor of ~ 3 over which one would obtain for an E3/M2 mixing of the source magnitude as above, but opposite sign.

---

† Brookhaven National Laboratory, Upton, Long Island, New York 11973.

1. D.J. Millener, E.K. Warburton, K.A. Snover, R. Von Lintig, and P. G. Ikossi, Phys. Rev., to be published.
2. E.G. Adelberger, *et al.*, Phys. Rev. Lett. 34, 402 (1975).
3. C.A. Barnes, *et al.*, Phys. Rev. Lett. 40, 840 (1978).
4. M. Gari and J.H. Reid, Phys. Lett. 53B, 237 (1974); B. Desplanques and J. Micheli, Phys. Lett. 68B, 339 (1977); J. Donoghue, Phys. Rev. D13, 2064 (1976); DIS, 184 (1977).
5. H. Grawe *et al.*, Zeitschrift für Physik A280, 271 (1977).
6. R.M. Freeman, F. Haas, B. Heusch, and A. Gallmann, Nucl. Phys. A261, 471 (1976).

2.11 Parity Mixing in ^{21}Ne II: Measurement of the Parity Nonconserving Circular Polarization of the 2.789 MeV γ-Ray

E. G. Adelberger, C. A. Barnes†, E. D. Earle††, A. B. McDonald††, K. A. Snover, H. E. Swanson, T. A. Trainor, and R. Von Lintig

We populated the 2.789 MeV, $1/2^-$ level of ^{21}Ne with the ^{21}Ne(p,p') reaction at $E_p = 4.08$ MeV, near the peak of a 30 keV wide resonance in the yield of γ's from this level. In preliminary measurements at Chalk River[1] this reaction was determined to be significantly more favorable than either the ^{18}O(α,n)^{13} or ^{20}Ne(d,p) reaction. The 4.8 mm long gas target contained 1.25 atmospheres of ^{21}Ne Gas (94.5% enriched) between a 2.5 μm molybdenum foil and a water-cooled platinum beam stop. A 7 μA proton beam from the University of Washington FN tandem was diffused over a 2 mm dia spot by passing it through a 50 μgm/cm^2 carbon foil 2 meters before the target. The circular polarization was analyzed in two transmission-type gamma-ray polarimeters developed for a previous measurement in ^{18}F.[2] The lead shielding was modified slightly to accommodate two magnetically-shielded and gain stabilized 7.5 cm × 7.5 cm NaI(Tℓ) detectors. The polarimeters were carefully designed so that gamma rays from the target, other than those passing through the Fe core are strongly attenuated by heavy metal shielding (ρ=17). The analyzing power (η) of the polarimeters was previously measured[2] for γ's from a ^{60}Co source. An extrapolation to 2.8 MeV using known Compton cross sections yields a value of $\eta = (3.41 \pm 0.10) \times 10^{-2}$. The magnetizations of the two polarimeters were always parallel and reversed every two seconds. The magnetic fields in the polarimeters were monitored continuously by sense coils wound around the polarimeter cores. Pulse height spectra from the two NaI detectors were recorded in separate multichannel analyzers with the spectra for the two senses of polarimeter magnetization routed into different memory regions using apparatus developed for the ^{19}F parity experiment. Data collection was halted for a period of 150 msec beginning 1 msec before each change of magnetization. Every 15 minutes the accumulated spectra were transferred to a computer for on-line analysis, written on magnetic tape, and the analyzer memories were cleared. Twice each day the current connections to the polarimeter coils were reversed so that the sense of polarization was changed relative to the remainder of the electronic circuitry. Data were accumulated for a total integrated charge of 0.5 Coulombs.

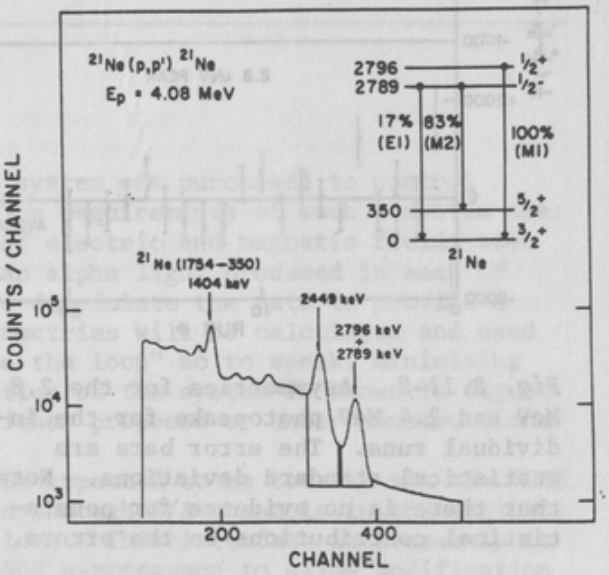

Fig. 2.11-1. Spectrum of γ-rays observed in one of the 3" × 3" NaI detectors.

A typical γ-ray spectrum is shown in Fig. 2.11-1. The photopeak at 2.8 MeV from the unresolved $1/2^- \rightarrow 3/2^+$ and $1/2^+ \rightarrow 3/2^+$ transitions is clearly

resolved from the peak at 2.4 MeV from the $1/2^- \rightarrow 5/2^+$ transition. The small, slowly-varying background is due to high-energy-neutron-capture gamma rays. For the 2.8 and 2.4 MeV photopeak regions indicated on the figure, asymmetries

$$A = \frac{1}{4}\left(\frac{R_-L_+}{R_+L_-} - 1\right)$$

were calculated, where R_-, R_+, L_-, L_+ denote the excess counts above the smooth background for the right and left detectors in the two magnetization states. Very small gain differences ($\lesssim$0.05%) were observed in the spectra for the two magnetization states. Therefore, the centroids of the 2.4 and 1.4 MeV peaks $\left({}^{21}Ne(1.746) \rightarrow {}^{21}Ne(0.350)\right)$ were used to determine an energy calibration for each spectrum from which identical energy windows were selected for the determination of R_+, R_-, etc.

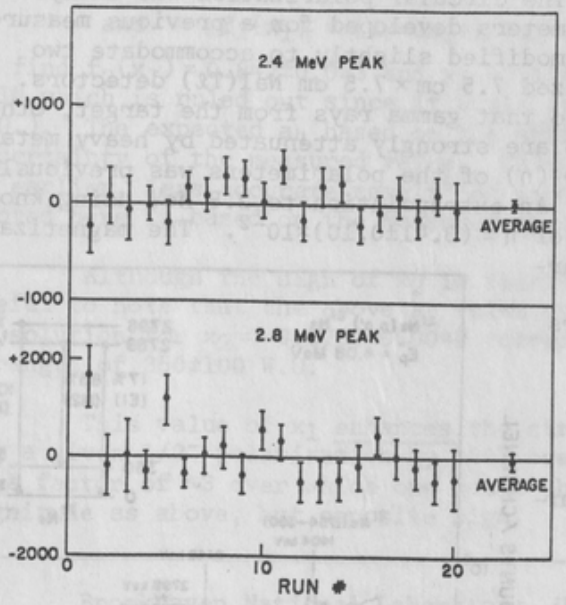

Fig. 2.11-2. **Asymmetries for the 2.8 MeV and 2.4 MeV photopeaks for the individual runs. The error bars are statistical standard deviations. Note that there is no evidence for nonstatistical contributions to the errors.**

The asymmetries measured for the 2.4 MeV and 2.8 MeV peaks for various 12 hour periods are plotted in Fig. 2.11-2. Mean values of $A = (.24 \pm .44)\times10^{-4}$ and $(-.17\pm.90)\times10^{-4}$ were obtained for the two peaks with reduced χ^2 of 0.9 and 1.3 respectively. Asymmetries evaluated for background regions at energies above and below these peaks were found to be consistant with zero within statistical errors. The null asymmetry obtained for the 2.4 MeV peak has a statistical accuracy significantly smaller than the asymmetry of the 2.8 MeV peak, confirming the abasence of systematic errors at this precision. The asymmetry of the 2.8 MeV photopeak, A, is related to $P_\gamma(2.789)$ by $P_\gamma(2.789) = A/(f\eta)$ where f (0.52) is the fraction of the photopeak due to the $1/2^- \rightarrow 3/2^+$ transition determined from the yield of 2.4 MeV γ-rays and the known branching ratio. Our measurement yields a value of $P_\gamma(2.789) = (-9\pm51)\times10^{-4}$ for the circular polarization of the 2.789 MeV γ-ray. This corresponds to a parity violating matrix element $|\langle H_{pv}\rangle| = .009\pm.054$ eV between the 2.80 J=1/2 levels, which is considerably smaller than the measured parity mixing[3] in the ${}^{19}F$ J-1/2 doublet.

In contrast to ${}^{19}F$ and ${}^{18}F$, no theoretical calculations of parity mixing in ${}^{21}Ne$ have been published. However, Millener[4] has made a preliminary prediction of $\langle|H_{PNC}|\rangle = 0.13$ eV using shell model wavefunctions with an SU(3) basis and an effective one-body PNC potential. Brandenburg *et al.*[5] have used two-body PNC matrix elements determined for ρ and π exchange in the factorization approximation with various shell model wavefunctions to calculate Cabibbo model PNC

matrix elements ranging from 0.02 to 0.19 eV. In all of these calculations, a strong ($f_\pi/f_{\pi_c} \geq 10$) neutral current enhancement would lead to values of $\langle H_{PNC} \rangle$ at least a factor of 2 bigger than our present upper limit. Calculations using a two-body potential in a more complete shell model basis are in progress.[4,5]

We would like to thank Prof. B. H. J. McKellar for pointing out the interest in the ^{21}Ne system and further stimulating our interest by presenting us with a very large, if evanescent, predicted effect.

---

† Kellogg Lab, California Institute of Technology, Pasadena, California 91125.

†† Chalk River Nuclear Laboratories, Atomic Energy of Canada Ltd., Chalk River, Ontario K0 J1 J0, Canada.

1. A.B. McDonald, E.D. Earle, and M.A. Lone, BAPS 23, 520 (1978).
2. C.A. Barnes, M.M. Lowry, J.M. Davidson, R.G. Marrs, F.B. Morinigo, B. Chang, E.G. Adelberger, and H.E. Swanson, Phys. Rev. Lett. 40, 840 (1978).
3. E.G. Adelberger, H.E. Swanson, M.D. Cooper, J.W. Tape, and T.A. Trainor, Phys. Rev. Lett. 34, 402 (1975).
4. D.J. Millener, private communication.
5. R.A. Brandenburg, B.H.J. McKellar, and I. Morrison, to be published; and B.H.J. McKellar, private communication.

2.12 H-Atom Control Computer

E. Swanson

A DEC PDP 11/03 minicomputer-based system was purchased to control switching patterns and data acquisition. The requirements of such a system are: to modulate the directions and magnitudes of electric and magnetic fields seen by the neutral H* beam, to measure the lyman alpha light produced in each of the field modulation configurations, and to demodulate the data to provide a "PV" signal. In addition instrumental asymmetries will be calculated and used to modify the switching algorithm to "close the loop" so to speak, minimizing these asymmetries. A schematic representation of the system is shown in figure 2.12-1. Here the parts shown dashed are either proposed or under construction.

Communication with the experiment is expected to be totally via the IEEE 488 bus. Power supplies will be programmed through D/A channels in the control interface which also contains the master clock. This interface is presently in the design stage and will use a Motorola 6800 μ-processor to allow modification as familiarity with the experiments operation increases. A/D channels will be used to monitor ion source parameters.

To obtain an understanding of the features and limitations of the "IEEE bus" an interface was built to allow us to use a Calcomp plotter. Plot software in the form of Fortran callable subroutines was obtained from "DECUS" (DEC Users Group) and converted for use on our system. The plotter is now completely operational.

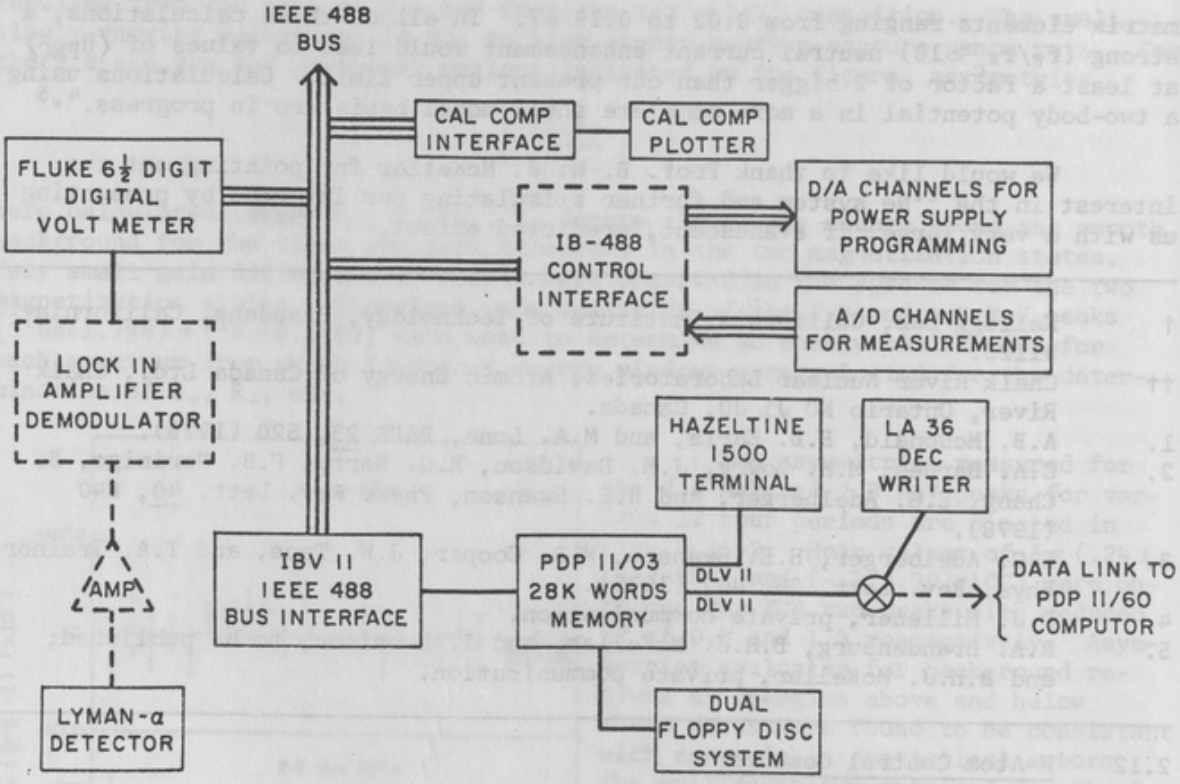

Fig. 2.12-1. **H-atom control computer schematic dashed lines indicate items proposed or under construction.**

The primary data acquisition device is a Fluke 8500A 6 1/2 Digit Digital Volt Meter. A maximum sample rate of 240 Hz can be obtained using the IEEE bus interface or implementing an optional direct parallel interface a 500 Hz rate can be obtained.

We are presently investigating the use of a lock-in amplifier upstream of the Fluke DVM to pre-demodulate the signal thus allowing us to modulate the static E field at a kiloHertz.

Programming of the system can be done in FORTRAN IV, Basic, and MACRO. Data and programs are stored on floppy disks and eventually sent via a data link to the lab's PDP 11/60 computer.

3. NUCLEAR STRUCTURE

3.1 An Accurate Value for the ^{20}Ne 2^+,T=1 (10.27) → 2^+,T=0 (1.63 MeV) Gamma-Decay Strength

K. A. Snover, K. Kim, and P. A. Dickey

The absolute magnitude of the ^{20}Ne(2^+,T=1) → (2^+,T=0) γ-decay strength is important for comparisons with the analagous ^{20}F and ^{20}Na β-decay which test the "strong form" of conserved-vector-current (CVC) theory and/or the possible existence of second class currents. Although the most difficult ingredients in such comparisons are the β-decay experiments, it is essential that the absolute γ-decay strength be known reliably. Hence we have remeasured the strength of the E_γ = 6.97 MeV resonance in the ^{16}O(α,γ1)^{20}Ne*(1.63) reaction.

Our experiment consists of 3 parts: an ^{16}O(α,γ_1) resonance yield measurement using an anodized tantalum target and the large NaI spectrometer, an accurate spectrometer efficiency calibration using the ^{13}C(^{3}He,pγ) coincidence reaction, and an ^{16}O(d,nγ) and (d,pγ) study to determine the absolute oxygen content of the anodized tantalum target.

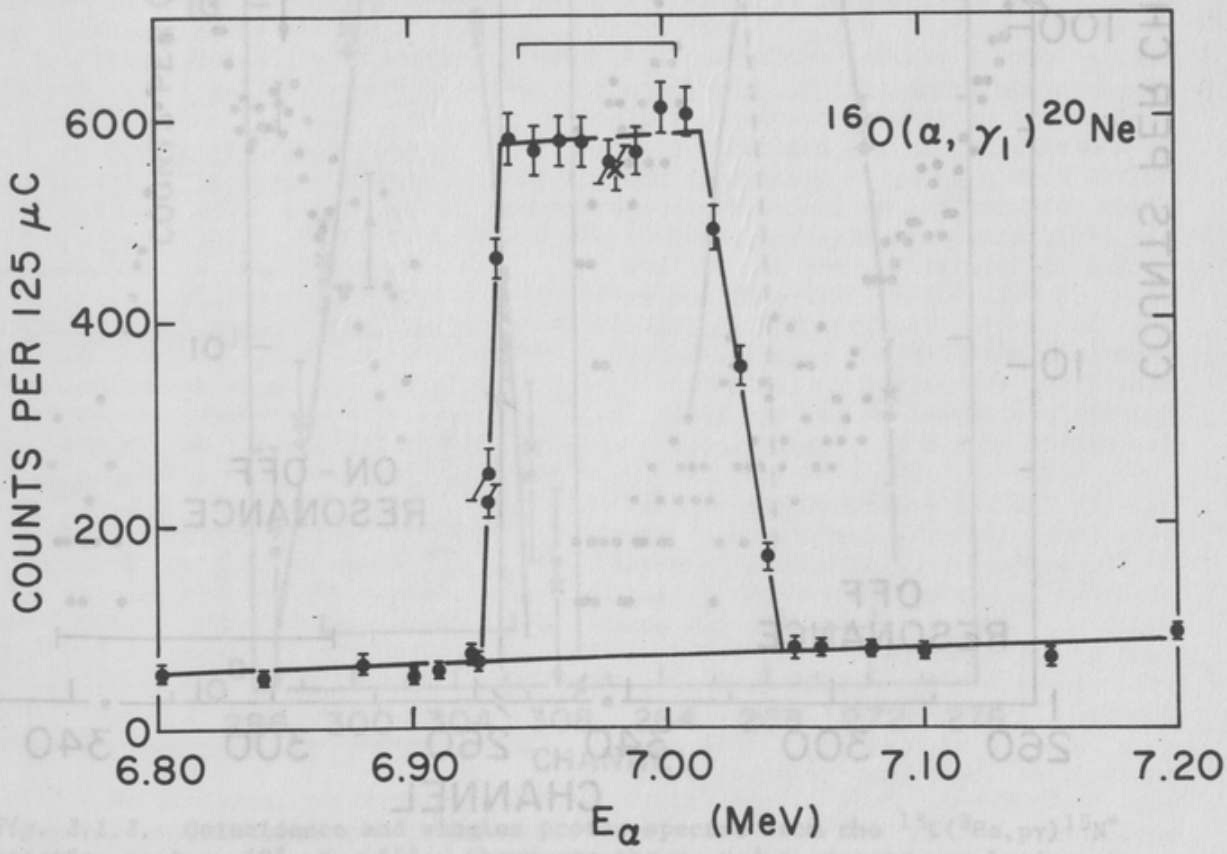

Fig. 3.1-1. ^{16}O(α,γ_1) yield curve measured at θ_γ = 55° with an anodized tantalum target.

The $^{16}O(\alpha,\gamma_1)$ resonance yield curve measured at $\theta_\gamma = 55°$ with a $^4He^{++}$ beam of 250 nA striking an anodized tantalum target is shown in Fig. 3.1-1. The nearly rectangular resonance shape is characteristic of small beam spread

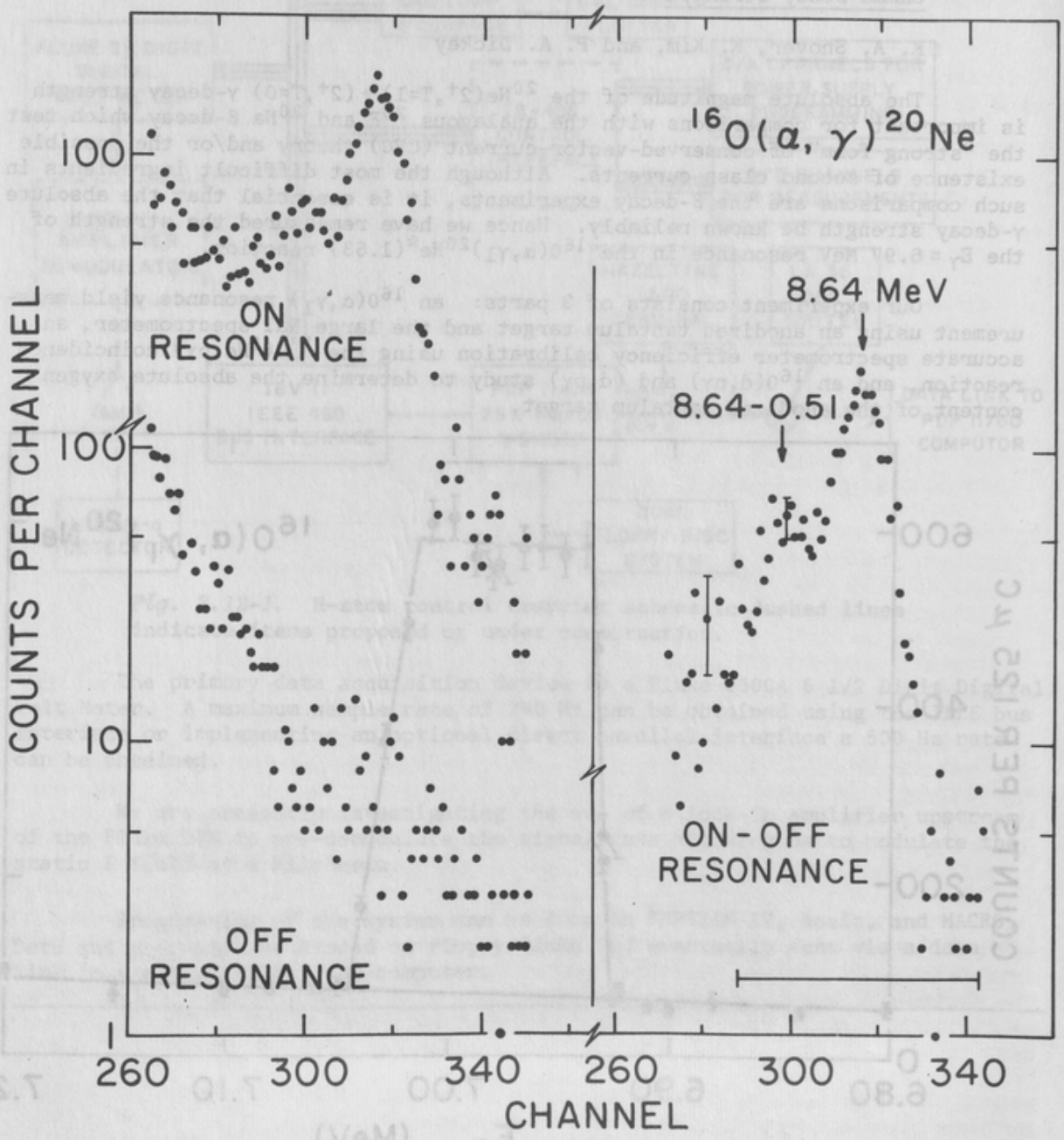

Fig. 3.1-2. γ-ray spectra from $^{16}O(\alpha,\gamma)^{20}Ne$. Each of the on and off-resonance spectra are the sum of 6 runs.

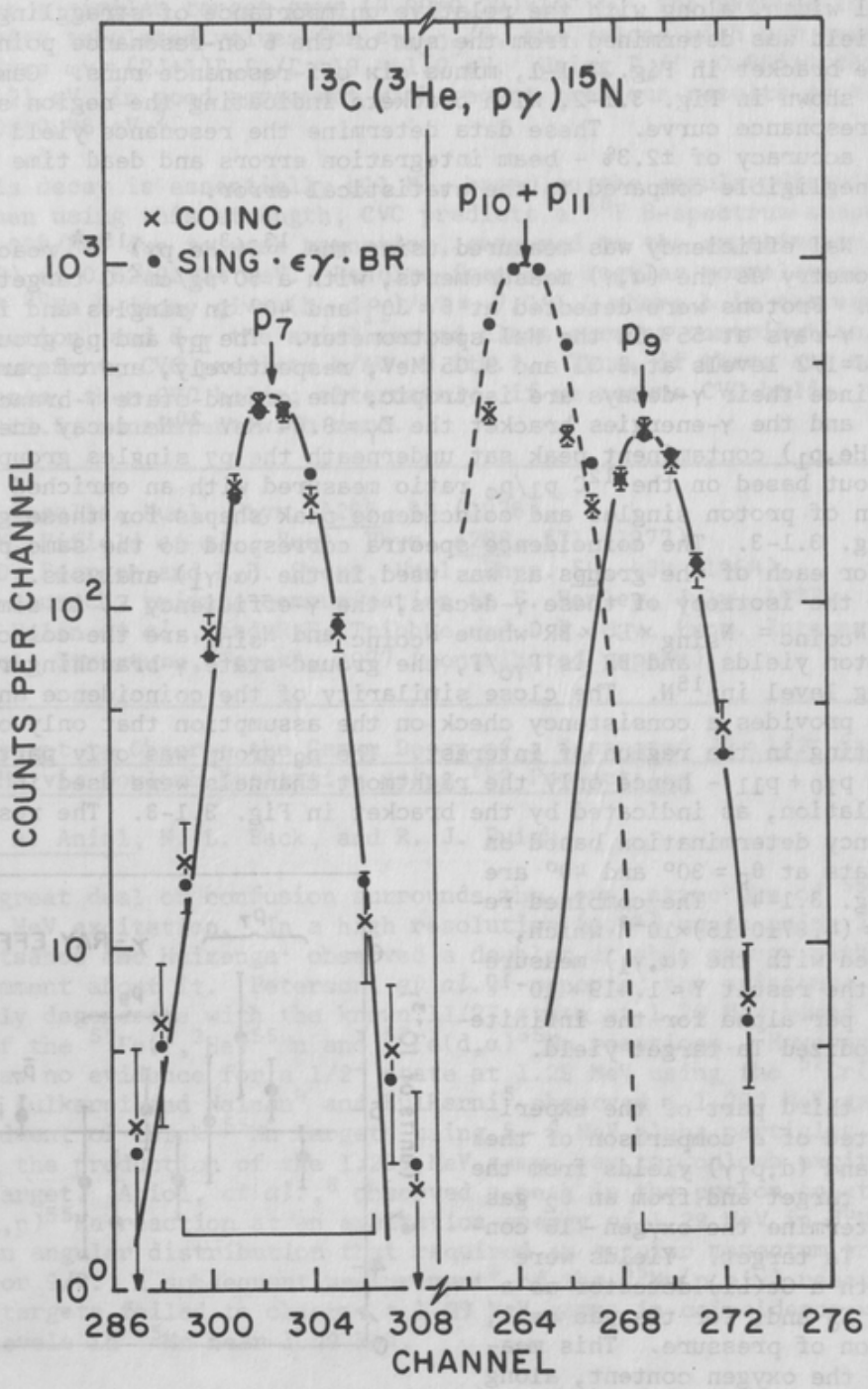

Fig. 3.1.3. Coincidence and singles proton spectra from the $^{13}C(^3He,p\gamma)^{15}N^*$ reaction at $\theta_p = -40°$, $\theta_\gamma = 55°$. Shown are the p_7 and p_9 groups populating the J=1/2 states at 8.31 and 9.05 MeV, respectively. The solid line represents the peak shape determined from an isolated proton group elsewhere in the spectrum.

plus natural width, along with the relative unimportance of straggling. The resonance yield was determined from the sum of the 6 on-resonance points indicated by the bracket in Fig. 3.1-1, minus six off-resonance runs. Gamma ray spectra are shown in Fig. 3.1-2, with brackets indicating the region summed to obtain the resonance curve. These data determine the resonance yield with a statistical accuracy of ±2.3% - beam integration errors and dead time corrections were negligible compared to the statistical error.

The NaI efficiency was measured using the $^{13}C(^{3}He,p\gamma)^{15}N^{*}$ reaction in the same geometry as the (α,γ) measurements, with a 50 $\mu g/cm^2$ C target enriched to >95% ^{13}C. Protons were detected at $\theta = 30°$ and 40° in singles and in coincidence width γ-rays at 55° in the NaI spectrometer. The p_7 and p_9 groups populating the J=1/2 levels at 8.31 and 9.05 MeV, respectively, are of particular interest, since their γ-decays are isotropic, the ground-state γ-branches are well-known, and the γ-energies bracket the $E_\gamma = 8.64$ MeV ^{20}Ne decay energy. A small $^{12}C(^{3}He,p_1)$ contaminent peak sat underneath the p_7 singles group and was subtracted out based on the ^{12}C p_1/p_o ratio measured with an enriched ^{12}C target. A comparison of proton singles and coincidence peak shapes for these groups is shown in Fig. 3.1-3. The coincidence spectra correspond to the same percentage E_γ window for each of the groups as was used in the (α,γ_1) analysis. As a consequence of the isotropy of these γ-decays, the γ-efficiency E_γ is simply determined from $N_{coinc} = N_{sing} \times E_\gamma \times BR$ where N_{coinc} and N_{sing} are the coincidence and singles proton yields, and BR is $\Gamma_{\gamma o}/\Gamma$, the ground-state γ-branching ratio of the decaying level in ^{15}N. The close similarity of the coincidence and singles peak shapes provides a consistency check on the assumption that only one group is contributing in the region of interest. The p_9 group was only partly resolved from $p_{10} + p_{11}$ - hence only the rightmost channels were used in the efficiency calculation, as indicated by the bracket in Fig. 3.1-3. The results of the efficiency determination based on p_7 and p_9 data at $\theta_p = 30°$ and 40° are shown in Fig. 3.1-4. The combined result is $E_\gamma = (4.87 \pm 0.15) \times 10^{-3}$ which, when combined with the (α,γ_1) measurement gives the result $Y = 1.419 \times 10^{-10}$ (±3.9%) γ's per alpha for the infinitely-thick anodized Ta target yield.

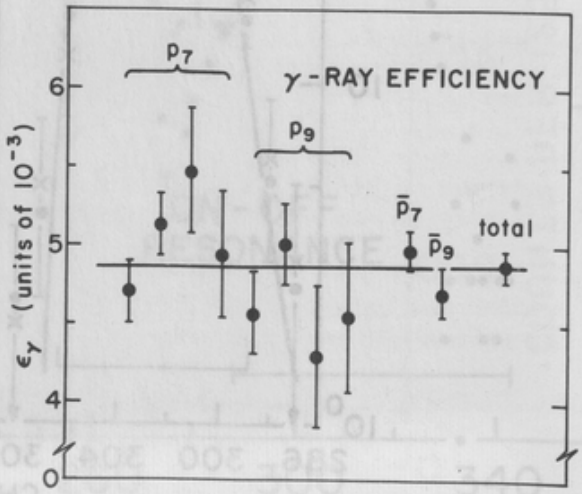

Fig. 3.1-4. Gamma efficiency determined from the $^{13}C(\ He,p\gamma)^{15}N^{*}$ reaction.

The third part of the experiment consisted of a comparison of the $^{16}O(d,n_1\gamma)$ and $(d,p_1\gamma)$ yields from the anodized Ta target and from an O_2 gas cell, to determine the oxygen-16 content of the Ta target. Yields were measured with a Ge(Li) detector as a function of E_d and, for the gas cell, as a function of pressure. This measurement of the oxygen content, along with the observed width of the (α,γ_1) resonance curve imply $E = (3.85 \pm 0.20) \times 10^{-17}$ keV - cm^2/O atom for the stopping power of $E_\gamma = 6.97$ MeV alpha particles in anodized Ta. A measurement by

Ingalls[1] for a similar target gave $(4.09\pm0.20)\times10^{-17}$. The average is in good agreement with tabulated values for $\epsilon_{Ta_2O_5}/5$, and, along with our measured strength gives $\omega\gamma = (2J+1)\Gamma_\gamma\Gamma_\gamma/\Gamma = 19.4\pm1.0$ eV. Using $\Gamma_\alpha/\Gamma = 0.965\pm0.005$ we obtain $\Gamma_\gamma = 4.02\pm0.21$ eV, in good agreement with recent previous results of 4.08 ± 0.33 eV[1] and 4.08 ± 0.46 eV.[2]

This decay is essentially all M1, based on the angular distributions of ref. 4. Then using this strength, CVC predicts a ^{20}F β-spectrum shape factor of $\approx1.07\pm0.03\%$/MeV due to weak magnetism, compared to the experimental value (see ref. 3) of $0.62\pm0.33\%$ MeV. Results from β-γ angular correlation studies of the ^{20}F and ^{20}Na β-decay give $(b - d_{II})/AC = -7.0\pm1.5$ where b is the weak magnetism contribution, and d_{II} the axial second class current contribution. Based on our Γ_γ measurement, CVC predicts $b/AC = 8.1\pm0.2$. Thus, if there are no second class currents, then CVC holds; alternately, if we assume CVC holds, then $d_{II}/AC = 1.1\pm1.5$, consistent with zero.

1. P. Ingalls, Nucl. Phys. A265, 93 (1976).
2. L,K. Fifield *et al.*, Nucl. Phys. A288, 571 (1977).
3. J.D. Pearson and R.H. Spear, Nucl. Phys. 54, 434 (1964).
4. J. Deutsch, private communication to E. Henley, July, 1977. See also N. Rolin *et al.*, and R.E. Tribble and D.P. May, Proc. Internat. Conf. Nucl. Structure, Toyoko, 1977 (contributed papers).

3.2 Attempt to Observe the Gamma Decay of a Suspected $J^\pi = 1/2^-$ State in ^{55}Mn via Coulomb Excitation using ^{16}O Projectiles

K. A. Aniol, N. L. Back, and R. J. Puigh

A great deal of confusion surrounds the level structure of ^{55}Mn at about 1.29 MeV excitation. In a high resolution (p,p') study using 7.975 MeV protons Katsanos and Huizenga[1] observed a doublet at this energy although they made no comment about it. Peterson, *et al.*,[2] reported the existence of a $1/2^-$ state nearly degenerate with the known $11/2^-$ state at 1.29 MeV based on their analysis of the $^{57}Fe(P,^3He)^{55}Mn$ and $^{57}Fe(d,\alpha)^{55}Mn$ reactions. However, Hichwa, *et al.*,[3] saw no evidence for a $1/2^-$ state at 1.29 MeV using the $^{52}Cr(\alpha,p\gamma)^{55}Mn$ reaction. Kulkarni and Nainan[4] and Kulkarni[5] observed a 1.293 MeV gamma ray in the bombardment of thick ^{55}Mn targets using 5 - 8 MeV alpha particles. They attributed the production of the 1.293 MeV gamma ray to Coulomb excitation of the ^{55}Mn target. Aniol, *et al.*,[6] observed a peak in the proton spectrum from the $^{52}Cr(\alpha,p)^{55}Mn$ reaction at an excitation energy of 1.29 MeV in ^{55}Mn. This peak had an angular distribution that required an angular momentum transfer of $1/2 + 11/2$ or $9/2$. A subsequent measurement[6] of the $^{55}Mn(p,p'\gamma)$ reaction using thin ^{55}Mn targets failed to observe a 1.29 MeV gamma in coincidence with protons exciting levels in ^{55}Mn near 1.29 MeV.

We attempted to detect the production of the 1.29 MeV state both in gamma-ray singles and particle gamma coincidence using 30 and 38 MeV ^{16}O ions. For this purpose a thick Mn target was bombarded by ^{16}O ions and viewed by a Ge(Li) detector at 90° and an angular surface barrier detecter at a mean angle of 165°. The only gamma rays which were observed, both in singles and

coincidence, that could be definitely assigned to ^{55}Mn were the 0.126 and 0.860 MeV decays from the first and second excited state. We could have observed the 1.29 MeV gamma if $0.2 < B(E2)(1.29\ MeV)/B(E2)(0.984\ MeV)$ whereas Kulkarni and Nainon[4] claim that $B(E2)(1.29\ MeV)/B(E2)(0.984\ MeV) = 0.4$. Moreover, the upward transition to the 5th excited state was also not observed requiring $B(E2)(1.884\ MeV)/B(E2)(0.984\ MeV) < 0.3$, whereas ref. 4 claim that this ratio is 0.6. It appears that the transitions to the 1.29 and 1.88 MeV state seen in (4) were not due to single step Coulomb excitation. Consequently the origin of the 1.29 MeV gamma ray seen in α particle bombardment of ^{55}Mn is uncertain. Deviation from the single step Coulomb Excitation yield for thin targets of Mn were observed for $E_\alpha > 2$ MeV.[7]

The puzzle surrounding the level structure of ^{55}Mn at 1.29 MeV still remains.

1. A.A. Katsanos and J.R. Huizenga, Phys. Rev. 159, 931 (1967).
2. R.J. Peterson, S. Pittel, and H. Rudolph, Phys. Lett. 37B, 278 (1971).
3. B.P. Hichwa, J.C. Lawson, L.A. Alexander, and P.R. Chagnon, Nucl. Phys. A202, 364 (1973). B.P. Hichwa, J.C. Lawson, and P.R. Chagnon, Nucl. Phys. A215, 132 (1973).
4. R.G. Kulkarni and T.D. Nainon, Can. J. Phys. 52, 1676 (1974).
5. R.G. Kulkarni, Phys. Scr. 13, 213 (1976).
6. K. Aniol, D. Gebbie, C. Hollas, and J. Nurzynski, submitted to Nucl. Phys. A. K. Aniol, Ph.D. thesis (1977) Australian National University, Canberra, A.C.T., Australia, unpublished.
7. G.M. Temmer and N.P. Heydenburg, Phys. Rev. 96, 426 (1954).

3.3 The α-width of the lowest T=2 state in ^{28}Si

E. G. Adelberger, P. G. Ikossi, A. B. McDonald†, J. L. Osborne††, and K. A. Snover

In last year's annual report[1] we have presented excitation function data for the $^{24}Mg(\alpha,\alpha_0)^{24}Mg$ reaction in the vicinity of the lowest T=2 state in ^{28}Si. We have extended these data by measuring cross-sections over the 5.99 MeV resonance at laboratory angles of 50, 70, 85, 115, 130 and 150° (Fig. 1). Resonance analysis of these data under the assumption of a linear background establishes that the spin of this state is 0^+, the width $\Gamma = 11\pm2$ keV and $\Gamma_\alpha/\Gamma = 0.7\pm0.1$. The $J^\pi = 0^+$ assignment is important because it suggests this state as a possible candidate for isospin mixing with the lowest $J^\pi = 0^+$, T=2 state which occurs at $E_\alpha = 6.114$ MeV.

Two sets of data measured over the T=2 state in steps of 1 keV at laboratory angles 125°, 145° and 165°, using 0.5 and 2 μg/cm^2 thick targets, respectively, were analyzed to obtain the width of this state. In this analysis we have written the cross-section as

$$\frac{d\sigma_{obs}}{d\Omega}(E,\theta) = \int_{-\infty}^{+\infty} \frac{d6}{d\Omega}(E',\theta)\, f(E'E',\Delta,t)dE' \qquad (1)$$

where $\frac{d\sigma}{d\Omega}(E,\theta) = \sigma_B(E,\theta) + \frac{1}{4K^2}$

$$\frac{\Gamma_\alpha^2}{(E-E_\alpha)^2+\Gamma^2/4}\left[1+4K\sqrt{\sigma_B}(E,\theta)\times\left(\cos\phi(\theta)\frac{E_R-E}{\Gamma_\alpha} + \sin\phi(\theta)\frac{\Gamma}{2\Gamma_\alpha}\right)\right] \quad (2)$$

where σ_B is the background cross-section, assumed to vary linearly with energy and $\phi(\theta)$ the interference phase.

The width and shape of the resolution function was estimated from (α,p_0) data measured at 65° and 85° using the same targets over a resonance at 3.191 MeV with $\Gamma = 660\pm30$ eV.[2] This width is an order of magnitude smaller than our observed width of the resonance anomaly. Also the (a,p) cross-section off-resonance is zero. Thus the observed width and shape of the anomaly was taken to represent the width and shape of the resolution function. This energy resolution function was much broader than we would expect for uniform targets, and was well described as a convolution of a Gaussian and a Landau distribution function with adjustable width and asymmetry parameters.

In analyzing the excitation function data over the T=2 state we have treated all parameters in eq. 2 as variables. The width of the energy resolution function was also allowed to vary. The χ^2 as a function of Γ_α with Γ_α/Γ held constant exhibits well pronounced minima and thus provides an accurate estimate of the width of the T=2 state (Figs. 2, 3). Furthermore the phase $\phi(\theta)$ and the width of the energy resolution function which minimize the χ^2 are in agreement with the estimates obtained from the analyses of the 5.99 and 3.191 MeV resonances respectively.

Given that $\Gamma_\alpha/\Gamma = 0.7\pm0.1$ (ref. 3., fig. 4) the best estimate for the α-width of the T=2 state is $\Gamma_\alpha = 222\pm25$

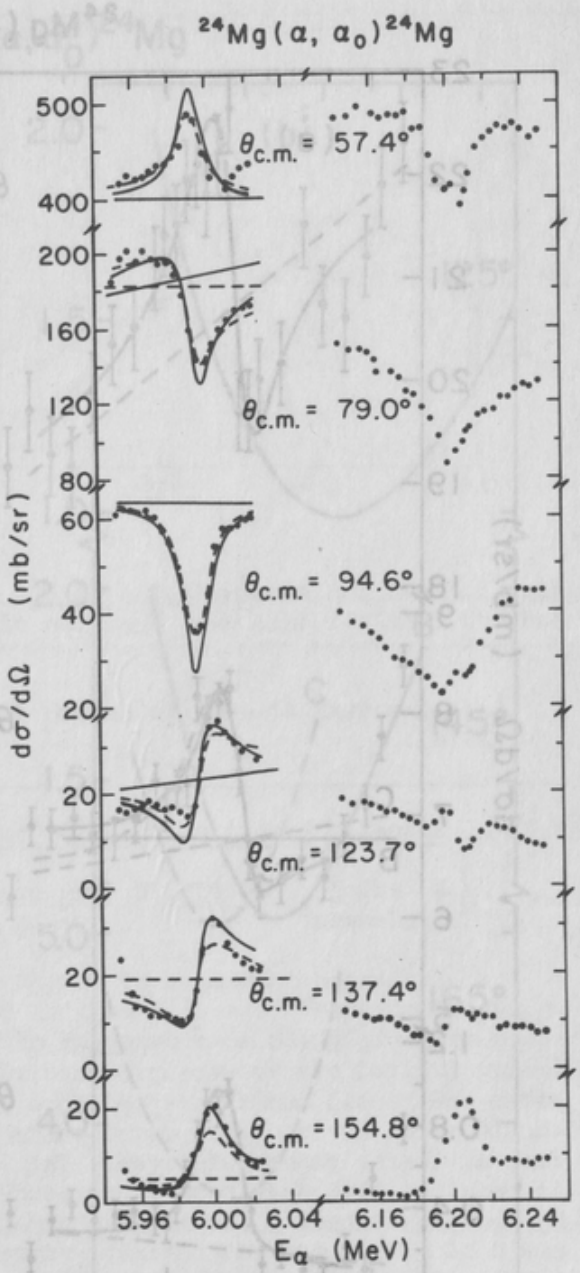

Fig. 3.3-1. Excitation functions for the $^{24}Mg(\alpha,\alpha_0)$ reaction. The solid curves are fits to the data with Γ_α/Γ = 0.8 and the background cross-sections as shown by the straight lines. The dashed curves are calculated for $\Gamma_\alpha/\Gamma = 0.6$.

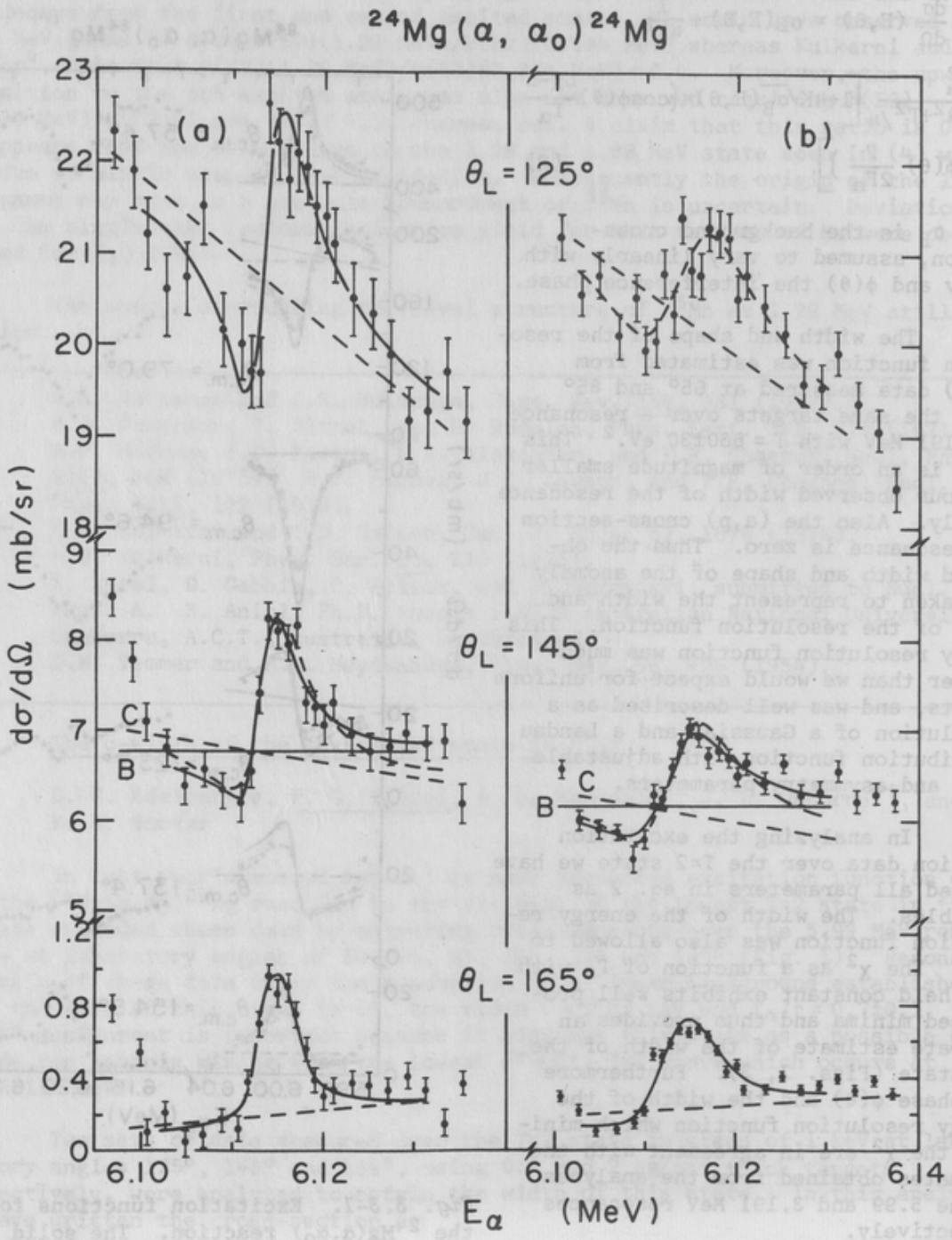

Fig. 3.3-2. Excitation functions over the lowest T=2 state in ^{28}Si measured with 0.5 μg/cm^2 (a) and 2 μg/cm^2 (b) thick targets. The solid lines are fits obtained as described in the text.

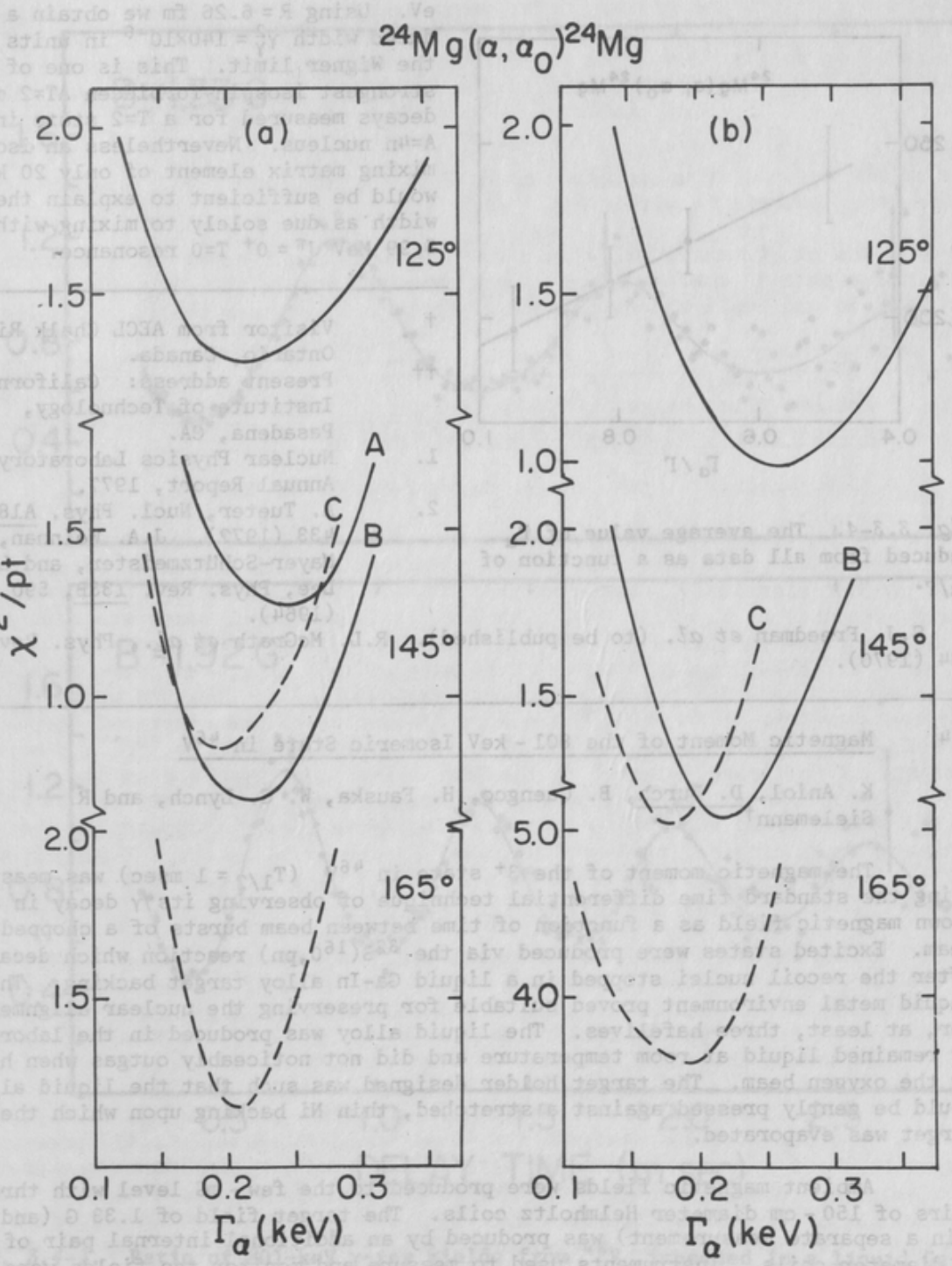

Fig. 3.3-3. The χ^2 as a function of Γ_α. The curves labelled A, B, C for 145° corresponds to a different choice of the background cross-section.

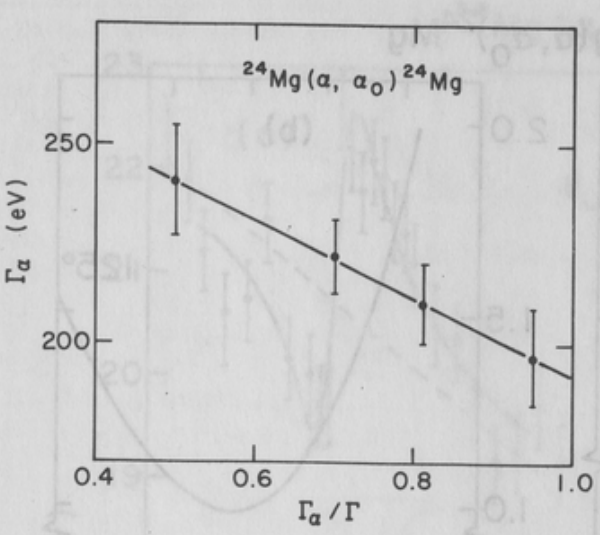

Fig. 3.3-4. **The average value of Γ_α deduced from all data as a function of Γ_α/Γ.**

eV. Using R = 6.26 fm we obtain a reduced width $\gamma_\gamma^2 = 140\times10^{-6}$ in units of the Wigner limit. This is one of the strongest isospin-forbidden $\Delta T=2$ α-decays measured for a T=2 state in on A=4n nucleus. Nevertheless an isospin mixing matrix element of only 20 keV would be sufficient to explain the width as due solely to mixing with the 5.99 MeV $J^\pi = 0^+$ T=0 resonance.

---

† Visitor from AECL Chalk River, Ontario, Canada.

†† Present address: California Institute of Technology, Pasadena, CA.

1. Nuclear Physics Laboratory Annual Report, 1977.
2. A. Tueter, Nucl. Phys. A185, 433 (1972). J.A. Weinnan, L. Mayer-Schützmeister, and L.L. Lee, Phys. Rev. 133B, 590 (1964).
3. S.J. Freedman *et al.* (to be published). R.L. McGrath *et al.*, Phys. Rev. C1, 184 (1970).

3.4 Magnetic Moment of the 801-keV Isomeric State in ^{46}V

K. Aniol, D. Burch, B. Cuengco, H. Fauska, W. G. Lynch, and R. Sielemann†

The magnetic moment of the 3^+ state in ^{46}V ($T_{1/2}$ = 1 msec) was measured using the standard time differential technique of observing its γ decay in a known magnetic field as a function of time between beam bursts of a chopped beam. Excited states were produced via the ^{32}S(^{16}O,pn) reaction which decayed after the recoil nuclei stopped in a liquid Ga-In alloy target backing. This liquid metal environment proved suitable for preserving the nuclear alignment for, at least, three hafelives. The liquid alloy was produced in the laboratory; it remained liquid at room temperature and did not noticeably outgas when heated by the oxygen beam. The target holder designed was such that the liquid alloy could be gently pressed against a stretched, thin Ni backing upon which the Cds target was evaporated.

Ambient magnetic fields were produced to the few-mG level with three pairs of 150-cm diameter Helmholtz coils. The target field of 1.33 G (and 1.92 G in a separate measurement) was produced by an additional internal pair of 45-cm diameter coils. Instruments used to measure and monitor the fields were calibrated with yet another pair of single-loop coils constructed to an accuracy of 1%.

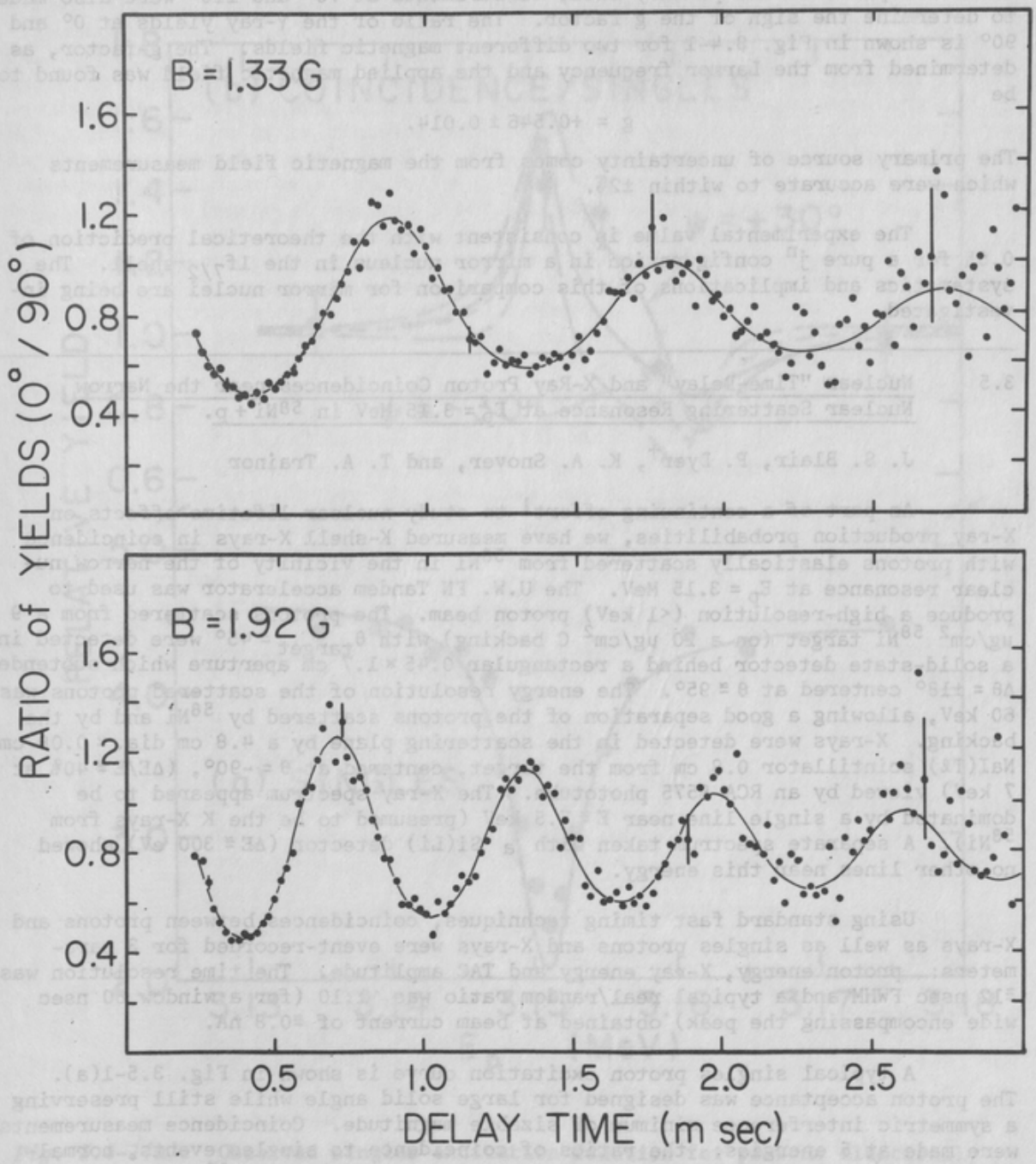

Fig. 3.4-1. Ratio of 801-keV γ-ray yields from ^{46}V imbedded in a liquid Ga-In alloy in weak magnetic fields as a function of time between beam bursts.

Two thin NaI detectors (5-cm diameter) placed at 0° and 90° to the beam

direction provided the primary data; measurements at 70° and 110° were also made to determine the sign of the g factor. The ratio of the γ-ray yields at 0° and 90° is shown in Fig. 3.4-1 for two different magnetic fields. The g-factor, as determined from the Larmor frequency and the applied magnetic field was found to be

$$g = +0.546 \pm 0.014.$$

The primary source of uncertainty comes from the magnetic field measurements which were accurate to within ±2%.

The experimental value is consistent with the theoretical prediction of 0.55 for a pure j^n configuration in a mirror nucleus in the $1f_{7/2}$ shell. The systematics and implications of this comparison for mirror nuclei are being investigated.

3.5 Nuclear "Time-Delay" and X-Ray Proton Coincidences near the Narrow Nuclear Scattering Resonance at $E_p = 3.15$ MeV in $^{58}Ni + p$.

J. S. Blair, P. Dyer†, K. A. Snover, and T. A. Trainor

As part of a continuing effort[1] to study nuclear lifetime effects on X-ray production probabilities, we have measured K-shell X-rays in coincidence with protons elastically scattered from ^{58}Ni in the vicinity of the narrow nuclear resonance at $E_p = 3.15$ MeV. The U.W. FN Tandem accelerator was used to produce a high-resolution (<1 keV) proton beam. The protons scattered from a 9 μg/cm^2 ^{58}Ni target (on a 20 μg/cm^2 C backing) with $\theta_{target} = 45°$ were detected in a solid-state detector behind a rectangular 0.45 × 1.7 cm aperture which subtended $\Delta\theta = \pm 18°$ centered at $\theta \cong 95°$. The energy resolution of the scattered protons was 60 keV, allowing a good separation of the protons scattered by ^{58}Ni and by the backing. X-rays were detected in the scattering plane by a 4.8 cm dia. × 0.08 cm NaI(Tℓ) scintillator 0.8 cm from the target, centered at $\theta = -90°$, ($\Delta E/E \cong 40\%$ at 7 keV) viewed by an RCA 8575 phototube. The X-ray spectrum appeared to be dominated by a single line near $E \cong 7.5$ keV (presumed to be the K X-rays from ^{58}Ni). A separate spectrum taken with a Si(Li) detector ($\Delta E \cong 300$ eV) showed no other lines near this energy.

Using standard fast timing techniques, coincidences between protons and X-rays as well as singles protons and X-rays were event-recorded for 3 parameters: proton energy, X-ray energy and TAC amplitude. The time resolution was ≅12 nsec FWHM and a typical real/random ratio was ∿1:10 (for a window 60 nsec wide encompassing the peak) obtained at beam current of ≅0.8 nA.

A typical singles proton excitation curve is shown in Fig. 3.5-1(a). The proton acceptance was designed for large solid angle while still preserving a symmetric interference minimum of sizable magnitude. Coincidence measurements were made at 5 energies: the ratios of coincidence to singles events, normalized to unity off-resonance, are shown in Fig. 3.5-1(b). The middle points (at $E_p = E_R$, $E_R + 4$ and $E_R + 8$ keV where E_R is the nuclear resonance energy and the K-shell binding energy $B \cong 8$ keV are in the region where interference effects due to the nuclear lifetime are expected to be greatest. These ratios show a clear variation with energy in the region of the resonance.

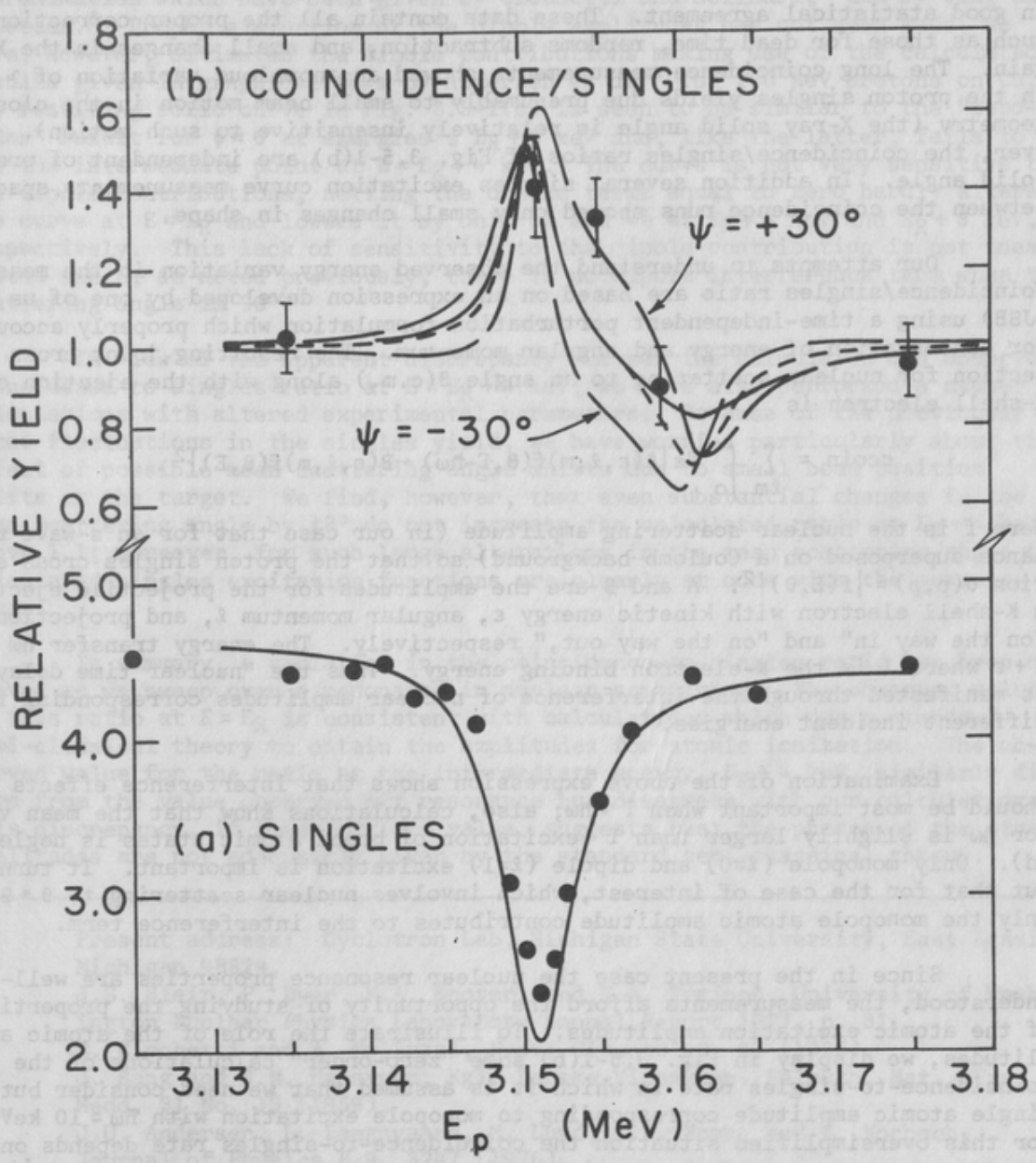

Fig. 3.5-1(a). Observed singles excitation function for protons elastically scattered from ^{58}Ni (together with calculated excitation function which takes into account the large solid angle subtended by the proton detector). *(b)* Ratio of proton yield in coincidence with K X-rays to the singles proton yield. The long-dashed curves correspond to "zero-order" calculations for the atomic phase angle $\psi = 30°$ and $-30°$, the short-dashed curve to the same with $\psi = 0$, and the solid curve to a detailed theoretical calculation (see text).

Each ratio is the sum of 3 separate runs, ∿6 hours/run, which were all in good statistical agreement. These data contain all the proper corrections such as those for dead time, randoms subtraction, and small changes in the X-ray gain. The long coincidence measurements showed an anomalous variation of ∿ ±10% in the proton singles yields due presumably to small beam motion in the close geometry (the X-ray solid angle is relatively insensitive to such motion). However, the coincidence/singles ratios of Fig. 3.5-1(b) are independent of proton solid angle. In addition several singles excitation curve measurements spaced between the coincidence runs showed only small changes in shape.

Our attempts to understand the observed energy variation in the measured coincidence/singles ratio are based on an expression developed by one of us (JSB) using a time-independent perturbation formulation which properly accounts for conservation of energy and angular momentum. The resulting joint cross section for nuclear scattering to an angle θ(c.m.) along with the ejection of a K-shell electron is

$$\sigma\text{coin} = \sum_{\ell m} \int_0^\infty d\varepsilon \left| A(\varepsilon,\ell,m) f(\theta, E-\hbar\omega) + B(\varepsilon,\ell,m) f(\theta,E) \right|^2 .$$

Here f is the nuclear scattering amplitude (in our case that for an s-wave resonance superposed on a Coulomb background) so that the proton singles cross section $\sigma(p,p) = |f(E,\theta)|^2$. A and B are the amplitudes for the projectile ejecting a K-shell electron with kinetic energy ε, angular momentum ℓ, and projection m "on the way in" and "on the way out," respectively. The energy transfer $\hbar\omega = I + \varepsilon$ where I is the K-electron binding energy. Thus the "nuclear time delay" is manifested through the interference of nuclear amplitudes corresponding to different incident energies.

Examination of the above expression shows that interference effects should be most important when $\Gamma \sim \hbar\omega$; also, calculations show that the mean value for $\hbar\omega$ is slightly larger than I (excitation of bound atomic states is neglected). Only monopole (ℓ=0) and dipole (ℓ=1) excitation is important. It turns out that for the case of interest, which involves nuclear scattering to θ ≈ 90°, only the monopole atomic amplitude contributes to the interference term.

Since in the present case the nuclear resonance properties are well-understood, the measurements afford the opportunity of studying the properties of the atomic excitation amplitudes. To illustrate the role of the atomic amplitudes, we display in Fig. 3.5-1(b) some "zero-order" calculations of the coincidence-to-singles rate in which it is assumed that we need consider but a single atomic amplitude corresponding to monopole excitation with $\hbar\omega = 10$ keV. For this oversimplified situation the coincidence-to-singles rate depends only on the relative phase of the atomic amplitude, ψ, defined through $B = |B|e^{i\psi}$. (In the canonical semiclassical approximation, A and B are related by the condition $A^* = B$.) One sees that the predicted curves are indeed sensitive to the value of ψ and that the curve for ψ = +30° is in reasonable agreement with the experimental results.

From this exploratory calculation we turn to more detailed theoretical predictions in which there is proper integration over the electron kinetic energy. Here we use expressions for the monopole amplitudes in the semi-classical

approximation which have been given by Ciochetti and Molinari,[2] and by Bang and Hansteen.[3] Proper evaluation of the dipole amplitudes has not been made; we have, however, estimated the dipole contributions making use of the calculated results given in graphical form by Andersen *et al.*[4] for 2.0 MeV protons on Cu. The resulting solid curve in Fig. 3.5-1(b) is seen to be similar to the "zero-order" result for $\psi = 0$ at energies $\leq E_R + 8$ keV and, like the latter, fails to fit the intermediate point at $E = E_R + 4$ keV. The curve is not very sensitive to the dipole contributions; setting the dipole terms equal to zero hardly alters the curve at $E = E_R$ and lowers it by only 3% and 4% at $E_R + 4$ keV and $E_R + 8$ keV, respectively. This lack of sensitivity to the dipole contribution is not unexpected since, as noted previously, there is no dipole interference term when the scattering angle is 90°.

In view of the apparent discrepancy between the calculated and observed coincidence-to-singles ratio at $E = E_R + 4$ keV, we have also performed a number of calculations with altered experimental parameters. Because of the previously noted fluctuations in the singles yield, we have worried particularly about the effect of possible mean scattering angle shifts due to small beam position shifts on the target. We find, however, that even substantial changes in the mean scattering angle by ±8° do not increase the calculated ratio at $E_R + 4$ keV above 1.1; moreover, for such large alterations in the mean scattering angle the calculated singles excitation functions are clearly at odds with the measurements.

In summary, a variation in the coincidence-to-singles ratio has been observed as we sweep over a resonance in nuclear scattering. The observed value of this ratio at $E = E_R$ is consistent with calculations which use a standard semi-classical theory to obtain the amplitudes for atomic ionization. The observed value for the ratio at the intermediate energy, $E_R + 4$ keV, similarly differs from the value observed off resonance but disagrees with our calculations. This discrepancy, if taken at face value, suggests that the phases of the atomic amplitudes are not adequately given by the standard semi-classical theory.

---

† Present address: Cyclotron Lab, Michigan State University, East Lansing, Michigan 48824.

1. J.S. Blair, P. Dyer, K.A. Snover, and T.A. Trainor, University of Washington Nuclear Physics Laboratory Annual Report 1977, p. 31.
2. G. Ciochetti and A. Molinari, Nuovo Cimento 40, 69 (1965).
3. J. Bang and J.M. Hansteen, Kgl. Danske Videnskab. Selskab, Mat.-Fys. Medd. 31 No. 13 (1959).
4. J.U. Andersen, L. Laegsgaard, M. Lund, C.D. Moak, and L. Kocbach, Journal of Physics B 9, 3247 (1976).

3.6 A Schematic Model for Isospin Mixing in Light Nuclei

E. G. Adelberger and A.B. McDonald†

In this report we discuss a simple schematic model which relates off-diagonal mixing matrix elements to mass differences in isobaric multiplets. The model gives results in qualitative agreement with the systematics of isospin

nonconserving (INC) particle decay widths of $T = 3/2$ and $T = 2$ levels in light nuclei and in quantitative agreement with measured mixing matrix elements between $T = 0$ and $T = 1$ states. On the other hand, conventional mechanisms (see ref. 1) for generating isospin impurities, i.e., mixing of the antianalog "configuration" by the monopole Coulomb force and mixing of the isovector monopole state, produce very small isotensor matrix elements and therefore fail to account for the main features of the experimental results.

Considerable information now exists[2-6] concerning INC particle decays of $T = 3/2$ and $T = 2$ levels and a number of trends are observable in the results.

1. The reduced widths for INC nucleon decay of the lowest $T = 3/2$ and $T = 2$ levels for $A < 44$ are similar in size and show a systematic variation with mass. This implies that the isospin mixing is not dominated by the chance near degeneracy of lower isospin states and suggests that a general model for isospin mixing might account for the gross features of the data.

2. Reduced widths for INC neutron decays of the lowest $T = 3/2$ levels of $A = 4N + 1$ nuclei with $T_z = N-Z/2 = +1/2$ are generally about 10 times greater than the analogous proton decays of $T_z = -1/2$ nuclei. The conventional mechanisms involving one-body potentials can only generate $\Delta T = 1$ mixing which implies identical INC widths for mirror decays.

3. Ratios of reduced widths for decay of $A = 4N + 1$, $T = 3/2$ levels to various excitated states of $A = 4N$ nuclei are different for $T_z = +1/2$ and $-1/2$. This requires that more than one $T = 1/2$ configuration be admixed into the $T = 3/2$ states or that $T = 2$ states be admixed in the $A = 4N$ nucleus.

4. Reduced widths for INC nucleon decays of $T = 3/2$ levels to negative parity states are relatively large. This implies significant admixtures of configurations in which two particles are promoted to the next major shell.

5. Alpha particle reduced widths for INC decay of $T = 2$ levels in $A = 4N$ nuclei are similar in magnitude to those for proton decay, implying that $\Delta T = 2$ mixing is significant in this case.

We assume that the wave functions for the lowest $T = 1/2$, 1, 3/2 and 2 analog states are given by a simple schematic model with up to seven valence nucleons in a pair of four-fold degenerate orbits outside a closed $A_o = 4N$ core see Fig. 3.6-1). This model is analogous to the supermultiplet, Nilsson, or generalized quartet model. The isospin mixing is assumed to arise predominantly from the anti-analog configuration ($\bar{A}$) which may dominate the wave function of one state, or be distributed among several $T_<$ states. For the $A = A_o + 5$, $T = 3/2$ levels the mixing is also considered for other $T = 1/2$ configurations (such as configuration B in Fig. 3.6-1) wherein the two highest valance nucleons have been promoted to a third orbit which could be in the next major shell (i.e., $\hbar\omega$ above orbit 2).

We express isospin mixing matrix elements between the analog and anti-analog configurations in terms of elementary particle-core and particle-particle INC matrix elements which can be evaluated from fits to mass differences in isobaric multiplets. If the only INC interaction is the Coulomb force, then for

each pair of orbits there are only 5 elementary matrix elements: C(1) and C(2)- effective INC matrix elements between a single proton in orbit 1 or 2 and the $A = 4N$ core and C(11), C(22), C(12) - effective two particle INC matrix elements between two protons in orbit 1 etc. For example, the mass difference between the $T = 3/2$, $T_z = \pm 1/2$ levels shown in Fig. 3.6-1 may be written

$$\Delta E = \frac{1}{3}\left\{ C(1) + 2C(2) + C(11) + C(22) + 4C(12) \right\}.$$

We assume that the C parameters vary with mass as $\left(\frac{A-1}{A_o}\right)^{-\lambda/3}$ where A_o is the mass of the 4N core. For values of λ ranging from +3 to -3, linear least squares fits were obtained for a total of 15 mass differences of ground states or their analogs with $T = 1/2$ to $T = 2$ ranging in mass from $A = A_o + 1$ to $A_o + 7$. All mass differences were weighted equally, and the root mean square difference between experimental and fitted values (Δ) was determined for each value of λ. The number of parameters was reduced by equating C(1) and C(2) when orbits 1 and 2 had the same spherical shell model quantum numbers.

Table 3.6-1 lists the values of the parameters obtained by the fitting procedure, as well as the value of λ obtained for minimum Δ in each case. In general, fits were acceptable and Δ was a minimum for $\lambda \approx 1$, implying a variation with mass inversely proportional to the nuclear radius. The minimum value of Δ was largest for the lightest nuclei, partly due to energy level shifts caused by nearby thresholds.

Two general features emerge. First, for the cases involving different orbits $|C(2)-C(1)|$ is generally quite small ($\lesssim 170$ keV) in agreement with the small shell effects observed as deviations from an $A^{2/3}$ (i.e., Z/R) dependence of $A = 4N+1$, $T = 1/2$ ground state mass differences. Secondly, $C(11) \approx C(22) > C(12)$, exhibiting the fact that Coulomb interaction is stronger for two protons which are coupled in a spatially symmetric configuration.

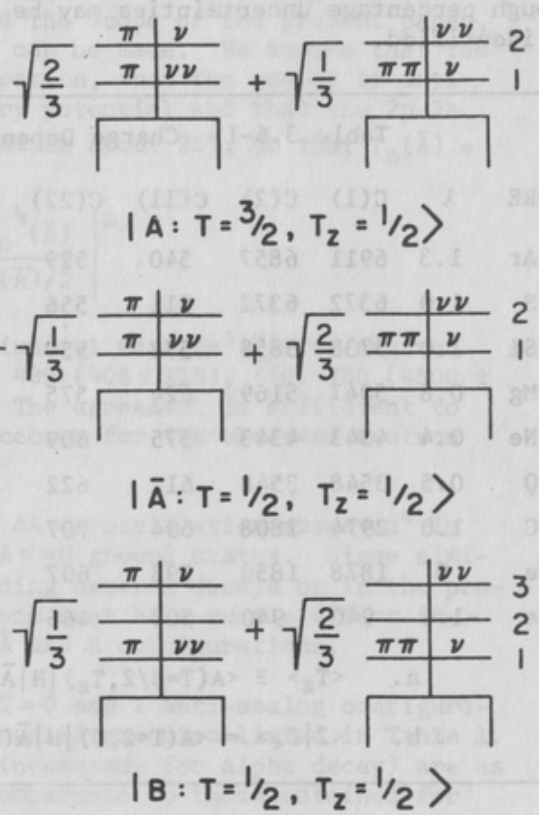

Fig. 3.6-1. Schematic representation of the wave functions for $A = A_o + 5$, $T = 3/2$, $T_z = +1/2$ levels (A), the $T = 1/2$ anti-analog configurations ($\bar{A}$), and configurations (B), in which the particles in orbit 2 have been promoted to the next major shell. For $T_z = -1/2$ all neutrons and protons are interchanged.

It is straightforward to write the matrix elements for isospin mixing between analog and anti-analog configurations in terms of the elementary matrix

elements. For example, for the $A = A_0 + 5$, $T = 3/2$ nuclei illustrated in Fig. 3.6-1,

$$\langle A\left(\frac{3}{2},-\frac{1}{2}\right)|H|\bar{A}\left(\frac{1}{2},-\frac{1}{2}\right)\rangle = -\frac{\sqrt{2}}{3}\left\{C(2)-C(1)+C(22)-C(11)\right\} \quad (1)$$

$$\langle A\left(\frac{3}{2},+\frac{1}{2}\right)|H|\bar{A}\left(\frac{1}{2},+\frac{1}{2}\right)\rangle = -\frac{\sqrt{2}}{3}\left\{C(2)-C(1)+C(12)-C(11)\right\} \quad (2)$$

These matrix elements involve differences of the fitted parameters and are therefore sensitive to the details of the fit and the validity of the model wave functions. Typical uncertainties can be estimated from the results for Δ. Although percentage uncertainties may be large in some cases, general trends can be identified.

Table 3.6-1. Charge Dependent Matrix Elements (keV)

CORE	λ	C(1)	C(2)	C(11)	C(22)	C(12)	Δ	$\langle +\frac{1}{2}\rangle^a$	$\langle -\frac{1}{2}\rangle^a$	$\langle 2\|0\rangle^b$	$\langle 2\|1\rangle^b$
^{36}Ar	1.3	6911	6857	540	529	363	43	107	30	80	-34
^{32}S	1.0	6372	6372	511	556	383	24	61	-20	71	13
^{28}Si	1.0	5738	5858	572	559	374	11	35	-48	88	63
^{24}Mg	0.8	5047	5169	624	575	377	23	57	-33	100	55
^{20}Ne	0.4	4343	4343	575	609	403	17	80	-16	88	10
^{16}O	0.5	3548	3548	612	622	459	34	71	-4	73	3
^{12}C	1.0	2974	2808	694	707	491	47	158	65	92	-85
^{8}Be	0	1878	1850	793	607	529	70	138	101	81	-70
^{4}He	-1.6	940	940	502	466	306	52	119	22	114	-14

a. $\langle T_z\rangle \equiv \langle A(T=3/2,T_z)|H|\bar{A}(1/2,T_z)\rangle$, MASS = CORE + 5

b. $\langle 2|\Gamma_<\rangle = \langle A(T=2,0)|H|\bar{A}(T_<,0)\rangle$, MASS = CORE + 4

The mixing matrix elements for $T_z = +1/2$ tend to be larger (see Table 1), implying larger neutron decay widths, in agreement with experimental trend 2. This arises because $|C(2)-C(1)|$ is generally small and $C(11) \approx C(22) > C(12)$ as discussed above.

To investigate the influence of charge dependent nuclear forces, fits to the masses were obtained with three additional parameters representing two-particle matrix elements of a charge symmetric nuclear interaction[7] ($V_{pp} = V_{nn} \neq V_{np}$). Slightly improved fits were obtained, but for values of λ within $\pm$ 0.5 of those listed in Table 1, the two-particle-matrix elements were small and changed the calculated mixing matrix elements by less than 30 keV in all cases. Effects of $V_{pp} \neq V_{nn}$ would be already included in the C matrix elements as derived from the masses.

In general, configurations of type B (fig. 3.6-1) for any orbit 3 will have vanishing matrix elements for $T_z = +1/2$, because the neutron configurations are completely different in A and B, but will have finite matrix elements for $T_z = -1/2$. It is therefore appropriate to expect significant proton decay branches to negative parity levels from $T = 3/2$, $T_z = -1/2$ levels, as is observed (trend 4) and to expect ratios of reduced widths for decay to excited states to be different for $T_z = \pm 1/2$ (trend 3) since both $\bar{A}$ and B configurations are mixed into the $T_z = -1/2$ level.

A detailed calculation of isospin forbidden decay widths for these $T = 3/2$ levels requires a knowledge of the average excitation energy of the $\bar{A}$ and B configuration components and of their isospin allowed decay widths for the various channels. Such a calculation is beyond the scope of the present paper, but a simple estimate for neutron decay widths can be made. We assume that the mixing is dominated by the anti-analog configuration, that the analog to anti-analog energy splitting is given by the symmetry potential and that the 2p-2h strength in the ground state of the $A_o + 4$ nuclei is about 25%, so that $\Gamma_n(\bar{A}) \approx (0.25)^2\Gamma$ (single particle).

Then
$$\Gamma_n(\bar{A}) = \left| \frac{\langle A|H|A\rangle\, \Gamma_n^{\frac{1}{2}}(\bar{A})}{E_A - E_{\bar{A}} + i\Gamma_n(\bar{A})/2} \right|^2 .$$

On this basis the theoretical estimates (experimental results[3,8]) for neutron decay widths in eV are: ^{9}Be: 190 (9 ± 8), ^{13}C: 439 (406 ± 115), ^{17}O: 750 (4500 ± 1200), ^{21}Ne: 32(< 1000), ^{25}Mg: 3.7 (13 ± 1.3). The agreement is sufficient to indicate that anti-analog mixing alone could account for the observed neutron widths and their variation with mass.

We cannot account for the very regular $\Delta A = 8$ oscillation observed[4] in the proton decays of the $T = 3/2$ levels to the $A = 4N$ ground states. Since similar oscillations are not seen in the corresponding neutron decays or in the proton decays to 2^+ excited states, the oscillations must be a subtle effect involving the mixing and decay probabilities of $\bar{A}$ and B configurations.

The matrix elements for the mixing of $T = 0$ and 1 anti-analog configurations into the lowest $T = 2$ state of the $A = 4N$ nuclei are also listed in Table 1. Note that the matrix elements for $T = 0$ mixing (necessary for alpha decay) are as large or larger than for $T = 1$ mixing and are comparable to those obtained for $T = 1/2$ or $T = 3/2$ mixing (trends 5 and 1 above).

The parameters of Table 1 can also be used to calculate $\langle A|H^{INC}|\bar{A}\rangle$ for cases where isospin mixing matrix elements have been explicitly derived from experiment. For

$$\langle A(2,+1)|H|\bar{A}(1,+1)\rangle = \frac{1}{2}\big(C(2) - C(1)\big) \qquad (3)$$

in ^{28}Al we obtain 60 keV compared with the experimental result 17 ± 5 keV,[9] which confirms that C(2)-C(1) is relatively small within a major shell. For

$$\langle A(1,0)|H|\bar{A}(0,0)\rangle = \frac{1}{2}\big(C(2)-C(1)+C(12)-C(11)\big) \qquad (4)$$

we obtain: ^{8}Be (-133 keV); ^{12}C (-146 keV); ^{16}O (-171 keV). The extraction of a comparable quantity from the experimental results is somewhat indirect. In addition, a recent paper by Barker[10] emphasizes that the influence of nearby particle thresholds must be properly taken into account. However, the matrix elements we calculate are in reasonable agreement with published experimental values.[11]

We conclude by noting that although the pure isovector one-particle INC matrix elements are substantially larger than the two-particle INC matrix elements, isospin mixing of anti-analog states (see formulae 1 to 4) invariably involves differences of these matrix elements which are of similar size for both types. This explains why analog states in light nuclei, for which anti-analog mixing may be expected to dominate, have comparable isovector and isotensor mixtures.

---

† Colleague at Chalk River Nuclear Laboratories, Atomic Energy of Canada Ltd., Chalk River, Ontario K0 J1 J0, Canada.

1. G. Bertsch and A.Z. Mekjiian, Ann. Rev. Nucl. Sci. 22, 25 (1972).
2. E.G. Adelberger, Proc. Int. Conf. on Nuclear Structure and Spectroscopy Amsterdam, ed. H.P. Blok and E.A.L. Dieperink (Scholar's Press, Amsterdam, 1974) p. 641.
3. A.B. McDonald, *et al.*, Nucl. Phys. A273, 477 (1976).
4. P.G. Ikossi, *et al.*, Nucl. Phys. A274, 1 (1976).
5. R.L. McGrath, *et al.*, Phys. Rev. C1, 184 (1971).
6. S.J. Freedman, *et al.*, to be published.
7. R. Sherr, Phys. Rev. C16, 1159 (1977).
8. H. Weigmann, R.L. Macklin, and J.A. Harvey, Phys. Rev. C14, 1328 (1976).
9. P.A. Dickey, E.G. Adelberger, and J.E. Bussoletti, to be published.
10. F. Barker, Aust. J. Phys. 31, 27 (1978).
11. F.C. Barker, Nucl. Phys. 83, 418 (1966); E.G. Adelberger, *et al.*, Phys. Rev. C15, 484 (1977); G.J. Wagner, *et al.*, Phys. Rev. C16, 1271 (1977).

4. RADIATIVE CAPTURE

4.1 Polarized Proton Radiative Capture into ^{16}O Below the Giant Dipole Resonance

K. A. Snover, P. G. Ikossi, L. Stokes, T. A. Trainor, and R. Helmer†

Recent studies[1,2] in this Laboratory of the $^{15}N(\vec{p},\gamma)^{16}O$ reaction indicated that the measured angular distributions in the incident proton energy region of 8 - 18 MeV can be described as due mainly to E1 radiation with a small E2 contribution. However, the angular distributions at 7.07 and 7.57 MeV could not be fitted under the assumption that only E1 and E2 radiations were present. This result prompted our study of the $^{15}N(\vec{p},\gamma)^{16}O$ reaction below the giant dipole resonance to look for possible M1 contributions in the region of $E_p \sim 7$ MeV. M1 decays to the ground state of ^{16}O are particularly interesting since the independent particle shell model, the doubly magic ^{16}O ground state can have essentially no M1 excitations.

We have measured angular distributions of the γ-rays to the ^{16}O ground state for the $^{15}N(\vec{p},\gamma)^{16}O$ reaction using a polarized proton beam ($P_b \sim 0.7$) at proton energies 6.8, 6.97, 7.10, 7.25, 7.40, 7.70 and 7.75 MeV. The measured cross-section angular distributions are asymmetric around 90° indicating considerable E2 or M1 radiation. In addition the analyzing powers at 90° deviate considerably from zero. Least squares fits to these data under the assumption that only E1 and E2 radiation are present fail to reproduce these distributions. In fact the reduced χ^2 is ≈ 50 at 7.10 MeV and has a resonance-like behavior centered near this energy with a width of 150 - 300 keV. Including M1 contributions on the same general footing as E1 and E2 increases the number of unknowns beyond the number of determined a_i and b_j coefficients. Nevertheless fits assuming constant E2 amplitudes near 7.1 MeV together with arbitrary M1 amplitudes but with the M1 phases restricted to follow a resonance-like behavior permit good χ^2 fits. A crude estimate of the M1 strength obtained in this manner yields $\Gamma_\gamma \gtrsim 5$ eV (where the inequality results from $\Gamma_p \lesssim \Gamma$) which is comparable to that of the 16.22 1^+ T=1 state.[3] For a rough comparison, this corresponds to a reduced M1 strength $\gtrsim 6\%$ of the strength of the strong $15.1 \rightarrow 0.0$ M1 decay in ^{12}C.

However further work is necessary to prove the uniqueness of this result. The failure to reproduce the data around 7.1 MeV assuming only E1 and E2 radiations unambiguously indicated the presence of M1 contributions. Nevertheless it is not necessarily true that the resonance-like behavior of the χ^2 is due to an M1 resonance and not to a constant M1 contribution which accidentally becomes evident at these energies due to the particular phases of the s-d E1 amplitudes in this energy region.

In order to further investigate this problem we have measured excitation functions in the energy region 6.0 - 9.0 MeV in 100 keV steps (Fig. 4.1-1). Preliminary analyses of these data indicate that the major features could be qualitatively accounted for by E1 resonances and slowly varying E1 and E2 backgrounds. The simultaneous analysis of the angular distribution data together with the excitation functions in a manner where the amplitudes and phases are restricted to have a resonance energy dependence plus a smooth

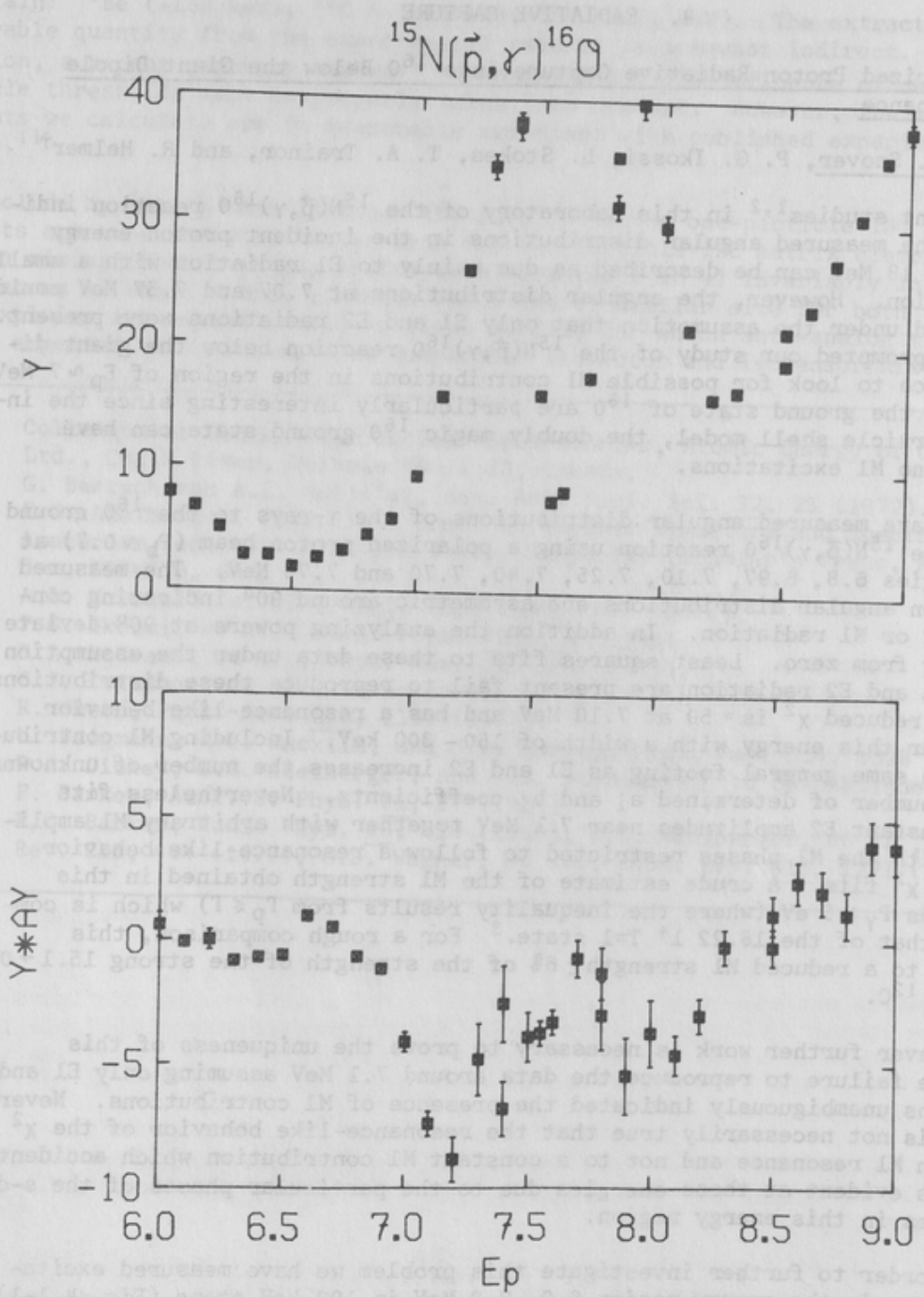

Fig. 4.1-1. Excitation function at $\theta = 90°$ for the $^{15}N(\vec{p},\gamma)^{16}O$ reaction (arbitrary normalization). Top half: cross-sections; bottom half: cross-section times analyzing power.

background is under way. This minimizes the number of variables and would perhaps clarify the nature of the M1 contribution.

---

† Chalk River Nuclear Laboratories, AECL, Chalk River, Ontario, Canada.

1. Nuclear Physics Laboratory Annual Report (1977) p. 43.
2. J.E. Bussoletti, Ph.D. Dissertation, University of Washington (1978).
3. F.A. Jzenberg-Selove, Nucl. Phys. A281, 1 (1977).

4.2 The Absolute Strength of the $E_x = 13.02$ MeV Resonance in $^{16}C(\alpha,\alpha_o)^{16}O$

K. A. Snover, P. Ikossi, and H. C. Bhang

A recent study[1] of the charged particle decay of the isoscalar giant quadrupole resonance in ^{16}O in an $^{16}O(\alpha,\alpha'c)$ coincidence experiment permits a direct comparison with model-independent E2 strength determined in the $^{12}C(\alpha,\gamma_o)$ ^{16}O reaction[2] since, in the coincidence experiment, the α_o decay channel has been studied. Of particular interest is the 2^+ state near $E_x = 13.0$ MeV which appears to be of the order of a factor of 3 stronger in (α,γ) compared to $(\alpha,\alpha'\alpha_o)$. Because of the possibility that the original $^{12}C(\alpha,\gamma_o)$ measurements may have suffered from energy averaging effects due to $t \gtrsim \Gamma$ where t is the energy loss in the target and Γ is the resonance width, we have remeasured angular distributions in the vicinity of this resonance using a thin target. Analysis of these data is presently in progress.

---

1. K.T. Knopfle, G.J. Wagner, P. Paul, H. Brever, C. Mayer-Boricke, M. Rogge, and P. Turek, preprint.
2. K.A. Snover, E.G. Adelberger, and D.R. Brown, Phys. Rev. Letts. 32, 1061 (1974).

4.3 Fast Neutron Radiative Capture

K. Aniol, E. Arthur†, D. Drake†, M. Drosg†, I. Halpern, and L. Nilsson†

We have pointed out in earlier reports that fast neutron radiative capture is a particularly suitable tool to explore the location of E2 strength in nuclei. As in radiative proton capture, one meaures the forward-backward asymmetry of the photon distribution to pick up the dipole-quadrupole interference. The advantage of neutron capture over proton capture is that there is no *direct* quadrupole amplitude for neutrons and that any observed asymmetry can therefore be ascribed to an E2 excitation of the entire nucleus. That is, one does not have a large and somewhat uncertain asymmetry to subtract in extracting the quantity of interest.

The disadvantage of using neutrons stems mainly from the fact that they are a secondary and therefore relatively weak beam. Nonetheless, it is possible, with large NaI detectors and modern techniques for suppressing background, to measure front-back asymmetries well enough to determine asymmetry coefficients when they are not too small. In collaboration with D. Drake and his

coworkers in the Los Alamos neutron physics group we have had a run on (n,γ_0) in ^{208}Pb using the d+d reaction to provide neutrons up to 19 MeV. This work extends the work in a run at lower neutron energies using protons on tritium.

The counting statistics are still fairly poor. In Fig. 4.3-1 we show preliminary results for the ground state transition to ^{209}Pb. The curve in the figure is the expected asymmetry for an E2 isovector resonance at 23 MeV assuming a strength consistent with sum rules and a width of 4 MeV. The calculated curve shows that if the E2 isovector resonance is not significantly broader than the E1 resonance one should be able to detect it easily by measuring the asymmetry at neutron energies from say 20 to 25 MeV. We plan to make such measurements just as soon as adequate pulsing of the ion source becomes available at Los Alamos with 3 stage operation of the tandem facility.

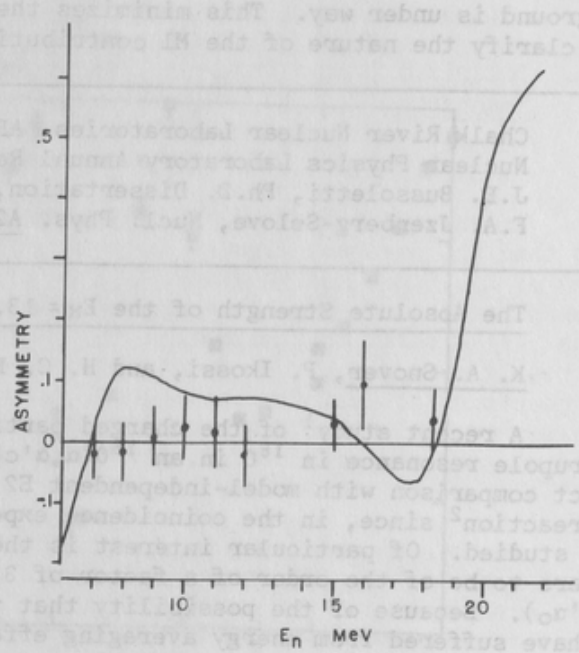

Fig. 4.3-1. Preliminary results for the front to back (55° to 125°) asymmetry in (n,γ_0) on ^{208}Pb. The curve is the theoretical expectation if there is a narrow isovector E2 resonance at 23 MeV.

† Coworkers at the Los Alamos tandem facility.

5. REACTIONS WITH POLARIZED PROTONS

5.1 Inelastic Scattering of Polarized Protons on ^{206}Pb

N. L. Back, J. G. Cramer, T. A. Trainor, and R. Von Lintig

Much experimental and theoretical work has been done on isobaric analog resonances (IAR's) in the lead region. Most recently, in experiments at this Laboratory, polarized protons have been used to measure the analyzing power in the elastic scattering on ^{206}Pb and ^{207}Pb near the $3p_{1/2}$ IAR[1] and on ^{208}Pb over all the single-particle IAR's.[2] These measurements demonstrated the advantages of this method in extracting accurate elastic partial widths. These advantages can be seen by considering the form of the cross section and analyzing power when "direct" (non-resonant) and resonant processes are both important:

$$\sigma = \sigma(\text{direct}) + \sigma(\text{interference}) + \sigma(\text{IAR}) \quad (1)$$

$$\sigma A = \sigma A(\text{direct}) + \sigma A(\text{interference}) \quad (2)$$

There is no $\sigma A(\text{IAR})$ for an isolated resonance, since the analyzing power is identically zero whenever only one partial wave is present in the entrance channel.[3] Therefore, for sub-Coulomb elastic scattering or for inelastic scattering to collective states, the analyzing power will be the sum of the interference term and a small, slowly-varying background term. Furthermore, since the interference term is linear in the resonance amplitude, a measurement of the analyzing power can be used to determine both the magnitude and the phase of the partial width.[1]

Because of the vanishing of $\sigma A(\text{IAR})$, this method is applicable only where the off-resonance cross section is large. This is the case for the first 2^+, 3^-, and 5^- states of the even lead isotopes, and for the states in the odd isotopes which consist of a single particle weakly coupled to these states. Previous measurements of the inelastic scattering to the first 3^- and 5^- states of ^{208}Pb have shown that the analyzing power is large and has a large resonant enhancement.[4] For the first 4^- state, on the other hand, the analyzing power is near zero.

An attempt was made to measure the analyzing power in inelastic proton scattering on ^{206}Pb. The University of Washington Lamb-shift polarized ion source was used; it was operated in the Sona scheme, and produced a beam of about 30 nA with a polarization of 73%. The scattered particles were detected by two pairs of symmetrically-placed Si(Li) detectors, separated by 30°. A ^4He polarimeter was used to continuously monitor the beam polarization. Two already-existing targets of isotopically-enriched ^{206}Pb were used. Unfortunately, these proved to be inadequate because of their thickness and contamination. The thinner of the two targets was approximately 1.0 mg/cm^2 thick, and this contributed to the poor resolution that was observed. This target contained, in addition to carbon and oxygen, another contaminant which appeared to be chlorine. At 12.2 MeV (the energy of the $3p_{1/2}$ IAR), the chlorine peak masked the peak of interest, which was the 2^+ first excited state (0.803 MeV) of ^{206}Pb.

More experimental runs are planned, using new, thinner targets of ^{206}Pb and ^{208}Pb, and with more emphasis placed on improving the resolution.

1. N.L. Back, M.P. Baker, J.G. Cramer, and T.A. Trainor, Phys. Rev. C (to be published).
2. M.P. Baker, J.S. Blair, J.G. Cramer, E. Preikschat, and W. Weitkamp, in *Proceedings of the Fourth International Symposium on Polarization Phenomena in Nuclear Reactions*, ed. W. Grüebler and V. König (Birkhäuser Verlag, Basel, 1976) p. 781.
3. H.L. Harney, Phys. Lett. 28B, 249 (1968).
4. H.L. Harney, P. von Brentano, E. Grosse, J.L. Escudie, J.C. Faivre, P. Foissel, J. Gosset, B. Mayer, and L. Papineau, Nucl. Phys. A145, 282 (1970).

5.2 Measurement of Depolarization in the Continuum Portions of Particle Emission Spectra

W. Bartholet, H. C. Bhang, I. Halpern, T. A. Trainor, and W. G. Weitkamp

The depolarization paramater D, also denoted $K_y^{y'}$, is essentially the ratio of outgoing particle polarization to incident beam polarization. It has been measured in a few cases for proton elastic and inelastic scattering to discrete states in nuclei. In most cases the measured value of D is close to unity, i.e., spin flip forces have little effect. However, for inelastic scattering in which protons are emitted from the compound nucleus by the evaporation process, the depolarization ought to be near zero even in the presence of spin-flip forces because the average polarization of the protons in the nucleus, any one of which might be emitted, is approximately zero. In the preequilibrium region between inelastic scattering to discrete states and evaporation, the degree of depolarization should change with excitation energy, and may shed some new light on the inelastic scattering process.

We have investigated the feasibility of measuring D in inelastic scattering to the preequilibrium and evaporation regions. Measurements of D necessarily involve double scattering with a polarized incident beam. Thick targets, large solid angles and an intense polarized beam are required to obtain acceptable counting rates. Neutron-induced background must be minimized. We have built a prototype polarimeter, using elastic scattering from ^{4}He as the analyzing reaction. A large solid angle proportional counter-silicon detector telescope has been used to reduce background. Tests indicate that this geometry, with some refinements, together with available polarized proton beam intensities, can be used to make reasonable measurements.

5.3 Analyzing Power in the Continuum Portions of Particle Spectra

H. Bhang, J. S. Blair, I. Halpern, W. Lynch, and T. A. Trainor

During the past year we have perfected several techniques required for this experiment, extended the data set for $^{63}Cu(\vec{p},p)^{63}Cu$ over a greater angular range, and have observed some striking regularities in the differential analyzing power above 6 MeV excitation in the residual ^{63}Cu.

Subtraction of impurity contributions to the particle spectra is a subtle problem when small polarization asymmetries are to be measured. The subtraction technique described in last year's report[1] combined with left-right particle-telescope pairs better matched for energy resolution and use of 50% thicker ΔE detectors has resulted in subtracted spectra free of artifacts at levels well below the observed analyzing powers. Subtraction of oxygen peaks was accomplished by a combination of spectra from Ta and Ta_2O_5 targets. These spectra and those for a carbon target were obtained at each angle. Since the oxygen and carbon lines are sharp in the spectral regions where the spectra from

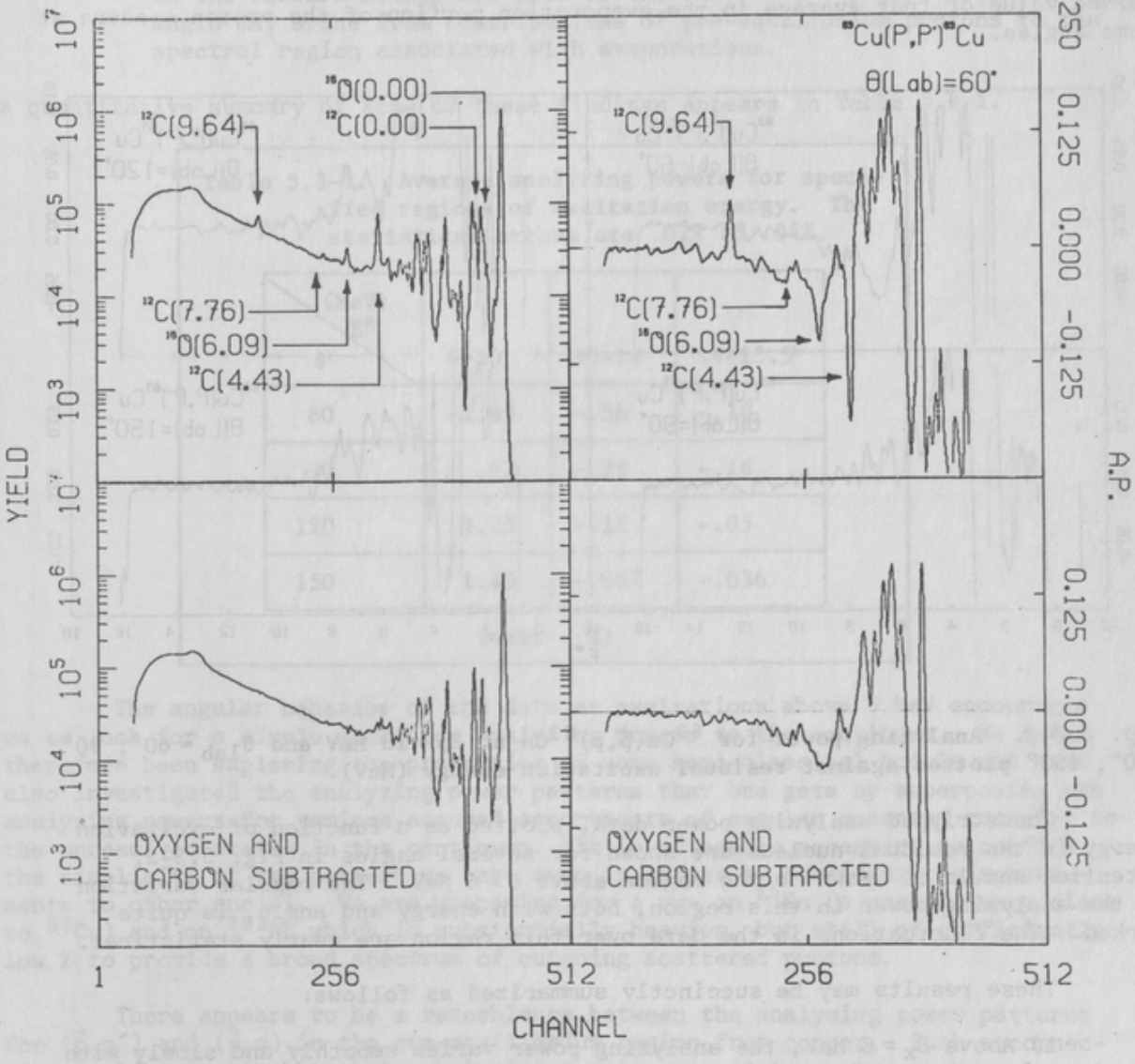

Fig. 5.3-1. Analyzing-power and yield spectra for $^{63}Cu(\vec{p},p)^{63}Cu$ at Ep = 18 MeV and $\theta_{lab} = 60°$.

copper are continuous, they can be used as gain shift monitors when they are corrected for the kinematic shifts with angle. A comparison of spectra with and without impurity contributions is shown in Fig. 5.3-1.

The data set has been extended to more angles. Data are now available for $\theta_{lab} = 30°$, 45°, 60°, 90°, 120° and 150°. Data taken before installation of the rapid spin-reversal system in the polarized ion source have been set aside because of the superiority of the new system in terms of demonstrated freedom from false asymmetries. The statistical errors of the average analyzing power have been reduced to the extent that they are now ten times less than the observed value of that average in the evaporation portion of the proton spectra at some angles.

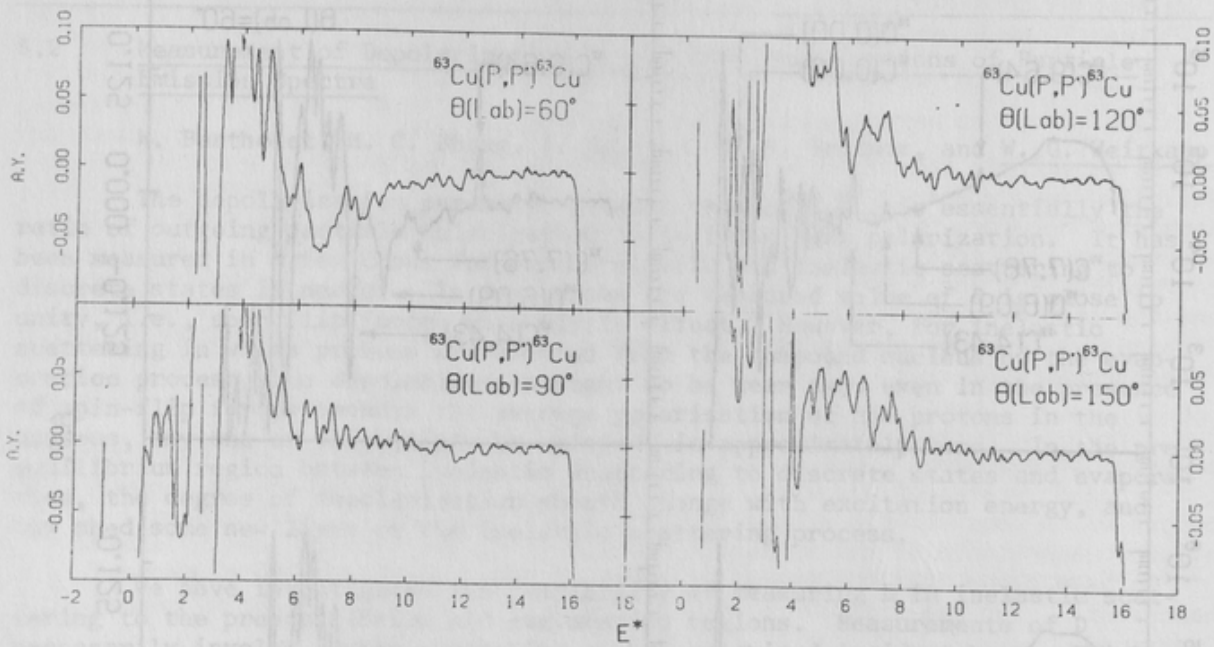

Fig. 5.3-2. **Analyzing power for $^{63}Cu(\vec{p},p)^{63}Cu$ at Ep = 18 MeV and $\theta_{lab} = 60°$, 90°, 120°, 150° plotted against residual excitation energy (MeV).**

The stripped analyzing power data, plotted as a function of excitation energy in the residual nucleus are shown for several angles in Fig. 5.3-2. Attention should be drawn to the region above $\theta = 6$ MeV. The regular variation of the analyzing power in this region, both with energy and angle, is quite marked. The fluctuations in the data over this region are nearly statistical.

These results may be succinctly summarized as follows:

1) Above $E_x = 6$ MeV, the analyzing power varies smoothly and slowly with angle and with excitation energy, i.e., the fluctuations tend to be small compared with average values.

2) The analyzing power in this higher excitation region is negative in

the forward hemisphere and positive in the back hemisphere. (In particular, it does not oscillate nearly as much as the analyzing power to a residual state of definite spin and parity.)

3) The analyzing power decreases from levels near 5% to very small values as the reaction Q is decreased, i.e., as the residual excitation energy increases.

4) The analyzing power in the evaporation region of the spectrum (-Q = 12 to 16 MeV) is uniformly negative with somewhat larger magnitude ($\sim\frac{1}{4}$%) in the forward hemisphere than in the back one. This variation with angle may arise from contributions of pre-equilibrium protons to the spectral region associated with evaporations.

A quantitative summary of some of these findings appears in Table 5.3-1.

Table 5.3-1. Average analyzing powers for specified regions of excitation energy. The statistical errors are .02% to .04%.

θ \ E* (MeV)	6-10	10-14	14-15.5
60	-2.65	-.58	-.18
90	.63	-.25	-.16
120	1.25	-.12	-.05
150	1.43	-.067	-.036

(unit: %)

The angular behavior of the data at excitations above 6 MeV encourages us to look for a simple model for analyzing powers to the continuum. We have therefore been exploring the properties of some semi-classical models and have also investigated the analyzing power patterns that one gets by superposing the analyzing powers for various assumed assortments of angular momentum transfer to the unresolved states in the continuum. It is of course necessary to confirm the simplicity of the pattern we have seen in copper by extending the measurements to other nuclei. We are preparing for a run on ^{64}Zn (a nuclide very close to ^{63}Cu) and on ^{103}Rh which is substantially heavier, but still of sufficiently low Z to provide a broad spectrum of outgoing scattered protons.

There appears to be a resemblance between the analyzing power patterns for $(\vec{p},p')$ and $(\vec{p},\alpha)$ in the pre-equilibrium region from copper. Such a connection would suggest that these analyzing powers are mainly entrance channel effects. The comparison of analyzing powers for different outgoing particles will certainly be pursued.

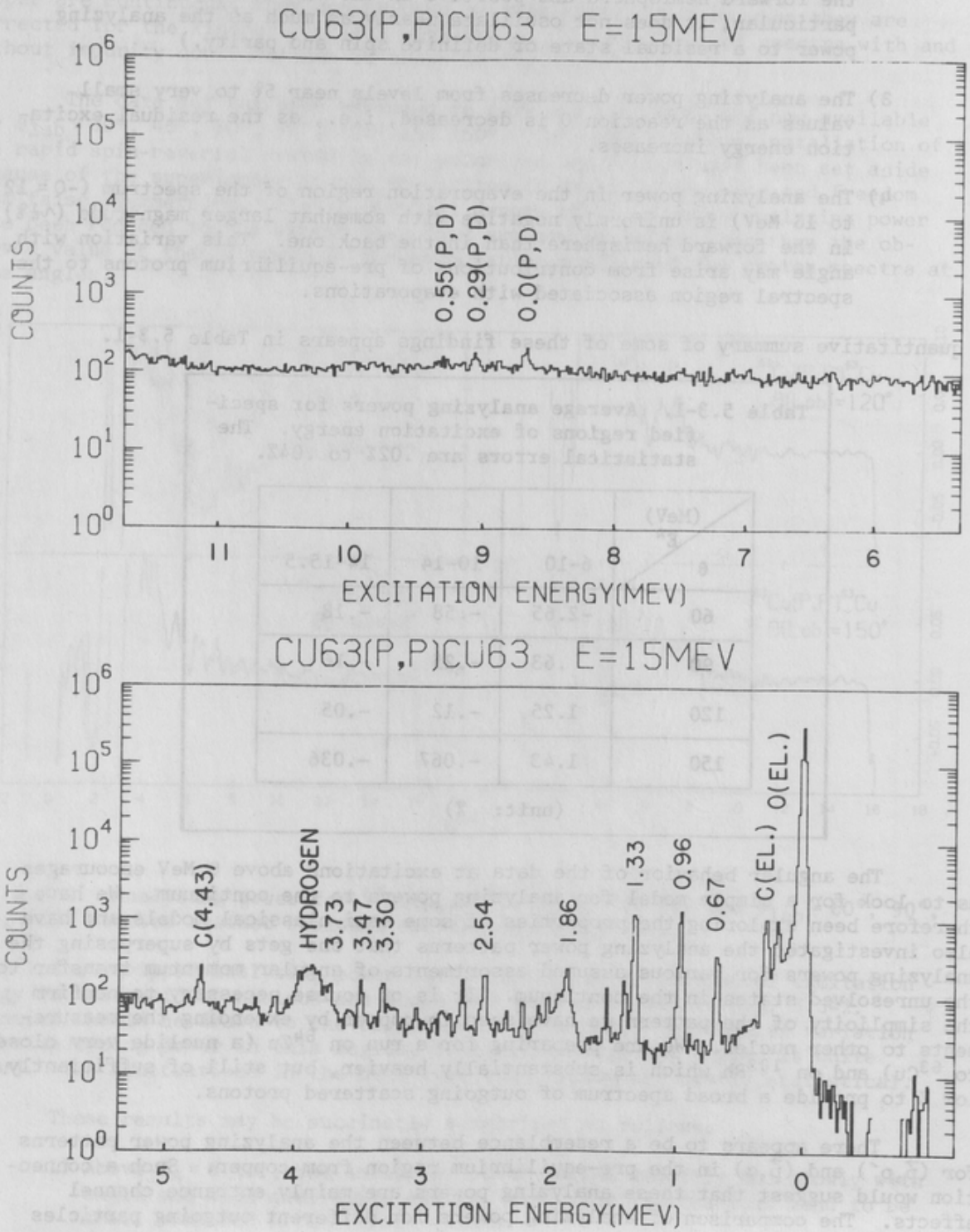

Fig. 5.3-3. Yield spectrum for $^{63}Cu(p,p')^{63}Cu$ at Ep = 15 MeV and at $\theta_{lab} = 45°$.

The investigation of the higher excitations in copper has recently been complemented with studies of lower resolvable states or groups of states. Any model parameters to be used in accounting for the continuum observations should adequately describe levels of known spin and parity. The first goal was to see at what rate with increasing excitation energy the levels tend to merge and become unresolvable. To maintain adequate resolution, the telescope was replaced with a single high-resolution solid-state detector and the beam was carefully collimated to produce clean spectra. A brief development period resulted in uncooled detector resolutions with a Ta target of 18-20 keV (about 5 to 6 times better than that of the telescope) and an elastic peak to slit-scattered background ratio of about 5000. A p,p′ spectrum obtained from ^{63}Cu at 15 MeV is shown in Fig. 5.3-3. The stronger levels have been labeled with their excitation energy. They generally agree with previous observations. It is seen that the levels become unresolved by excitations of around 5 MeV. At higher energies, the fluctuations around the mean are roughly those expected on the basis of the statistics of the numbers of counts observed.

---

1. Nuclear Physics Laboratory Annual Report, University of Washington (1977) p. 66.

---

6. HEAVY ION INDUCED REACTIONS

6.1 Coincidence Study of the $^{27}Al(^{16}O,^{12}C\alpha)^{27}Al$ Reaction at 65 MeV

W. G. Lynch, R. Puigh, A. Seamster, M. B. Tsang, and R. Vandenbosch

In recent years, particle-particle coincidence techniques have been used as a tool to investigate the time scale and mechanism by which energy is transferred into internal degree of freedom in deeply inelastic reactions[1-5]. In a recent publication,[2] Harris *et al.* reported the results of their investigation of the $^{27}Al(^{16}O,^{12}C\alpha)^{27}Al$ reaction at 65.6 MeV with coincidence techniques. The α-carbon angular correlation showed a guassian shaped distribution peaked along the recoil direction of $^{31}P^*$, $E^* \sim 14.5$ MeV. The angular correlation was not symmetric with respect to the plane perpendicular to the recoil direction as would be expected for evaporation from $^{31}P^*$. Harris *et al.* interpreted the reaction mechanism as predominantly pre-equilibrium decay from a ^{31}P intermediate. In view of the surprisingly sharply focused angular correlation along the recoil direction and the absence of any indication of an evaporation component at backward directions we decided to explore this system further with a particular emphasis on improving the ability to detect low energy alphas in the backward direction. In the course of this work, we have repeated the previous measurement at forward angles. Our results differ significantly from theirs.

The experiment was performed by bombarding ^{27}Al with 65 MeV ^{16}O from our FN tandem Van de Graaff. The self-supporting 0.7 mg/cm^2 ^{27}Al foil was produced by evaporation of 99.999% pure ^{27}Al wire. Carbon and alpha particles were detected in coincidence with a two telescope system. The carbon telescope, fixed at 30° and consisting of 17.3μ - 300μ ΔE-E Si detectors, subtended a solid angle of ∿8 msr. In order to increase the efficiency of detecting low energy alpha particles at backward angles, two ΔE-E telescope systems were used to detect alpha particles. For the backward angles past -90° and +60° (∓ indicates the opposite side of the beam from the C-telescope), we used a 5μ - 300μ ΔE-E telescope subtending a solid angle of ∿5 msr. For more forward angles, 8.7μ - 300μ thick ΔE-E Si detectors subtending a solid angle of 1.5 msr were used. The α-telescope was moved in the reaction plane defined by the beam axis and the C-telescope.

^{16}O and ^{12}C contaminants in the targets were determined by studying the elastic scattering of 3 MeV protons at backward angles. These elements were shown to be originally present in less than 1% atomic abundance. Events from $^{12}C(^{16}O,^{12}C\alpha)$ reaction are kinematically distinguishable from events corresponding to $^{27}Al(^{16}O,^{12}C\alpha)$ reactions. As a check on possible effects due to carbon buildup during the experiment, we bombarded a carbon target at a

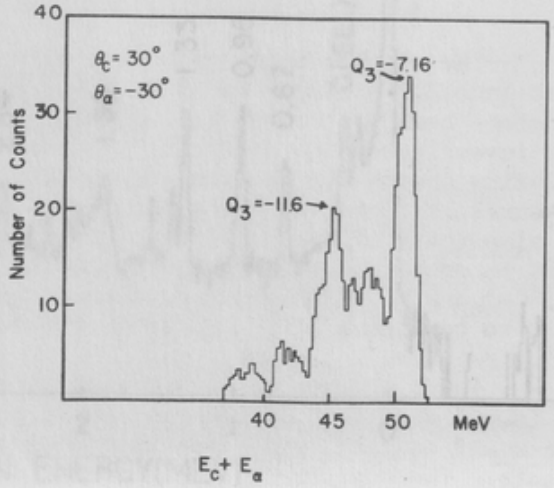

Fig. 6.1-1. Total energy spectrum of $^{27}Al(^{16}O,^{12}C\alpha)$ at $\theta_\alpha = -30°$, $\theta_C = 30°$.

forward alpha angle ($\theta_\alpha^{lab} = 30°$). We conclude that although carbon buildup was significant, its effect is negligible in the region of the peak corresponding to those events leaving ^{12}C and ^{27}Al in their ground states.

In our data analysis, we assume a 3-body final state of $^{27}Al + ^{26}O \rightarrow ^{12}C + \alpha + ^{27}Al(g.s.) + Q_3$. The two peaks observed in the total energy spectrum (Ec+Eα) kinematically correspond to ground state of carbon with $Q_3 = -7.16$ MeV and 4.43 (2^+) state of carbon with $Q_3 = -11.59$ MeV (Fig. 6.1-1). The valley between the peak is probably filled with events that correspond to residual excited states of ^{27}Al and the contributions from $^{12}C(^{16}O,^{12}C\alpha)$ and $^{16}O(^{16}O,^{12}C\alpha)$ events.

In contrast to the previous report, we do not find the most probable excitation energy of $^{31}P^*$ to be independent of lab detection angle. In Fig. 6.1-2, we show the most probable ^{31}P excitation energy corresponding to events

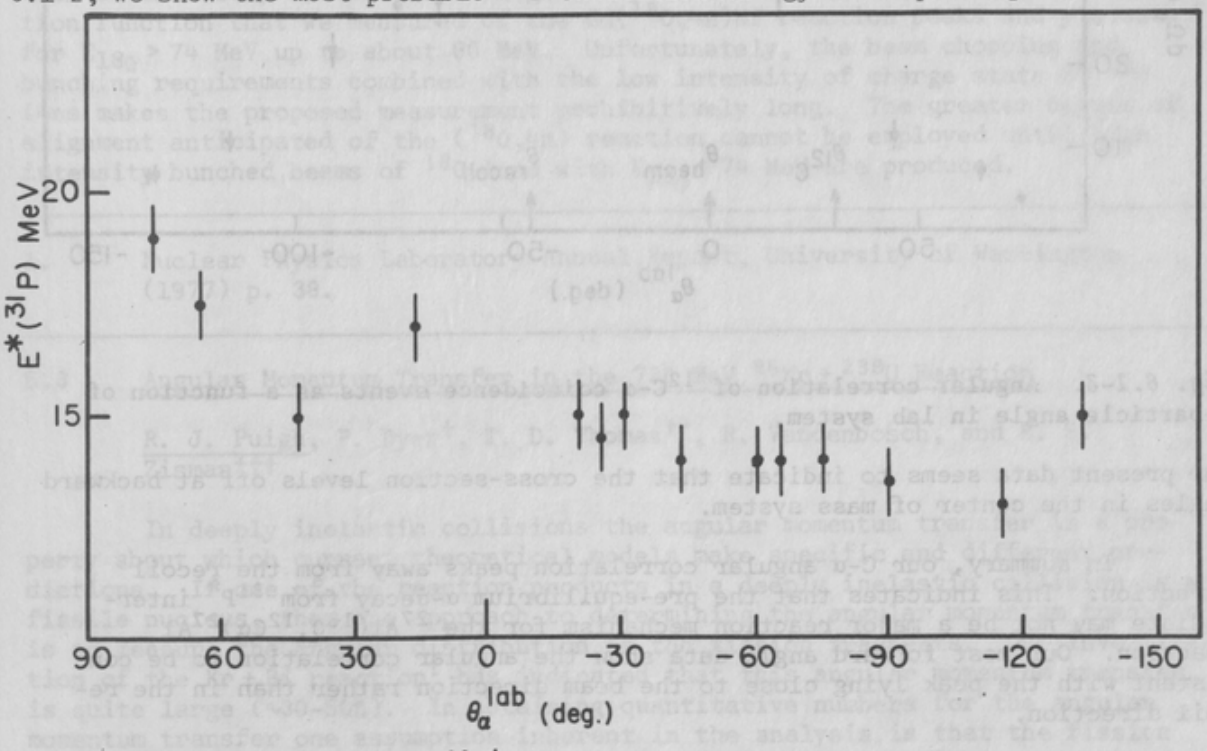

Fig. 6.1-2. Most probable $^{31}P^*$ energy for events corresponding to ground state ^{12}C ($Q_3 = -7.16$ MeV) as a function of α-particle lab angle.

with $Q_3 = -7.16$ MeV for different measured lab angle. For $\theta_\alpha^{lab} = 65°$ and 75°, the most probable excitation energy of ^{31}P is about 4 MeV higher than those observed in other angles.

The angular correlation of events with $Q_3 = -7.16$ MeV are shown in Fig. 6.1-3. The data are plotted in the lab system and show a strong forward peak towards the incident beam direction rather than at the recoil direction ($\theta_\alpha^{lab} = 43°$) of the $^{31}P^*$ intermediate as reported previously. Even with a 5μ-300μ ΔE-E Si telescope at the backward angle, we still encountered some slight cut off of low energy alphas at the most backward angle measured ($\theta_\alpha^{lab} = -133°$).

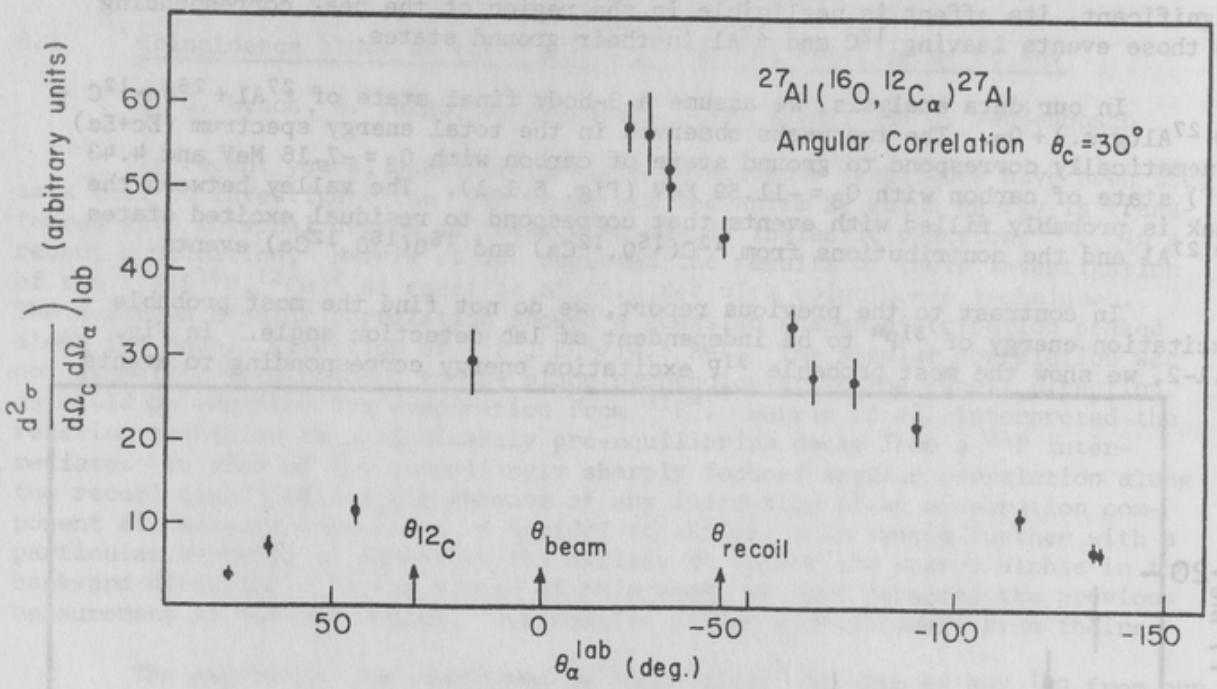

Fig. 6.1-3. Angular correlation of ^{12}C-α coincidence events as a function of α-particle angle in lab system.

Our present data seems to indicate that the cross-section levels off at backward angles in the center of mass system.

In summary, our C-α angular correlation peaks away from the recoil direction. This indicates that the pre-equilibrium α-decay from $^{31}P^*$ intermediate may not be a major reaction mechanism for the $^{27}Al(^{16}O,^{12}C\alpha)^{27}Al$ reaction. Our most forward angle data show the angular correlation to be consistent with the peak lying close to the beam direction rather than in the recoil direction.

1. D.C. Slater, J.R. Hall and J.R. Calarco, B.A. Watson and J.A. Becker, Phys. Rev. Lett. 33, 784 (1974).
2. J. Harris, T.M. Cormier, D.F. Geesaman, L.L. Lee Jr., R.L. McGrath, and J.P. Wurm, Phys. Rev. Lett. 38, 1460 (1977).
3. H. Ho, R. Albrecht, W. Dunnweber, G. Graw, S.G. Steadman, J.P. Wurm, D. Disdier, V. Rauch, and F. Scheibling, Z. Physik A283, 238 (1977).
4. C.K. Gelbke, M. Bini, C. Olmer, D.L. Hendrie, J.L. Laville, J. Mahoney, M.C. Mermaz, D.K. Scott, and H.H. Wieman, Phys. Lett. 71B, 83 (1977).
5. T. Shimoda, M.G. Ishihara, H. Kamitsubo, T. Motobayashi, and T. Fukuda, preprint.

6.2 Assessment of the Gd(^{18}O,4n) Hf Reaction as a Means of Producing Aligned Isomeric States

K. Aniol, D. Chiang, B. Cuengco, R. Puigh

The isomeric states in ^{174}Hf discussed in last year's annual report[1] were again studied with the hope of obtaining the electric quadrupole moment of the 180 nsec 6^+ state at 1.549 MeV. Time differential measurements with NaI detectors at 0° and 90° did not produce discernible oscillations in the gamma ray intensity when the 1.549 MeV state was produced in the ^{175}Lu(p,2n)^{174}Hf reaction.

A possible cause for the absence of oscillations in the time distribution of the decay is the small alignment produced in the reaction. An excitation function that we measured of the Gd(^{18}O,4n)Hf reaction peaks and plateaus for $E_{^{18}O} > 74$ MeV up to about 80 MeV. Unfortunately, the beam chopping and bunching requirements combined with the low intensity of charge state 8^+ ^{18}O ions makes the proposed measurement prohibitively long. The greater degree of alignment anticipated of the (^{18}O,4n) reaction cannot be employed until high intensity bunched beams of ^{18}O ions with $E_{^{18}O} > 74$ MeV are produced.

---

1. Nuclear Physics Laboratory Annual Report, University of Washington (1977) p. 38.

6.3 Angular Momentum Transfer in the 730 MeV ^{86}Kr + ^{238}U Reaction

R. J. Puigh, P. Dyer†, T. D. Thomas††, R. Vandenbosch, and M. S. Zisman†††

In deeply inelastic collisions the angular momentum transfer is a property about which current theoretical models make specific and different predictions. If one of the reaction products in a deeply inelastic collision is a fissile nucleus, then one approach to determining the angular momentum transfer is to measure the angular distribution of the fission fragments. Our investigation of the Kr + Bi reaction[1] has indicated that this angular momentum transfer is quite large (∿30-50ħ). In obtaining quantitative numbers for the angular momentum transfer one assumption inherent in the analysis is that the fission process is sequential. Instantaneous fission is another possible mechanism in these reactions. Because of the high fission barrier associated with Bi-like nuclei we have assumed sequential fission to be the predominant mechanism for the Kr + Bi reaction. The Kr + U reaction was investigated in the hope of observing some evidence for instantaneous fission since uranium-like nuclei have much lower fission barriers. Kinematically it is not possible to differentiate between sequential and instantaneous fission; however, it was hoped that the fission fragment angular correlations might give some evidence for this type of reaction mechanism.

A 730 MeV Kr beam from the LBL Super-HILAC was incident on a 200 μg/cm^2 ^{238}U target mounted on a 50 μg/cm^2 carbon backing. A semi-conductor counter telescope was fixed at 35° (lab) and used to measure the charge and energy loss

associated with the Kr-like particles. Two semi-conductor detectors were placed at different angles on the other side of the beam to measure the fission fragments. One of these detectors could be moved above the reaction plane (defined by the beam direction and the counter telescope). Conventional electronics were used to shape and handle the signals from the detectors to produce linear signals for the counter telescope, ΔE and E, and for each of the fission fragment detectors, $E_F^{(i)}$ $(i = 1,2)$. Timing signals from the telescope's stopping counter and each of the fission fragment detectors were input into time-to-pulse-height converters (TAC's) in order to differentiate real from random coincident events. An event was then characterized by four linear signals, ΔE, $\Delta E + E$, $E_F^{(i)}$ and $TAC^{(i)}$, which were digitized and recorded event by event on magnetic tape. In a two-dimensional array of counts versus telescope energy ($\Delta E + E$) and fission fragment energy ($E_F^{(i)}$) the events of interest were well separated from other coincident events.

Theoretically, if one neglects the spins of the projectile and target, then the shape of the angular correlation of fission fragments with respect to a space fixed Z axis (chosen here normal to the reaction plane) is given by

$$W(\theta) \alpha \sum_{J=0}^{\infty} \sum_{M=-J}^{J} \sum_{K=-J}^{K} P(J)P(M)P(K)W^{J}_{M,K}(\theta) ,$$

where

$$W^{J}_{M,K}(\theta) = \frac{2J+1}{2} \left| d^{J}_{M,K}(\theta) \right|^2$$

gives the shape of the fission fragment angular correlation in the center of mass frame of fissioning nucleus whose transition state quantum numbers are J, M, and K.[2] The angle θ is between the space fixed Z axis and the nuclear symmetry axis, and the $d^{J}_{M,K}(\theta)$ functions are the rotational wavefunctions. The weighting factor P (K) reflects the distribution of K states for the fissile nucleus at its saddle point. A Gaussian distribution of K states is predicted for this distribution by the liquid drop model with K_o^2 charecterizing the width of the distribution. This width, K_o^2, is strongly dependent upon the charge and excitation energy of the fissile nucleus; therefore, experimental values of K_o^2 obtained from light ion compound nucleus reactions have been used in our calculations. The weighting factor P(M) depends upon the details of the interaction between the two colliding nuclei. Since experimental evidence exists for strong alignment[1,3] and since the calculation of the rotational wave functions becomes time consuming when $M \neq J$, the following simplification in our calculations has been made. The shape of the $M = J$ angular correlation is taken from the $d^{K}_{J,K}(\theta)$ rotational wavefunction and a classical prescription is then used to account for components of $M = J$. The spin vectors for the fissile nucleus are assumed to have a Gaussian distribution in the plane perpendicular to the recoil direction of the fissile nucleus. The shape of the angular correlation is then given by

$$P(\theta,\phi) = \int_o^{2\pi} \exp\left(-\frac{\alpha^2}{2\alpha_o^2}\right) W(\theta')d\alpha ,$$

where α is the angle between the spin vector and the fixed Z axis and θ' is the angle between the spin direction and the nuclear symmetry axis. The spreading width parameter α_o is proportional to the width of the M distribution; hence it

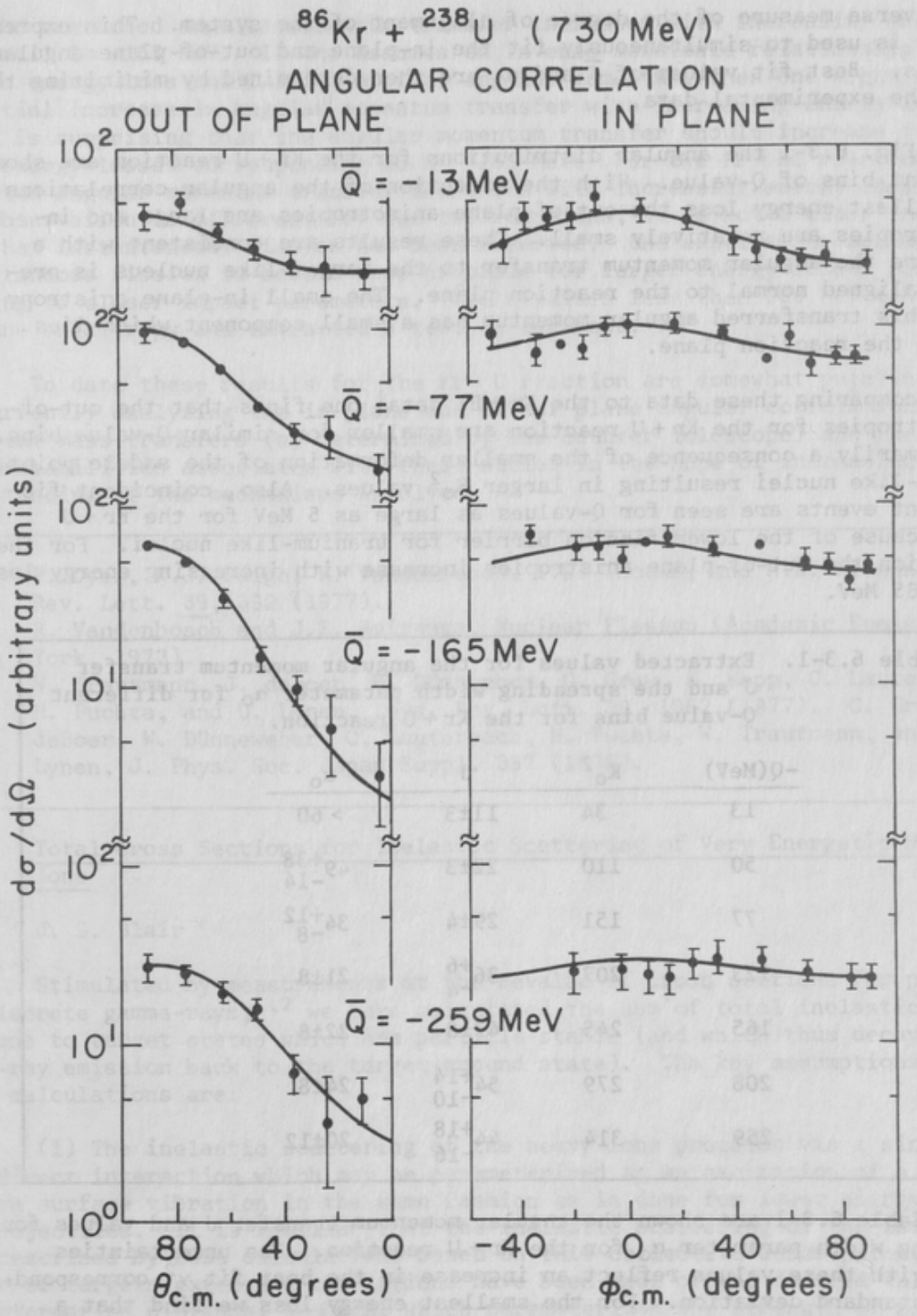

Fig. 6.3-1. In-plane and out-of-plane fission fragment angular correlations for different bins of Q-value. The solid curves represent best fit theoretical calculations.

gives an inverse measure of the degree of alignment of the system. This expression $P(\theta,\phi)$ is used to simultaneously fit the in-plane and out-of-plane angular correlations. Best fit values of $\overline{J}$ and α_o are then determined by minimizing the χ^2 fit to the experimental data.

In Fig. 6.3-1 the angular distributions for the Kr + U reaction are shown for different bins of Q-value. With the exception of the angular correlations for the smallest energy loss the out-of-plane anisotropies are large and in-plane anistropies are relatively small. These results are consistent with a picture where the angular momentum transfer to the target-like nucleus is predominantly aligned normal to the reaction plane. The small in-plane anistropy indicates this transferred angular momentum has a small component which lies parallel to the reaction plane.

In comparing these data to the Kr + Bi data[1] one finds that the out-of-plane anisotropies for the Kr + U reaction are smaller for similar Q-value bins. This is primarily a consequence of the smaller deformation of the saddle point for uranium-like nuclei resulting in larger K_o^2 values. Also, coincident fission fragment events are seen for Q-values as large as 5 MeV for the Kr + U reaction because of the lower fission barrier for uranium-like nuclei. For the Kr + U reaction the out-of-plane anistropies increase with increasing energy loss until $Q \cong -165$ MeV.

Table 6.3-1. Extracted values for the angular momentum transfer J and the spreading width parameter α_o for different Q-value bins for the Kr + U reaction.

-Q(MeV)	K_o^2	J	α_o
13	34	11±3	> 60
50	110	22±3	49^{+38}_{-14}
77	151	29±4	34^{+12}_{-8}
123	207	36^{+6}_{-4}	21±8
165	245	47±8	22±8
208	279	54^{+14}_{-10}	24±8
259	314	44^{+18}_{-16}	20±12

In Table 6.3-1 are shown the angular momentum transfer J and values for the spreading width parameter α_o for the Kr + U reaction. The uncertainties associated with these values reflect an increase in the best fit χ^2 corresponding to one standard deviation. For the smallest energy loss we find that a large value for the spreading width parameter is needed to fit these data. This implies the transferred angular momentum has a significant component not perpendicular to the reaction plane. For the larger energy losses the spreading width parameter decreases indicating better alignment of the system. Also we

find the extracted angular momentum transfer increases with increasing energy loss until Q = -165 MeV. If one assumes an inverse monotonic relationship between energy loss and initial orbital angular momentum, then one might expect an initial increase in angular momentum transfer with increasing energy loss. But it is surprising that the angular momentum transfer should increase for large energy losses corresponding to Q = -165 MeV. For the Kr + Bi reaction the extracted angular momentum transfer decreases with increasing energy loss. While this observation is different for the two reactions, it is not a clear indication that instantaneous fission has been observed. One expects the mechanism of instantaneous fission to become more probable for larger energy losses corresponding to closer impact parameters. For Q-values less than 208 MeV the out-of-plane anisotropy and extracted J tend to decrease.

To date these results for the Kr + U reaction are somewhat puzzling. We are currently analyzing the in-plane and out-of plane angular correlations for different mass transfers (as determined by the counter telescope) and the fission probabilities associated with these nuclei in the hope of increasing our understanding of the mechanisms involved.

---

1. P. Dyer, R.J. Puigh, R. Vandenbosch, T.D. Thomas, and M.S. Zisman, Phys. Rev. Lett. 39, 392 (1977).
2. R. Vandenbosch and J.R. Huizenga, Nuclear Fission (Academic Press, New York, 1973).
3. W. Trautmann, J. deBoer, W. Dünnweber, G. Graw, K. Kopp, C. Lauterbach, H. Puchta, and U. Lynen, Phys. Rev. Lett. 39, 1062 (1977). G. Graw, J. deBoer, W. Dünneweber, C. Lauterbach, H. Puchta, W. Trautmann, and U. Lynen, J. Phys. Soc. Japan Suppl. 357 (1978).

6.4 Total Cross Sections for Inelastic Scattering of Very Energetic Heavy Ions

J. S. Blair

Stimulated by measurements at the Bevalac of cross sections for producing discrete gamma-rays,[1,2] we have calculated the sum of total inelastic cross sections to target states which are particle stable (and which thus decay by gamma-ray emission back to the target ground state). The key assumptions in these calculations are:

(1) The inelastic scattering of the heavy ions proceeds via a single step direct interaction which may be parameterized as an excitation of a collective surface vibration in the same fashion as is done for lower energy light ion projectiles. It is familiar that the inelastic scattering of the latter is well described by DWBA calculations based on this collective description; for a number of targets extensive tabulations have been made of the deduced values of the deformation distance, $\delta_L \equiv \beta_L R$, which parameterizes the strength of particular inelastic transitions, and these values are also presumed to apply for the inelastic scattering of very energetic heavy ions.

(2) The inelastic diffraction model[3] may be used as an approximation to

DWBA computations, which at these energies become quite cumbersome. It has been found that this simple model can be quite accurate, especially in situations of strong absorption, and the reasons for this are well understood.[4] The smooth transition from complete to no absorption in the surface region is accounted for by multiplying the familiar results for a sharp cutoff radius, R, by the square of a form factor, F(y); here $y = kd\theta$, where d is a diffuseness distance parameterizing the width of the transition region and k is the wave number. In the present calculations, the transition was taken to have the form of a Fermi function so that F becomes

$$F(y) = \frac{\pi y}{\sinh(\pi y)}.$$

Total cross sections for particular transitions are obtained by numerically integrating over solid angle the differential cross sections of the inelastic diffraction model for various reasonable values of the ratio R/d.

Preliminary values[2] have been given for the observed cross sections for producing discrete gamma-rays in ^{207}Pb and ^{88}Sr and, more recently,[1] in ^{40}Ca. Using the values of δ_L extracted from a high resolution study[6] of the scattering of 35 MeV protons from ^{207}Pb and the assumption that d = 0.35 fm, we calculate that the total inelastic cross section to the particle unbound states of ^{207}Pb > 73 mb; the inequality expresses the fact that values of δ_L could not be deduced in Ref. 6 for many of the higher excited states of ^{207}Pb. This is to be compared to 137 ± 17 mb, which is the measured summed cross section for producing gamma rays proceeding from the two lowest excited states to the ground state of ^{207}Pb. In a similar fashion for ^{88}Sr, using values of δ_L obtained[7] for scattering of 20.3 MeV protons, we calculate that the total inelastic cross section >70 mb. The cross section for producing the transition for the first 2^+ to the ground state of ^{88}Sr was found to be 83 ± 23 mb.

But while these comparisons are not unreasonable, in view of the uncertainties in the analysis of the experiments, a distinct discrepancy is encountered for the target ^{40}Ca. Here, using values of δ_L determined from the scattering of 35 MeV protons[8] we compute that the total inelastic cross section >80 mb while the observed cross section for producing the 3.73 MeV (3^-) gamma-ray of ^{40}Ca is only 14 mb. The computed total inelastic cross section to the first 3^- level and to the first 5^- level (which decays 100% to the 3^- level) alone equals 50 mb; thus one cannot attribute the discrepancy to cascades from higher excited states which proceed through states other than the 3^- level. It is possible that there is a reduction in the effective deformation parameter when the projectiles are very energetic heavy ions. Alternatively, it may be that we have underestimated the greyness of the surface region; the total inelastic cross sections are inversely proportional to the diffuseness, d, so that a larger value of d will lead to smaller cross sections. Such explanations, however, create other difficulties and, at the moment, the puzzle is unresolved.

---

1. T. Shibata, H. Ejiri, J. Chiba, S. Nagamiya, K. Nakai, R. Anholt, H. Bowman, J.G. Ioannou, E.A. Rauscher and J.O. Rasmussen, submitted to Nuclear Physics A.
2. H. Ejiri and T. Shibata, private communication.
3. See for example J.S. Blair in *Lectures in Theoretical Physics*, Vol.

VIII-C, University of Colorado Press (1966).
4. N. Austern and J.S. Blair, Annals of Phys. 33, 15 (1965).
5. W.E. Frahn and R.H. Ventner, Annals of Phys. 24, 243 (1963).
6. W.T. Wagner, G.M. Crawley, and G.R. Hammerstein, Phys. Rev. C11, 486 (1975).
7. J. Picard, O. Beer, A. El Behay, P. Lopato, Y. Terrien, G. Vallois, and R. Schaeffer, Nucl. Phys. A128, 481 (1969).
8. C.R. Gruhn, T.Y.T. Kuo, C.J. Maggiore, H. McManus, F. Petrovich, and B.M. Preedom, Phys. Rev. C6, 915 (1972).

6.5 Total Reaction Cross Sections for Near-Relativistic Heavy Ions

J. G. Cramer, R. M. DeVries†, and H. C. Britt‡

We have submitted a letter of intent describing an experiment to be performed on the new low-energy beam line of the BEVELAC. The experiment would involve the systematic measurement of forward angle elastic scattering as a function of energy in the energy region of about 30 MeV/A to 200 MeV/A, employing the quarter point of the forward angle elastic scattering as a measure of the total reaction cross section.

A variety of new phenomena have been predicted to occur in this region. In this region the collision velocity exceeds the velocity of sound in nuclear matter, the normally attractive nuclear potential is predicted to change sign and become repulsive, and the center of mass energy crosses the thresholds for both coherent and incoherent pion production. Several experiments proposed or in progress have focused on specific details of final states in order to search for new phenomena in this energy region. The experiment which we intend to propose is designed to be a complementary study using the good energy and angular resolution of projected low energy beam line of the BEVELAC to study the gross properties of the reactions, in particular the total reaction cross section σ_R, as a function of bombarding energy. Specifically, we will propose to measure σ_R over the complete energy range available with the BEVELAC low energy beam line for ^{12}C ions on targets of ^{12}C, ^{40}Ca, and ^{208}Pb, resolving elastic scattering from inelastic and inferring σ_R as described below.

In the absence of new phenomena we would expect σ_R to saturate at its geometrical value (πr_s^2) at the low energy end of our energy range (30 MeV/A) and remain relatively constant until "normal" (i.e., incoherent) pion production becomes significant. At this energy (about 150 MeV/A) σ_R might be expected to slowly increase. Thus the "baseline" for studies of total reaction cross section studies would be expected to be quite constant (or at least smooth) and small perturbations (5% or less?) in σ_R should stand out clearly. Of course it is possible that the predicted new phenomena will not perturb the total reaction cross section enough to be apparent in this type of survey measurement. However, it is also possible (perhaps even probable) that completely unanticipated phenomena will be observed in this unexplored volume of nuclear reaction space. It is our contention that the lack of information about heavy ion reactions in this region argues strongly for survey measurements of the gross reaction properties such as σ_R at an early stage.

There are three possible ways of determining the total reaction cross section for nuclear reactions such as those proposed here: (1) Summation of all reaction channels, (2) transmission measurements, and (3) interferrence from elastic scattering. We presently favor the latter method because it requires only relative (not absolute) measurements, because it seems least susceptible to systematic errors, and because it offers to provide additional information about elastic and inelastic scattering in addition to a determination of σ_R. We propose to infer the total reaction cross section from the elastic scattering quarter point angle (i.e., the angle at which $\sigma/\sigma_{rutherford} = 1/4$). At energies well over the Coulomb barrier the semiclassical formula $\sigma_R \simeq \pi\lambda^2[\eta \mathrm{Cot}(\theta/2)]^2$ gives a quite accurate estimate of σ_R. Alternatively, an optical model analysis of the angular distribution in the quarter-point region will provide a reliable value for σ_R. We also note that if it is possible to observe the inelastic cross sections simultaneously, an interference minimum should be present in the inelastic cross sections in the same angular region as the elastic quarter-point which yields information on the relative phase between the nuclear and Coulomb inelastic amplitudes, a quantity which might also be sensitive to the onset of new phenomena in the reaction channels. In any case, all of the measured experimental quantities will require good energy resolution ($\Delta E \simeq 2$ MeV) and good angular resolution in both the beam and the detection system.

We hope to achieve the required energy and angular resolutions using the low energy beam line of the BEVELAC and simple experimental geometry. The beam ($\Delta E/E \simeq 1/2000$) would be cleansed of its high emittance components with a suitable choice of optics to achieve a small beam spot (5 mm) and a small angular divergence ($\lesssim 0.05°$). At a relatively large distance downstream of the target (5-20 m) a high resolution liquid argon detector (see BEVELAC proposal by DeVries, Flynn, Gruhn, Hendry, and Van Bibber) will measure energy loss and total energy, while a drift chamber placed in front of the liquid argon detector would measure reaction angle. Although liquid argon detectors are very new and their expected energy resolution for the detection of near-relativistic heavy ions has not yet been established, we expect that the resolution should be adequate to resolve scattering to the ground state and probably also the first excited state of suitably chosen target nuclei. We note that at the low energy end of the range of interest ($E/A < 75$ MeV/nucleon) the measurements can be performed with well developed systems involving gas ion chamber detectors.

At first glance, the expected beam intensities at the BEVELAC low energy beam line (about 10^8 particles/spill) would seem to indicate that the count rates in experiments of the type described here would be hopelessly low. However, the huge Rutherford scattering cross sections involved (example: $\sigma_{ruth}(0.5°) = 6.7 \times 10^5$ barns/steradian for 100 MeV/A $^{12}C + {}^{208}Pb$) are very helpful. In the above example a 4 mg/cm^2 lead target bombarded with 10^6 carbon ions per second yields a count rate for a 100 cm^2 counter placed 17.2 meters downstream from the target of 260 counts/sec. It appears that the angular resolution effects of beam spot size, position detector resolution, and multiple scattering in the target are all negligible compared to the beam angular divergence of 0.05°.

In conclusion, we are presently investigating an experimental design for measuring the total reaction cross sections as a function of energy for selected targets in the energy region which will become available with the BEVELAC low

energy beam line. We plan to submit a proposal this fall which will request beam time for these experiments.

---

† Los Alamos Scientific Laboratory, Los Alamos, NM 87545.

6.6 Q and Z Dependence of Angular Momentum Transfer in Deeply Inelastic Collisions of ^{86}Kr with ^{209}Bi.

P. Dyer†, R. J. Puigh, T. D. Thomas††, R. Vandenbosch, and M. S. Zisman†††

Last year we reported[1] an in-plane and out-of-plane angular correlation for the above reaction. These results were integrated over all energies and all Z's of the outgoing projectile-like particles. We have now analyzed these data in a more differential way.

We have first divided the data into 50 MeV wide bins of Q-value as deduced from the light-particle energy assuming two-body kinematics. Several features are revealed by the resulting in-plane and out-of-plane correlations. We first note that the symmetry angles of the in-plane angular distributions seem to qualitatively track with the recoil direction. Secondly, both in-plane and especially the out-of-plane anisotropies decrease with increasing energy loss. The direction of this effect is to be expected simply from the fact that the width of the K-distribution will increase with increasing excitation energy. A dependence of the angular momentum transfer on Q may either enhance or attenuate the trend expected from this effect.

We have performed a quantitative analysis of these data to extract the dependence of the angular momentum transfer on Q-value. Since for a restricted range of energy loss the range of J values contributing is expected to be fairly narrow, and since we can determine only the first moment of the J distribution from such data, we have assumed a single J value in this analysis. By simultaneously fitting the in-plane and out-of-plane anistropy we determine the best-fit J. The results are given in Table 6.6-1. The J values show a tendency to

Table 6.6-1. The heavy-fragment momentum J as determined by fits to the Q-divided in-plane and out-of-plane correlations.

$-\bar{Q}$	$J/\hbar$
92	50±8
130	41±3
170	38±3
220	28±4

decrease with increasing energy loss. If there is an inverse relation between the energy loss and the initial orbital angular momentum in the entrance channel, the results indicate a correlation between the transferred angular momentum J

Table 6.6-2. The heavy-fragment angular momentum J as determined by fits to the Q and Z-divided in-plane and out-of-plane correlations

$-\bar{Q}$	Z	$J/\hbar$	P_f
	28-30	$60^{+\infty}_{-24}$	1.1
	31-33	42^{+9}_{-5}	0.44
81	34-36	44^{+13}_{-7}	0.08
	37-39	$92^{+\infty}_{-36}$	0.05
	40-42	>50	0.07
	28-30	30±8	0.98
	31-33	38±5	0.88
154	34-36	36±4	0.44
	37-39	51^{+10}_{-7}	0.27
	40-42	>60	0.24
	28-30	29^{+11}_{-8}	1.11
228	31-33	35^{+9}_{-7}	0.77
	34-36	36 6	0.45
	37-39	31^{+10}_{-6}	0.42

and the initial orbital angular momentum. Such a correlation is reasonable, except one would expect that for the highest partial waves (corresponding to very small energy losses) the fraction of the orbital angular momentum transferred would decrease. Because the fission probability becomes negligible for very small energy losses we might not see this decrease since we sample only those events with inelasticities greater than about 50 MeV. The apparent J values for the smallest inelasticities may be biased toward larger values due to angular momentum fractionation in the fission and neutron emission channels. Calculations are in progress to assess the magnitude of this effect.

We have also investigated the Z-dependence of the angular correlations. The counter telescope used to define the projectile-like particle had a Z resolution of approximately 1.5 charge units and can therefore be used to study the dependence of the angular correlations on the Z as well as the energy of the scattered particle. The Z of the complementary fissioning nucleus is expected to be within one Z unit of the difference between the sum of the target and projectile Z and the observed Z. We have divided the data into three moderately broad ranges of Q values, one centered near the most probable Q and the others above and below the most probable Q value. For each of the Q bins, we have sorted the data into bins 3 Z units wide. The extracted values of J obtained in the fitting of these data are summarized in Table 6.6-2. The values for the Z = 31-33 and Z = 34-36 bins are similar to the values obtained from the analysis of the data sorted with respect to Q only. For the Z = 37-39 bin, corresponding to low Z less fissionable complementary fragments, there is evidence for a higher J value than obtained for the other Z bins. This may be a consequence of the previously mentioned angular momentum fractionation which can be important if the average absolute probability for fission is low. If there is a distribution of J values for the heavy reaction partner, the increase in fissionability with increasing angular momentum can lead to a preponderance of fissioning events from the high-J end of the range of J-values. The attribution of the high J-values for the lower excitation energy Z = 37-39 bins to angular momentum fractionation is supported by the absolute fission probabilities given in the last column. (These values have been obtained by comparing the angle-integrated coincident fission rate with the singles rate.) It is seen that the absolute fission probabilities are small for these cases.

In an attempt to relate the observed dependence of transferred angular momentum on Q to a dependence on the initial orbital angular momentum ℓ_i we have deduced a dependence of ℓ_i on energy loss assuming an inverse monotonic relation between ℓ_i and Q. Such a dependence is expected for the higher partial waves in all theoretical models. In order to obtain the dependence of ℓ_i on Q we have angle-integrated the double differential cross section of Wolf *et al.*[2] The resulting dependence of ℓ_i on energy loss enables us to assign an average ℓ to each bin of Q-values for which average transferred angular momenta J_{Bi} have been obtained. A plot of the J_{Bi} values versus initial orbital angular momentum is given in Fig. 6.6-1. The error bars reflect only the statistical uncertainties in determining J_{Bi} from the angular distributions. Also shown are some simple estimates of J_{Bi} for the cases of rolling and sticking spheres and for sticking spheroids where the elongation (ratio of semi-axes ∿1.4) has been chosen to give a Coulomb interaction energy consistent with the most probable

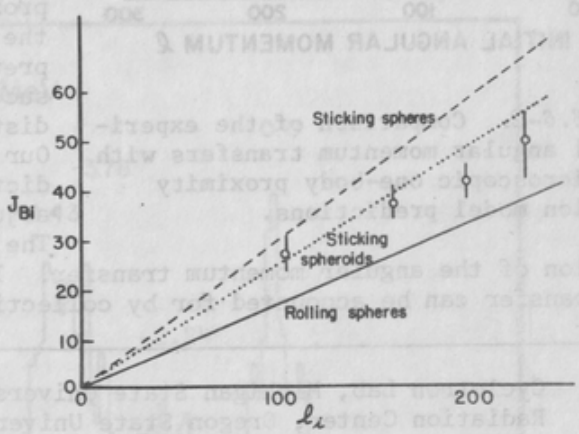

Fig. 6.6-1. **Comparison of the experimental angular momentum transfers to the heavy fragment with simple macroscopic friction model expectations.**

total kinetic energy in the deeply inelastic scattering. The results are qualitatively consistent with the expectation for sticking spheroids. One might in fact expect J_{Bi} to be close to the sticking limit for low ℓ_i and to be closer to the rolling limit for the more peripheral reactions where the overlap of target and projectile is small. Unfortunately the fission barrier of ^{209}Bi is large enough that the fission probability is rather small at the low excitation energies associated with the more peripheral collisions. We observe few events when the fission probability is low and what events are observed may be biased due to the possibility of angular momentum fractionation.

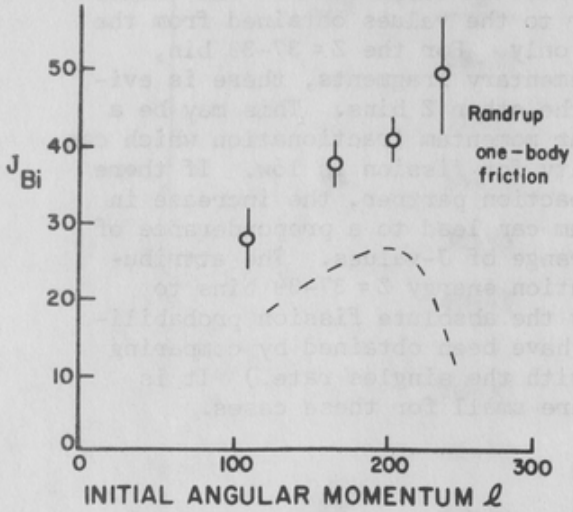

Fig. 6.6-2. **Comparison of the experimental angular momentum transfers with the microscopic one-body proximity friction model predictions.**

We have also compared our results on angular momentum transfer with other more detailed nuclear model calculations. In general we find that most theoretical calculations underestimate the angular momentum transfer. One of the more successful models is the one-body proximity friction model of Randrup.[3] This model takes into account the energy and angular momentum loss due to particle exchange between the moving fragments. Both the conservative potential determining the trajectory and the transparency factor for particle transfer are based on a proximity treatment which incorporates the diffuse nuclear surface. We have previously found that this model is successful in accounting for charge distributions in similar reactions.[4] Our results are compared with the prediction of this model, which has no adjustable parameters, in Fig. 6.6-2. The calculation accounts for the major fraction of the angular momentum transfer. It remains to be seen if the remaining transfer can be accounted for by collective effects.

---

† Cyclotron Lab, Michigan State University, East Lansing, Michigan 48824.
†† Radiation Center, Oregon State University, Corvallis, Oregon 97331.
††† Lawrence Berkeley Lab, Berkeley, California 94720.

1. P. Dyer, R.J. Puigh, R. Vandenbosch, T.D. Thomas, and M.S. Zisman, Phys. Rev. Lett. 39, 392 (1977).
2. K.L. Wolf and C.T. Roche, Proc. of the Symposium on Macroscopic Features of Heavy-Ion Collisions, Argonne, Ill., Vol. 1, p. 295 (ANL/PHY-72-2) 1976.
3. J. Randrup, to be published.
4. P. Dyer, R.J. Puigh, T.D. Thomas, R. Vandenbosch, M.P. Webb, and M.S. Zisman, Nuclear Physics Laboratory Annual Report, University of Washington (1977), p. 91.

6.7 Elastic and Inelastic Scattering of ^{32}S on ^{12}C

Y-d. Chan, J. G. Cramer, W. Lynch, R. J. Puigh, and B. Tsang

Introduction

We have carried out an experiment to measure the angular distribution for elastic and inelastic scattering of ^{32}S on ^{12}C in order to investigate the systematic dependence of enhanced backward cross sections and structures for this mass region. This particular system was chosen because it has the same channel compound nucleus as the $^{28}Si + ^{16}O$ and $\alpha + ^{40}Ca$ channels, where very pronounced backward angle phenomena have been observed.[1] The fact that $^{32}S + ^{12}C$ and $^{28}Si + ^{16}O$ are closer to each other in kinematics makes a detailed comparison of these two systems useful so that various models trying to explain these phenoma can be tested.

So far, data has been accumulated only for relatively low bombarding energies ($E_{c.m.} = 21.8$ and 27.0 MeV). Further measurements, including the application of the UW spectrometer, are still in progress.

Experiment

Measurements have been performed for $E_L(^{32}S) = 80$ and 99 MeV. The ^{32}S beam was extracted from the NPL Sputter Ion Source with an LiS cone and was accelerated towards an isotopic ^{12}C foil target inside the 60" scattering chamber.

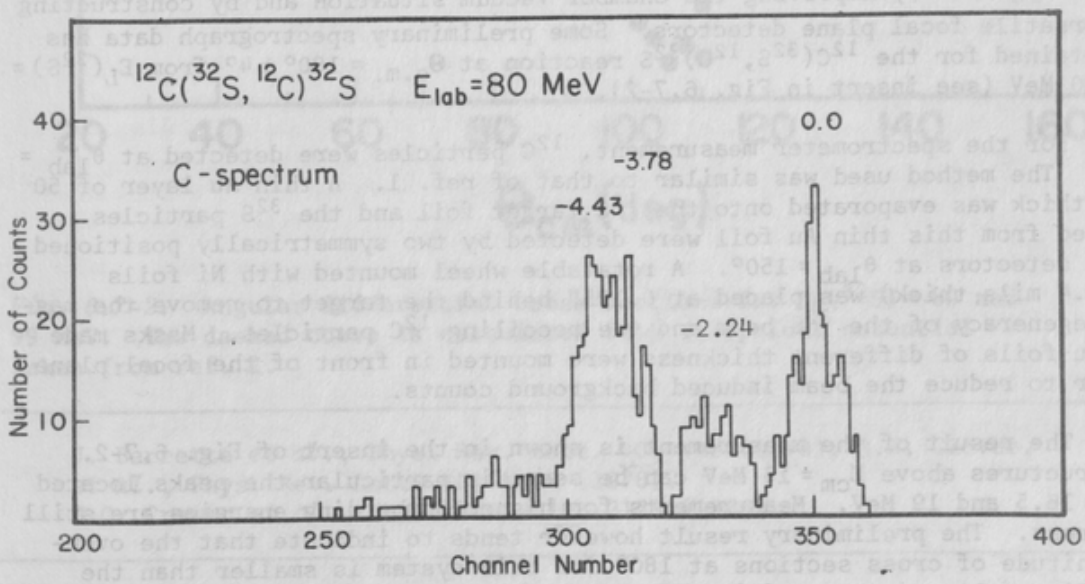

Fig. 6.7-1. Carbon energy spectra at $E(^{32}S) = 80$ MeV with the telescope positioned at $\theta_{lab} = 12°$ for the $^{12}C(^{32}S,^{12}C)^{32}S$ reaction.

Depending on the center of mass angle, the angular differential cross

sections were measured either by singles detection of S or C (outside the kinematic cone of S) particles with a S_i detector array or by doing particle identification at forward laboratory angles to obtain data corresponding to very backward c.m. angles. Particle identification was achieved by mounting a S_i ΔE-E telescope on top of a radially movable mechanical device so that the detection solid angle could be changed to optimize the counting efficiency. The counting rate was limited mainly by pile-ups in the ΔE detector. The thickness of the ΔE detector was chosen (20.6 μm) so that all S particles were stopped. Target thickness ranging between 50 - 150 μg/cm^2 were used. Due to the low cross section for backward angles, the telescope angle was kept fixed while the detector array angles were changed between consecutive runs until the summed telescope data reached about 10% statistics. A sample energy spectrum for the C particles from the telescope is shown in Fig. 6.7-1. A S_i detector was also mounted at $\theta_{lab} = 15°$ for normalization purpose.

Results

The measured elastic and inelastic differential cross sections are shown in Fig. 6.7-2. Also plotted are optical model calculations by using the global potential E18[2] which can reproduce the forward scattering between p- and sd-shell nuclei quite well. Since the c.m. energy is quite low in our case, the 80 MeV data falls off smoothly from the Rutherford cross section and diffractive patterns are apparent only for the 99 MeV data.

In order to further pursue this experiment, the UW magnetic spectrometer has been upgraded by improving the chamber vacuum situation and by constructing more versatile focal plane detectors. Some preliminary spectrograph data has been obtained for the $^{12}C(^{32}S,^{12}C)^{32}S$ reaction at $\Theta_{c.m.} = 180° \pm 4°$ from $E_L(^{32}S) =$ 40 to 80 MeV (see insert in Fig. 6.7-2).

For the spectrometer measurement, ^{12}C particles were detected at $\theta_{lab} =$ $0° \pm 2°$. The method used was similar to that of ref. 1. A thin Au layer of 50 μg/cm^2 thick was evaporated onto the ^{12}C target foil and the ^{32}S particles scattered from this thin Au foil were detected by two symmetrically positioned monitor detectors at $\theta_{lab} = 150°$. A rotatable wheel mounted with Ni foils (0.1 - 0.4 mils thick) was placed at 0.125" behind the target to remove the magnetic degeneracy of the ^{32}S beam and the recoiling ^{12}C particles. Masks made up of Au foils of different thickness were mounted in front of the focal plane detector to reduce the beam induced background counts.

The result of the measurement is shown in the insert of Fig. 6.7-2. Some structures above $E_{cm} = 15$ MeV can be seen, in particular the peaks located at $E_{cm} = 16.5$ and 19 MeV. Measurements for higher bombarding energies are still in progress. The preliminary result however tends to indicate that the overall magnitude of cross sections at 180° for this system is smaller than the $^{16}O + ^{28}Si$ results as reported in ref. 1.

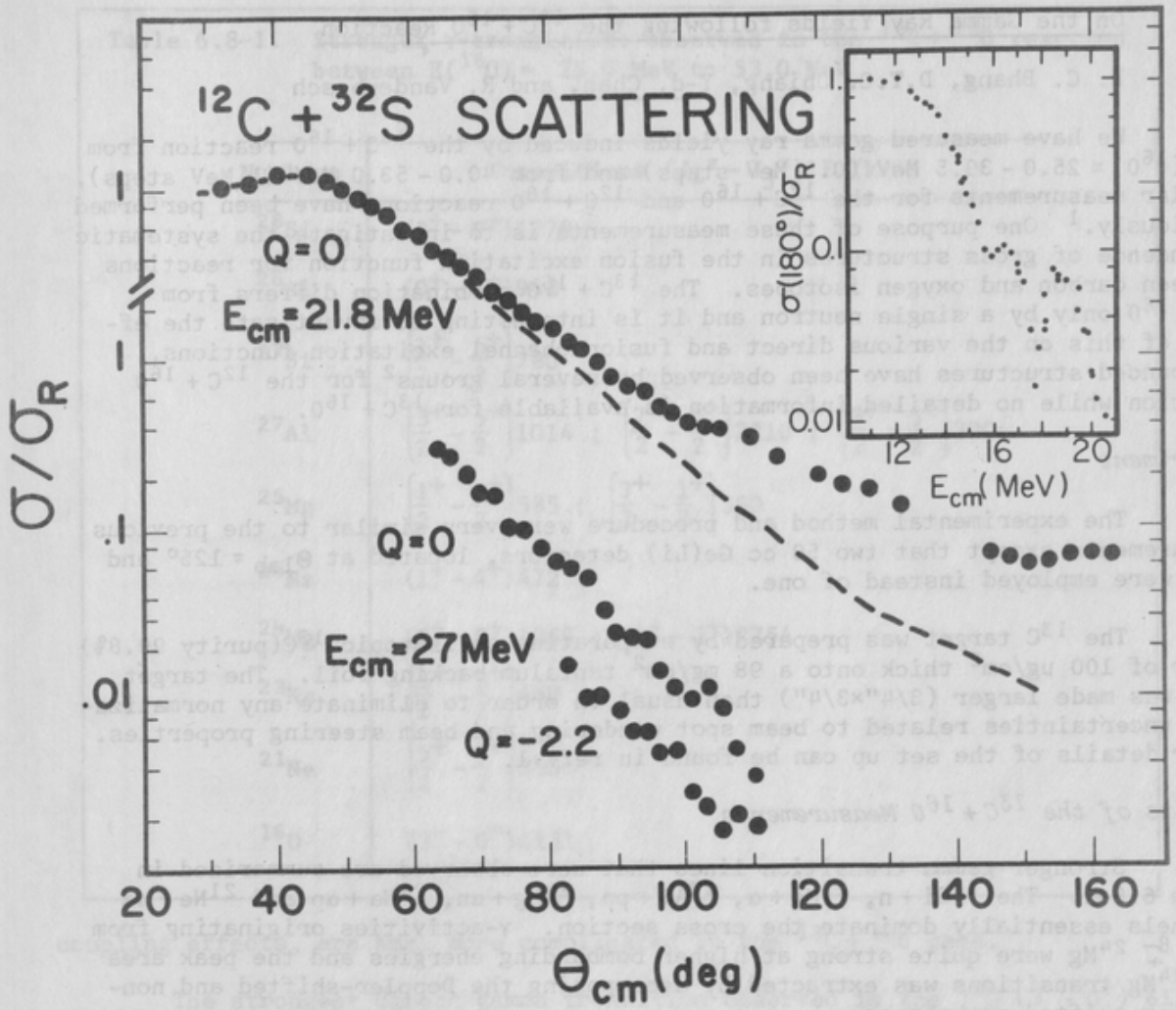

Fig. 6.7-2. Angular differential cross sections for $E_L(^{32}S) = 80$ and 99 MeV. The dashed curve is calculated from an optical potential taken from ref. 2.

1. J. Barrette *et al.*, Phys. Rev. Lett. 40, 445 (1978); M.R. Clover, *et al.*, Phys. Rev. Lett. 40, 1008 (1978).
2. J.G. Cramer *et al.*, Phys. Rev. C14, 2158 (1976).

6.8 On the Gamma Ray Yields following the $^{13}C + ^{16}O$ Reaction

H. C. Bhang, D.T.C. Chiang, Y-d. Chan, and R. Vandenbosch

We have measured gamma ray yields induced by the $^{13}C + ^{16}O$ reaction from $E_{lab}(^{16}O) = 25.0 - 39.5$ MeV (0.5 MeV steps) and from 40.0 - 53.0 MeV (1 MeV steps). Similar measurements for the $^{12}C + ^{16}O$ and $^{12}C + ^{18}O$ reactions have been performed previously.[1] One purpose of these measurements is to investigate the systematic dependence of gross structures in the fusion excitation function for reactions between carbon and oxygen isotopes. The $^{13}C + ^{16}O$ combination differs from $^{12}C + ^{16}O$ only by a single neutron and it is interesting to investigate the effect of this on the various direct and fusion channel excitation functions. Pronounced structures have been observed by several groups[2] for the $^{12}C + ^{16}O$ reaction while no detailed information is available for $^{13}C + ^{16}O$.

Experiment

The experimental method and procedure were very similar to the previous measurements except that two 50 cc Ge(Li) detectors, located at $\Theta_{lab} = 125°$ and 75°, were employed instead of one.

The ^{13}C target was prepared by evaporating an isotopic ^{13}C(purity 99.8%) layer of 100 μg/cm^2 thick onto a 98 mg/cm^2 tantalum backing foil. The target area was made larger (3/4"×3/4") than usual in order to eliminate any normalization uncertainties related to beam spot wandering and beam steering properties. Other details of the set up can be found in ref. 1.

Results of the $^{13}C + ^{16}O$ Measurements

Stronger gamma transition lines that were observed are summarized in Table 6.8-1. The $^{28}Si + n$, $^{25}Mg + \alpha$, $^{27}Al + pn$, $^{24}Mg + \alpha n$, $^{24}Na + \alpha p$ and $^{21}Ne + \alpha\alpha$ channels essentially dominate the cross section. γ-activities originating from $^{24}Na \xrightarrow{\beta-} {}^{24}Mg$ were quite strong at higher bombarding energies and the peak area for ^{24}Mg transitions was extracted by decomposing the Doppler-shifted and non-Doppler shifted peakshapes.

The resulting excitation functions for various transitions are plotted in Fig. 6.8-1. Also shown are the Coulomb excitation transition lines from the ^{181}Ta backing foil. The yields of these ^{181}Ta transitions are used to monitor the accuracy of the beam charge integration. As can be seen from the figure, they are smooth and monotonically increasing over the entire energy range of interest.

Excitation functions for most transitions are found to be smooth and structureless (e.g., $^{27}Al(\frac{9}{2}^+ - \frac{5}{2}^+)$ 3004 keV, $^{24}Mg(4^+ - 2^+)$ 2754 keV and ^{24}Na $(1^+ - 4^+)$ 472 keV) except possibly for transitions belonging to the $^{25}Mg + \alpha$ channel, where large deviations from a smoothed trend curve are apparent, especially in the lower energy portion. It is interesting to point out the resemblance with the $^{12}C + ^{16}O$ reaction where the α-out channel (^{24}Mg) also carries the strongest structural feature. However, the $^{13}C + ^{16}O$ data does seem to fluctuate more. This may be due to the fact that even though gross envelopes in the excitation functions are similar, the finer details, presumably due to channel

Table 6.8-1. Stronger γ-transitions observed in the $^{13}C + ^{16}O$ reaction between $E(^{16}O) =$ 25.0 MeV to 53.0 MeV

Nucleus	Transitions $(J_i^\pi - J_j^\pi)$ E_γ(keV)
^{28}Si	$(2^+ - 0^+)1778$
^{28}Al	$(0^+ - 2^+)942$
^{27}Si	$\left(\frac{1}{2}^+ - \frac{5}{2}^+\right)780$
^{27}Al	$\left(\frac{3}{2}^+ - \frac{5}{2}^+\right)1014$; $\left(\frac{7}{2}^+ - \frac{5}{2}^+\right)2210$; $\left(\frac{9}{2}^+ - \frac{5}{2}^+\right)3004$
^{25}Mg	$\left(\frac{1}{2}^+ - \frac{5}{2}^+\right)585$; $\left(\frac{3}{2}^+ - \frac{1}{2}^+\right)390$
^{24}Na	$(1^+ - 4^+)472$
^{24}Mg	$(2^+ - 0^+)1369$; $(4^+ - 2^+)2754$
^{23}Na	$\left(\frac{5}{2}^+ - \frac{3}{2}^+\right)440$
^{21}Ne	$\left(\frac{5}{2}^+ - \frac{3}{2}^+\right)350$
^{16}O	$(3^- - 0^+)6131$

coupling effects, are much more complicated in the $^{13}C + ^{16}O$ case.

The strongest direct gamma transition observed is the ^{16}O $(3^- - 0^+)$ 6131 keV line. The corresponding cross section, deduced from the full energy peak, is also plotted in Fig. 6.8-1. This transition stands up above the continuum background only for $E_{lab} \geq 38$ MeV, and in the energy range we have studied, no significant structures were observed. Transitions corresponding to inelastic excitation of the ^{13}C target are very weak, only the $^{13}C(\frac{5}{2}^+ - \frac{1}{2}^+)$ 3.85 MeV transition can be tentatively identified in the singles energy spectra.

Comparison of Results from the $^{12}C + ^{16}O$, $^{13}C + ^{16}O$ and $^{12}C + ^{18}O$ Measurements

Excitation functions for the p-, α-, pn- and αα-out channels for these reactions are plotted in Fig. 6.8-1 and 6.8-2. The α-out channels stand out among the others in structural features, with the pn-out channel being the smoothest. According to our work there are also some structures in the αα-channels but the peak to valley ratios are smaller than those of the α-out case. Based on the predominance of structure only in the α-out channel and the fact that α-emission is favored to p- and n-emissions for high spin compound nuclei, one would conclude that these structures are mainly confined to the peripheral partial waves,

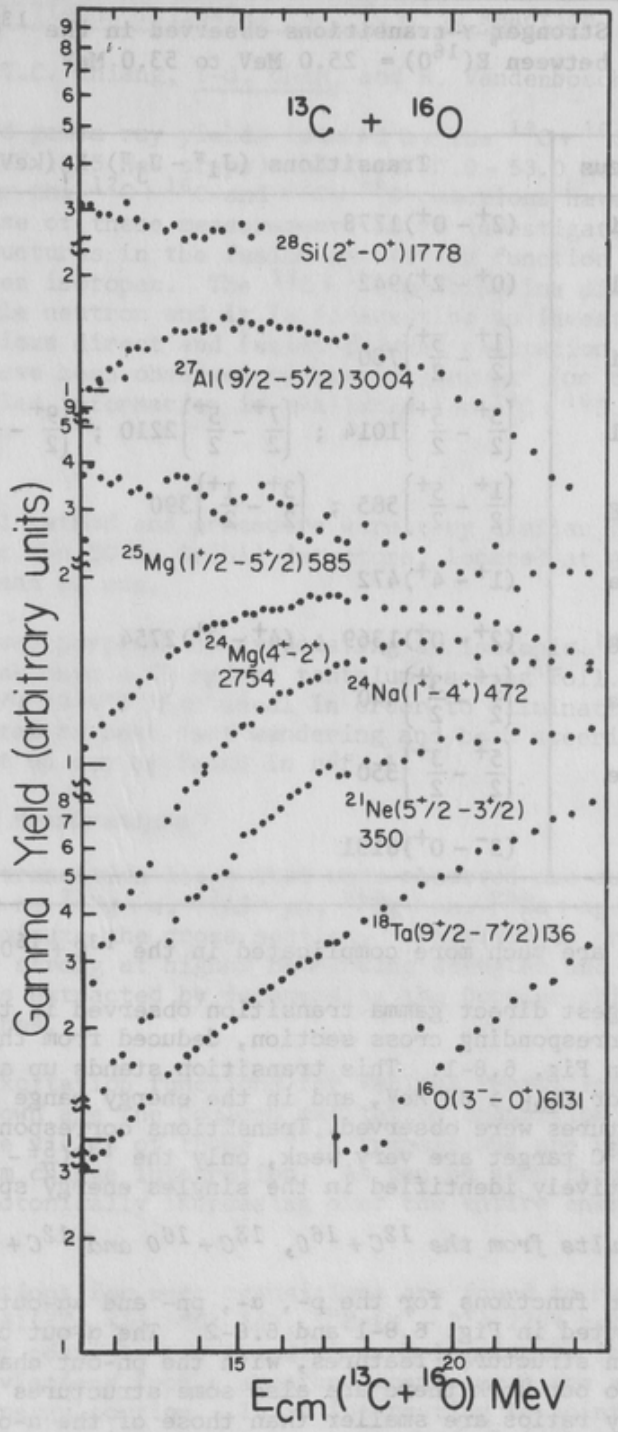

Fig. 6.8-1. Excitation functions for discrete gamma transitions from the reaction $^{13}C + ^{16}O$. Also shown are the Coulomb excitation lines from the ^{181}Ta backing foil.

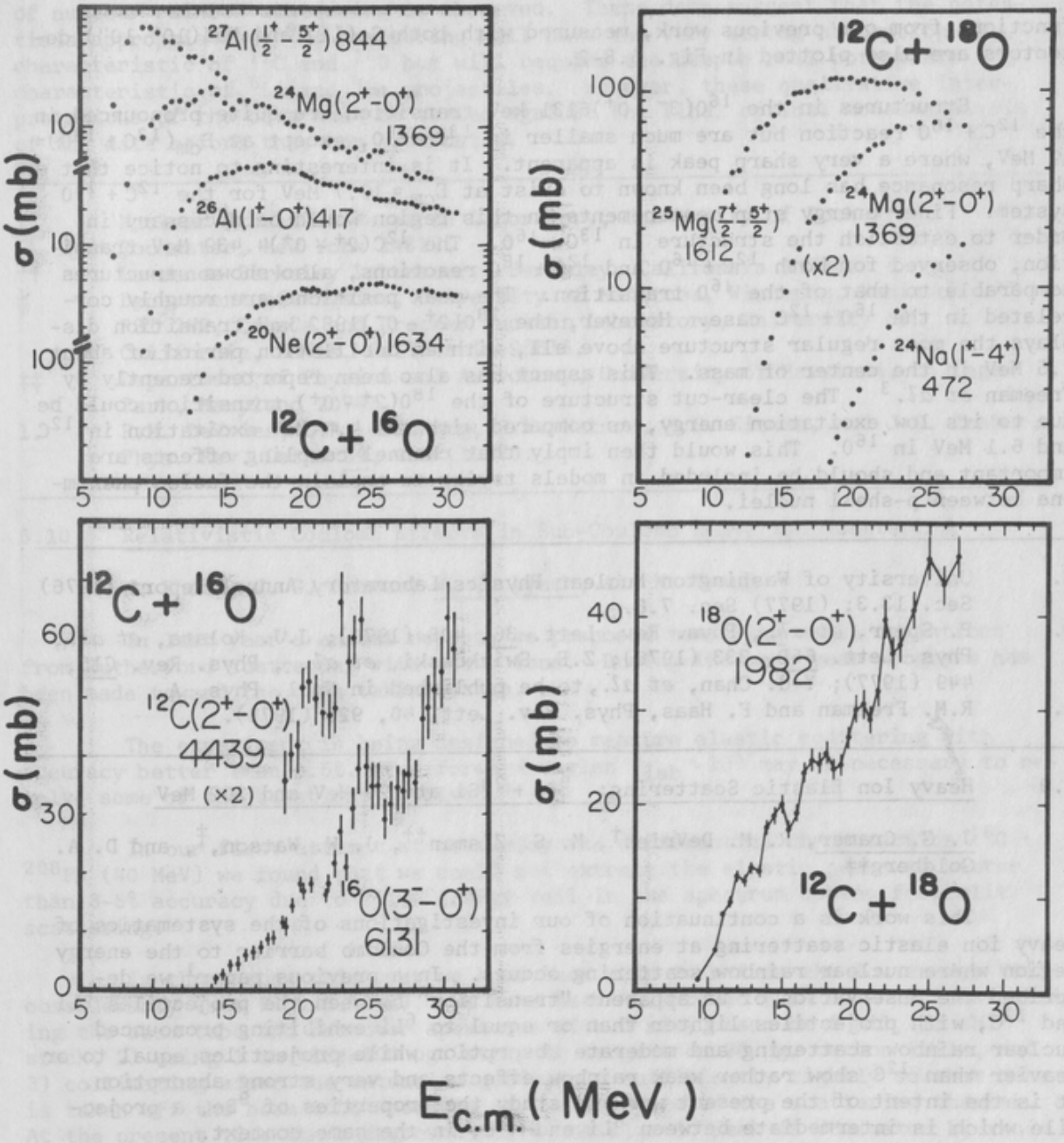

Fig. 6.8-2. Comparison of gamma ray excitation functions for the $^{12}C + ^{16}O$ and $^{12}C + ^{18}O$ reactions.

and would expect to see much stronger correlations of these structures with the various direct channels.

To investigate this, a collection of inelastic gamma ray excitation

functions from our previous work, measured with both Ge(Li) and NaI(10" 10") detectors are also plotted in Fig. 6.8-2.

Structures in the $^{16}O(3^- - 0^+)$6131 keV transition are quite pronounced in the $^{12}C + ^{16}O$ reaction but are much smaller in $^{13}C + ^{16}O$, except at $E_{cm}(^{13}C + ^{16}O)$= 19 MeV, where a very sharp peak is apparent. It is interesting to notice that a sharp resonance has long been known to exist at $E_{cm} \simeq 19.7$ MeV for the $^{12}C + ^{16}O$ system. Finer energy step measurements in this region would be necessary in order to establish the structure in $^{13}C + ^{16}O$. The $^{12}C(2^+ - 0^+)$4.439 MeV transition, observed for both $^{12}C + ^{16}O$ and $^{12}C + ^{18}O$ reactions, also shows structures comparable to that of the ^{16}O transition. The peak positions are roughly correlated in the $^{16}O + ^{12}C$ case. However, the $^{18}O(2^+ - 0^-)$1982 keV transition displays the most regular structure above all, with an oscillation period of about 2.5 MeV in the center of mass. This aspect has also been reported recently by Freeman *et al.*[3] The clear-cut structure of the $^{18}O(2^+ - 0^+)$ transition could be due to its low excitation energy, as compared with the 4.4 MeV excitation in ^{12}C and 6.1 MeV in ^{16}O. This would then imply that channel coupling effects are important and should be included in models trying to explain the fusion phenomena between p-shell nuclei.

---

1. University of Washington Nuclear Physics Laboratory Annual Report (1976) Sec. 13.3; (1977) Sec. 7.6.
2. P. Sperr, *et al.*, Phys. Rev. Lett. 36, 405 (1976); J.J. Kolata, *et al.*, Phys. Lett. 65B, 333 (1976); Z.E. Switkowski, *et al.* , Phys. Rev. C15, 449 (1977); Y-d. Chan, *et al.*, to be published in Nucl. Phys. A.
3. R.M. Freeman and F. Haas, Phys. Rev. Lett. 40, 925 (1978).

6.9 Heavy Ion Elastic Scattering: $^{9}Be + ^{28}Si$ at 120 MeV and 202 MeV

J. G. Cramer, R. M. DeVries†, M. S. Zisman††, J. W. Watson,‡, and D. A. Goldberg‡‡

This work is a continuation of our investigations of the systematics of heavy ion elastic scattering at energies from the Coulomb barrier to the energy region where nuclear rainbow scattering occurs. In a previous paper[1] we described the observation of an apparent "transition" between the projectiles ^{6}Li and ^{12}C, with projectiles lighter than or equal to ^{6}Li exhibiting pronounced nuclear rainbow scattering and moderate absorption while projectiles equal to or heavier than ^{12}C show rather weak rainbow effects and very strong absorption. It is the intent of the present work to study the properties of ^{9}Be, a projectile which is intermediate between ^{6}Li and ^{12}C, in the same context.

We will not show the data here, since it is still undergoing final analysis. We will, however, comment that the measurements done at bombarding energies of 120 MeV and 202 MeV with the ^{9}Be beam from the LBL 88" Cyclotron seem to indicate that the projectile ^{9}Be is indeed intermediate between ^{6}Li and ^{12}C. In the forward part of the angular distributions measured the ^{9}Be data follows predictions made with potential H12 derived from the ^{12}C analysis with surprising accuracy. However, at the more backward angles the interference oscillations damp out and in the data taken at 202 MeV a structureless falloff characteristic

of nuclear rainbow scattering is observed. These data suggest that the potentials appropriate to ^{9}Be scattering will have the very strong absorption characteristic of ^{12}C and ^{16}O but will require the deeper real potentials characteristic of ^{6}Li and ^{4}He projectiles. However, these qualitative interpretations of the data must be tested against the final optical model analysis of the data before they can be trusted.

---

† Nuclear Structure Research Laboratory, University of Rochester, Rochester, New York 14627.

†† Lawrence Berkeley Laboratory, Berkeley, California 94720.

‡ Department of Physics, University of Manitoba, Winnepeg, Manitoba R3T 2N2, Canada and Crocker Nuclear Laboratory, University of California, Davis, California 95616.

‡‡ Department of Physics and Astronomy, University of Maryland, College Park, Maryland 20743.

1. R.M. DeVries, D.A. Goldberg, J.W. Watson, M.S. Zisman, and J.G. Cramer, Phys. Rev. Lett. 39, 450 (1977).

6.10 Relativistic Coulomb Effects in Sub-Coulomb Heavy Ion Scattering

H. Bhang, J. G. Cramer, W. G. Lynch, and M. Tsang

In last year's annual report, we proposed measuring small deviations from Rutherford scattering with heavy ions. During the past year progress has been made toward the data taking stage.

The experiment is being designed to measure elastic scattering with accuracy better than 0.5%. Far forward angles $\theta_{lab} \sim 10°$ may be necessary to resolve some of the questions involved.[1]

In our first attempt at measuring the differential cross section ^{16}O + ^{208}Pb (40 MeV) we found that we could not extract the elastic peaks to better than 3-5% accuracy due to a low energy tail in the spectrum coming from slit scattering.

In three runs this year we have been able to reduce the low energy tail considerably (see Fig. 6.10-1). We have been able to do this by: 1) constructing the beam tube and detector apertures with 3 mil. brass or 2 mil. Ta shim stock, 2) using 1 mm wide 100 μg. strip Pb targets on 20 μg. carbon foils, and 3) collimating after the extension quadrupole sufficiently tightly so that beam is taken off the beam tube aperture at the entrance of the scattering chamber. At the present time the background below the elastic peak is dominated by trace target contaminents and by the yield from the carbon foil, and we get a peak to background ratio under the elastic peak of $2\times10^{-3}(\theta_{lab}=20°)$.

The major remaining difficulties have to do with determining the properties of the beam well enough to do accurate measurements at forward angles. The important effects are: multiple scattering and uncertainties in beam spot position and beam direction. For the angles we are attempting, the multiple scattering can probably be handled by the conventional multiple scattering formulae.[2]

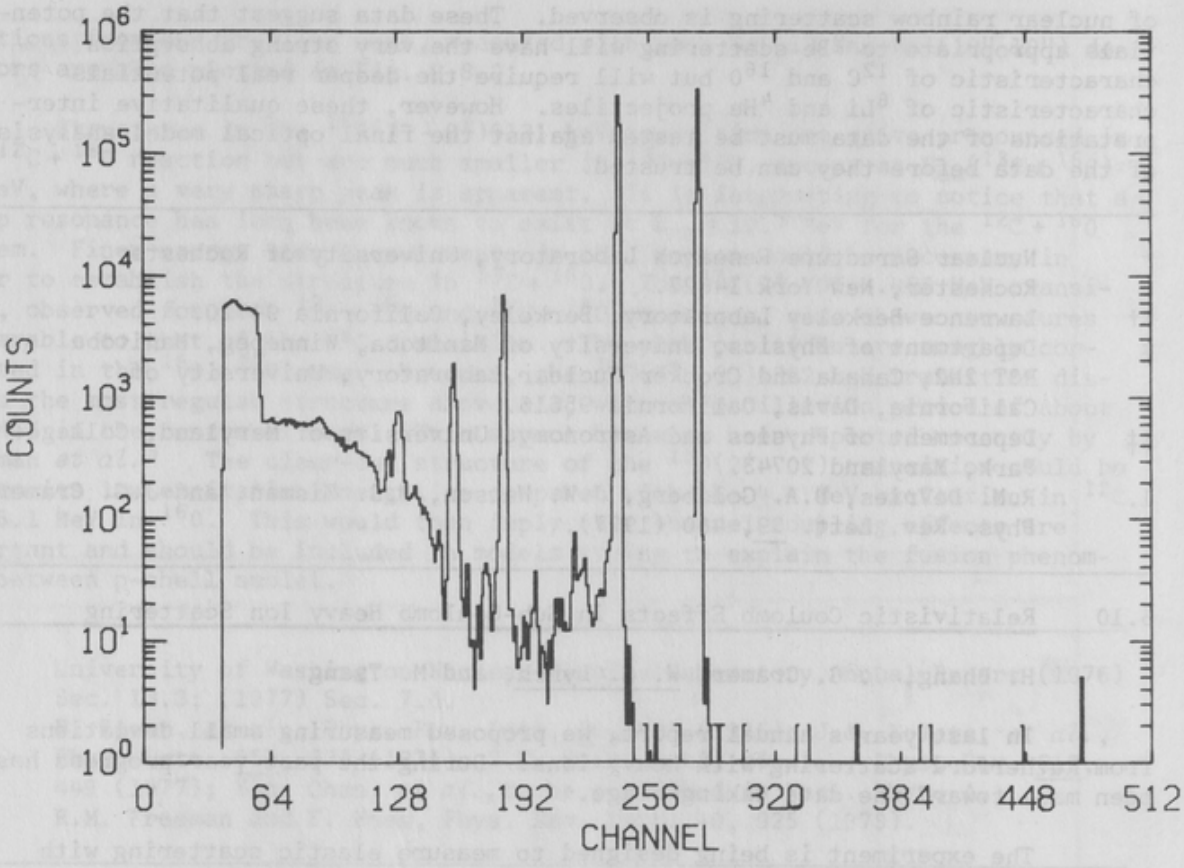

Fig. 6.10-1. Energy spectrum for ^{12}C beam on strip ^{108}Pb target at 46 MeV (lab) and 30° (lab). The elastic peak for lead strip is in channel 280. The elastic peak for the carbon backing is in channel 240.

Stability in the beam spot position is insured by coupling a split Faraday cup to the beam position regulator.[3] The beam spot position and beam direction (i.e., scattering angle) we would like to determine by a method involving the kinematics of elastic scattering of ^{16}O off of an ^{27}Al target.[4] In a recent run we have attempted to use this technique to determine the scattering angle in the 60" chamber. Due to equipment failure, we were unable to determine the target angle and as a result we had to give up on determining the scattering from the data we had taken.

Shortly we will try again to determine the effective scattering angle. Concurrently we will do excitation functions on several targets and projectiles in addition to Pb to determine other suitable targets and projectiles for these sub-Coulomb energies.

---

1. J. Rafelski and A. Klien, *Reactions between Complex Nuclei*, North-Holland (1974), Vol. 2, p 412.
2. B.W. Hooten, J.M. Freman, and P.P. Kane, Nuclear Instruments and Methods

124, 29 (1975).

3. J.G. Cramer and H. Fauska, University of Washington Nuclear Physics Laboratory Annual Report, 1974, p. 7.

7. MEDIUM ENERGY PHYSICS

7.1 The ^{11}C Production Yield Ratios from ^{12}C vs. ^{13}C and ^{12}C vs. ^{16}O for Incident $\pi^{\pm}$ from 100 to 250 MeV

K. Aniol, D. Chiang, D. Drake†, I. Halpern, and G. Haouat†

In a run on the LEP channel at Los Alamos last summer we measured the ratio of ^{11}C production cross-sections from ^{12}C and ^{13}C across the (3,3) resonance for both π^+ and π^-. In a similar series of measurements, we also measured the ratio of ^{11}C production cross-sections from ^{12}C and ^{16}O. This is a preliminary report of both sets of measurements.

There were two motivations for the experiment; to look for possible evidence for intermediate structure in the (3,3) resonance and to measure cross-section ratios that could be useful in establishing the reaction mechanisms of pions with light nuclei.

The special feature of the measurement was the use of a direct comparison technique which provided cross-section ratios having uncertainties of about 2%, where the uncertainties of the individual cross-section measurements[1,2] are considerably larger because of uncertainties in beam calibrations and absolute counting efficiencies. In our measurement the samples being compared were exposed to the beam simultaneously and subsequently counted in identical geometries.

The results for the measured cross-section ratios are shown in Figs. 7.1-1 and 7.1-2. It is seen that all four sets of ratios lie on some sort of smooth curve. If there were any characteristic intermediate structure in the (3,3) resonance that differed for different reactions (because of the different couplings among the nucleons in the different targets) one would expect to see fluctuations in the curve of cross-section ratios against bombarding energy. Within the accuracy of the measurements ($\lesssim$2%), there is no evidence for such fluctuations.

It is possible to give at least a qualitative account of some of the features in Figs. 7.1-1 and 7.1-2 in terms of the reaction mechanisms involved.

Why the curve giving the ratios for π^+ lies lower than the curve giving them for π^-: The ^{11}C yield from carbon targets in the π^- bombardments is due to inelastic scatterings only. That is, an absorption of the incident pion would reduce the nuclear Z by unity and there would be no way to reach ^{11}C. With incident π^+ on the other hand, one can reach ^{11}C starting with pion absorption in both ^{12}C and ^{13}C. It is likely that the absorption mechanism is a substantial contributor to the ^{11}C yield in the bombardment of ^{13}C since it is known to dominate the scattering contribution in the production of ^{10}C in ^{12}C bombardments.[3] The evidence is that the ^{10}C cross-section in π^- bombardment of ^{12}C at 175 MeV is less than half a millibarn whereas the corresponding π^+ cross-section is 5 mb.[4] Since the π^+ reaction involves absorption + scattering whereas the π^- cross-section involves only scattering, it appears that the scattering contribution to 2 neutron removal from ^{12}C is small and that there is $\sim$5 mb worth of removal that starts with an absorption. There are good reasons to expect that

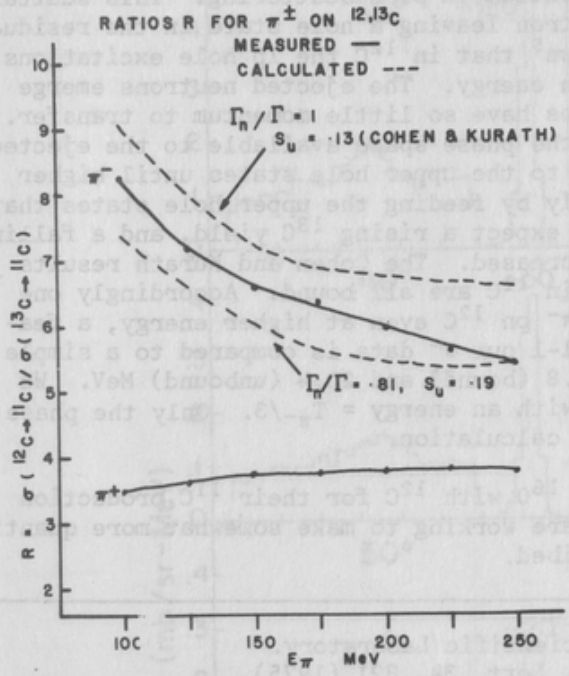

Fig. 7.1-1. Measured excitation functions for the ratios of ^{11}C production cross sections from $^{13,12}C$ with $\pi^{\pm}$. These data do not include the relatively small corrections for secondary reactions in the targets. The calculated curve (for π^-) takes into account mainly the phase space available to neutrons ejected from ^{13}C. It is seen to depend somewhat on spectroscopic factors S_u and n branching ratios.

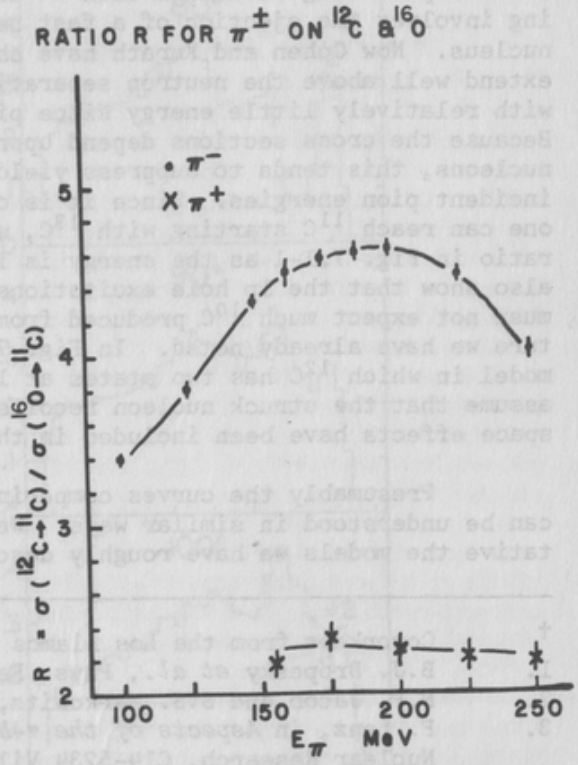

Fig. 7.1-2. Measured excitation functions for the ratios of ^{11}C production cross-sections from ^{12}C and ^{16}O with $\pi^{\pm}$.

the 2 neutron removal yields due to scattering depend sensitively on nuclear structure (see below) but this is less likely to be so for the absorption yields. Thus it would appear that the $^{12}C/^{13}C$ ratio in Fig. 7.1-1 due to π^+ is smaller than that due to π^- because of the contribution of pion absorption in ^{13}C to the ^{11}C yield. This assumes of course that pion absorption is not playing as significant a role in the production of ^{11}C from a ^{12}C target as from ^{13}C. For ^{11}C to be made in pion absorption on ^{12}C, one of the two nucleons which are presumably involved would have to emerge from the nucleus as a proton carrying virtually all the energy made available. The partner nucleon would have to recoil into the nucleus with too little energy for subsequent particle evaporation. This seems unlikely. Thus it would appear that π^+ absorption is a significant contributor to the ^{11}C production in the ^{13}C bombardment.

Another striking feature in Fig. 7.1-1 is the fairly rapid fall off with increasing π^- energy of the ^{12}C to ^{13}C production ratio of ^{11}C. This can be understood in terms of the nuclear structure of ^{12}C. As has been indicated,

the ^{11}C-producing mechanism with π^- is inelastic pion scattering. This scattering involves the ejection of a fast neutron leaving a hole state in the residual nucleus. Now Cohen and Kurath have shown[5] that in ^{12}C the 1p hole excitations extend well above the neutron separation energy. The ejected neutrons emerge with relatively little energy since pions have so little momentum to transfer. Because the cross sections depend upon the phase space available to the ejected nucleons, this tends to suppress yields to the upper hole states until higher incident pion energies. Since it is only by feeding the upper hole states that one can reach ^{11}C starting with ^{13}C, we expect a rising ^{13}C yield, and a falling ratio in Fig. 7.1-1 as the energy is increased. The Cohen and Kurath results also show that the 1p hole excitations in ^{11}C are all bound. Accordingly one must not expect much ^{10}C produced from π^- on ^{12}C even at higher energy, a feature we have already noted. In Fig. 7.1-1 our π^- data is compared to a simple model in which ^{12}C has two states at 12.8 (bound) and 20.4 (unbound) MeV. We assume that the struck nucleon recoils with an energy = $T_{\pi^-}/3$. Only the phase space effects have been included in the calculation.

Presumably the curves comparing ^{16}O with ^{12}C for their ^{11}C production can be understood in similar ways. We are working to make somewhat more quantitative the models we have roughly described.

---

† Coworkers from the Los Alamos Scientific Laboratory.

1. B.J. Dropesky *et al.*, Phys. Rev. Lett. 34, 821 (1975).
2. N.P. Jacob and S.S. Markowitz, Phys. Rec. C13, 754 (1976).
3. F. Lenz, in *Aspects of the π-Nucleus Interaction,* Swiss Inst. for Nuclear Research, C14-5234 Villigen, Switzerland, Nov. 30 (1976).
4. D.T. Chivers *et al.*, Nucl. Phys. A126, 129 (1969).
5. S. Cohen and D. Kurath, Nucl. Phys. A141, 145 (1970).

7.2 Inelastic Scattering of Pions to the Continuum

K. Aniol, D. Chiang, I. Halpern, and G.A. Miller

In April '77 we and our collaborators from Carnegie-Mellon University, University of Wisconsin, and Los Alamos had a short run at LAMPF on a single target, nickel.[1] The incident pion energy was 67 MeV and broad range inelastic pion spectra were recorded at a number of angles with a telescope made of intrinsic Germanium detectors. These spectra, corrected for efficiency etc., are shown in Fig. 7.2-1.

Our main interest in this run was in any gross-structures which might appear in these spectra. Such structures seen in other inelastic scatterings have been associated with giant collective resonances. It was hoped that because of their light mass (compared with other strongly interacting probes) the pions would not excite higher multipole resonances and that it would therefore be easier with pions to identify the lowest multipole giant resonances.

In Fig. 7.2-1 the data suffer from poor statistics (we hope to improve matters in an upcoming run) but even so, one can see a bump in the spectra at many angles at 19 ± 1 MeV and an even more conspicuous bump at back angles at

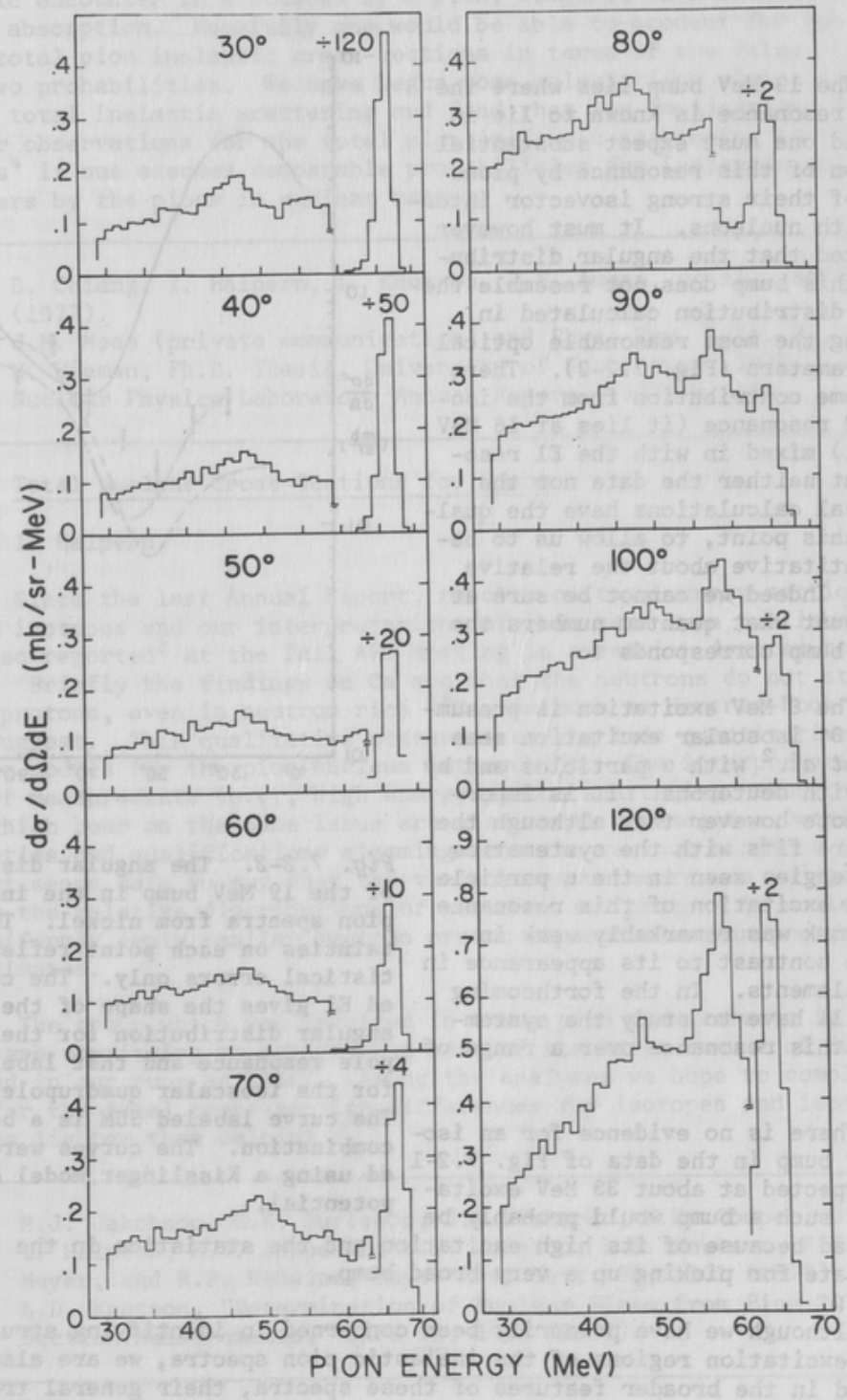

Fig. 7.2-1. **Spectra for the inelastic scattering of 67 MeV pions from natural nickel at a number of angles.**

8 MeV.

The 19 MeV bump lies where the E1 giant resonance is known to lie in nickel and one must expect substantial excitation of this resonance by pions because of their strong isovector interaction with nucleons. It must however be admitted that the angular distribution of this bump does not resemble the expected distribution calculated in DWBA using the most reasonable optical model parameters (Fig. 7.2-2). There may be some contribution from the isoscalar E2 resonance (it lies at 16 MeV in nickel) mixed in with the E1 resonance, but neither the data nor the theoretical calculations have the quality, at this point, to allow us to become quantitative about the relative mixture. Indeed we cannot be sure at present just what quantum numbers the observed bump corresponds to.

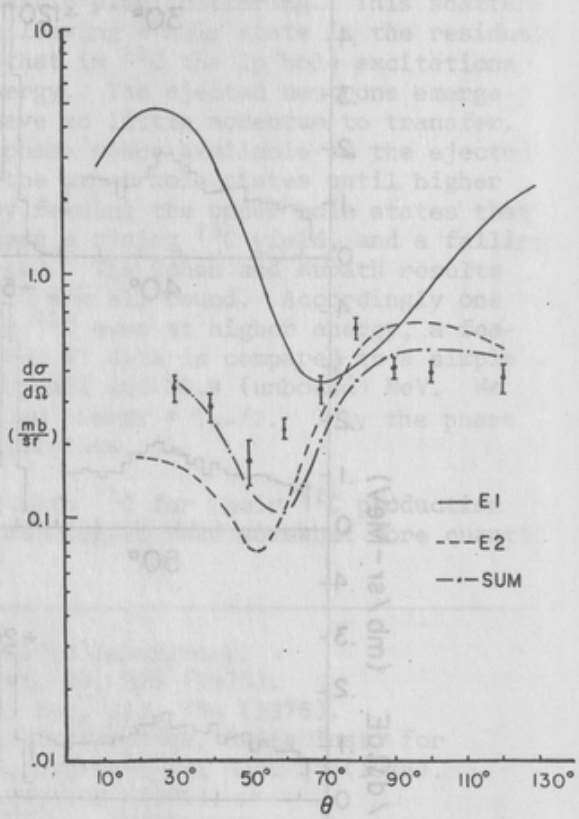

Fig. 7.2-2. **The angular distribution of the 19 MeV bump in the inelastic pion spectra from nickel. The uncertainties on each point reflect the statistical errors only. The curve labeled E1 gives the shape of the expected angular distribution for the giant dipole resonance and that labeled E2 is for the isoscalar quadrupole resonance. The curve labeled SUM is a best fit combination. The curves were calculated using a Kisslinger model optical potential.**

The 8 MeV excitation is presumably the 3^- isoscalar excitation seen by Moss *et al.*[2] with α particles and by Wieman[3] with deuterons. It is important to note however that although the energy here fits with the systematics for 3^- energies seen in the α particle work, the excitation of this resonance in that work was remarkably weak in nickel in contrast to its appearance in heavier elements. In the forthcoming run we will have to study the systematics of this resonance over a range of targets.

There is no evidence for an isovector E2 bump in the data of Fig. 7.2-1 (it is expected at about 33 MeV excitation) but such a bump would probably be quite broad because of its high excitation and the statistics in the figure are not adequate for picking up a very broad bump.

Although we have primarily been concerned in identifying structures in the high excitation regions of the inelastic pion spectra, we are also very much interested in the broader features of these spectra, their general trends with excitation energy, their angular distribution, their integrals and the A dependence and bombarding energy dependence of these quantities. In particular we are anxious to see whether it is possible to assign a relative probability for an

inelastic encounter in a nucleus by a pion, compared with an encounter leading to pion absorption. Hopefully one would be able to account for the A dependence of the total pion inelastic cross-sections in terms of the value of the ratio of these two probabilities. We have begun some calculations with a simple model for the total inelastic scattering and find that its implications fit reasonably with our observations for the total pion inelastic scattering in different elements[4] if one assumes comparable probabilities for inelastic and absorbing encounters by the pions in nuclear matter.

---

1. D. Chiang, I. Halpern, L. Knutson, J.F. Amann, *et al.*, BAPS 22, 525 (1977).
2. J.M. Moss (private communication) and Phys. Rev. Lett. 31, 816 (1976).
3. H. Wieman, Ph.D. Thesis, University of Washington, 1975.
4. Nuclear Physics Laboratory Annual Report, 1977, p. 125.

7.3 Total Nuclear Cross-Sections for Pions

I. Halpern

Since the last Annual Report, results on total cross-sections of the calcium isotopes and our interpretations of them have been published.[1] (They were also reported[2] at the fall APS meeting in a session devoted to nuclear radii.) Briefly the findings on Ca are that the neutrons do not stick out beyond protons, even in neutron rich ^{48}Ca, as much as Hartree-Fock calculations would suggest. This qualitative statement can be made quantitative in terms of specific models for the pion-nucleus interaction. The interpretation of other kinds of measurements (e.g., high energy proton scattering, electron scattering), which bear on the same issue are also model dependent. Despite the uncertainties and qualifications stemming from the various kinds of model dependence, it seems safe to say that the various measurements are in agreement concerning the relative distributions of neutrons and protons in nuclei and that they uniformly imply smaller neutron proton separations than present theoretical estimates.

The group which was involved in these pion measurements is now dispersed, but we are continuing to analyze the rest of the large amount of data that was obtained in our runs at LAMPF. Among the analyses we hope to complete soon are those for the total cross-section differences for isotopes and isotones of elements lighter than calcium.

---

1. M.J. Jakobson, G.R. Burleson, J.R. Calarco, M.D. Cooper, D.C. Hagerman, I. Halpern, R.J. Jeppeson, K.F. Johnson, L.D. Knutson, R.E. Marrs, H.O. Meyer, and R.P. Redwine, Phys. Rev. Lett. 38, 1201 (1977).
2. L.D. Knutson, "Determination of Nuclear Sizes from Pion Total Cross-Section Measurements," BAPS 22, 1009 (1977).

7.4 Low Energy Pion Elastic Scattering on ^{208}Pb and ^{90}Zr

M. D. Cooper†, J. G. Cramer, and W. G. Lynch

We have submitted a proposal[1] to measure low energy pion elastic angular distributions at energies 8, 10, and 12 MeV on two targets ^{90}Zr and ^{208}Pb. At these energies and with these targets we can investigate two questions: 1) Is low energy pion elastic scattering on ^{208}Pb below the Coulomb barrier described well by the Klein-Gordon equation? 2) What is the pion-nucleon optical potential at these energies?

The standard method of dealing with nuclear reactions involving charged particles is to factor the problem into a point Coulomb interaction problem which can be solved exactly and a Coulomb-modified nuclear part which has no exact solutions and usually must be dealt with numerically. When the particles involved are in the relativistic domain it is appropriate to employ a wave equation which is relativistically invariant (e.g., The Klein-Gordon equation), but it has been known[2] that severe difficulties are encountered in solving the point Coulomb problem for spinless particles when $ZZ'>137/2$, and it has been stated[2] that the $\ell=0$ Coulomb equation has no solution under these circumstances. Recently, however, methods of dealing with these difficulties have been devised[3,4] and it is now possible to predict the equivalent of Rutherford scattering from finite nuclei using a relativistically invariant wave equation, even in the domain where $ZZ'>137/2$. We note that π^+ scattered from any target heavier than Erbium (Z=68) satisfies this criterion.

It is thus of great interest to study the pure Coulomb scattering of π^+ in order to make comparisons with properly relativistic predictions of Coulomb scattering. However, although a body of information exists on the elastic scattering of π^+, in all cases the action of the nuclear potential prevents a study of the Coulomb effects in isolation, and uncertainties about the pi-nucleus interaction prevent any serious study of these Coulomb effects. On the other hand, it can be rather important to verify our understanding of the Coulomb part of the interaction as well as possible or one may come to rather incorrect conclusions concerning the nuclear interaction. We note, in particular, that the relativistic corrections to Rutherford scattering increase with energy. Even though the predictions of the Klein-Gordon equation are likely to be correct, it is useful to verify them experimentally.

A unified treatment of the pi-nucleus optical potential for fitting both pionic atom and 50 MeV elastic scattering data has been tried by Stricker, McManus and Carr.[5] The phenomenalogical potential form they use which we will call the MSU potential is:

$$\frac{1}{2\pi}\,\omega\,\mathrm{Vopt} = -[\bar{b}_o\rho - \varepsilon_\pi b_1(\rho_n-\rho_p)] \qquad \text{s-wave scattering} \qquad (1)$$

$$+\vec{\nabla}L(r)C(r)\vec{\nabla} \qquad \text{p-wave scattering with Ericson effect}$$

$+\vec{\nabla}C_o\rho^2\vec{\nabla}$ p-wave absorption

$-B_o\rho^2$ s-wave absorption

$-\frac{\omega}{2m}\nabla^2 C(r)$ Kinematic angle transformation

where $C(r) = c_o\rho - \varepsilon_\pi C_1(\rho_n - \rho_p)$,

$$L(r) = \left[1 + \frac{4\pi\lambda}{3}C(r)\left(\frac{A-1}{A}\right)\right]^{-}, \text{ and}$$

ε_π is the sign of the pionic charge

Equation (1) contains a great number of complex parameters ($b_o, b_1, c_o, c_1, B_o, C_o$) which cannot possible be determined by a single set of data. It has therefore been necessary to invoke theoretically intuitive arguments to try and reduce the number of free parameters. Some parameters which may be adjusted are always required to fit the data since values calculated from free pi-nucleon scattering give, at best, only rough agreement with the data. The approach used in ref. 5 has been to take the best values of the parameters from atoms[6] and leave those parameters which cannot be determined from pionic atoms as variable in order to tune the predictions to the scattering data. Fig. 7.4-1 shows a comparison of the predictions of the MSU and pionic atom potentials for 50 MeV π^+ scattering from ^{12}C.

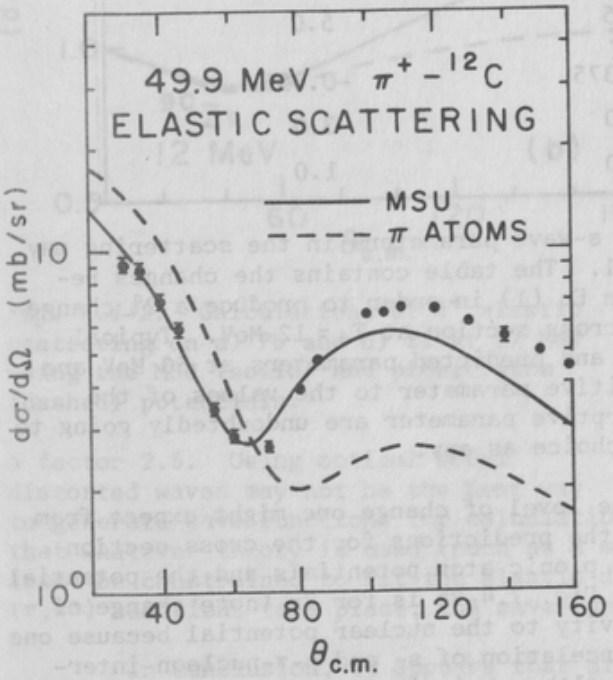

Fig. 7.4-1. $\pi^+ - {}^{12}C$ elastic scattering at 50 MeV. The solid (dashed) curve are calculations using the MSU[1] (pionic atom potential.

Turning to the question of what part of the phenomenology is most likely to be illuminated by these measurements, the answer is the s-wave interaction. By doing sub-Coulomb scattering, the pion must interact in the tail of the nuclear potential or by barrier penetration. As will be discussed below, this selectively suppresses the sensitivity to most effects except the π-nucleus s-wave scattering. Thus, it will probably be sufficient to use "standard" value for all but two coefficients in Eq. (1). At this point, the most likely candidates would be $\mathrm{Re}\bar{b}_o$ and $\mathrm{Im}B_o$. These are supposedly related to real shape scattering (remember that quasi-elastic knockout is suppressed) and

true pion absorption.

It is worthwhile to emphasize the need for understanding these data with statistical precision. The nuclear effects are small in the sub-Coulomb region, and any calculation (e.g., no nuclear potential) will produce qualitatively acceptable fits to the undemanding eye. The interesting nuclear physics lies in the quantitative predictions of the data.

Table 7.4-1.

Nucleus	Parameter	Parameter Value	Change to produce 2% change in cross section
Pb	$4\pi \mathrm{Re}\bar{b}_o$	-0.235	-0.11
Pb	$4\pi \mathrm{Re}C_o$	6.5	3.0
Pb	$4\pi \mathrm{Im}C_o$	0.0	2.0
Pb	$4\pi \mathrm{Im}B_o$	2.5	5.0
Zr	$4\pi \mathrm{Re}\bar{b}_o$	-0.375	-0.055
Zr	$4\pi \mathrm{Re}C_o$	7.0	3.0
Zr	$4\pi \mathrm{Im}B_o$	2.0	1.0

The dominance of the π-nucleus s-wave parameters in the scattering may be appreciated by examining Table 7.4-1. The table contains the changes required for representative parameters in Eq (1) in order to produce a 2% change (two standard deviations) in the 120° cross section at $T_\pi = 12$ MeV. Typical fluctuations between fitted parameters and predicted parameters at 50 MeV are ±1. Thus $\mathrm{Re}\bar{b}_o$ is by far the most sensitive parameter to the values of the measurements. Variations in some absorptive parameter are undoubtedly going to be necessary, and $\mathrm{Im}B_o$ is as likely a choice as any.

As a further illustration to the level of change one might expect from different potentials, Fig. 7.4-2 shows the predictions for the cross section ratio to Rutherford calculated from the pionic atom potentials and the potential of ref. 5. Figure 7.4-2a is for Pb and Fig. 7.4-2b is for Zr (note change of scale). The Zr shows much more sensitivity to the nuclear potential because one is just at the Coulomb barrier. The cancelation of s- and p-π-nucleon interactions is somewhat more delicate in Zr although it is important to have both present in Pb also.

These potentials which predict the different cross sections in Fig. 7.4-2 also predict different distorted waves. Figure 7.4-3 shows the l=0 distorted scattering wave functions for 12 MeV pions on Pb. Note that in the nuclear interior that the wave functions differ by a factor of 1.5.

For a reaction which is influenced by the scattering waves, such as (p,π^+), these differences are important. These models produce differences in the probability of a produced pion propagating to the outside of the nucleus of

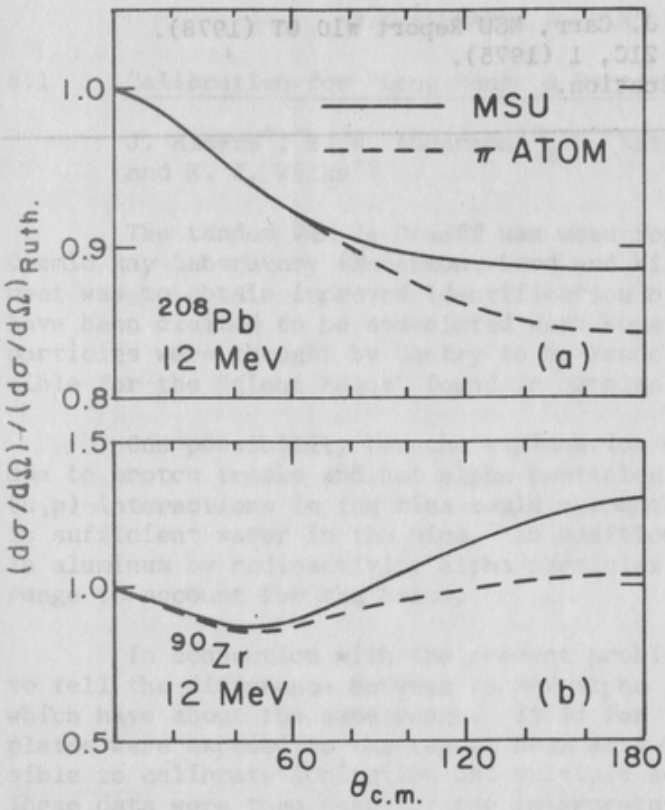

Fig. 7.4-2. Calculations of π^+ elastic scattering on a) Pb and b) Zr at 12 MeV using the MSU (solid) and pionic atom (dashed) potentials.

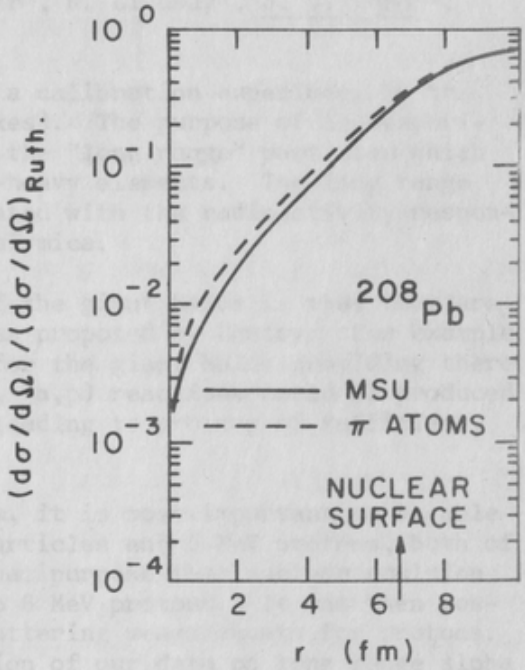

Fig. 7.4-3. ℓ=0 distorted π-Pb scattering wave functions at 12 MeV. The distortion is produced by the Coulomb potential plus either the MSU (solid) or the pionic atom (dashed) potential.

a factor 2.5. Using optical model distorted waves may not be the best way to generate wave functions for calculations of (p,π^+) reactions, but it seems that whatever theory is used (such as a multiple scattering series) should at least be constrained to fit the elastic data also. Even in the surface, where (π,π') reactions take place, the wave functions are different.

In conclusion, it appears that pion scattering at sub-Coulomb energies can provide useful information about the nature of the π-nucleus optical potential, particularly the s-wave part.

---

† Coworker from the Los Alamos Scientific Laboratory.

1. LAMPF LEP Proposal #370.
2. N.F. Mott and H.S.W. Massey, *The Theory of Atomic Collisions*, pp. 40-41 and 78 ff., Clarendon Press, Oxford (1965).
3. J.G. Cramer, W.G. Lynch, and J.G. Wills, *Proceedings of the VIIth Conference on High Energy Physics and Nuclear Structure*, Zürich (1977).
4. M.D. Cooper, R.H. Jeppeson, and N.B. Johnson, *ibid.*

5. K. Striker, H. McManus, and J. Carr, MSU Report π10 OT (1978).
6. J. Hüffner, Physics Reports 21C, 1 (1975).
7. G.A. Miller, private communication.

8. RESEARCH - USERS AND VISITORS

8.1 Calibration for "Long Range α Particles"

J. Albers†, S. N. Anderson††, P. Kotzer†, R. Lindsay†, J. J. Lord††, and R. J. Wilks††

The tandem Van de Graaff was used for a calibration experiment by the Cosmic Ray Laboratory (Anderson, Lord and Wilkes). The purpose of the experiment was to obtain improved identification of the "long range" particles which have been claimed to be associated with super-heavy elements. The long range particles were thought by Gentry to be associated with the radioactivity responsible for the "giant halos" found in samples of mica.

One possibility for the explanation of the giant halos is that they are due to proton tracks and not alpha particles as proposed by Gentry. For example, (α,p) interactions in the mica could account for the giant halos providing there is sufficient water in the mica. In addition, (α,p) reactions could be produced in aluminum by radioactivity alpha particles leading to protons of sufficient range to account for the halos.

In connection with the present problem, it is most important to be able to tell the difference between 16 MeV alpha particles and 5 MeV protons, both of which have about the same range. It is for that purpose that nuclear emulsion plates were exposed to the tandem beam of 5 to 6 MeV protons. It was then possible to calibrate ionization and multiple scattering measurements for protons. These data were then used for the interpretation of our data on long range alpha particles which was presented at the INTERNATIONAL SYMPOSIUM ON SUPER HEAVY ELEMENTS, Lubbock, Texas, March 9-11, 1978.

Although it was important to have a good calibration for protons, it is still necessary to have a similar exposure of plates to alpha particles of low energies.

---

† Western Washington University.
†† University of Washington Department of Physics

8.2 Radiation Environment Simulation - Mechanical Properties*

R. H. Jones† and D. L. Styris†

The use of penetrating light ions to produce displacement damage in materials offers a degree of control over irradiation parameters not attainable with any neutron source. The long term objective for the ion irradiation for mechanical properties program is the development of an ion irradiation system with sufficient flexibility to perform a variety of mechanical property experiments while the short term objective is a correlation between the microstructure and mechanical properties of light ion and neutron irradiated materials.

The ion irradiations are performed in a UHV (5×10^{-10} torr) irradiation

chamber on the 30° beam line of the tandem Van de Graaff accelerator at the University of Washington. This system has been upgraded to include mass analysis of the cooling gas, vacuum Faraday cup monitoring of the ion beam in the gas, and dosimetry by the $^{51}V(p,n)^{51}Cr$ reaction.

The displacement damage produced in MRC marz grade nickel and niobium and reactor grade 316 SS by 16 MeV protons and $^{3}H(d,n)$ and Be(d,n) neutrons is being correlated on the basis of cluster size and density and yield strength. The effects of steady state flux and temperature and cyclic flux, temperature and stress on the microstructure and flow properties and the relationships between the radiation induced microstructure and flow properties are also being studied.

The damage produced in nickel and niobium by 16 MeV protons and $^{3}H(d,n)$ neutrons has been correlated as a function of particle fluence on the basis of microstructure and flow stress. Proton and neutron irradiations were performed on material taken from the same source given the same geometry and identical heat treatments, prepared and evaluated by the same techniques, and irradiated at 20-30° C at a flux 10^{12} particles/cm^2-s.

The 16 MeV protons produced an amount of hardening per particle in the MRC marz grade nickel equivalent to that produced by the H(d,n) neutrons and about 20% more hardening per particle in the MRC marz grade niobium at 10^{17} particles/cm^2. The fluence dependence of the yield strength increase of 16 MeV proton irratiated nickel and niobium were equal to their respective $^{3}H(d,n)$ neutron fluence dependence, within the experimental error.

---

* Funded by the United States Department of Energy, Magnetic Fusion Division.

† Battelle Northwest Laboratory.

8.3 Simulation of In-Reactor Creep

P. L. Hendrick† and C. Henager†

Materials placed under stress and subjected to the elevated neutron fluxes of both breeder and fusion reactors will exhibit a form of accelerated deformation termed irradiation-induced creep. Due to the difficulty, cost and time required in making precise in-reactor creep measurements, there is a worldwide interest in simulating in-reactor creep by bombarding materials of interest with energetic light ions under well-controlled conditions. Such experiments could enhance our understanding of the operating creep mechanisms and permit screening of potential reactor alloys. Several early experiments have demonstrated the ability to simulate irradiation-induced creep and have generated a limited amount of creep data.[1-4]

The Radiation Effects on Metals program supported by the Division of Basic Energy Sciences/Department of Energy at Battelle Northwest is conducting a creep simulation program using the tandem Van de Graaff accelerator at the Nuclear Physics Laboratory. Development of an apparatus located on the straight-ahead line in Cave III, has been completed. The apparatus features a

helium circulating system for removing the irradiation-induced heat from the test specimen. The specimen is heated and its temperature controlled by direct ohmic heating. Temperature is redundantly sensed by measuring the specimen electrical resistance, emitted infrared radiation, and thermocouple output. Stress is applied uniaxially by a remotely-driven tensioning spring. Specimen elongation (i.e., creep strain) is continuously monitored by a non-contacting laser extensometer.

Early experiments have tested the creep response of high purity nickel bombarded with 17 MeV deuterons. Specimens are stressed to between 34 and 340 MPa (5,000 to 50,000 psi), heated to between 100 and 300° C (212 to 572° F) at ion fluxes between 1 and 10 $\mu a/cm^2$. Creep rates are measured as a function of stress, temperature, and flux. This data is then compared with electron microscopy data obtained from the irradiated test specimens to elucidate operating creep mechanisms.

---

† Battelle Northwest, Richland, Washington.

1. S.D. Harkness, F.L. Yagee, and F.V. Nolfi, Jr. ANL-7883, Argonne National Laboratory, 1972.
2. P.L. Hendrick, A.L. Bement, Jr., and O.K. Harling, Nucl. Instr. and Methods 124, 389 (1975).
3. R.J. McElroy, J.A. Hudson, and R.S. Nelson, Proceedings of the International Conference on Radiation Effects and Tritium Technology for Fusion Reactors (CONF -750989, Vol. II), 1975.
4. P.L. Hendrick, D.J. Michel, A.G. Pieper, and R.E. Surratt, J. of Nuclear Materials 59, 229 (1976).

8.4 Equilibrium Delayed Neutron Spectra*

P. J. Grant† and G. L. Woodruff†

Data were recently obtained for directly measured equilibrium delayed neutron energy spectra associated with fast neutron fission of ^{240}Pu. The data were collected using a cyclical sequence consisting of 0.1-sec irradiation, 0.04-sec delay, 0.1-sec count, and a 0.02-sec wait.

The experimental apparatus used was that developed by G. W. Eccleston for his measurements of ^{232}Th, ^{235}U, ^{233}U, ^{238}U, and ^{239}Pu.[1] Although data reduction is not yet complete, the spectrum appears to be similar to the over-all shape of that obtained by Eccleston for ^{232}Th.[2]

---

* Work supported by Department of Energy Contract EY-76-5-06-2225, Basic Agreement No. 31 Mod A007.

† Department of Nuclear Engineering, University of Washington.

1. Nuclear Physics Laboratory Annual Report, University of Washington (1977), p. 148.
2. G. W. Eccleston, "Measurements of Near-Equilibrium Neutron Spectra from Fast Fission," Ph.D. Dissertation (1976).

8.5 Fast Neutron Beam Radiotherapy - Medical Radiation Physics*

H. Bichsel†, J. Eenmaa†, P. Wooton†

The Medical Radiation Physics Division continued its routine support of neutron beam radiobiology and treatment of cancer patients until patient therapy was interrupted in August, 1977, pending the appointment of a new Director of the Division of Radiation Oncology.

Meanwhile, investigations into the determination of absolute neutron dose with ionization chambers continued. New and recent W- and stopping power data were used to calculate the average value of W_n for neutrons and of the dose conversion factor $r = D_W/D_g$ for various neutron energies for finite chamber volumes in A-150 Shonka plastic/TE gas ionization chambers.[1] The results show that W_n is about 31.1 ± 0.6 eV/i.p. (stochastic uncertainty only) for neutron energies ranging from 2 to 14 MeV. A change from the value of 30.5 eV/i.p. used in the past is thereby suggested. The ratio r is found to be quite close to 1.00 for a 2.0 cc chamber, but has an uncertainty of about 4%, most of which is due to the stopping power uncertainty of protons and alpha particles in tissue equivalent materials. For the carbon/carbon dioxide chamber, r increases with chamber volume toward the Kerma ratio. The uncertainty decreases due to a growing dose contribution from insiders.

Dosimetry intercomparisons were conducted with FermiLab (FNL), the Naval Research Laboratory (NRL) and the University of Washington (UW) at the Fermi National Laboratory in August, 1977. The parameters that were intercompared at this meeting were the ion chambers' gamma ray calibrations in the FNL Cs-137 calibration source, and the relative chambers' sensitivity in the FNL neutron beam, as a test of the constancy of the TE plastic composition. The agreement between the gamma ray calibrations of the NRL and FNL chambers was well within the reproducibility of the measurements. The UW chamber calibration differed initially by a larger factor than should be expected but the chamber was subsequently recalibrated at UW against an NBS transfer standard ion chamber and was found to agree within 0.2% of the other groups' FNL measurements.

Measurements in the FNL neutron beam indicated that the standard spread in the relative response of the chambers was about 0.5%, with a maximum spread of 0.9%. This level of agreement was well within the reproducibility of this type of measurement.

Absorbed dose measurements were conducted at UW with the Sloan-Kettering tissue equivalent A-150 plastic calorimeter in cooperation with J. C. McDonald from Sloan-Kettering. The calorimeter is similar to previous designs originated at Sloan-Kettering.[2] The central absorbing element, in which dose is determined, is cylindrical in shape, 2 cm in diameter and 2 mm in thickness. The calorimeter is constructed nearly entirely of A-150 plastic so that the measurement represents the absorbed dose at a point in an extended TE medium. Measurements with spherical, thimble, and cylindrically shaped TE ionization chambers at a depth of 5 cm in A-150 plastic were in agreement with the calorimeter to 2%. Since the absolute uncertainty in the calorimeric measurements is felt to be ±2.5% due mainly to the thermal defect, it appears that the constants employed in the ion chamber measurements are good to within a few percent.

Additional measurements of this type will be carried out at the other neutron therapy centers in the U.S. later this year.

A neutron beam dosimetry protocol to be used by all current and future neutron therapy facilities in the U.S. is being prepared in coordination with the AAPM RTC-TG #18, Fast Neutron Beam Dosimetry Physics. The protocols are being developed according to previous agreements of the neutron dosimetry physics group; these have been based on dosimetry studies and practice, and on dosimetry intercomparisons among participating institutions. An outline of the proposed dosimetry protocols was presented at the meeting of TG #18 at RSNA/AAPM-'77, Chicago.

---

* Supported by NCI Grant No. CA-12441.

† Division of Medical Radiation Physics, Department of Radiology, University of Washington.

1. H. Bichsel and A. Rubach, Third Symposium on Neutron Dosimetry, Munich, 1977.

2. J.C. McDonald, J.S. Laughlin, and R.E. Freeman, Medical Physics 3, 80 (1976).

8.6 Fast Neutron Beam Radiation Therapy Clinical Program*

T. W. Griffin†

On September 10, 1976, a program of phase I clinical trials was instituted to study the efficacy of fast neutron beam teletherapy in the treatment of human cancer. These initial studies were designed to develop treatment techniques applicable to practical patient problems, study of normal tissue reactions to fast neutron beam therapy to define proper dose schedules, and to observe and record tumor responses to this new treatment method. Since that time, patients have been assessed and results of treatment analyzed in several areas.

Table 8.6-1. Tumor control for metastatic squamous cell carcinoma of the head and neck region

	Size of Adenopathy		
	≤3 cm	3-6 cm	>6 cm
All patients	100%	82%	40%
Mixed beam	100%	96%	50%

Table 8.6-1 outlines the results of treatment for patients who have been treated for metastatic squamous cell carcinoma of the head and neck region and have achieved primary tumor control. The first group of patients represents all patients who received neutrons as part of their therapy and the second group of patients represents only those who received mixed beam therapy (neutrons on Monday and Friday and photons on Tuesday, Wednesday and Thursday). These

results are superior to those previously reported for conventional radiation therapy alone.

Table 8.6-2. $T_3N_{0-3}M_0$ Carcinomas of the Oral Cavity

	Number of Patients	Percent Survival*
All Patients	35	46**
Neutrons only	9	33
Mixed beam	26	50

*Mean followup 1.2 years.
**9% died of intercurrent disease without evidence of malignancy.

Table 8.6-3. $T_4N_{1-3}M_{0-1}$ Carcinomas of the Nasopharynx

	Number of Patients	Disease free Survival*
All Patients	9	6/9
Neutrons only	2	1/2
Mixed beam	7	5/7**

*Mean followup 11 months.
**Death due to intercurrent disease.

Table 8.6-4. $T_{2-3}N_{0-3}M_0$ Carcinomas of the Oropharynx

	Number of Patients	Percent Survival*
All Patients	49	35**
Neutrons only	17	6
Mixed beam	32	50

*Mean follow up 1.3 years.
**12% died of intercurrent disease without evidence of malignancy.

Table 8.6-5. $T_3N_{0-3}M_0$ Carcinomas of the Hypopharynx

	Number of Patients	Percent Survival*
All Patients	17	35
Neutrons only	4	1/4(25%)
Mixed beam	13	5/13(38%)**

*Mean follow up 1 year.
**69% tumor control after exclusions for death due to intercurrent disease.

Tables 8.6-2 through 5 report the results of treatment for squamous cell carcinoma of the oral cavity, nasopharynx, oropharynx, and hypopharynx respectively. The results reported in these patients, again, are superior to those previously reported with conventional therapy.

These early results have prompted the formulation of national cooperative protocols where all neutron projects will submit patients to protocol studies randomizing therapy between the various fast neutron beams and the best available standard treatment. Hopefully, in this way the full potential of high LET therapy can be realized.

* Supported by NCI Grant No. CA-12441.
† Division of Radiation Oncology, Department of Radiology, University of Washington.

8.7 Fast Neutron Beam Radiotherapy Experimental Oncology*

Janet S. Rasey†

The research program in Experimental Oncology has been supportive of the neutron beam therapy project, in which cancer patients were treated with the neutron beam from the University of Washington cyclotron from September 1973 to August 1977. Our program has attempted to answer clinically relevant questions in the neutron radiobiology of tumor cells and selected normal tissues.

Projects continued or completed in the past year include studies of (1) potentially lethal damage repair, and (2) sublethal damage repair in the EMT-6 sarcoma-like tumor of the BALB/c mouse. Experiments were done with tumor cells growing *in vitro* (tissue culture) and *in vivo* (solid subcutaneous tumor in the mouse).

These investigations are described in more detail below:

Table 8.7-1. Potentially Lethal Damage Repair in the EMT-6 Tumor System Growth Modes and Postirradiation Treatment Used

Growth Mode	Postirradiation Conditions which may allow PLD-R	Repair after X-rays?	Repair after Neutrons?
In vitro - 1-day-old exponentially growing cells	Cover cells with depleted growth medium for 6 hours after irradiation	Yes* small amount	Yes* small amount
In vitro - 6-day-old cultures in nutritionally limited plateau phase of growth	Delay trypsinization and subculture of cells for survival determinations	Yes* large amount of repair	Yes* large amount of repair but less than X-rays
In vitro - 4-day-old fed cultures (i.e., fresh growth medium daily) in spatially limited plateau phase of growth	Delay trypsinization and subculture of cells for survival determination	Yes* large amount of repair	No
In vivo - tumors 100 mm^3 in volume	Delay excision and preparation of cell sample for survival determination	Yes* large amount of repair	No

*A large amount of repair means that cell survival increased by a factor of 2.5 or more in samples subjected to repair conditions. A small amount of repair means survival increased by a factor of less than 2.0. Comparisons were made at a survival level of 2% (*in vitro*) or 6-10% (*in vivo*).

1. Potential lethal damage repair (PLD-R) following X- or neutron irradiation was studied in EMT-6 mouse tumor cells growing *in vivo* or *in vitro*. Potentially lethal radiation damage is defined as damage whose repair can be modified by the conditions cells or tumors are subjected to immediately after irradiation. Generally, conditions which maintain the cells without encouraging growth and cell division allow this type of damage to be repaired; the repair is expressed as an increased survival level in the treated cell population subjected to the proper conditions. Table 8.7-1 shows the growth modes and postirradiation treatment used.

   The conclusion is that PLD-R does occur after neutron irradiation as well as after X-ray treatment, contrary to several reports published by others. However, the conditions under which this repair occurs post-neutrons are fewer. In direct comparison with X-rays within the same experiment, the amount of repair is less after the high LET radiation.

2. Sublethal damage repair following irradiation was studied using the classic split dose techniques of Elkind. This type of repair is defined as an increase in cell survival as the time interval between 2 doses of radiation is increased; the reference point is survival following a single (non-split) dose of radiation equal to the sum of the 2 doses. All permutations of X-ray and neutron radiation were employed: x-x, n-n, n-x and x-n. In the x-x combination, survival increased up to 1-2 hours between dose with no further increase with up to 8 hours between doses. With the n-n combination, repair occurred more slowly, requiring 4-5 hours between doses before the survival leveled off. In the n-x and x-n combinations, the time course and amount of repair was characteristic of the quality of the first dose of radiation. Reports by others of an absence of sublethal damage repair in x-n and n-x combinations were thus not confirmed.

3. The radiation response of mouse skin to different energy neutron beams used for cancer therapy was continued. These experiments, part of a program sponsored by the National Cancer Institute, were designed to determine relative biological potentency of the different neutron beams. While agreement on physical dose at these centers is excellent (±1%), equivalent rad doses do not have the same biological effect. These results and those of other intercomparison biologists will be useful in comparing tumor response and late normal tissue damage in patients treated in different neutron therapy programs.

   Nine neutron beams, including the University of Washington beam, have been intercompared to date. As part of each intercomparison, an "at home" experiment with the University of Washington neutrons was done. The University of Washington beam was thus assigned a potency of 1.0 and other neutron sources were related to this. The potencies were determined from the ratio of neutron doses required to produce a specified level of skin response over the 7 - 35 day postirradiation observation period. The level of skin response chosen was 1.25 on an arbitrary scale, which is equivalent to a maximum response of moist desquamation of slightly less than 1/4 of the foot skin by days 17 - 21 post-treatment. This is followed by complete or virtually complete healing by day 35. With the University of Washington beam, this response was produced by a dose of 1580 - 1700 rad. This value

varied slightly between experiments, requiring a University of Washington control experiment as part of each study.

Table 8.7-2. Relative potencies of neutron beams at cancer treatment facilities determined using mouse skin as a biological dosimeter

Beam[a]	Incident Charged Particle Energy and Target Material	Relative Potency at Average Response Level = 1.25
TAMVEC	16 MeV d^+ - Be	1.24
IMS	16 MeV d^+ - Be	1.22
U of W	21.5 MeV d^+ - Be	1.0
Cleveland Clinic -NASA	25 MeV d^+ - Be	in progress
NIRS	30 MeV d^+ - Be	0.936
NRL	35 MeV d^+ - Be	0.943
TAMVEC	35 MeV d^+ - Be	0.984
TAMVEC	50 MeV d^+ - Be	0.904
Fermilab	66 MeV p^+ -Be	0.898

[a] Abbreviations used:

TAMVEC	Texas A&M University variable energy cyclotron
IMS	Institute of Medical Sciences, Tokyo
Cleveland Clinic-NASA	Cleveland Clinic-National Aeronautics and Space Administration - Lewis Research Center joint project
NIRS	National Institute of Radiological Science, Chiba-shi, Japan
Fermilab	National Accelerator Laboratory, Batavia, Illinois

The physical characteristics of the different neutron beams and their relative potencies are compared in Table 8.7-2. Some beams were mentioned in last year's report and are included here for completeness.

---

* Supported by NCI Grant No. CA-12441.

† Division of Radiation Oncology, Department of Radiology, University of Washington.

8.8 Fast Neutron Beam Radiotherapy-Radiation Biology*

J. P. Geraci†, A. M. Spence‡, K. L. Jackson†, G. M. Christensen†, P. D. Thrower†, and M. Mariano†

During the past year the effects of cyclotron-produced fast neutrons and ^{60}Co gamma rays on an ethylnitrosourea-induced rat astrocytoma transplanted to the intracerebral site have been examined. Unirradiated animals usually succumb from the mass effects of relentless tumor growth 17 to 21 days after implantation of 5×10^4 cells. This mechanism of death is often seen in humans with brain tumors. Whole-head neutron or photon irradiation in a single dose one week after transplantation delays the onset of neurological signs and prolongs survival. This response is dose-dependent with both types of irradiation (Fig. 8.8-1). However, neutrons are clearly more effective per rad resulting in a RBE of 3.0 to 3.5. Preliminary results using five daily fractions at a neutron dose per fraction of 200 rad indicate that fractionation does not appreciably change this RBE value. The limited total-dose tolerance of the oral mucosa prevented delivery of a higher curable dose of neutrons or photons to the tumor implants.

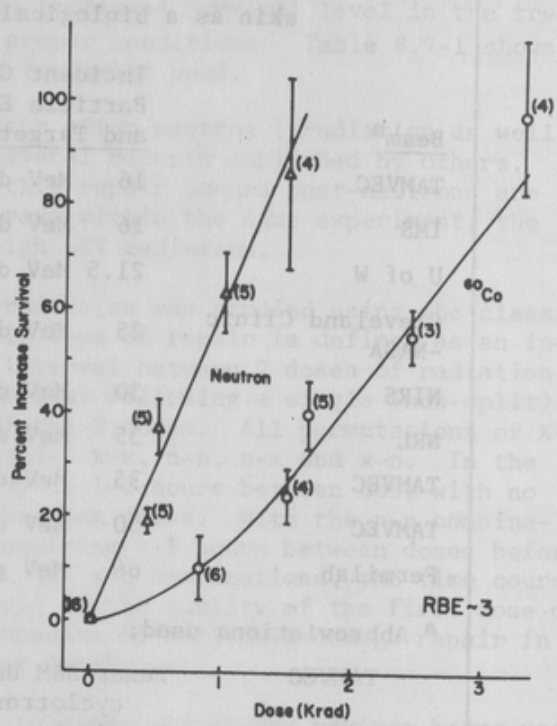

Fig. 8.8-1. Dose-response curves for increased survival due to photon and neutron irradiation of rat astrocytoma.

* Supported in part by NCI Grants No. CA 22431 and CA 18385.

† Department of Radiology, University of Washington.
‡ Department of Neurology, University of Washington.

8.9 Plastic Track Detector Calibration

R. A. Johnson†, H. B. Knowles†, and G. E. Tripard†

Since 1974 a research group at Washington State University has been employing plastic track detectors for the measurement of heavy ions emitted by high-energy negative pions and captured negative pions when either interacts with tissue-resident nuclei. Starting in 1975, track detector measurements of heavy ions produced by therapeutic fast neutron beams has been initiated.

The most sensitive of the plastics employed (Kodak Pathe CA 80.15

cellulose nitrate) had never been completely calibrated for range and etch rate against beams of heavy ions of known energy. This is especially significant because the WSU group employs a much lower etch temperature than do other groups using tract detectors to measure heavy ions of very low energy. During the etch of several callulose nitrate films exposed to low-energy ^{16}O ions at Los Alamos, a previously unremarkable etch parameter, etch induction time, was found to show a quasilinear dependence on incident particle energy. The existence of a third etch parameter, other than range and etch rate, would provide a simple method for measuring energy, charge, and mass (isotope) of an incident heavy ion, thus extending useful domain of heavy ion spectroscopy down to a region of $\sim$0.1 - 0.2 MeV/amu specific kinetic energy. This would extend the domain of heavy ion measurements well below those feasible with conventional counter systems and has application not only to current biophysical problems, but also to astrophysical and nuclear structure investigations.

Currently ^{4}He and ^{3}He beams from the University of Washington tandem Van de Graaff are being used to investigate the functional dependence of etch induction time upon mass, energy and charge state.

---

† Department of Physics, Washington State University, Pullman, WA.

8.10 Total Body Calcium by Neutron Activation

C. H. Chesnut†, T. K. Lewellen†, R. Murano†, and W. B. Nelp†

The Division of Nuclear Medicine is continuing its measurements of total body calcium by means of whole-body neutron activation and whole-body counting. The cyclotron is used as the neutron source, and the 3.1 MeV gamma ray of 8.7 minute ^{49}Ca is counted.

Two therapy regimes are being tested for the control of post menopausal osteoporosis. Twenty-five patients are being treated with Calcitonin, while 25 more are used as controls. Both treated and control groups are women over 50 years who show several signs of osteoporosis, including a history of fractures. Treatment is continued for a two-year period, with 5 neutron activation measurements. A number of other tests are made on these patients, including blood and urine chemistries, photon transmission densitometry of the arm bones, and bone biopsies with tetracycline labeling to measure new bone growth on the microscopic level. A similar group of patients and controls is being studied for the effects of the drug Winstral (Winthrop Laboratories).

Twenty-one percent of the patients in these two programs have completed the series of measurements, and all patients have had at least 3 of the scheduled 5 measurements.

A few osteoporotic patients have been measured in conjunction with a study conducted by Drs. Meaney and Recker of Creighton University in Omaha, Nebraska.

Another small group of patients has been measured for Dr. Marchioro, of

the University of Washington School of Medicine. These are renal transplant patients who will undergo parathyroidectomy. Changes in their calcium metabolism are expected.

---

† Division of Nuclear Medicine, Department of Radiology, University of Washington.

8.11 Development of a ^{81}Kr Production Facility for Nuclear Medicine

T. K. Lewellen†, G. M. Hinn†, R. Murano†, and W. B. Nelp†

Trial runs were made on the University of Washington cyclotron to determine the potential production yield of ^{81}Rb using the 40 MeV α beam and the standard powder target plate. If sufficient ^{81}Rb can be produced, than a system to automatically load the ^{81}Rb on shielded columns can be built, thus producing ^{81}Rb - ^{81}Kr generators.

The yield was found to be sufficient to produce 8 - 10 10-mCi generators with an hour and a half bombardment time. However, the radiation levels at the target box at the end of bombardment are several hundred rads/hour. Thus, a remote control handling system will have to be designed and installed.

---

† Division of Nuclear Medicine, Department of Radiology, University of Washington.

8.12 Production of ^{11}C Labeled Morphine

D. R. Allen and P. Beaumier

As part of the continuing efforts by the University Nuclear Pharmacy to provide new and innovative radiopharmaceuticals to the nuclear medical community, Carbon-11 production and chemistry was studied. Carbon-11, the 20 minute half life positron emitter, is ideally suited for many *in vivo* dynamic radiotracer applications to determine organ function as well as imaging.

In completed work, our group studied the synthesis of N-($^{11}CH_3$)-morphine and its biodistribution in the rabbit model. Carbon-11 dioxide can be produced in relatively abundant yield (≈350 mCi/30 min) by the $^{14}N(p,\alpha)^{11}C$ nuclear reaction. Subsequent reduction of $^{11}CO_2$ by $LiAlH_4$ over anhydrous THF and hydrolysis, produced $^{11}CH_3OH$ which was oxidized over silver wool at 450° C to produce Carbon-11 formaldehyde, $^{11}CH_2O$. Reductive alkylation of normorphine with $^{11}CH_2O$ over $NaBH_4$ produced the desired N-($^{11}CH_3$) morphine.

This work demonstrated the feasibility of the University of Washington cyclotron to produce C-11 material for radiopharmaceutical production and will be the basis for further study with short-lived radiopharmaceuticals.

---

9. ACCELERATOR AND ION SOURCE DEVELOPMENT

9.1 Van de Graaff Accelerator Operations and Development

Staff

Among Van de Graaff accelerator development activities were the following projects: improvements of the generating voltmeter for use in regulating the terminal voltage (see Sec. 9.3 and 9.4); improvement of the polarized ion source, including the ^{3}He recovery system (see Sec. 9.5); modernization of the accelerator control circuitry; improvement of the vacuum in the accelerator beam tube, and construction of a revised sputter source.

Statistics of Van de Graaff accelerator operations are given in Table 9.1-1.

As a first step in modernizing the accelerator control circuitry, we have installed a programmable controller (Texas Instrument T15) to control part of the low energy vacuum system, the high energy beam line valves, the vacuum system on the 60 inch scattering chamber, and the accelerator safety interlocks. A programmable controller is a small, inexpensive computer which receives input signals from devices such as switches, current relays, vacuum gauge contacts, etc., and uses a stored logic program to interpret these inputs and connect power to appropriate output lines, which may operate valves, motors, heaters, etc. The logic operations which can be programmed include "and," "or," and "not" as well as delay timers and counters, arranged so that programs can be written in a simple notation similar to ladder diagrams used with relay networks.

The controller has exhibited a number of advantages over the relay networks it replaced:

1) It has led to a greatly simplified wiring network for the accelerator. Since only one wire connects each device to the controller, and since all interconnections are made by the program, the number of wires has been reduced by at least an order of magnitude.

2) The controller appears to operate more reliably. With no moving parts and a rugged electrical design, this system has operated without any failure attributable to the hardware so far. It has survived a number of power outages.

3) The controller is easier to modify. New inputs and outputs can be added by simply plugging in the appropriate modules. Changes to the logic of the program or changes in the settings of timers and counters can be entered with a small keyboard while the rest of the program is continuing to function.

4) It is much easier to keep documentation for the system up to date. Since any part of the program in the controller can be read out at any time, it is not necessary to maintain circuit diagrams and wire lists.

The one disadvantage of the controller is that it takes time to learn to program and troubleshoot it. As a result, these skills have not become as

Table 9.1-1. Statistics of Van de Graaff Operation from April 16, 1978 to April 15, 1978

	Time (Hrs)	Per Cent
1. Division of time among activities		
Normal operations[a]	6,520	75
Scheduled maintenance and accelerator development	732	8
Unscheduled maintenance	179	2
Unrequested time	1,329	15
Total[b]	8,760	100
2. Division of beam time among particles		
a. Two stage operation		
Protons	1,080	21
Polarized protons	903	18
Deuterons	178	4
^{3}He	332	7
^{4}He	525	10
^{12}C	116	2
^{14}N	10	<1
^{16}O	1,278	25
^{18}O	123	3
^{28}Si	150	3
^{32}S	96	2
^{58}Ni	2	<1
^{107}Ag	3	<1
Subtotal	4,796	95
b. Three stage operation		
Protons	65	1
^{16}O	20	1
^{35}Cl	160	3
Subtotal	245	5
TOTAL BEAM TIME	5,041	100
3. Division of normal operation among activities		
University of Washington Nuclear Physics Laboratory	5,724	88
Battelle Northwest Laboratories	639	10
University of Washington Department of Nuclear Engineering	130	2
Washington State University	24	<1
University of Washington Physics Department	3	<1
Total	6,520	100

a) Includes all the time the accelerator was under the control of an experimenter.

b) This is the number of hours in a year.

widespread in the Laboratory as desirable.

Studies of the effect of a poor vacuum in the beam tube on heavy ion transmission have shown that substantial losses occur for some ions at pressures as low as 10^{-6} Torr. In order to improve the beam tube vacuum the following tasks have been completed: the buncher tube at the lower energy end of the tandem has been reworked to minimize virtual leaks; at the same time, provisions have been made to install a titanium sublimation pump in this device; two ion pumps in the low energy region have been overhauled to improve pumping speed; and, a titanium sublimation pump has been installed in the terminal of the tandem. As a result, the vacuum in the beam tube has improved by a factor of 2 to 5 and it is possible to attain a pressure of 1×10^{-7} Torr at the low energy end of the tandem.

A new sputter source has been designed and is nearly completely constructed. This source, which has been constructed to circumvent problems inherent in the old source, will have an improved vacuum system, view ports for trouble shooting sparking problems, better focusing geometry for the cesium beam, a lock to permit installation of cones without breaking vacuum, and the capability of measuring ionizer temperature precisely.

9.2 Polarized Ion Source Development

E. G. Adelberger, W. R. Ingalls, H. E. Swanson, T. A. Trainor, and R. Von Lintig

The polarized source has operated with the spin filter and rapid spin reversal system for somewhat over a year. During this time much experience has been acquired during a succession of ^{19}F parity runs, which probably complete the data-acquisition phase of that experiment. Beam polarization during the most recent runs has typically been 81% with occasional variations over a ±2% range. The corresponding polarization with straight spin-filter operation is 90-92%.

The upper limit on false asymmetries due to transverse spin-correlated beam motion is about 10^{-5} as inferred from the 74 KeV "normalizer" gamma ray in the ^{19}F experiment. This is consistent with earlier inferences made from results with a beam-motion analyzer and artificially large rapid-reversal fields.

Minor refinements of the rapid-reversal system included a redesigned electrode set for the compensating electric field. The design was a result of a detailed 3-dimensional study of the magnetic field generated by the T-coil and electrolytic tank studies of various electrode geometries to determine what would best reduce the net Lorentz force over the beam region. These studies were performed with AC currents and voltages and a lock-in amplifier to eliminate various DC offset difficulties.

Various polarized beam properties are monitored on-line with the quad polarimeter discussed in previous reports. These include polarizations and spin-axis orientations for both spin states and the ratio of beam intensities in the two states. Some of these parameters were observed to vary with time in

ways that could not easily be explained by any reasonable model of ion source operation. The problem was finally traced to silicon build-up on the polarimeter carbon-gold target. The source of the silicon is a popular brand of O-ring grease. The polarimeter and nearby vacuum components have been thoroughly degreased and a carbon-based low vapor-pressure grease is now used, since carbon build-up causes no problems. With these steps and additional electron suppression to improve energy resolution the polarimeter computer-ion source system now maintains the spin angle to better than 0.1°.

The ^{3}He recirculator system constructed for use with the old Lithium charge-exchange source[1] has been made portable, and quick-disconnect hardware has been introduced into the polarized ion source fore-vacuum system so that ^{3}He beams can be economically produced. For ^{3}He runs the recirculator is rolled inside the polarized source high-voltage cage and connected with the hardware provided. Performance is similar to that for ^{4}He beams, with typically 2 μA and up to 4 μA of He^{++} analyzed at 3-5 MeV.

Two regulated high voltage power supplies based on a high-frequency oscillator system have recently been purchased, one to replace an unregulated supply for the duoplasmatron extraction electrode, which gets much abuse, and another to replace the main frame voltage supply. The latter purchase is motivated by a desire to time bunch helium beams from the polarized source. The existing power supply, although regulated to a certain degree, suffers long term drifts which are unacceptable for bunching purposes.

Because the two devices share several similar subsystems much of the technical progress made on the hydrogen atom parity experiment described elsewhere in this report[2] can be transferred to the polarized ion source. The first instance of this is a recirculating cesium canal constructed for the hydrogen experiment. This device has been extensively studied[2] and a modified version is now being constructed based on the results. The original device is, however, quite serviceable for use in the polarized source and represents a factor of 10 reduction in rate of cesium loss from the canal ends. This should substantially extend the lifetime of the source during helium runs.

---

1. Nuclear Physics Laboratory Annual Report, University of Washington (1972), p. 11.
2. See Section 10.3 of this report.

9.3 Cyclotron Operations and Improvements

H. Fauska, B. Lewellen, J. Orth†, G. Saling, and W.G. Weitkamp

The cyclotron has continued to be used predominantly for medical research. Articles describing cancer therapy, *in vivo* neutron activation analysis and nuclear pharmacy are given in Chapter 8. Statistics of cyclotron operations are given in Table 9.3-1.

An improved main magnet regulator is under development. Plans are being made for upgrading the cyclotron somewhat to support future medical

research.

Table 9.3-1. Statistics of Cyclotron Operations from April 16, 1977 to April 15, 1978

	Time (Hrs)	Per Cent
1. Division of time among activities		
Normal operation	1,102	74
Scheduled maintenance	290	20
Unscheduled maintenance	88	6
Total	1,480	100
2. Division of beam time among projectiles		
Alpha particles	75.1	14
Protons	8.6	2
Deuterons	433.2	84
Total	516.9	100
3. Division of normal operating time among users		
University of Washington Cancer Therapy Group		
a. Therapy	146	13
b. Physics	86	8
c. Biology	78	7
d. Experimental Oncology	148	14
University of Washington Nuclear Medicine	566	51
University of Washington Nuclear Pharmacy	14	1
University of Washington Nuclear Physics Laboratory	64	6
Total	1,102	100

† Retired September 30, 1977.

9.4 Use of Van de Graaff as a Super Sensitive Mass Spectrometer, FY '78.

G. W. Farwell, H. Fauska, and F. H. Schmidt

Richard A. Muller (Lawrence Berkeley Laboratory) suggested using a cyclotron as a super sensitive mass spectrometer (Science 196, 489 [29 April 1977]). Although the basic idea is an old one, he revived it with new and important considerations which appear to make the technique especially attractive for ^{14}C, ^{10}Be and ^{3}H dating. Other potential uses might be in trace element detection, especially for investigation of nuclear reactions leading to stable isotopes.

During the summer of 1977, we explored the possibility of using the tandem Van de Graaff for this purpose. The Van de Graaff has a number of potential advantages over a cyclotron which we will not detail here, except to mention that a sputter ion source may be the ideal type to use.

Our first objective was to develop operational techniques such that the Van de Graaff could be "tuned" reliably to produce a particular analyzed beam, even if the "beam" could not be detected or controlled by usual techniques. In short, the terminal potential must be regulated by means other than the usual image slit-corona system, so we made various improvements to the generating voltmeter, and fed its signal into the regulating system.

In addition to holding the terminal potential constant independent of any actual beam, it is necessary to pre-set all magnetic parameters (bending magnets, quadrupoles, and steering magnets) to exact values to produce the desired beam.

During the summer we were reasonably successful with both objectives. For example, we could reliably "dial in" beams such as $^{13}C^{-1}$ stripped to $^{13}C^{+5}$, $(^{13}C^{14}N)^{-1}$ stripped to $^{13}C^{+5}$ or $^{14}N^{+5}$. To detect very small beams, we installed a solid state detector on an unused beam line just downstream from the switching magnet.

Unfortunately, just as we were ready to try looking for ^{14}C from a "young" source of carbon, our sputter ion source failed, and the summer ended.

Due to lack of man-power, very little further work has been accomplished since the Summer of 77, but work will resume vigorously during the summer of 78. At the time of writing, we are engaged in various electronic improvements to the regulating systems.

These efforts have been quite successful. The systems of regulation shown in figures 9.4-1 and 9.4-2 have both operated successfully. Details of the crucial improvements to the GVM circuit are discussed in Section 9.5.

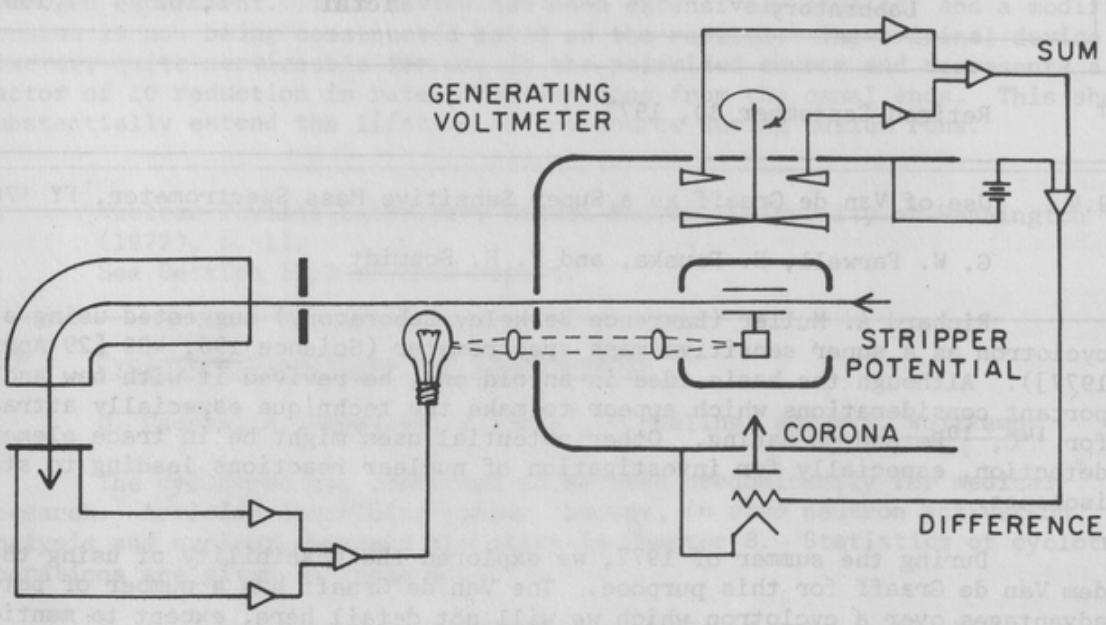

Fig. 9.4-1. **Twin regulator decoupled hybrid system.**

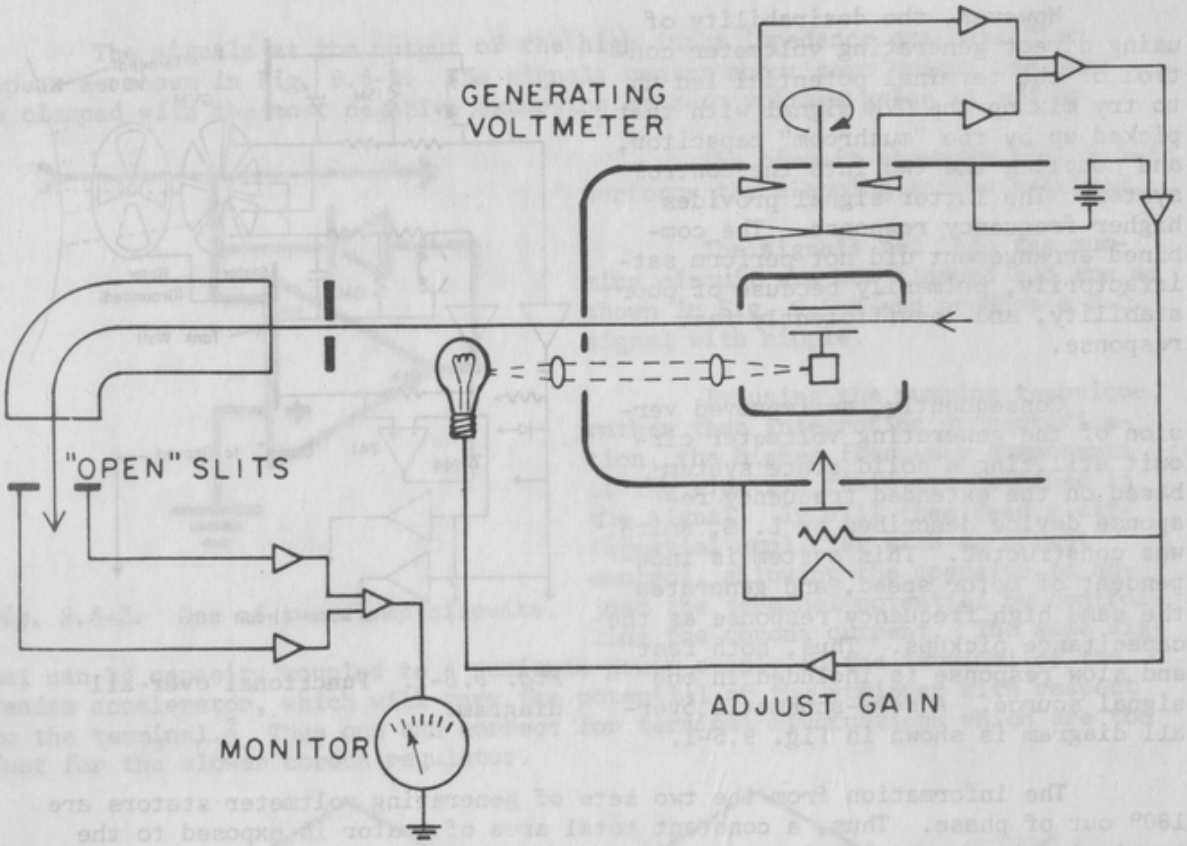

Fig. 9.4-2. The no-slit ultimate system.

In addition, improvements to the sputter ion source are being designed.

It is worth mentioning that regulation of the Van de Graaff very accurately without utilizing the customary image slits will have other important applications. For example, it could generate a "super-clean" beam, free of beam degredation due to slit scattering, the deleterious effects of which are well known.

9.5 Improvement of the Generating Voltmeter Corona Controller and Digital Readout

H. Fauska and F. Schmidt

The generating voltmeter, as initially supplied with the tandem Van de Graaff, used a vacuum tube rectifier circuit, together with a series battery to provide the proper voltage offset. The circuit was non-linear, and required considerable maintenance.

As the first step, an improved unit was constructed which employed solid state compensated feedback amplifiers.

However, the desirability of using direct generating voltmeter control of the terminal potential led us to try mixing the GVM signal with that picked up by the "mushroom" capacitor, and coupling the two into the control system. The latter signal provides higher frequency response. The combined arrangement did not perform satisfactorily, primarily because of poor stability, and insufficiently fast response.

Consequently, an improved version of the generating voltmeter circuit utilizing a solid state system based on the extended frequency response device described by L. G. Smith,[1] was constructed. This system is independent of motor speed, and generates the same high frequency response as the capacitance pickups. Thus, both fast and slow response is included in one signal source. A semi-schematic overall diagram is shown in Fig. 9.5-1.

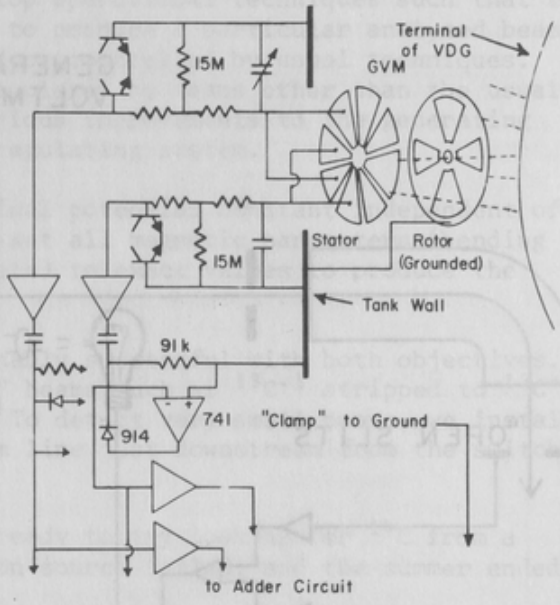

Fig. 9.5-1. Functional over-all diagram.

The information from the two sets of generating voltmeter stators are 180° out of phase. Thus, a constant total area of stator is exposed to the terminal voltage at all times.

By electronically clamping the signals from each set of stators to ground, and then summing the two triangular outputs, a fast response signal can be retained. The other criterion is to use a very high input impedance preamplifier, thus preserving the basic triangular-shaped signals from each set of stators.

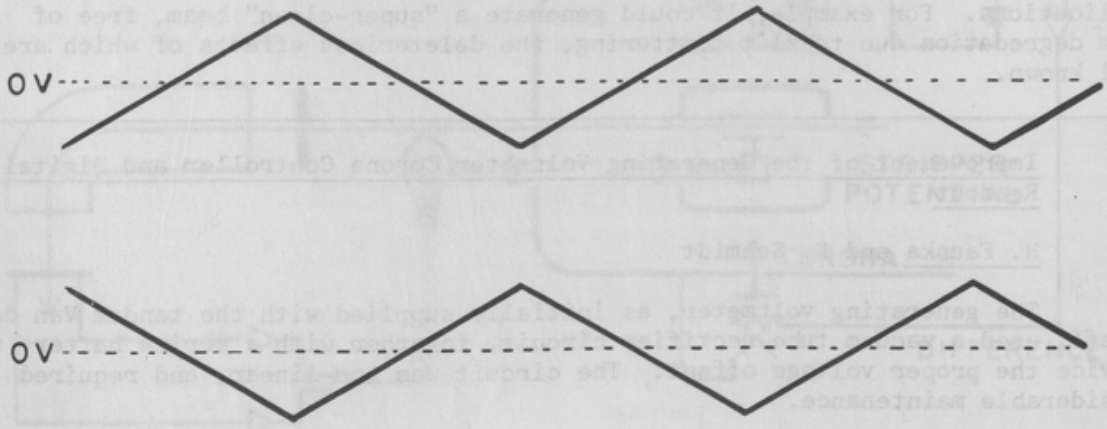

Fig. 9.5-2. (Upper) Stator pre-amp output #1; (Lower) Stator pre-amp output #2.

The signals at the output of the high input impedance pre-amplifier appear as shown in Fig. 9.5-2. The signals center about zero volts, and must be clamped with the most negative excursion at zero voltage prior to adding.

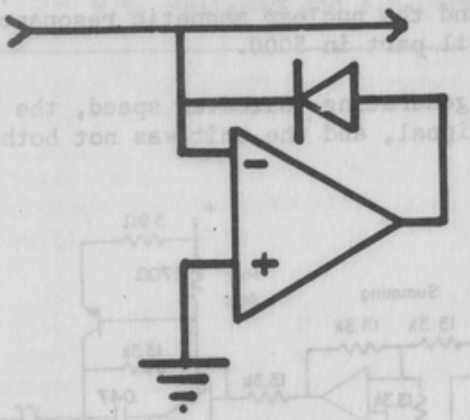

Fig. 9.5-3. **One of two clamp circuits.**

The circuit shown in Fig. 9.5-3 performs the clamping action required.

The signals fed into the summing circuit are now clamped and are as shown in Fig. 9.5-4 and produce a D.C. signal with ripple.

By using the summing technique, rather than integration or rectification, the higher frequency components of the electric field are retained in the signal. It will then feed a differential amplifier with an offset control, allowing the operator to adjust the terminal potential by controlling the corona current. The same signal can be capacity coupled to a variable power supply in the terminal of the tandem accelerator, which will vary the potential of the stripper with respect to the terminal.[2] Thus one can correct for terminal fluctuations which are too fast for the slower corona regulator.

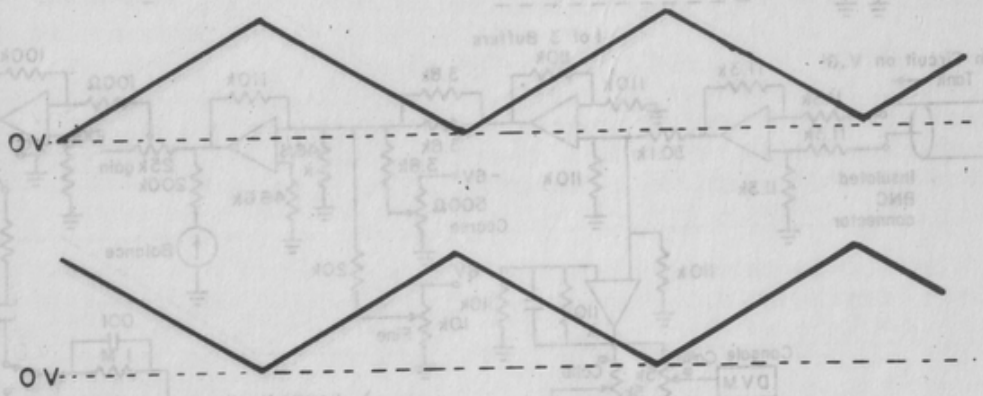

Fig. 9.5-4. **(Upper) Clamped signal stators #1; (Lower) Clamped signal stators #2.**

The optically coupled terminal stripper regulator does not have the stabilizing of negative feedback, therefore the operator must optimize the amount of gain used in the correction signal. The present system can be adjusted while observing a beam scanner or maximizing the beam intensity on target.

The circuit has operated with no image slits in the system thus preventing slit scattering, but more importantly the machine can be controlled on a very small beam of intensity too small to yield enough slit signals to allow the usual control of terminal voltage.

Stability of the voltmeter circuit has been tested by observing the output portion of the summing amplifier which is read out on a digital voltmeter display at the operation console. During several days and nights of continuous running while the machine was regulating via the image slits and corona, the energy was set by the analyzing magnet and the nuclear magnetic resonance regulator. The digital readout varied only ±1 part in 5000.

The accuracy does not vary with generating voltmeter speed, the high frequency response is preserved in the signal, and the unit was not bothered by temperature changes.

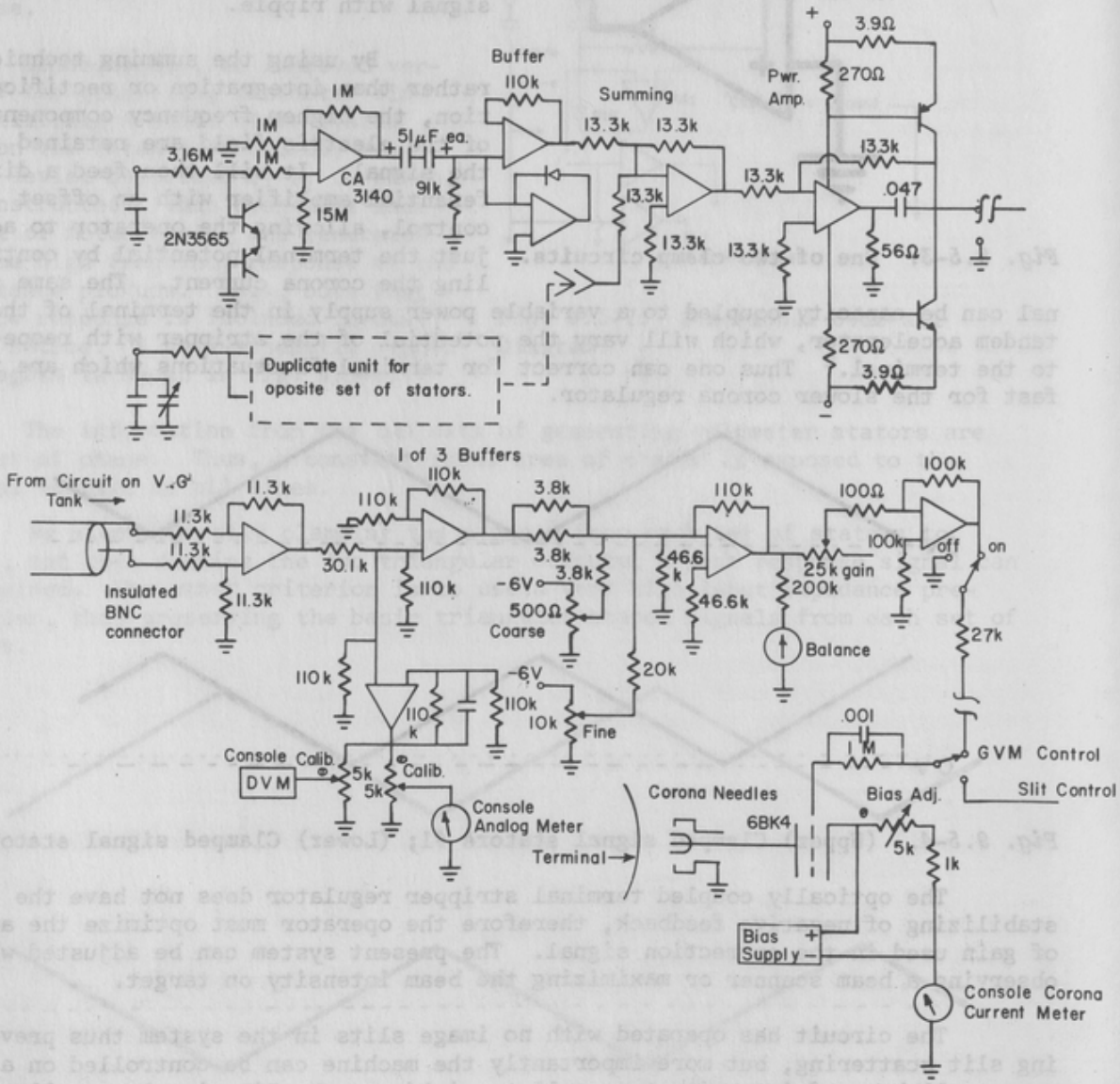

Fig. 9.5-5. Complete over-all schematic.

The currently used circuit schematic is shown in Fig. 9.5-5.

1. L.G. Smith, Rev. of Sci. Instr. 25, 510 (1954).
2. W.G. Weitkamp and F.H. Schmidt, Nucl. Instr. and Meth. 122, 65 (1974).

10. INSTRUMENTATION AND EXPERIMENTAL TECHNIQUE

10.1 Target Preparation

S. Hoffman

Over 200 thin targets varying in thickness from a few $\mu g/cm^2$ to several mg/cm^2 were produced by evaporation, rolling, plating or anodizing and include Adenine, Al, Au, Al_2O_3, Bi, Ca, ^{13}C, CdS, ^{63}Cu, Gd, ^{6}LiF, Mn, ^{58}Ni, Na, Mg, Pb, ^{206}Pb, ^{208}Pb, Rh, Sb, Se, Sn, Sr, Si, SiO_2, $Ta_2{}^{18}O$, and UF_4. The targets were self-supporting or deposited on carbon or metal backings. Film sandwiches of 3 layers and 1-2 mm strip targets of Al, Pb, and Au on carbon backings were used in some experiments.

Selenium targets are difficult to produce although the metal is very easy to evaporate and forms a reddish amorphous film that is tough. Unfortunately at 70°C the amorphous selenium crystallizes and shrinks by 15%[1] destroying the target. However, self-supporting films approximately 5 mg/cm^2 were produced at this laboratory. Se was evaporated from a resistance headed Ta tube boat (3 cm high, 1 cm diam.) onto a 20 $\mu g/cm^2$ carbon coated glass slide suspended just over the tube opening. After cooling in vacuum, a circle approximately 1 cm diam. was scribed around the thickest deposit of Se in order to relieve stress caused by later volume reduction. When the slide was baked 1/2 hour at 70°C and cooled, 50% of the time the selenium pulled up from the carbon in a large smooth cyrstalline piece that could be mounted between two carbon foils for protection from evaporation in beam.

Two pieces of apparatus were built for the target lab. A glove box enclosure with double entry doors was built onto a surplus vacuum evaporator and vented outside in order to provide a safe environment for the production of targets of highly toxic materials such as Be. A polypropylene stretching device was built after the design of D. B. Barrus and R. L. Blake.[2]

---

1. M.P. Givens, Rev. Sci. Instr., 25, 1130 (1954).
2. D.M. Barrus and R.L. Blake, Rev. Sci. Instr., 48, 116 (1977).

10.2 A Time-Zero Detector for Heavy Ion Spectroscopy

Alan G. Seamster and Robert Vandenbosch

A fast timing detector for heavy ions has been constructed which incorporates a stack of two microchannel plates as an electron multiplier. The device, based on the design of Zebelman *et al.*,[1] utilizes the isochronous transport of secondary electrons produced when a charged particle passes through a thin carbon foil. The transport is accomplished by crossed electric and magnetic fields.

A time resolution of 250±50 psec has been measured for 15 MeV ^{12}C using the time-zero unit and a silicon surface barrier detector. The nature of the stop detector is such that the contribution of the time-zero detector to the

resolution cannot be directly obtained. However, by comparing the time resolution obtained by detecting recoil and scattered ^{12}C ions with a pair of silicon surface barrier detectors and that obtained between a single silicon detector and the time-zero unit an upper limit of 150 psec was deduced.

The efficiency, measured with a 20 $\mu g/cm^2$ carbon foil, was found to be 55% for 5.48 MeV alpha particles. Measurements with 58.4 and 4.76 MeV ^{16}O gave 69% and 94% respectively.

---

1. A. M. Zebelman *et al.*, Nucl. Instr. and Meth. 141, 439 (1977).

10.3 Design and Construction of Electronic Equipment

H. Fauska and R. E. Stowell

The following electronic equipment was designed and constructed for use with the new terminal regulation system described in Chapter 9.3: Two generating voltmeter high impedance pre-amplifiers including clamping circuits, summing circuits and line driver amplifiers, several buffer amplifiers to drive the console digital and analog meters, a difference amplifier with set point control, and two pre-amplifiers for the capacity pick ups (mushrooms) on the tandem.

A new experiment controller was designed and constructed. The controller allows the experimenter to control the data taking process either with the computer or manually. Provision is made to take data only when the tandem or injector energy is at desired level. The error signal is derived from the digital voltmeter comparators described in our 1977 Annual Report.[1] Provision is also made to take data only when the beam current is at a desired intensity. The devices controlled include all analog-to-digital converters, scalers and optional control outputs to be used as the experimenter wishes.

New scaling circuits have been designed and are under construction. The scalers will be in two banks of 16, one bank in each counting area. Each scaler contains 10 decimal digits, a maximum counting rate is 75 megaHertz, and is provided with pulse inputs for standard NIM or fast NIM pulse signals. The scalers are interfaced to the computer via a standard IEEE 488-75 Bus, and can be both read out and written into (i.e., preset) providing maximum flexibility to the experimenter. Each scaler position is addressable by software, allowing all circuits to be identical and interchangeable.

The local telephone system for use during machine adjustments, repair, and experimental setup has been redesigned and updated.

Electronics designed and constructed for use in the measurements of g-factors for short lived nuclear states described in Chapter 3.4 include the following:

1. A beam chopper control and sequencer providing Activate, Wait, Count, Wait and Start Over functions.

2. A magnet sweep control.

3. A buffer amplifier system control interface unit.

Other electronics designed and constructed include:

1. An eight channel pre-scaler unit in a NIM plug-in.

2. A circuit to alert the experimenter in the event an ADC does not get reset. The device starts a clock run down and if it fails to receive a reset from an ADC clear it will sound an alarm to alert the experimenter.

3. A single pulser with a variable duration of up to one minute. The unit has received much use in checking electromechanical devices.

---

1. University of Washington Nuclear Physics Laboratory Annual Report, 1977, p. 175.

10.4 Focal Plane Detector for the Magnetic Spectrometer

Y-d. Chan, J. Cramer, W. Lynch, and R. J. Puigh

To measure low energy heavy ion particle yields at very small angles we have found it necessary to use the magnetic spectrometer.[1] However, there are several problems inherent with using this apparatus. First, the spectrometer is of the Brown-Beuchner design[2] and has focusing only in the horizontal plane. Therefore the solid angle of the detection system is small and determined by the vertical height of the detector at the focal plane. The maximum vertical dispersion for particle trajectories is approximately 5 cm (at the focal plane) and is determined by the hole gap of the magnet (3 cm). Most commercial solid state position sensitive detectors have a vertical dimension of approximately 1 cm. To use the largest solid angle allowed by the spectrometer's design we have decided to develop a gas position sensitive detector which has characteristics similar to the Rochester[3] and Argonne designs.[4]

A schematic diagram of our prototype gas detector is shown in Fig. 10.4-1. Initially, three (3) reactive wires (300 Ω/ft) are used to provide position information corresponding to the particle's track through the detector. Also, three anode plates are used to provide energy loss information. The major difference between our prototype detector and the detector of Ref. 4 is

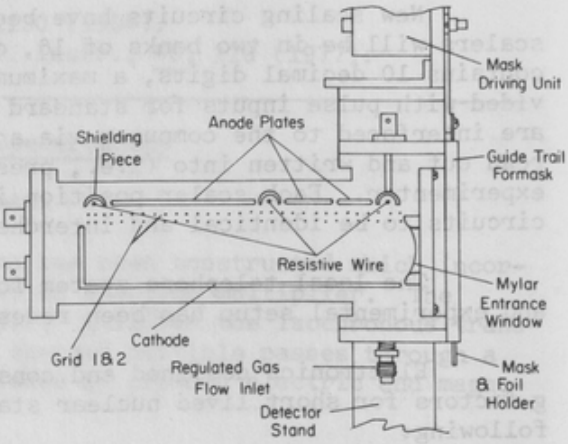

Fig. 10.4-1. Schematic of focal plane detector.

that our detector has a larger separation (4 cm) between the positive and negative electrodes due to solid angle consideration.

This detector has been tested both in the magnetic spectrograph and the 60" scattering chamber. The position resolution has been determined by placing a slotted mask before the entrance window. This technique has been used to determine the position resolution for different heavy ions and the results are shown in Fig. 10.4-2. Typical position resolution for the first wire (closest to the entrance window) is the order of 1.2 mm for ^{16}O ions.

One of the experiments which we hope to perform is to measure the excitation function for the $^{12}C(^{21}S,^{21}S)^{12}C$ elastic and inelastic scattering channel

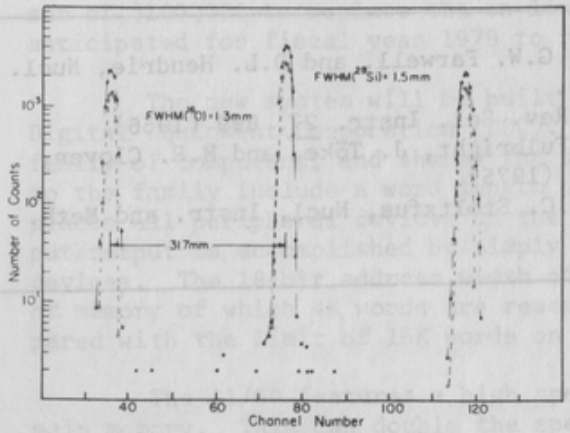

Fig. 10.4-2. **Position spectra from first wire for various particle types elastically scattered from Au.**

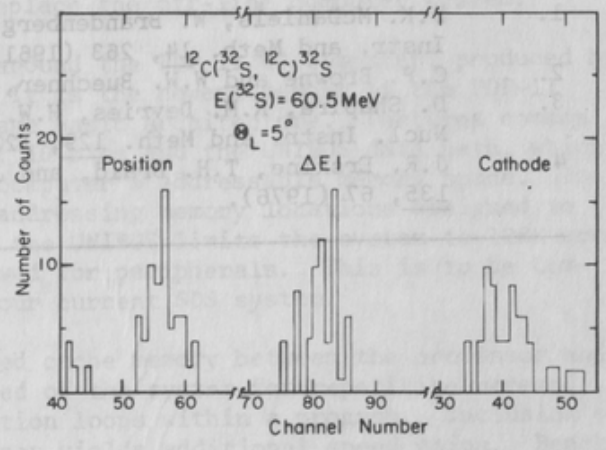

Fig. 10.4-3. **Spectra corresponding to energy loss for the $^{12}C(^{32}S,^{12}C)^{32}S$ reaction at 60.5 MeV and detected at 5° (lab).**

at 180°. To do this we intend to measure the recoil ^{12}C at 0°. To determine if our gas counter could detect the ^{12}C recoils we measured this reaction at 60.5 MeV at 5° (lab) in the magnetic spectrograph. The results of these measurements are shown in Fig. 10.4-3. That these events represent ^{12}C particles was verified by keeping the experimental set-up the same and measuring ^{12}C elastic scattering from a Au target at a beam energy which resulted in the ^{12}C ions having an energy equivalent to their energy from the $^{12}C(^{32}S,^{12}C)^{32}S$ reaction at 60.5 MeV.

There were several problems encountered in using this prototype gas counter in the spectrograph. First, the physical dimensions of the counter did not permit the placement of the front resistive wire on the focal plane at the end of the focal plane corresponding to less energetic particles. We next found that the particles to be detected entered the gas counter at an angle of 55° with respect to the normal to the detector face. Because of the large separation between the two resistive wires only 8.9 cm out of the 22.9 cm horizontal width of the entrance window could be used effectively.

We are currently building a new gas detector which will eliminate these problems. First, the physical dimensions of the detector will permit the location of the front resistive wire on the spectrograph's focal plane. The major feature of the new gas counter is that its detection length along the focal plane will be increased to 57.2 cm. This will increase the number of excited states for a given reaction that one could detect at one time. Also, one can detect more than one charge state of the heavy ion (at one time) from a particular reaction. This in turn reduces the run time needed to accumulate sufficient data. The usable vertical height of the gas counter will be increased to 5 cm in order to use the maximum possible solid angle permitted by the spectrograph's design.

---

1. D.K. McDaniels, W. Brandenberg, G.W. Farwell, and D.L. Hendrie, Nucl. Instr. and Meth. 14, 263 (1961).
2. C.P. Browne and W.W. Buechner, Rev. Sci. Instr. 27, 899 (1956).
3. D. Shapira, R.M. Devries, H.W. Fulbright, J. Tōke, and M.R. Clover, Nucl. Instr. and Meth. 129, 123 (1975).
4. J.R. Erskine, T.H. Braid, and J.C. Stoltzfus, Nucl. Instr. and Meth. 135, 67 (1976).

---

11. COMPUTERS AND COMPUTING

11.1 New Computer System

R. Seymour, H. E. Swanson, and K. Green

This laboratory has been conducting experiments with an on-line data acquisition system built around an SDS 930 computer for the past 11 years. The need to replace this system has become increasingly evident to us, for a number of reasons.

The age of the system is forcing a high maintenance overhead on our staff. Speed and memory limitations have restricted the experimental flexibility of the laboratory. As a result, we were granted for fiscal year 1978 the sum of $100,000 to replace the on-line system. A similar level of funding is anticipated for fiscal year 1979 to replace the off-line computer system.

The new system will be built around the PDP 11/60 computer, produced by Digital Equipment Corporation (DEC). It is the newest member of the PDP-11 family of computers, and shares the same basic architecture. Features common to the family include a word length of 16 bits and the UNIBUS data path, which places all peripheral devices in the computer's addressable memory space. Input/output is accomplished by simply addressing memory locations assigned to devices. The 18-bit address width of the UNIBUS limits the system to 128K words of memory of which 4K words are reserved for peripherals. This is to be compared with the limit of 16K words on our current SDS system.

The 11/60 features a high speed cache memory between the processor and main memory. This can double the speed of the system for repetitive access, such as is encountered during calculation loops within a program. Inclusion of a hardware fast floating-point processor yields additional speed gains. Benchmark programs run on the 11/60 typically execute at 5 times the speed of the SDS 930.

With the 11/60, we will receive a pair of RL01 Disc drives (5 MegaByte), a RM03 Disc drive (67 MegaByte) and the Disc based RSX-11M operating system. With the large disc space and interactive operating system, user programs will be entered either by cards or by typing them directly into files via video terminals. Once on the disc they can be compiled, edited and run without the usual delays and problems of card equipment.

For run-time data collection, we have one 7-track tape drive ordered. This will provide compatibility with the SDS machines, and allow us to read old tapes if needed. Next year we intend to install three 9-track tape drives, thus providing increased data packing ability and conforming to the current standards of the computer industry.

For printing and rough plotting, we are installing a Printronix 300 line-per-minute printer. Its matrix hammers can be individually controlled, giving 60 to 72 dot per inch resolution. For publication-quality plotting we are moving the old Calcomp plotter from the SDS to the 11/60.

Also on the system is a VT11 graphics unit. This device automatically displays data from memory on a 17" screen, with light pen and keyboard interaction with the computer operator. Its direct access of memory permits the computer to be busy calculating and moving data while the display is maintained without flicker of the image.

For interfacing to scalers and other laboratory instruments, the 11/60 is being provided with an IEEE488 interface. This device provides interconnection to an international-standard bus protocol. As a part of the equipment upgrade, we are designing and building 32 new 10-digit scalers. These will be able to be loaded, controlled and read via the IEEE bus. The hydrogen parity computer also can "talk" over an IEEE bus.

For the actual collection of the experimental data, an interface is being built to couple 12 200-megahertz Analog-to-Digital converters (ADC) to the computer. The user will set up the experiment's conditions, and then the ADC's will automatically analyze and store their data directly to the computer's memory. Each of the ADC's can be independently programmed for group size, coincidence grouping, signal routing and certain error checking. The ADC's can be set for both 16-bit and 32-bit capacity in channel put-away mode, allowing optimized use of limited memory.

Funding limitations required the choice of a 16-bit computer, as well as the acquisition of only 64,000 words of memory this year. We expect about a four to six month development lag between receipt of the computer and its taking over most of the data taking tasks from the real-time SDS machine. As we await delivery, the DEC LSI-11 computer used with the hydrogen parity experiment is providing some program writing and testing support, thanks to its commonality within the PDP-11 family.

11.2 On the Application of a Generalized Form Factor to the Optical Model Analysis of $^{16}O + ^{28}Si$ Elastic Scattering

Y-d. Chan and S. Y. Lee

We have applied optical model potentials of the following form

$$V(r) = (Vo+iWo)/(1+\alpha\exp(s/a1)+\exp(s/a2))$$

$$S \equiv r-ro(A_1^{1/3}+A_2^{1/3})$$

to study the elastic scattering of ^{16}O on ^{29}Si. The above form factor has the advantage that it contains both the conventional Woods-Saxon form and the (Woods-Saxon)^2 form as its limiting cases ($\alpha \to 0$ and $\alpha \to 2$, $a_1 \to 2a_2$). The latter (WS)^2 form has been applied successfully to the scattering of α on Ca isotopes.[1] By introducing two extra degrees of freedom (α and a_1), one hopes to improve the quality of data fitting (over large angular ranges) for even heavier systems.

As an application, we have fitted the angular distribution data of Braun-Munzinger *et al.*[2] for $^{16}O + ^{28}Si$ scattering at $E_L(^{16}O)$ = 50 and 55 MeV by the following potential:

V_o = 290 MeV r_o = 1.122 fm a_1 = 3.7 fm a_2 = 0.49 fm

W_o = 2.29 exp(0.0391 E_L) MeV α = 0.9 r_c = 1.2 fm

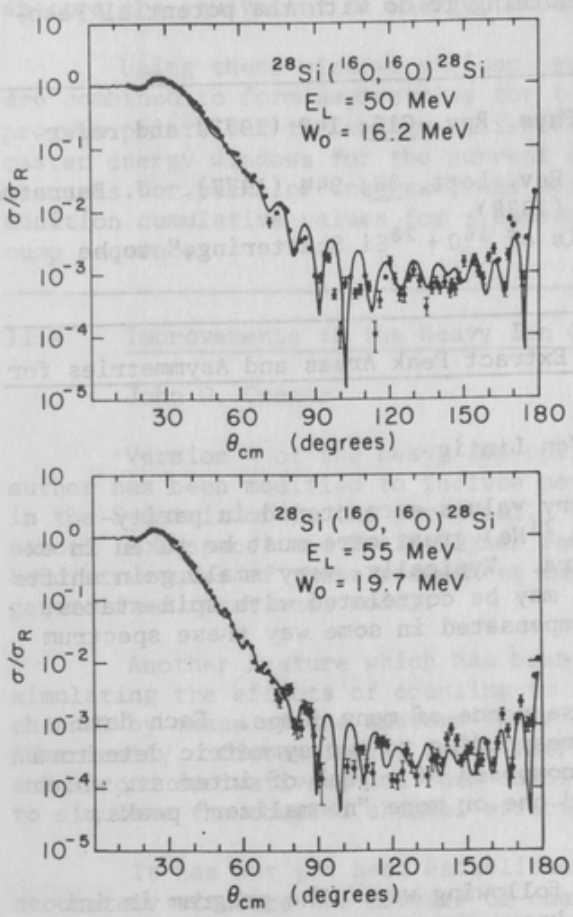

Fig. 11.2-1. Comparison of the experimental angular distributions and that of theoretical calculation. The potential is given in the text and the data are taken from ref. 2.

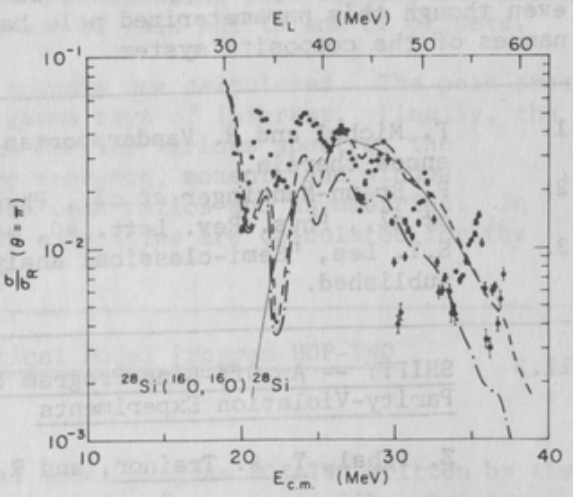

Fig. 11.2-2. Comparison of the experimental excitation function at θ = 180° (taken from ref. 2) and that of the optical model calculation. The dash-dotted curve in the excitation function calculation is the result of averaging the dashed curve (θ=180°) over an angular region of 5°. The thin solid line is the semiclassical internal wave contribution.

The calculated angular distributions and the elastic excitation functions at θ_{cm} = 180° for the above potential are shown in Fig. 11.2-1, 2. One can see that not only the angular distributions are being fit quite well, but also the general features of the oscillatory structure in the excitation function can be reproduced. The fact that this potential has identical real and imaginary geometries makes semi-classical interpretations simple. Our semi-classical analysis result[3] for the above potential indicates that the oscillatory structure in the excitation function is rather due to interference effects than molecular type resonances. In fact, the interference leads to a rather regularly spaced oscillation, with the energy spacing determined by

$$\Delta E = 2/\left(\frac{\delta\Lambda}{\delta E}\right)$$

where Λ is the grazing angular momentum. The same analysis also shows that the $P^2_{\Lambda-1/2}(\cos\theta)$ distribution in the differential cross section is due to undamped internal wave refractive-diffractive phenomena, and that the interval wave diffractive effort can be parameterized by a simple pole in the complex l-plane, even though this parameterized pole has nothing to do with the potential resonances of the composite system.

---

1. F. Michel and R. Vanderpoortan, Phys. Rev. C16, 142 (1977) and references therein.
2. P. Braun-Munzinger *et al.*, Phys. Rev. Lett. 38, 944 (1977). J. Barrette *et al.*, Phys. Rev. Lett. 40, 445 (1978).
3. S.Y. Lee, "Semi-classical analysis of $^{16}O + ^{28}Si$ Scattering," to be published.

11.3 SHIFTY -- An Off-Line Program to Extract Peak Areas and Asymmetries for Parity-Violation Experiments

Z. Iqbal, T. A. Trainor, and R. Von Lintig

Because of the very small asymmetry values encountered in parity-violation (PV) experiments (e.g., ^{19}F and ^{21}Ne) great care must be taken in extracting peak areas from the photon spectra. Typically, very small gain shifts and/or zero offsets are encountered which may be correlated with spin states, polarimeter magnet sense, etc. If not compensated in some way these spectrum alterations can lead to false asymmetries.

Data are typically acquired as a sequence of many dumps. Each data dump consists of four similar spectra corresponding to two symmetric detectors and two "spin states." Each spectrum is composed of a peak of interest, which is expected to exhibit a PV asymmetry, and one or more "normalizer" peaks, sensitive only to instrumental effects.

SHIFTY extracts peak areas in the following way. The program is initialized for a dump sequence by assigning known gamma-ray energies to several peaks in the spectra, and by entering initial peak and background windows for each spectrum. Centroids are calculated within these initial peak windows and combined with the peak energy assignments to yield initial gains and zero offsets for each spectrum of the first data dump. The peak and background window channels for one spectrum only are then converted to energy values using the initial energy calibration for that spectrum. These master energy windows are retained for use in the iterative procedure outlined below for successive dumps until the analysis program is reinitialized.

For each subsequent data dump centroids obtained with the channel windows resulting from a previously converged iteration are combined with peak energy assignments to yield initial spectrum calibrations. These are in turn used to convert the master energy windows to new channel windows, from which new spectrum calibrations are obtained, etc. This iterative procedure converges rapidly. The convergence criterion is that the relative changes in spectrum

gain and channel offset be less than some fraction of their respective statistical errors. A fraction of 1/10 requires 4-6 iterations for a typical photo spectrum. The result of this procedure is a self-consistent set of peak channel windows and spectrum energy calibrations. Corresponding peak windows in various spectra are equivalent in energy, independent of gain shifts and DC offsets.

Using these windows various peak moments are calculated. The peak areas are combined to form asymmetries for the gamma rays of interest. Finally, the program prints out the energy calibrations for the various spectra, the master energy windows for the current dump sequence, moments and window channels for peaks of interest, and various peak ratios and asymmetries. In addition cumulative values for a number of quantities are calculated for the cump sequence.

11.4 Improvements to the Heavy Ion Optical Model Program HOP-TWO

John G. Cramer

Version 4 of the heavy ion optical model program HOP-TWO written by the author has been modified to include several kinds of resonance-like structures in the S-matrix or in the potential. These include Regge-poles[1,2] (i.e., resonances in L-space) and Breit-Wigner resonances (i.e., resonances in energy). Band structures of these resonances can be specified in accordance with the generalized rotational model.

Another feature which has been added to the program is a capability for simulating the effects of coupling to inelastic channels from the elastic channel by means of the Austern-Blair approximation.[3] This is accomplished by numerically differentiating the S-matrix with respect to L to obtain the first and second derivatives, and then combining these with the optical model S-matrix to simulate the coupled channel effects.

It has not yet been established that the Austern-Blair procedure can accurately simulate the effects of channel coupling. We plan to investigate the accuracy of the approximation by direct comparison with coupled channel calculations.

---

1. K. McVoy, Phys. Rev. C3, 1104 (1971); and *Classical and Quantum Mechanical Aspects of Heavy Ion Collisions*, H.L. Harney, P. Braun-Munzinger, and C.K. Gelbke, Eds., p. 127, Springer Verlag, Berlin (1975).
2. P. Braun-Munzinger, G.M. Bertowitz, T.M. Cormier, C.M. Jachcinski, J.W. Harris, J. Barrette, and M.J. LeVine, Phys. Rev. Lett. 38, 944 (1977).
3. N. Austern, *Direct Reaction Theories*, (Wiley, New York, 1970), Chapter 5 and the references cited therein.

11.5 GENOA-II, A Major Revision of the Global Optical Model Search Program

John G. Cramer

The global optical model search code GENOA written by F. G. Perey[1] a number of years ago and more recently modified with improved Coulomb functions has proved to be a very powerful analysis tool in the study of heavy ion optical potentials.[2] However, the code in its standard form has a number of awkward aspects, particularly its input and plotting formats, and lacks the ability to search on potentials which are L-dependent or which include resonances in the S-matrix.

In the course of carrying out an extensive global analysis of $^{16}O + ^{28}Si$ elastic scattering from the point of view of the possible existence of a continuum rotational band, it was decided to extensively modify GENOA to include a long list of features and conveniences which would add to the usefulness of the program.

The input format of the program was simplified and rationalized, and many default options were added. In particular, it is no longer necessary to specify the integration step size, maximum integration radius, and maximum L-value, although each of these can be specified if desired. The size of the input parameter card deck had been reduced by about a factor of two. Several options for output have been included so that the amount of superfluous paper used in output can be drastically reduced. The plotting program has been modified from its two-cycle log form to a three cycle plot with "retrace" so that a plot which disappears off the bottom of the plot reappears at the top.

The definitions of the optical model potentials have also been expanded and revised. The "joined" Woods-Saxon potential with different diffusenesses inside and outside the potential radius has been eliminated, and replaced by a four parameter Woods-Saxon potential of the form $f(r) = [1 + \exp((r - R)/(\alpha a))]^{-\alpha}$ so that when $\alpha=1$ the potential is a normal Woods-Saxon. This form factor is used in all of the potentials (except the spin-orbit potential). Also included is J-dependent absorption (equivalent to L-dependent absorption for spin=0),[3] and any mixture of surface and volume absorption. Resonances in the S-matrix have been included which may be either of the Breit-Wigner form or in the form of a band structure of rather general energy dependence. Corrections for channel coupling effects of inelastic scattering coupling back to the elastic channel have been included, employing the Austern-Blair approximation.[4]

Finally, the definition chi-squared has been generalized to permit more emphasis on large angle data and to include "phase-sensitive" terms useful in rapid fitting of oscillating data, and provisions for "staged" searches have been expanded.

Extensive comment cards have been added to the beginning and body of the program to make its operation more understandable and to provide documentation as to input formats, definitions and options. The program is now running on the CDC computers at the Leibnitz Rechnungzentrum at the Technische Univer-

sität in Munich and at the University of Washington Computer Center.

1. F.G. Perey, Oak Ridge National Laboratory, Computer program GENOA (unpublished).
2. J.G. Cramer, R.M. DeVries, D.A. Goldberg, M.S. Zisman, and C.F. Maguire, Physical Review C14, 2158 (1976).
3. J.G. Cramer, K.A. Eberhard, J.S. Eck, and W. Trombik, Physical Review C8, 625 (1973).
4. N. Austern, *Direct Nuclear Reaction Theories*, (Wiley, New York, 1970), Chapter 5 and the references cited therein.

12. APPENDIX

12.1 Nuclear Physics Laboratory Personnel

Faculty

Eric G. Adelberger, Professor
John S. Blair, Professor
David Bodansky, Professor, Chairman, Department of Physics
David F. Burch, Research Assistant Professor[1]
John G. Cramer, Professor
George W. Farwell, Professor
I. Halpern, Professor
Fred H. Schmidt, Professor
Kurt A. Snover, Research Associate Professor
Thomas A. Trainor, Research Assistant Professor
Robert Vandenbosch, Professor
William G. Weitkamp, Research Professor;
Technical Director, Nuclear Physics Laboratory

Research Staff

Konrad Aniol, Research Associate
Philip A. Dickey, Research Associate[1]
Peggy L. Dyer, Research Associate[2]
Pitsa Ikossi, Research Associate
Raymond J. Puigh, II, Research Associate
Ruedi Risler, Research Associate

Laboratory Supervisory Personnel

Harold Fauska, Research Electronics Supervisor; Assistant Technical Director, Nuclear Physics Laboratory
John W. Orth, Accelerator Engineer; Assistant Technical Director, Nuclear Physics Laboratory[3]

Predoctoral Research Associates

Chemistry

Man-Yee B. Tsang

Physics

Norman L. Back
Hyoung C. Bhang
John E. Bussoletti[4]
Yuen-dat Chan
David T. C. Chiang
Bernardo D. Cuengco[1]
Katsuyaki Ebisawa
Zafar Iqbal
Kyunga Kim[5]
William G. Lynch
Richard Von Lintig

Research Assistants

Physics

Timothy E. Chupp
Keith Davis
Charles D. Hoyle
Loren F. Stokes[5]

Full-Time Technical Staff

Professional Staff

Kelly C. Green, Research Scientist
Sally A. Hoffman, Research Scientist
William B. Ingalls, Research Engineer
Shirley Kellenbarger, Chemist[1]
Gary Roth, Accelerator Engineer[1]
Alan G. Seamster, Research Engineer
Richard J. Seymour, Computer Systems Engineer
Rod E. Stowell, Electronics Engineer
H. Erik Swanson, Research Engineer

Accelerator Technicians

Barbara L. Lewellen
Carl E. Linder
Georgia J. Rohrbaugh
George E. Saling

Design and Drafting

Peggy Douglass, Graphics Designer/Illustrator[6]
Lewis E. Page, Designer

Instrument Makers

Louis L. Geissel, Student Shop Leadman
Norman E. Gilbertson
Charles E. Hart, Foreman[7]
Gustav E. Johnson
Allen L. Willman, Leadman

Administrative Staff

Julie L. Anderson, Secretary
Dana L. Jones, Administrative Secretary

Part Time Technical Staff

John F. Amsbaugh
William Bartholet
Joanne Beaubein[1]
Mike Bizak
Charles Bouldin[1]
Don Bovee
David Chamberlin[8]
Trevor Cramer[1]
Richard Deymonaz
Ronald Dickens[1]
Thomas Emrich[1]
Patrick J. Grant
Lynn D. Green[1]
Wilbur Jones[1]
Mark Killinger[1]
Roger Lapthorne[4]
Bruce Magnuson
Lyle Martin[1]
Kevin L. Michelsen
John L. Osborne[1]
Shawn Pannell
Leslie Pence
Daniel Quick[1]
Jan Sanislo[1]
Christopher Scofield[1]
John Soudas[1]
Thomas Schuch[1]
Mary Tobin[1]
Tim Van Wechel[1]
Chris Wagner
Steve Walker[1]
Richard Weisfield
R. Craig Wiren[1]

---

1. No longer associated with the Nuclear Physics Laboratory.
2. Present address: Cyclotron Lab, Michigan State University, East Lansing, Michigan 48824.
3. Retired September 30, 1977.
4. Present address: The Boeing Company, Seattle, Washington 98031
5. Not on appointment for part of FY '78.
6. Retired November 30, 1977.
7. Retired August 31, 1977.
8. Present address: Westinghouse, Richland, Washington 99352.

12.2 Advanced Degrees Granted, Academic Year 1977-1978

J. E. Bussoletti: Ph.D. "The Giant Quadrupole Resonance: Capture Amplitude Analysis of the $^{14}C(p,\gamma)^{15}N$ and $^{15}N(p,\gamma)^{16}O$ Reactions."

K. Ebisawa: Ph.D. "Measurements and Model Calculations of Radiative Proton Capture in Heavy Nuclei and Radiative Alpha Capture in Light Nuclei."

12.3 List of Publications

Published Papers:

"Electromagnetic Decays of T=2 States in T_z=1 Nuclei," D.P. Balamuth and E.G. Adelberger, Phys. Rev. C 16, 928 (1977).

"Electromagnetic Transitions in ^{13}C and ^{13}N," R.E. Marrs, E.G. Adelberger, and K.A. Snover, Phys. Rev. C 16, 61 (1977).

"Investigation of E2 and E3 Radiation above the Giant Dipole Resonance in $^{89}Y(p,\gamma_0)^{90}Zr$," K.A. Snover, F.S. Dietrich, and D.W. Heikkinen, Phys. Rev. Lett. 38, 156 (1977).

"Radiative Transitions and Isospin Mixing in ^{12}C," E.G. Adelberger, R.E. Marrs, K.A. Snover, and J.E. Bussoletti, Phys. Rev. C 15, 484 (1977).

"Distinguishing Between Stars and Galaxies Composed of Matter and Antimatter Using Photon Helicity Detection," J.G. Cramer and W.J. Braithwaite, Phys. Rev. Lett. 39, 1104 (1977).

"Radiative Proton Capture to the Ground State and First 3 Excited States of ^{12}C," K.A. Snover, P. Paul, and H.M. Kuan, Nucl. Phys. A285, 189 (1977).

"Spontaneously Fissioning Isomers," R. Vandenbosch, Ann. Rev. Nucl. Sci. 27, 1 (1977).

"Angular Momentum Transfer in Deeply Scattering of 610 MeV ^{86}Kr by ^{209}Bi," P. Dyer, R.J. Puigh, R. Vandenbosch, T.D. Thomas, and M.S. Zisman, Phys. Rev. Lett. 39, 392 (1977).

"The Transition between Light and Heavy Ion Elastic Scattering," R.M. Devries, D.A. Goldberg, J.M. Watson, M.S. Zisman, and J.G. Cramer, Phys. Rev. Lett. 39, 450 (1977).

"Back-angle Anomalies in ^{6}Li Scattering from ^{40}Ca and ^{44}Ca," H. Bohn, K.A. Eberhard, R. Vandenbosch, K.G. Bernhardt, R. Bangert, and Y-d Chan, Phys. Rev. 16, 665 (1977).

"Neutron Radii of Calcium Isotopes from Pion Total Cross-Section Measurements," M.J. Jakobson, G.R. Burleson, J.R. Calarco, M.D. Cooper, D.C. Hagerman, I. Halpern, R.H. Jeppeson, K.F. Johnson, L.D. Knutson, R.E. Marrs, H.O. Meyer, and R.P. Redwine, Phys. Rev. Lett. 38, 1201 (1977).

Papers Submitted or in Press:

"A Search for Neutral Weak Current Effects in the Nucleus ^{18}F," M.M. Lowry, J.M. Davidson, R.E. Marrs, C.A. Barnes, F.M. Morinigo, B. Chang, E.G. Adelberger, and H.E. Swanson, submitted to Physical Review Letters.

"Substate Excitation of the 3.73 MeV 3^- State of ^{40}Ca Produced by the Inelastic Scattering of 20.3 MeV Protons," T.K. Lewellen, submitted to Nuclear Physics.

"The Analyzing Power of $^{206}Pb(\vec{p},p_0)$ and $^{207}Pb(\vec{p},p_0)$ Near the $3p_{1/2}$ Isobaric Analog Resonance," N.L. Back, M.P. Baker, J.G. Cramer, and T.A. Trainor, submitted to Phys. Rev. C.

"Isospin Forbidden Beta Decay of ^{28}Mg," P.A. Dickey, J.E. Bussoletti, and E.G. Adelberger, submitted to Nuclear Physics.

"Total Width of the Lowest T=2 State in ^{24}Mg, J.L. Osborne, E.G. Adelberger, and K.A. Snover, submitted to Nuclear Physics.

"Decays of the Lowest T=2 State in ^{44}Ti," S.P. Freedman, C.A. Gagliardi, M.S. Oothoudt, A.V. Nero, R.G.H. Robertson, F.J. Zutavern, E.G. Adelberger, and A.B. McDonald, submitted to Phys. Rev. C.

"A Schematic Model for Isospin Mixing in Light Nuclei," A.B. McDonald and E.G. Adelberger, submitted to Phys. Rev. Lett.

"Heavy Ion Elastic Scattering II: 142 MeV ^{16}O on ^{28}Si, ^{59}Co and ^{60}Ni," G.R. Satchler, M.L. Halbert, N.M. Clarke, E.E. Gross, C.B. Fulmer, A. Scott, D. Martin, M.D. Cohler, D.C. Hensley, C.A. Ludemann, J.G. Cramer, M.S. Zisman, and R.M. DeVries, submitted to Nuclear Physics.

"Gross Structure in Gamma Ray Yields Following the ^{16}O + ^{12}C Reaction," Y-d Chan, H. Bohn, R. Vandenbosch, K.G. Bernhardt, J.G. Cramer, R. Sielemann, and L. Green, submitted to Nuclear Physics.

"Gamma Decays of the First T=3/2 States in ^{9}Be and ^{9}B^{+}," P.A. Dickey, P.L. Dyer, K.A. Snover, and E.G. Adelberger, submitted to Physical Review.

"Polarization Transfer Coefficients for ^{3}He(p,p)^{3}He Elastic Scattering below 11 MeV," W.G. Weitkamp, W. Grüebler, V. König, P.A. Schmelzbach, R. Risler, and B. Jenny, submitted to Nuclear Physics.

"The ^{50,52,54}Cr(α,p)^{53,55,57}Mn Reactions at E_α = 18 and 26 MeV," K.A. Aniol, D.W. Gebbie, C.L. Hollas, and J. Nurzynski, accepted for publication in Nuclear Physics A.

Invited Papers and Talks:

"Large Angle Oscillations in Heavy Ion Elastic Scattering and Contimuum VMI Rotational Band Structures," J.G. Cramer. Invited paper presented at the Symposium on Heavy Ion Elastic Scattering, University of Rochester, October 25-26, 1977.

"Angular Momentum Transfer in Deeply Inelastic Collisions," R. Vandenbosch. Invited talk presented at Symposium on Macroscopic Features of Heavy-ion Collisions and Pre-equilibrium Process, Hakone, Japan, September 2, 1977.

"Transfer of Orbital Angular Momentum in Fragment Spin as a Probe of Energy Damping Mechanisms," R. Vandenbosch. Invited paper at APS/DNP Meeting at Rochester, N.Y. BAPS 22, 1027 (1977).

"Nuclear and Atomic Probes of the Neutral Weak Currents," E.G. Adelberger. International Symposium on Nuclear Physics at Cyclotron Energies, Calcutta, September 1977 (proceedings to be published).

"Inelastic Scattering to the Continuum at Moderate Energies," I. Halpern. International Symposium on Nuclear Physics at Cyclotron Energies, Calcutta, September 1977 (proceedings to be published).

"Nuclear Parity Mixing - An Experimental Review," E.G. Adelberger. Ben Lee Memorial International Conference on Parity Non-conservation, Weak Neutral Currents and Gauge Theories, October 1977 (proceedings to be published).

"Determination of Nuclear Sizes from Pion Total Section Measurements," L. Knutson, BAPS 22, 1009 (1977).

Conference Proceedings Publications:

"Angular Momentum Transfer in Deeply Inelastic Scattering of 610 MeV ^{86}Kr by ^{209}Bi," P. Dyer, R.J. Puigh, R. Vandenbosch, T.D. Thomas, and M.S. Zisman. International Conference on Nuclear Structure, Tokyo, Japan, September 5-10, 1977.

"Das Magnetisch Moment des 3^+-Zustands im Selbstkonjugierten Kern ^{46}V," K. Aniol, D.F. Burch, B.D. Cuengco, H. Fauska, W.G. Lynch, and R. Sielemann. Annual Meeting of the German Physical Society, Heidelberg, March 13-18, 1978.

"Resonance Structure in $^{12}C + ^{18}O$ and $^{14}C + ^{16}O$ at Excitation Energies Between 40 and 50 MeV in ^{30}Si," K.G. Bernhardt, H. Bohn, K.A. Eberhard, R. Vandenbosch, and M.P. Webb. Contribution to "International Conference on Resonances in Heavy Ion Reactions," Hvar, Yugoslavia, May 31 - June 3, 1977.

"The Scattering of ^{6}Li Projectiles from ^{40}Ca and ^{44}Ca at Backward Angles," H. Bohn, K.A. Eberhard, R. Vandenbosch, K.G. Bernhardt, R. Bangert, and Y-d. Chan. Contribution to "International Conference on Resonances in Heavy Ion Reactions," Hvar, Yugoslavia, May 31 - June 3, 1977.

"The $^{12}C(^{18}O,^{8}Be)^{22}Ne$ Reaction between 15 and 22.5 MeV (c.m.)," K.G. Bernhardt, H. Bohn, K.A. Eberhard, R. Sielemann, and R. Vandenbosch. Contribution to "International Conference on Resonances in Heavy Ion Reactions," Hvar, Yugoslavia, May 31 - June 3, 1977.

"The $^{12}C + ^{16}O \rightarrow ^{8}Be + ^{20}Ne$ Reactions," K.G. Bernhardt, H. Bohn, K.A. Eberhard, W. Trombik, and R. Vandenbosch. Contribution to "International Conference on Resonances in Heavy Ion Reactions," Hvar, Yugoslavia, May 31 - June 3, 1977.

"A New Experiment to Measuring Parity Mixing in the Ground State Doublet in ^{19}F," E.G. Adelberger, H.W. Swanson, T.A. Trainor, W.G. Ingalls, Z. Iqbal, and R. Von Lintig. Submitted for the International Conference on Nuclear Structure, Tokyo, Japan, September 1977.

"A Search for Neutral Weak Current Effects in the Nucleus ^{18}F," C.A. Barnes, M.M. Lowry, J.M. Davidson, F.B. Morinigo, E.G. Adelberger, and H.E. Swanson. Submitted for the International Conference on Nuclear Structure, Tokyo, Japan, September 1977.

"The Inelastic Scattering of 67 MeV Pions from Nickel in the Continuum," D. Chiang, I. Halpern, G.A. Miller, L. Knutson, M. Cooper, J.F. Amann, P.D. Barnes, M. Doss, R. Eisenstein, S.A. Dytman, J. Sherman, and W. Wharton, VIth Conference on High Energy Physics and Nuclear Structure, Zürich, August 1977.

"Relativistic Coulomb Effects in Pion Scattering," J.G. Cramer, W.G. Lynch, and J.G. Wills, VIth Conference on High Energy Physics and Nuclear Structure, Zürich, August 1977.

Contributed Abstracts:

"Evidence for a Continuum VMI Rotational Band from Large-Angle Oscillations in $^{16}O + ^{28}Si$ Elastic Scattering," J.G. Cramer, J.C. Wiborg, Y-d. Chan, K-l Liu, M. S. Zisman, B.D. Cuengco, W.G. Lynch, and R.J. Puigh. Rochester meeting of the American Physical Society, October 27-29, 1977, BAPS 22, 1002 (1977).

"Cross Sections Relevant to Gamma-Ray Astronomy," P. Dyer, D. Chiang, D. Bodansky, BAPS 22, 583 (1977).

"Systematics of Matter Densities of Nuclei from ^{40}Ca to ^{68}Zn," C.N. Papanicolas, A.M. Bernstein, W.Q. Summer, and J.S. Blair, BAPS 23, 38 (1977).

"A Proposal for Monitoring Nuclear Power Plants," F.H. Schmidt and G.L. Woodruff, BAPS 22, 547 (1977).

"Inelastic Scattering of 60 MeV Pions to Continuum Excitations," D. Chiang, I. Halpern, L. Knutson, M.D. Cooper, J.F. Amann, P.D. Barnes, M. Doss, S.A. Dytman, R.A. Eisenstein, J.D. Sherman, J.N. Crain, and W. Wharton, BAPS 22, 525 (1977).

"The $^{12}C(\pi^+,d)^{10}C$(g.s.) and $^{10}B(\pi^+,d)^{8}B$(g.s.) Transitions at $E_\pi = 50$ MeV," J.F. Amann, P.D. Barnes, K.G.R. Doss, S.A. Dytman, R.A. Eisenstein, J.D. Sherman, W. R. Wharton, and D.T. Chiang, BAPS 22, 1007 (1977).

"The $^{12}C(\pi^+,p)^{11}C$ Reaction at $E_\pi = 50$ MeV," J.D. Sherman, J.F. Amann, P.D. Barnes, K.G.R. Doss, S.A. Dytman, R.A. Eisenstein, W.R. Wharton, and D.T. Chiang, BAPS 22, 1007 (1977).

"The E3/M2 Mixing Ratio of the ^{21}Ne $1/2^-(1.80) \rightarrow 5/2^+$ (0.35) Decay and its Role in Proposed Parity Mixing Measurements," K.A. Snover, R. Von Lintig, P.G. Ikossi, and E.K. Warburton, BAPS 23, 520 (1978).

"Nuclear 'Time-Delay' and the Probability for K-shell Ionization," J.S. Blair, BAPS 23, 597 (1978).

"X-Ray Proton Coincidences in the Vicinity of the Narrow Nuclear Scattering Resonance at $E_p = 3.15$ MeV in $^{58}Ni + p$," P. Dyer, K.A. Snover, T.A. Trainor, and J.S. Blair, BAPS 23, 597 (1978).

"The α-Width of the Lowest 0^+,T=2 State in ^{28}Si," P.G. Ikossi, K.A. Snover, J.L. Osborne, E.G. Adelberger, and A.B. McDonald, BAPS 23, 521 (1978).

"An Accurate Value for the ^{20}Ne 2^+,T=1 (10.27) $\rightarrow$ 2^+,T=0 (1.63 MeV) Gamma-Decay Strength," K.A. Snover, K. Kim, and P.A. Dickey, BAPS 23, 501 (1978).

"Calculations of Hydrogen Metastable-State Populations for a Parity Nonconservation Experiment at 571G," T.A. Trainor, M.Z. Iqbal, E.G. Adelberger, and E.M. Henley, BAPS 23, 546 (1978).

"Principles of an Experiment to Detect Parity Nonconservation in n=2 Hydrogen Atoms," E.G. Adelberger, T.A. Trainor, and E.N. Fortson, BAPS 23, 546 (1978).

"Analyzing Powers for Particles Emitted to Continuum Excitations from ^{63}Cu in 18 MeV proton Bombardment," T.A. Trainor, H.C. Bhang, I. Halpern, K-1 Liu, and W.G. Lynch, BAPS 23, 603 (1978).

"Van de Graaff Control Without Image Slits," F.H. Schmidt and H. Fauska, BAPS 23, 542 (1978).

Top Row, from left to right, Standing

Lewellen, Bovee, Cramer, Johnson, Mickelsen, Wagner, Page, Saling, Willman, Trainor, Schmidt, Deymonaz, Puigh, Back, Grant, Halpern, Eenmaa, Stokes, Bhang, Swanson, Seamster, Bizak, Anderson, Seymour, Linder, Snover, Weitkamp, Iqbal, Jones

Kneeling and Sitting, from left to right

Blair, Ingalls, Geissel, Fauska, Tsang, Farwell, Aniol, Green, Adelberger, Stowell, Rohrbaugh, Chupp, Hoffman, Hoyle, Ikossi, Davis, Von Lintig, Lapthorne